THE UNIVERSITY OF ADELAIDE

DEPARTMENT OF MECHANICAL ENGINEERING

NOISE CHARACTERISTICS AND EXHAUST PROCESS GAS DYNAMICS OF A SMALL 2-STROKE ENGINE

by

Adrian David Jones, B.E. (Hons.)

Thesis for the Degree of Doctor of Philosophy

December, 1978

Awarded April 1979

ABSTRACT

The thesis consists of two parts. Part 1 describes a theoretical and experimental study of the radiated exhaust noise from a single cylinder, piston ported 2-stroke engine. Part 2 consists of a study of the noise sources on a rotary 2-stroke lawnmower.

In part 1, a detailed study of the gas dynamics of the exhausting process in a 2-stroke engine and the associated sound power radiated by the exhaust of the engine has been made. The exhaust systems considered include straight pipes of lengths 0.4m and 1.3m and a tuned expansion chamber of length 1.38m. Measurements show the significance of non-linear behaviour which results in wave steepening and shock wave formation. A series of measurements of far field sound pressure level and the associated pressure at several locations in the exhaust pipe for the different exhaust systems are discussed. These results are then compared with theoretical predictions obtained by calculating, using the method of characteristics, the detailed unsteady flow in the exhaust pipe matched to the flow out of the engine cylinder, for several engine revolutions. The calculation includes entropy characteristics and therefore allows for the significant variations in entropy, arising mainly from variable shock strength at the exhaust port, which occur in the system. Of particular interest is the close agreement between the calculated third-octave radiated sound pressure spectra and the measured spectra, for both the straight pipe and tuned expansion chamber exhaust systems.

It has been found that the radiated noise is almost totally a result of the wave action, with the noise caused by the flow turbulence at the exhaust port being of relatively minor significance. Similarly, it has been found that the Helmholtz resonance effect of the cylinder volume and exhaust port, suggested as being significant by Mutyala and

Soedel, seems also to be a negligible factor in the present studies.

In part 2, the problem of rotary 2-stroke lawnmower noise is initially considered in terms of the four component parts: inlet, exhaust, mechanical and blade noise. Of these, all but inlet noise are found to be significant at moderate engine speeds, with blade noise dominating at high speed. Detailed investigations, both experimental and theoretical, into the nature of exhaust, mechanical and blade noise are then described. In particular the mechanical noise is investigated quite thoroughly with a detailed analysis made of piston slap. Finally, recommendations are made for design changes which, if implemented, would lead to the reduction of the major components of the total noise.

CONTENTS

STATEMENT OF ORIGINALITY

This thesis contains no material which has been accepted for the award of any other degree or diploma in any University. To the best of the author's knowledge and belief, this thesis contains no material previously published or written by another person, except where due reference is made in the text.

ADRIAN D. JONES

December, 1978

ACKNOWLEDGEMENTS

The author wishes to express his sincere thanks and appreciation to his supervisor, Dr. G.L. Brown, for the constant encouragement and support, together with the most valuable guidance he has given throughout the duration of the work, and for the criticism of the thesis.

The author is also indebted to Professor R.E. Luxton and his predecessor Professor H.H. Davis for providing the opportunity to conduct the research and for the encouragement they have given. The considerable help given by other staff members and post graduate students in the Mechanical Engineering Department is also acknowledged.

The assistance given by the many helpful technicians in the Mechanical Workshop under Mr. D. Kerr and the Electrical Workshop under Mr. H. Bode is most gratefully acknowledged.

The author also wishes to thank his parents for their support for the duration of the research and his father for producing the photographic prints in the thesis. Further, the author wishes to thank Miss E.A. Clarebrough for the considerable support she has always given and Mr. W.R. Johnston for his special encouragement.

Finally, the author wishes to thank Miss F. McLeod for typing this thesis.

GENERAL INTRODUCTION

The use of small machines powered by 2-stroke engines is often accompanied by undesirable levels of noise. Lawnmowers, chain saws, small motorcycles and many similar devices are usually produced cheaply, and so, are not designed carefully with regard to noise. As the size and complexity of the components is kept to a minimum, the exhaust silencers used, for instance, are frequently inadequate. Exhaust noise is then often significant for such machines. As a result of these problems, this investigation was undertaken to study both the exhaust noise radiated from 2-stroke engines and the total noise problem for small machines powered by 2-stroke engines.

The thesis is divided into two parts. The first deals with a theoretical and experimental study of the radiated exhaust noise alone. This analysis includes a description of a special calculation technique, based on the method of characteristics, which may be used to study the development of pressure waves in an exhaust system. The calculation includes variable entropy and non-linear effects. Comparisons between experiments and theoretical predictions show that the calculation method accurately determines the radiated noise from 2-stroke engine exhaust systems consisting of both straight pipes and slowly varying area ducts. The relation between the method developed in this study and the existing exhaust noise and muffler theories is also considered. In making these comparisons, the existing theories are not described in detail, as a knowledge of them has been assumed.

The second part of the thesis is a study of the noise sources on a rotary 2-stroke lawnmower. The rotary lawnmower was selected for investigation as it is a typical example of a machine powered by a small 2-stroke engine. It is also a problem of local importance and a local

manufacturer, Simpson Pope Pty. Ltd., supplied the lawnmower studied. The study involves, firstly, a description of a series of measurements which show the significance of the various possible noise sources. Secondly, from consideration of the fundamental noise making processes, recommendations are made for design improvements which would result in lower levels of total radiated noise.

Part 2 of this work was, in fact, the starting point for the thesis and Part 1 developed specifically from the investigation of exhaust noise on the lawnmower engine. As the work progressed it became clear that some of the early experiments were not as fundamental as later work so that in some cases, mentioned in Part 2, the conclusions are not as significant as they are in Part 1.

PART 1: THE GAS DYNAMICS OF THE EXHAUST PROCESS IN SINGLE CYLINDER 2-STROKE ENGINES AND THE RADIATED NOISE

CHAPTER 1

INTRODUCTION

It has long been recognised that small 2-stroke engines, as on motorcycles and lawnmowers, have a particular exhaust noise problem. They are often very harsh sounding, with the noise from the individual pulses being very annoying. The intention of the work was to provide a means for studying the noise associated with exhausts for 2-stroke engines with piston ports and crankcase scavenging. To do this it was considered necessary to model the exhausting process and then to calculate the resultant radiated noise. Results in this part show that this has been successfully done. The measurements described in this part were all performed on a motorcycle engine, details of which are given in Appendix 1. The results obtained may be applied to all small 2-stroke engines and, although it was not done in this study, to many 4-stroke engines.

1.1 SOURCE OF EXHAUST NOISE

The basic method of operation of a piston ported 2-stroke engine is shown in figure (1). As the piston moves down in the cylinder during the expansion stroke, first it uncovers the exhaust port and then the transfer ports. Ideally, the engine is designed to exhaust the combustion products through the exhaust port in the time between when the exhaust port opens and the transfer ports open.

The source of the exhaust noise must now be considered. When the exhaust port opens the ratio of cylinder pressure to exhaust pipe pressure is usually high enough for choked flow to occur momentarily, through the exhaust port. For the duration of the choked flow and the

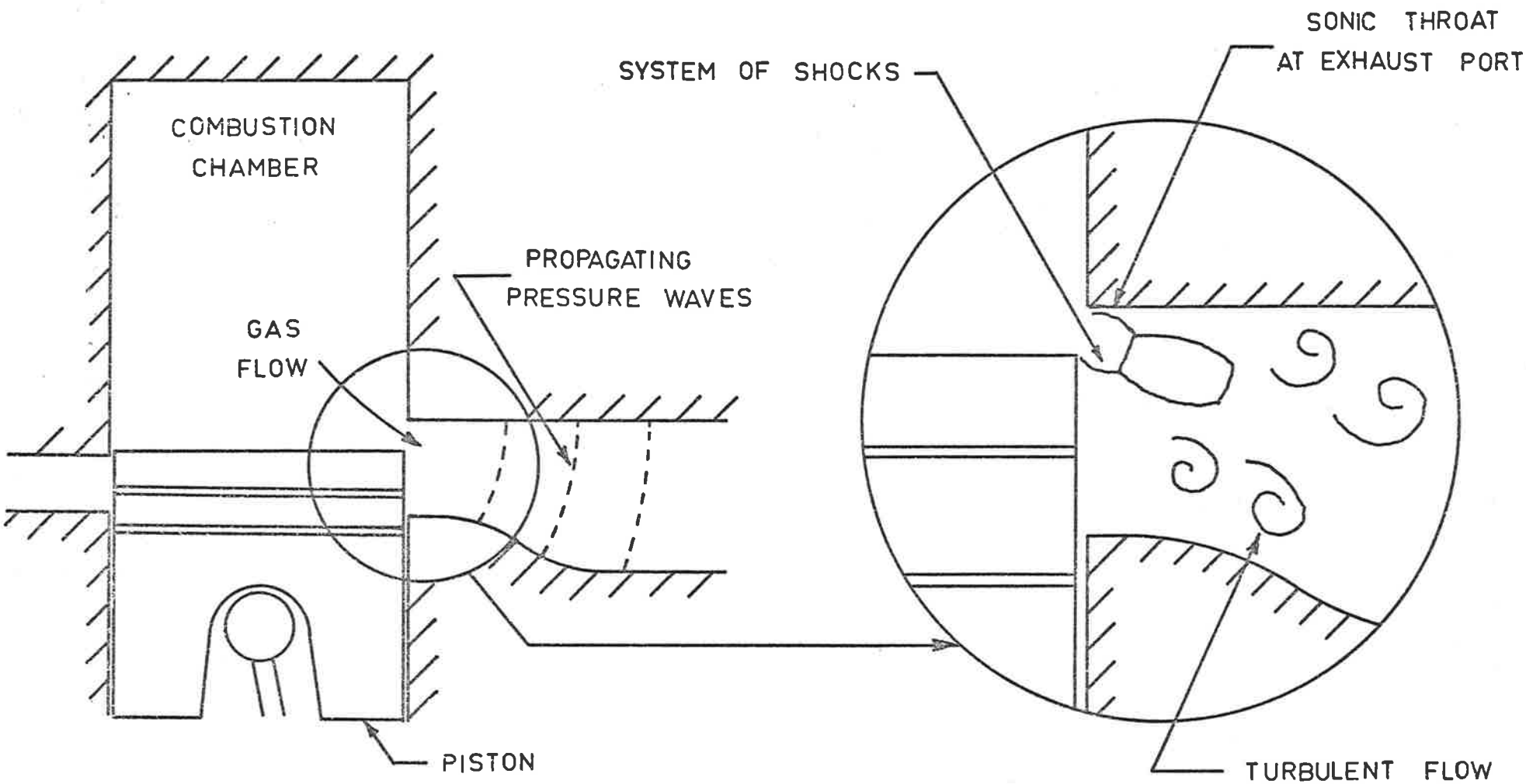

FIG.1 GAS FLOW AFTER EXHAUST PORT OPENS

subsequent subsonic flow, as shown in figure (1), turbulent flow exists downstream of the exhaust port. It was originally not clear how much of the exhaust noise was due to this choked turbulent flow. For choked valves, for example, it is well known that the passage of turbulence through a system of standing shocks gives rise to substantial noise (Heller and Franken (1)).

Apart from this possible flow generated noise, there is the noise resulting from the system of propagating pressure waves passing along the exhaust system, which are caused by variations in the mass flow rate at the exhaust port. These pressure waves cause the well known "wave action" in exhaust systems.

It has been found in this study that effectively all exhaust noise from a 2-stroke engine (and almost certainly from 4-stroke engines as well) is, in fact, caused by the "wave action", as originally studied by Bannister and Mucklow (2) and more recently by Benson and others (references (3), (4)).

A series of simple experiments and calculations showed the insignificance of the exhaust port flow generated noise. Firstly, from currently known flow noise theory, it was possible to estimate the contribution from this source.

As is well known (e.g. reference (1)), the flow noise created by the jet noise mechanism will be expected to vary with the flow velocity to the 8th power, very approximately. Most flow noise would then be expected when the flow is choked at the exhaust port, and the flow noise generated elsewhere in the exhaust system will be insignificant in comparison. Computer calculations of gas flow, as well as measurements of engine cylinder pressure show that the duration of choked flow is only about $\frac{1}{20}$th of a revolution at 4000 r.p.m.

In reference (1), Heller and Franken state that for valves with pressure ratios less than 3, which corresponds with a 2-stroke

engine exhausting, the creation of noise from both the shock noise mechanism and the turbulent mixing mechanism must be considered. Using relations given in section 16.6 of reference (1), and computer calculations of mass flow rate through the exhaust port, it was determined that the contributions to radiated sound power by the shock noise and turbulent mixing mechanisms were 107 dB and 102 dB re 10^{-12} watts respectively, for the motorcycle engine operating under certain conditions. As the actual measured value of radiated sound power under the same operating conditions (4000 r.p.m., high load) was 123dB it appears unlikely that the exhaust port flow noise would be significant. This was further verified by experiment.

The motorcycle engine was run using a number of exhaust systems which will be described in detail in chapter 3. These included simple straight pipes of lengths 0.4 m and 1.3 m and a tuned expansion chamber. In each case the engine was run at 4000 r.p.m. with a high load, and a pressure transducer was placed flush with the inside of the pipe 10 cm downstream of the port. If the exhaust port flow noise was evident it would have been recorded by the pressure transducer as high frequency pressure fluctuations on, and shortly after, the initial exhaust pulse. From chapter 16 of reference (1) the expected flow noise would have a peak in its spectrum at around 5kHz. As is shown in the oscilloscope traces in figure (2), no such high frequency pressure fluctuations are observed in any case. (As discussed more fully in section 3.1, the pressure transducer had a measured frequency response well in excess of 5kHz).

A further test showing the insignificance of the exhaust port flow noise involved a narrow band analysis of radiated exhaust noise. The engine was run with the 0.4 m straight exhaust pipe at the same speed and load as for the previous tests and the radiated sound was recorded at a distance 5 m from the source. The recording was then

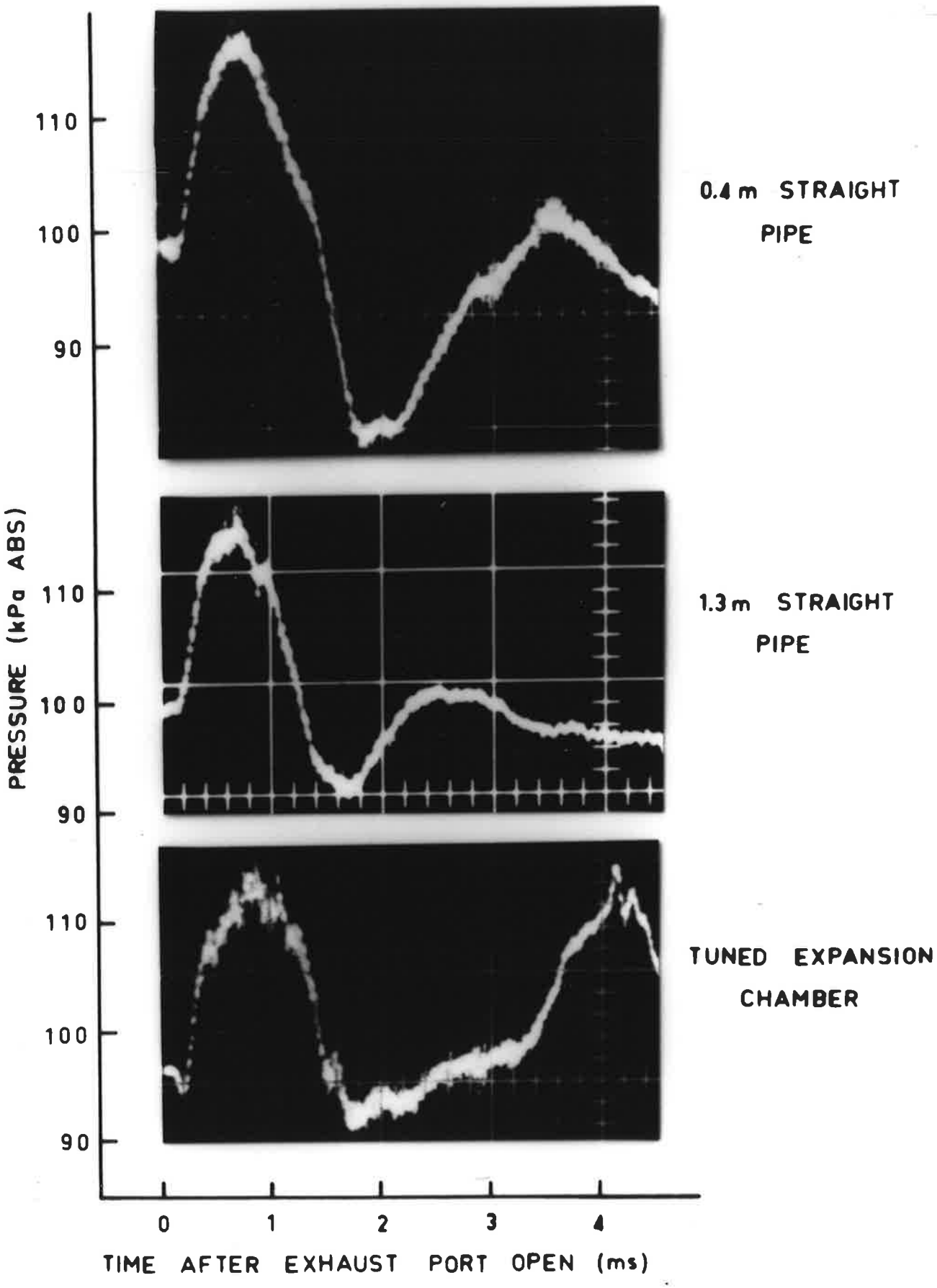

FIG. 2 INITIAL EXHAUST PULSE 0.10 m FROM PORT

analysed using a B & K 2010 narrow band analyser, with a constant bandwidth of 10Hz. If the flow noise was significant the spectrum would contain broadband noise rather than discrete harmonics at high frequencies (near 5kHz). However, as is shown in figure (3) the spectrum contains only harmonic peaks up to the 88th harmonic at 6kHz. Clearly, the flow noise is not significant. The spectrum in figure (3) was obtained from an analysis of the recorded sound on a loop of tape which contained well over 200 engine cycles.

It has been suggested by Mutyala and Soedel (5) that the Helmholtz resonance effect of the engine cylinder and the exhaust port area is significant in terms of radiated noise. For the motorcycle engine, this resonance would be expected at approximately 1kHz. Such a resonance would cause large fluctuations in cylinder pressure near bottom dead centre. To briefly test this theory, the engine was run with no exhaust system (to minimize damping of this resonance) and the cylinder pressure after exhaust port opening was recorded using a Kistler type 6005 pressure transducer. A sample pressure measurement shown in figure (4) does show these pressure fluctuations, at a frequency of slightly less than 1kHz. However, their magnitude is so small compared with the pressure at exhaust port opening, that the noise from the wave action resulting from the initial exhaust pulse must surely be far greater than that from the Helmholtz resonance effect. This is further verified by the fact that the radiated noise spectrum from the 0.4 m straight pipe system (figure (3)) shows no large peak near 1kHz.

Apart from the already conclusive evidence detailed above in this section, the fact that the pressure cycles both inside exhaust systems and as radiated to the far field are later shown to be accurately predicted using wave action calculations (see chapter 3), indicates that an exhaust noise study need only be concerned with the

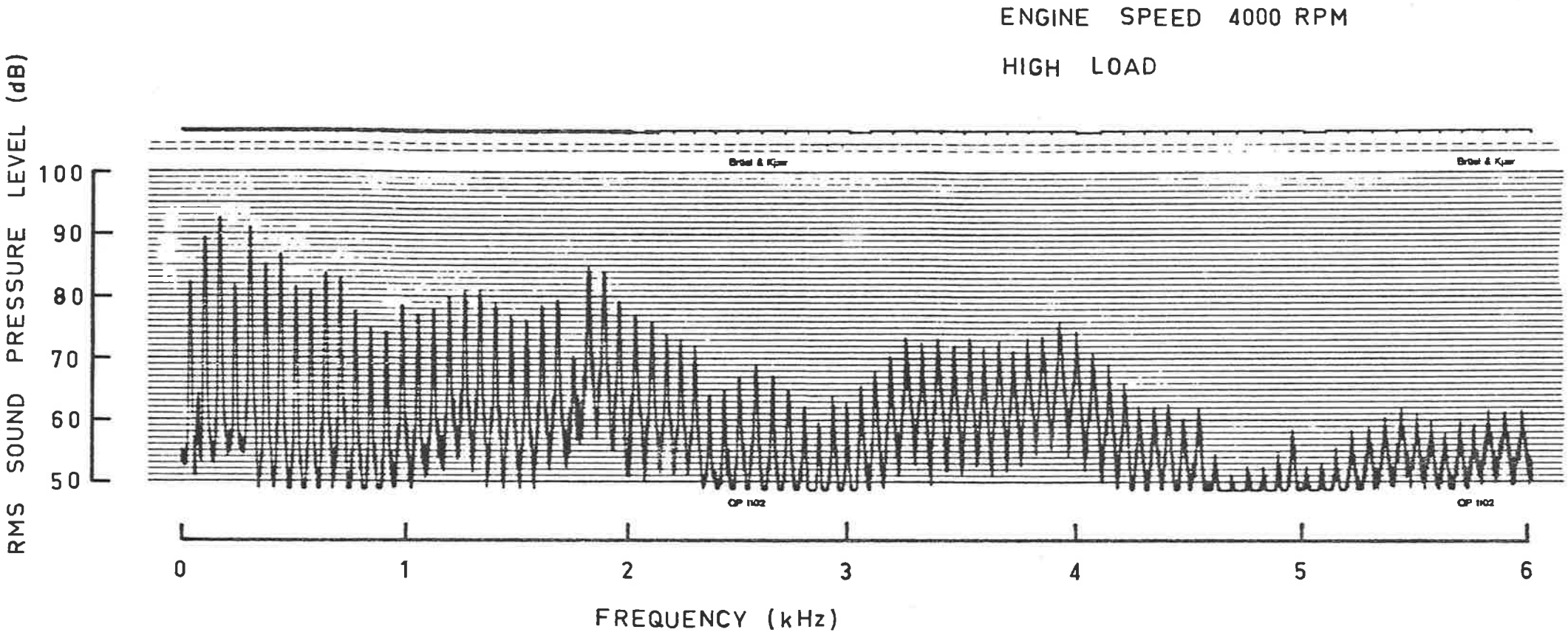

FIG.3 SPECTRUM OF RADIATED SOUND FROM 0.4 m STRAIGHT PIPE EXHAUST

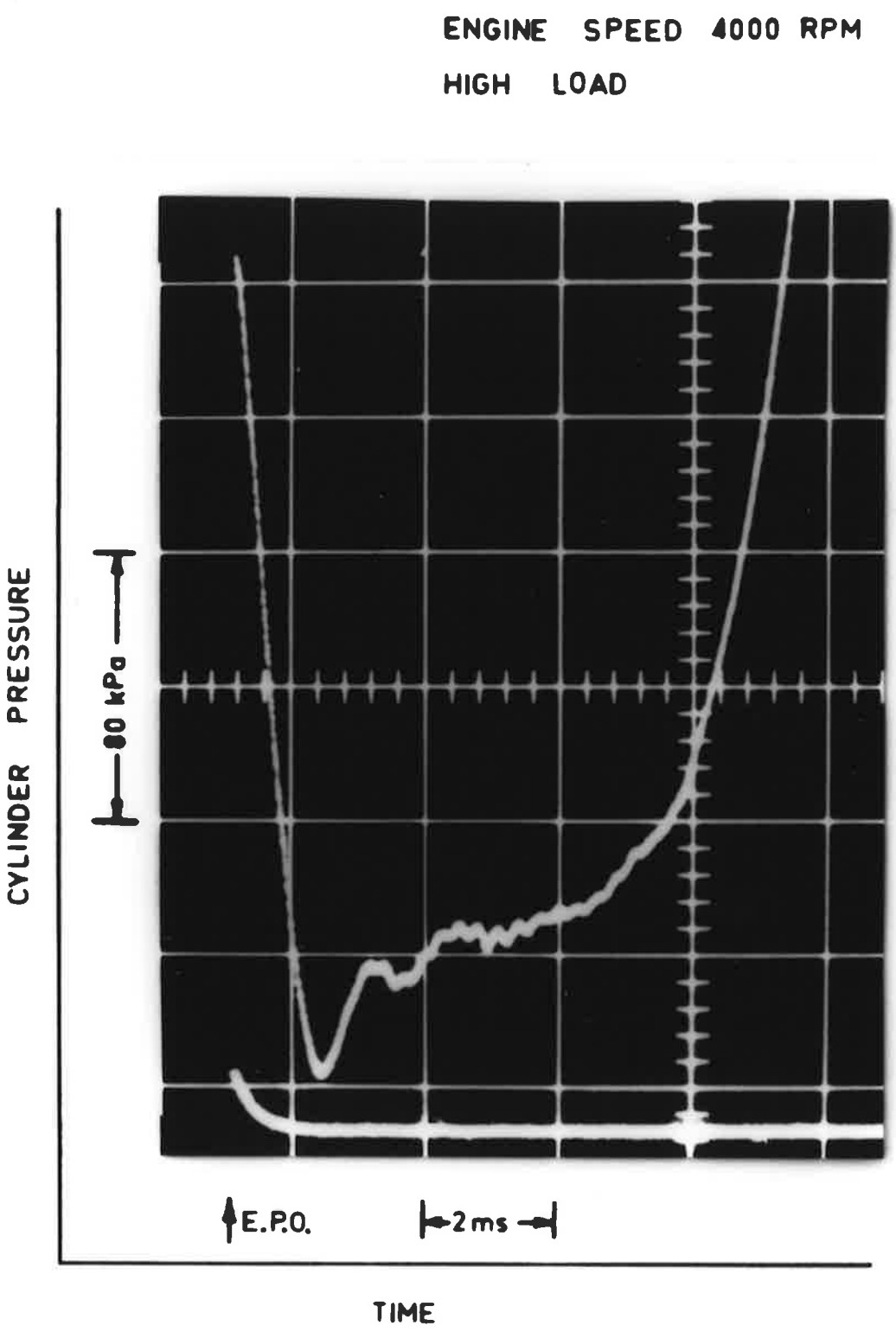

FIG.4 CYLINDER PRESSURE AFTER EXHAUST PORT OPENS

wave action. With this in mind, it is now possible to comment on why existing exhaust noise and muffler theories are often limited in application and sometimes very difficult to use.

1.2 EXISTING MUFFLER THEORY

The problems relating to the use of current exhaust noise and muffler theories concern the fact that most do not relate to the actual operation of an engine. The exhaust noise is caused by wave action and this causes short duration, high intensity pressure waves to pass down the exhaust and muffler systems. Also these pressure waves and their reflections have a large influence on the engine operation and, for example, usually determine at which speeds engines will run well.

Most current theories are based on linearized acoustic analyses which assume that muffler elements act as either lumped or distributed impedances with the nature of the sound source being greatly simplified, (e.g. Davis et al (6), Watters, Hoover and Franken (7), Davies (8), Alfredson (9)). The assumption of linear behaviour in muffler elements is only accurate at low sound pressure levels and the accuracy of this approximation for a given sound pressure is different for the different elements in the exhaust system. For example, the resistance of an orifice is linear provided the fluctuating velocity component is much less than the mean flow but the wave action in operating exhaust systems usually results in much larger fluctuating velocity values. Measurements of Davis, Watters and Alfredson, as well as results obtained using the motorcycle and lawnmower test engines of this study indicate that in at least some sections of all exhaust and muffler systems the peak sound pressure levels will be too high for general linear theory to be entirely valid. Discrepancies caused are usually worse for simple systems, such as those considered in this study. However, large multi-element mufflers progressively decrease sound pressure levels, and so,

often give good agreement with linear theory. For example, Alfredson (9), using distributed impedances and allowing for a mean flow, obtained good results for complex quarter wave type mufflers on engines with exhaust manifolds.

Apart from the possible non-linear behaviour of muffler elements, the nature of the sound source impedance poses a problem. Linear analysis usually requires that the sound source must be considered as either a zero or infinite impedance source. A consideration of the wave action effects may be used to clarify this situation. This is considered in detail in section 4.1, but briefly, because wave reflections in the exhaust system do strongly affect the flow at the exhaust port, modelling the engine as either a simple current or voltage source is not an accurate approximation.

As an alternative to linear theory, Davies (8) proposed a single pulse method, in which the passage of one wave through the exhaust system was studied. Usually a shock wave was considered and only the initial shock strength was investigated. This analysis took no account of expansion chamber lengths and only the area ratios at step changes in cross section reduced the strength of the initial shock. It is shown in more detail in section 4.5 how this method is unsatisfactory. This is partly because "wave-breaking", or specifically a shock wave, only forms in exhaust systems, if at all, some distance from the exhaust port. Also, the steepening of the initial pulse and reflections of this pulse are in general important in determining the radiated noise, certainly in the systems discussed in this work.

Bearing in mind the limitations of the current theories outlined above, it was the intention of this study to arrive at a means of investigating exhaust noise and muffling effects which took account of the importance of the wave action. Such a method would then tie

together the sound generation and the engine operation.

1.3 THE METHOD OF CHARACTERISTICS

The wave action effects in engine exhaust systems have been investigated for more than about thirty years now, by a number of people, using the method of characteristics. These investigations have almost always been concerned with studying engine operation with regard to efficiency as affected by exhaust tuning phenomena. Perhaps the best known work in the study of engine operation using the method of characteristics is that done by Benson and others (e.g. references (3), (4)) at, firstly, Liverpool and then Manchester. This work eventually resulted in the development of computer programs which compute all aspects of engine operation without, however, considering acoustics. It then appeared obvious when the present study was being undertaken, that, since the wave action causes the radiated noise, a similar method could be used to study 2-stroke engines with regard to exhaust noise. It was also believed that ultimately, by using such a method, the more general operation of mufflers could be studied. The method of characteristics was then adopted for this study.

When this work commenced it was decided to devise a calculation technique, by which the actual wave diagram, previously drawn graphically (as shown by Rudinger (10)), would be calculated on a computer. This was considered in preference to adapting the method of Benson for several reasons.

The programs developed by Benson are intended for studying engine operation and efficiency in terms of arriving at the initial design for an engine and exhaust system. As such, the accurate study of very rapid changes in pressure and velocity at certain points in the exhaust system is not of great concern. It is shown later in section 2.9 that the radiated exhaust noise is for most practical purposes dependent on the derivative of the cycle of velocity values at the

tailpipe outlet. A small error in this cycle of velocity values can, on differentiation, cause a large error in the radiated pressure cycle. For this reason a method of following very rapid changes in velocity at the tailpipe outlet was required.

Another associated reason for using the actual wave diagram relates to the importance of steepening of the initial exhaust pulse. As shown in section 2.9 it is necessary to follow very accurately the steepening and possible shock wave formation on the initial exhaust pulse. It was believed that the method of Benson would not do this with sufficient accuracy to satisfactorily determine the radiated noise. This is discussed further in section 2.11 where a comparison between the two methods is presented. The comparison does appear to support this initial point of view.

The method of characteristics was therefore used in a way which allowed very accurate determination of the events which are important in terms of the radiated noise from the tailpipe outlet. The method of its use in this study is detailed further in the following chapter. It may be noted here that it has been suggested (e.g. Alfredson (9)) that the method of characteristics would require too much computing time to study muffler systems. This study shows that this need not be so. Also, Benson (3) considered that for studying engine operation, the plotting of an actual wave diagram ("non-mesh" method) would be too difficult to program for a computer. As mentioned earlier, Benson's mesh method was not used because of the difficulties expected in accurately computing the radiated sound. Chapter 2 shows that the computation method developed in this study is, in fact, accurate but not excessively complicated. It is worth noting in passing that the method solves the unsteady flow in detail and therefore can be used to examine the actual non-linear effects that do occur in the various muffler elements.

The author notes that more recently Coates and Blair (29) and Karnopp, Dwyer and Margolis (30) have also used the method of characteristics for studying the noise associated with simple engine exhaust systems. As in this study the unsteady gas flow has been considered.

Coates and Blair obtained good agreement between theory and experiment, however, the actual experiments used controlled unsteady flows with a rotary valve acting as an unsteady current source. Due to the constant high pressure upstream of the valve and an almost constant pressure downstream (small fluctuations) the unsteady flows were essentially isentropic. It is the extension of the basic method of characteristics to the more difficult problem of a real engine exhaust with very large differences in entropy and more complicated matching of gas flow to and from the exhaust pipe through the exhaust port which was the concern of this study.

The work of Karnopp, Dwyer and Margolis seems similar in approach to that of this study. It was, of course, not available when this work was in progress. Published results of their work (for example, reference (30)) do not, however, give any significant comparison between theory and experiment, as is given in this study.

CHAPTER 2

THE METHOD OF CHARACTERISTICS SOLUTION FOR A SINGLE CYLINDER 2-STROKE ENGINE

The method of characteristics solution of a one-dimensionalized flow in a duct, and its general use, has been described by many researchers previously; for example by Rudinger (10) and Whitham (11). The mathematical derivation will then be assumed and the basic solution only covered briefly, however, the application of the method for modelling engine exhaust systems will be considered in some detail. Following this, the computational techniques and the actual calculations involved in constructing the x- t diagram will be described.

2.1 BASIC METHOD OF SOLUTION

The solution is based on the conservation equations for mass, momentum and energy for one-dimensional flow in a duct. These are as shown below (from, for example, Whitham (11), for a constant area duct:-

$$\frac{\partial \rho}{\partial t} + u\frac{\partial \rho}{\partial x} + \rho\frac{\partial u}{\partial x} = 0 \qquad (2.1)$$

$$\rho\left(\frac{\partial u}{\partial t} + u\frac{\partial u}{\partial x}\right) + \frac{\partial p}{\partial x} = 0 \qquad (2.2)$$

$$\frac{\partial S}{\partial t} + u\frac{\partial S}{\partial x} = 0 \qquad (2.3)$$

After manipulation, these equations may be rewritten in characteristic form, with the set of characteristic equations obtained, shown below (as in Whitham (11)):-

$$\frac{dp}{dt} + \rho a\frac{du}{dt} = 0 \qquad \text{on } C_+ : \frac{dx}{dt} = u + a \qquad (2.4)$$

$$\frac{dp}{dt} - \rho a\frac{du}{dt} = 0 \qquad \text{on } C_- : \frac{dx}{dt} = u - a \qquad (2.5)$$

$$\frac{dS}{dt} = 0 \qquad \text{on P: } \frac{dx}{dt} = u \qquad (2.6)$$

Information about the flow may then be considered to be carried along the duct by the right-facing C_+ and left-facing C_- characteristics, which travel with the local sonic velocity. The motion of the C_+ and C_- characteristics may be likened to the motion of pressure waves. The P characteristics, travelling with the local particle velocity, describe particle paths. If the flow in a constant cross-section duct is isentropic, the following non-dimensionalized relations, obtained by integrating equations (2.4) and (2.5), hold:-

$$P_1 = \left(\frac{2}{\gamma-1}\right)\frac{a}{a_o} + \frac{u}{a_o} \qquad \text{on } C_+ \qquad (2.7)$$

$$Q_1 = \left(\frac{2}{\gamma-1}\right)\frac{a}{a_o} - \frac{u}{a_o} \qquad \text{on } C_- \qquad (2.8)$$

as in, for example, Rudinger (10), where a_o = reference speed of sound. (The subscript "1" is used in equations (2.7) and (2.8) to avoid confusion with P, an entropy characteristic). P_1 and Q_1 are the Riemann invariants, and for isentropic flow in a constant cross section duct, are constant for the C_+ and C_- characteristics, respectively. In the non-isentropic flow in the exhaust duct, the entropy is assumed constant between P characteristics and the Riemann invariants, P_1 and Q_1, for the C_+ and C_- characteristics are then constant in this region. The change in either P_1 or Q_1 at an intersection between either a C_+ or C_- characteristic and a P characteristic is easily found and is discussed in section 2.6. The resultant flow in the duct is then found by plotting the paths of a finite number of C_+, C_- and P characteristics on an x - t diagram. Section 2.10 shows how the analysis is extended to consider ducts of slowly varying cross section.

This then describes the basis of the method of characteristics solution of a one-dimensional flow in a duct. For investigating radiated exhaust noise, the ideal use of the method appears to be, for reasons already given, the actual calculation of the paths of the C_+, C_- and P characteristics on the x - t plane. The way the method is applied to engine exhaust systems is described in the next section.

2.2 MATCHING THE CYLINDER CONDITIONS TO THE EXHAUST PIPE FLOW

As it is desired to obtain a computer program to calculate an x - t diagram, this section considers how the method of characteristics in terms of the x - t diagram may be used to study engine exhaust systems. The logic of the computational techniques, to be described later, then becomes obvious.

To best illustrate the modelling of an engine exhaust system on an x - t diagram, the simplest possible case is considered first:- a single cylinder, piston ported engine exhausting into a long straight pipe. Figure (5) shows the exhaust system to be modelled and also the corresponding x - t diagram which is subsequently drawn for this purpose. For reasons of simplicity this x - t diagram is by no means complete, but shows all the essential features as is described below.

The engine and exhaust pipe shown in the figure are depicted at a time shortly after the exhaust port has opened. The initial cylinder pressure is considerably higher than that for the gas initially at rest at atmospheric pressure in the exhaust pipe, so that choked flow exists at the exhaust port. The hot exhaust gas coming from the cylinder may be considered to act on the gas initially at rest, like a massless piston, accelerating it downstream. In terms of the x - t diagram in the figure, the massless piston sends downstream a system of C_+ characteristics representing increasing pressure values. Three such C_+ characteristics are shown emanating from the surface of the

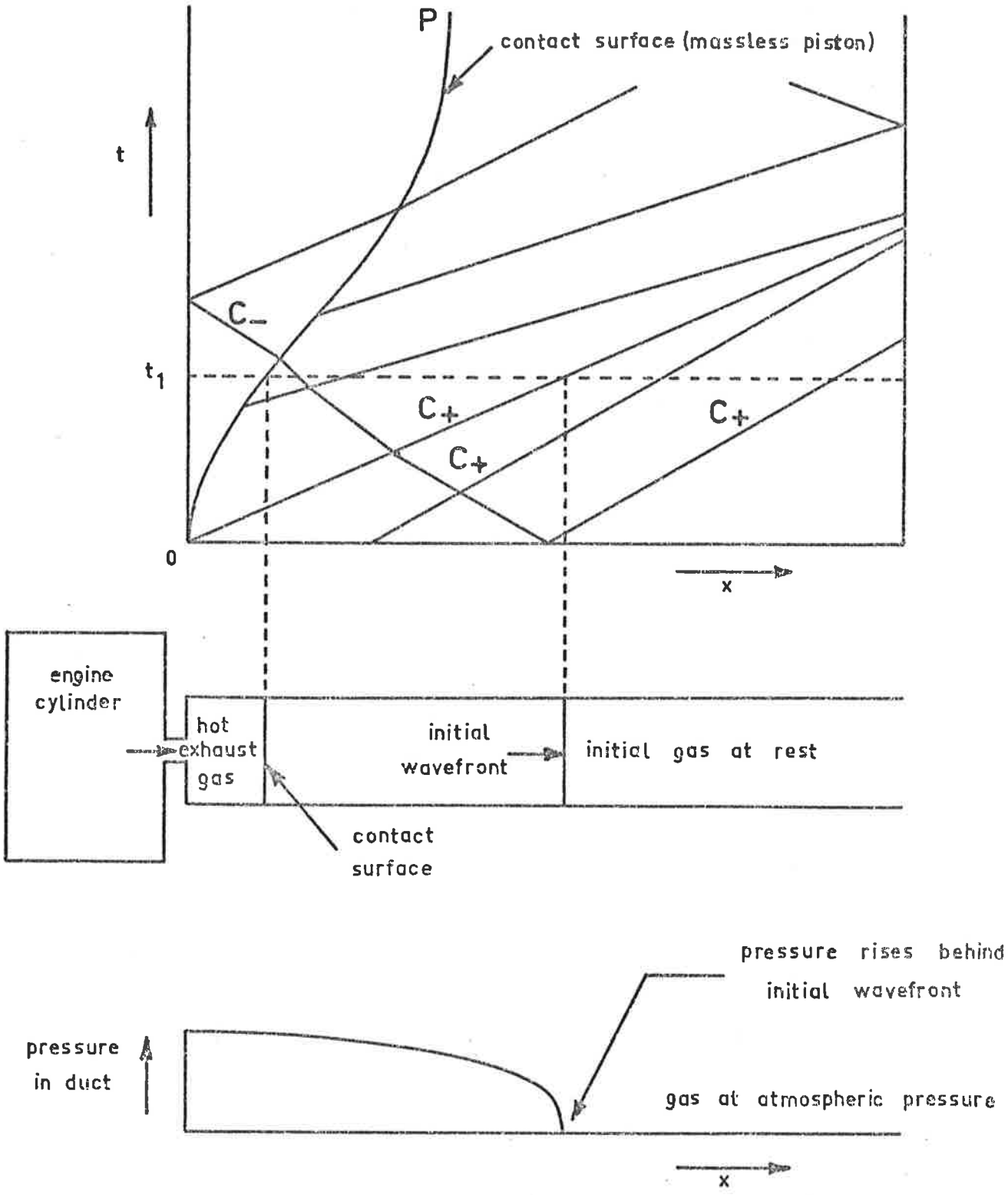

FIG. 5 x-t DIAGRAM FOR ENGINE WITH STRAIGHT PIPE EXHAUST

massless piston, the first coming from the exhaust port just as it opens at time $t = 0$.

The contact surface between the massless piston and the original gas in the pipe is the leading P or entropy characteristic which travels at the local particle velocity and marks a discontinuity in entropy levels in the pipe. This entropy discontinuity exists as the cylinder gas is of very high temperature. In the resultant exhaust gas flow, this P characteristic is first accelerated and then decelerated as the flow rate rises and then declines. For an engine exhaust the region behind the contact surface is of gradually decreasing entropy, as the shock strength at the port is less when the cylinder pressure decreases. There are, in fact, very large entropy differences between the initial outflow gas and the final outflow gas, particularly when the cooler crankcase gases are admitted into the cylinder as a fresh charge. In fact it has been shown by calculations, that any entropy increases caused by the passage of the strongest conceivable shock are small in comparison with the entropy differences caused by this varying cylinder outflow.

Figure (5) shows how information about the flow may be obtained from the x - t diagram. Information may be desired at either fixed positions in the duct, over the whole engine cycle, or at all positions in the duct at certain times. For example, figure (5) shows how the positions of the leading C_+ and P characteristics may be determined at time t_1. The third diagram in the figure shows that this C_+ characteristic, sent downstream when the exhaust port opens, represents the initial wavefront of the exhaust pressure wave. If enough C_+ characteristics are included the shape of the pressure pulse, as shown, may be obtained. (See section 2.8 for a calculated example of this).

Also of particular interest, is the determination of the velocity values at the tailpipe outlet as a function of time. Section

2.9 describes how these values may be used to calculate the radiated sound pressure. The tailpipe outlet velocity may be determined every time a C_+ characteristic reaches the open pipe end. The first diagram in figure (5) shows five such instances for which an outlet velocity may be determined. Clearly, by plotting the actual x - t diagram very rapid changes in outlet velocity may be followed, as shown by the way some C_+ characteristics arrive at the outlet in quick succession. This is discussed further in section 2.11.

The method of solution used to draw the x - t diagram is to represent a known exhaust port mass flow rate as a one-dimensional flow just downstream of the port. Just after the exhaust port opens at time t = 0, the flow will usually be choked and the mass flux may easily be calculated from the cylinder conditions and the exhaust port opening area. Then, using known values of density and cross-sectional area for the exhaust pipe, the whole flow in the pipe near the port may be determined. The C_+ characteristic starting at x = 0, t = 0, in the x - t diagram, is then known, as is its velocity. All features of the leading P characteristic are then also known at this time. The flow conditions determined at the exhaust port are assumed to remain constant over a small finite time interval. Over this time interval all the characteristics in the x - t diagram are advanced to new positions, and then, following updating of the cylinder conditions and exhaust port area, the flow for the next time interval is calculated. Simultaneously, the next C_+ characteristic is sent downstream. In figure (5) to emphasize the concept of the massless piston, these subsequent C_+ characteristics are shown as emanating from the initial contact surface. Obviously, when the flow through the port becomes subsonic, more detailed matching is required, and this is discussed in section 2.7.1.

If the exhaust gas flow rate rises rapidly enough, the initial wavefront, as shown in the third diagram in figure (5) becomes a shock.

In terms of the x - t diagram, this may be assumed to occur when C_+ characteristics, which have increasing velocities, catch up with each other. In fact, if shock wave formation is not assumed, the C_+ characteristics pass each other and multi-valued regions exist on the x - t diagram. Shock wave formation is discussed further in section 2.5. When C_+ characteristics crowd together but do not have enough duct length to catch up to each other, as indicated in the first diagram in figure (5), "wave steepening" occurs. Wave steepening is shown to be very significant in exhaust systems, in chapters 3 and 4.

The characteristic diagram is more complicated than shown in figure (5) as there are C_- characteristics, in the flow, travelling upstream at the local sonic velocity. One such C_- characteristic is shown in figure (5) to demonstrate this point. The complication is shown by the way the C_- characteristic is slowed down as it passes through the gas which has been accelerated downstream by the initial wavefront. The C_- characteristic then speeds up again as it passes through the hot exhaust gas. When it reaches the open exhaust port the new mass flux at the port and the simultaneous reflection of a C_+ characteristic and addition of a P characteristic must be determined (reflected C_+ characteristic shown in figure (5)). Actually, the method used in the computation technique to add C_+ characteristics at the port is to wait until a C_- characteristic reaches the port and then calculate the correct final flow and add the C_+ characteristic reflection on the basis of the current conditions. This is described in section 2.7.1.

As well as the complications listed above, the computation of the x - t diagram involves the correct description of a number of events which concern the effects of either boundary conditions or events within the flow itself. In total, these are as follows:-

1. C_+ crossing C_-
2. C_+ or C_- passing P
3. C_+ catching C_+ or C_- catching C_-
4. C_- (or C_+) reaching open exhaust port
5. C_- (or C_+) reaching closed exhaust port
6. P reaching open exhaust port
7. C_+ (or C_-) reaching open tailpipe
8. P reaching open tailpipe.

The calculations concerning each of these events are considered in detail in following sections in this chapter. Before these events are considered, it is first necessary to describe the basic computation technique by which the plotting of the x - t diagram and the calculation of the required output information is obtained.

2.3 COMPUTATION TECHNIQUE

Essentially, the computation method used numerically plots an x - t diagram using the basic principles outlined in the previous section. The means of doing this has been arranged to suit the kind of information that has been required. Specifically, the pressure cycle at certain points in the exhaust pipe, and the velocity cycle at the tailpipe outlet were required. Apart from this consideration, the computation method needed to be adaptable to study exhaust systems other than simple straight pipes. Section 2.10 shows how this has been done and section 5.1 shows how the computation may be adapted to study further different systems.

The computation method described below refers to a single cylinder, piston ported, crankcase scavenged 2-stroke engine with a straight pipe exhaust. Although the full wave action in the exhaust pipe is considered, certain simplifying assumptions have been made

concerning the cylinder and crankcase. Both the cylinder and crankcase volumes have been assumed to be concentrated at a point, with the length of the connecting transfer ports being assumed to be zero. As a consequence, both the respective cylinder and crankcase contents are assumed to be instantly and completely mixed, with any flow between the two volumes entirely dependent on the overall cylinder and crankcase conditions and the area of the transfer ports open at that particular time.

The calculation for the x - t diagram starts with an even distribution of C_+ and C_- characteristics in the duct at a time $t = 0$. Typically a total of 60 C_+ and C_- characteristics is often used. The initial particle velocity throughout the pipe is zero, the pressure being atmospheric and the entropy value throughout the duct is set equal to that in the cylinder when the exhaust port opens. This is done as this entropy value turns out to be a rough average of the resultant entropy levels of the exhaust gas in the duct. The initial cylinder conditions are based on actual measured pressure values at exhaust port opening, and estimated temperature values. The initial crankcase conditions are based on the assumption of atmospheric pressure and temperature in the crankcase at the time of the inlet port closing. The compression in the crankcase volume from the time of inlet port closing to transfer port opening has, of course, been assumed isentropic.

At regular small intervals of time Δt, typically 10^{-6} secs, the characteristics are moved to new positions along the duct. The time interval is so small that for most such time intervals all characteristics move to new positions without contacting either boundaries in the duct or other characteristics. Such events are therefore rare and may be considered in isolation from each other, with the resultant accuracy of plotting the x - t diagram being high. For each of the C_+ and C_- characteristics, the values of the speed of sound, particle

velocity, velocity of the characteristic, type of characteristic (whether C_+, C_- or P), entropy of gas, position, and the value of the Riemann invariant, are all kept in arrays which are updated after each Δt advancement. The same arrays are used to describe the P characteristics, however the values in the entropy and speed of sound arrays refer to the gas to the left hand side of the entropy discontinuity. The value of entropy to the right hand side of the discontinuity is held in the array which also contains the Riemann invariants of the C_+ and C_- characteristics. As events in the x - t diagram are rare, mostly the characteristics are simply moved to new positions with only the position arrays being updated. When any of the eight events listed in the previous section occur, the correct final flow situation is put into the x - t diagram by updating the appropriate values in the arrays. The presence of the P characteristics, effectively divides the duct into isentropic constant area sections for which practically the only event is the crossing of C_+ and C_- characteristics. As shown in section 2.7.1 a subroutine is used to limit the number of P characteristics, so that for constant cross section ducts the crossing of C_+ and C_- characteristics is by far the most common event. This considerably simplifies the calculations with very little loss of accuracy.

The two boundaries considered are the exhaust port end and the open tailpipe end of the straight pipe. Whenever a C_- characteristic reaches the open exhaust port, the cylinder and crankcase conditions are updated, and together with a new value of exhaust port area, a C_+ characteristic reflection is calculated. For the flow through the exhaust port, quasi-steady flow is assumed and the usual steady flow relations are used to calculate the local flow occurring at that particular time. If the flow is from the cylinder to the pipe, a P characteristic is also added. Whenever a C_+ characteristic reaches the tailpipe outlet a C_- characteristic reflection is added and a new value

of outlet velocity is computed with the velocity and time being stored in an array. Obviously, very fine resolution of this time is possible. Detailed consideration of each of these boundary conditions is given in section 2.7.

When the pressure as a function of time at any point is calculated in the program, it is obtained from the x - t diagram at regular large intervals, typically 100 Δt or 10^{-4} secs. It is, in fact, obtained by interpolation between the values behind the nearest characteristics. This resolution of the pressure is, of course, not as fine as that of the velocity, but greater resolution has not been necessary.

If the calculation is to proceed beyond one revolution, as it almost always does, the cylinder and crankcase conditions are simply reset to those used at the start of the revolution.

The calculations for all of the events occurring in the x - t diagram, listed in the previous section, must now be considered. The simple case of C_+ and C_- characteristics crossing will not be described. The calculation used for this case is as, for example, in Rudinger (10). It may be stated now that the calculations, to be described in further sections, have all been checked numerically with known solutions derived for simple finite waves. That is, in test calculations, pressure waves of a constant finite magnitude were reflected from an open pipe end, a closed pipe end and an open exhaust port, and were sent down a duct which included an entropy discontinuity. This was achieved by running the program to simulate a very large cylinder exhausting through a very fast opening port into a straight pipe. The computations always gave precisely the same answers as those calculated directly from the known solutions. It may also be mentioned that apart from the simplifications already described in this section, two other approximations have been made. The effects

of heat loss through the duct walls and also viscous losses have both been neglected. Comment on these omissions is made in sections 3.2.4 and 3.3.4. In order to somewhat simplify the calculations, only subsonic flows in the duct have been considered. This is clearly quite reasonable.

Before the events in the x - t diagram are considered, however, the calculations for the cylinder and crankcase conditions will be given. These calculations are not part of the x - t diagram computation itself, but must be understood for occasions when C_- characteristics reach the open exhaust port.

2.4 CYLINDER AND CRANKCASE CONDITIONS

A number of features of the calculations for the cylinder and crankcase conditions have already been mentioned in the previous section. These include defining the initial conditions at the start of the exhaust cycle, and the assumptions relating to the cylinder and crankcase volumes and the connecting transfer ports. It will further be assumed that all expansion and compression of gas in either the cylinder or crankcase volumes is adiabatic, if the gas flow is out of the volume. That is, no heat transfer to the walls of the volumes or the transfer and exhaust ports will be assumed to occur.

In the process of computing the x - t diagram, the cylinder and crankcase conditions are calculated every time a C_- characteristic reaches the open exhaust port. These calculations are made by assuming that a steady flow has existed since the previous C_- characteristic reached the port. Immediately after the new cylinder and crankcase conditions are determined, the calculations for the reflection of the current C_- characteristic are performed. These are described later in section 2.7.1. Clearly, the method described above is accurate for a piston moving in a series of jumps, in time with the C_- characteristics reaching the port. However, the expected error in describing a real

engine, with continuous piston motion, is very small.

In the calculations to update the cylinder and crankcase conditions, first the mass exchange between the cylinder and exhaust pipe, over the whole time period involved, is considered separately. New cylinder conditions are obtained. Then, using these cylinder conditions together with the unchanged crankcase conditions, the mass exchange between the two volumes is determined and new conditions in each are obtained. Again this is an approximation as the two flows are not considered simultaneously, however the error is clearly very small. In all cases, the values of cylinder and crankcase volumes, transfer and exhaust port areas relate to when the previous C_- characteristic reached the exhaust port.

The mass transfer calculations are noteworthy as they are performed in terms of a variable $\lambda(t)$ which represents the reciprocal of a characteristic time to exhaust the cylinder (or crankcase). In this way the values of pressure, temperature, etc. of the mass remaining in the cylinder (or crankcase) are obtained as a function of the rate of port opening. The derivation of the variable $\lambda(t)$ and the subsequent relations for the mass flow out of the cylinder, as obtained by Dr. G.L. Brown, are detailed in Appendix 2.

From Appendix 2, $\lambda(t)$ is defined as:-

$$\lambda(t) = \frac{C(t)\, a_c(t)\, A(t)}{V_c(t)} \qquad (2.9)$$

for flow out of the cylinder through the exhaust port. Following Appendix 2 the properties of the gas in the cylinder may now be expressed in terms of $\lambda(t)$ and various initial conditions. For example the pressure may be expressed as:-

$$p_c(t) = p_c(o)\left[\frac{V_c(o)}{V_c(t)}\right]^{\gamma} e^{-\gamma\int_o^t \lambda(t)dt} e^{\frac{-(\gamma-1)(s_c(o)-s_c(t))}{R}} \qquad (2.10)$$

where $p_c(t)$ = pressure in cylinder as a function of time

$s_c(t)$ = entropy in cylinder (dimensional value).

Therefore, to obtain the cylinder conditions, the integral of $\lambda(t)$ is progressively obtained numerically. The only other value which needs to be calculated to get the cylinder conditions is the flow parameter, C(t). This is considered in Appendix 2.

As well as the $\lambda(t)$ integral for the cylinder, there is a separate similar integrating calculation performed for the crankcase in terms of a variable, $\lambda_{cr}(t)$.

The flow between the cylinder and the crankcase results in an entropy change in one of the volumes. It has been assumed that the flow in the higher pressure volume is isentropic up to the transfer ports, with a loss in total pressure occurring in the lower pressure volume. The expression used to determine the entropy in the lower pressure volume, as a result of such a flow, is derived in Appendix 2. It is found, for example, that the entropy change in the cylinder, as a result of a flow from the crankcase to the cylinder, is given in terms of $\lambda(t)$ and the pressures and temperatures of the cylinder and crankcase gases.

The subroutine MASSEX, which performs these calculations in the computer program is listed in Appendix 6. The calculation of the exhaust and transfer port areas and the cylinder and crankcase volumes, which are required to determine the cylinder and crankcase conditions, is given in Appendix 2.

The following sections 2.5 to 2.7 consider the calculations for the more important of the events in the x - t diagram mentioned in

section 2.2. Section 2.8 studies a sample of a computed x - t diagram.

2.5 SHOCK WAVE FORMATION

The possibility of a travelling shock forming in an exhaust pipe is of interest in this study as a shock would greatly influence the radiated exhaust noise. Studies of non-linear wave motion (e.g. Whitham (11)) show that, with a large enough duct length, shocks will ultimately form in all compressive parts of a disturbance. Given the wave action in engine exhaust systems, shock formation is therefore possible. It is then necessary to see what relation shock wave formation has with the motion of characteristics on an x - t diagram. The ability of the calculation method to follow shock wave formation will then become clear.

Whitham (11) shows that if a series of right-facing pressure waves are travelling down a duct, wave breaking will first occur on the C_+ characteristic, for which the rate of change of speed of sound with distance along the duct has the largest negative value. It is also shown that the time t_B, from $t = 0$, for this to occur is given by -1 times the reciprocal of the derivative at $t = 0$ of the speed of sound with distance along the duct. On an x - t diagram, with an infinite number of characteristics, wave breaking or shock wave formation first occurs when a C_+ characteristic catches a slower C_+ characteristic (or a C_- catches a C_-). If, in fact, a shock is not included when these characteristics meet, there becomes an unacceptable fold in the x - t plane. Therefore, in the computation method, whenever two such characteristics meet, they are replaced by a single finite disturbance. The necessity of using a finite number of characteristics in computing the x - t diagram will obviously cause some error in the timing and position of the shock wave formation, however, it has been assumed that the number of characteristics usually used minimizes this error.

Shocks which are likely to occur in engine exhaust systems are of low pressure ratio. Therefore, as the entropy rise across a shock varies with pressure ratio to the third order, such entropy changes may be assumed negligible. The shocks may accurately be regarded as weak shocks. As such, to a first order approximation, in the x - t diagram, the propagation velocity of the resulting shock is then the average of the velocities of the two combining C_+ characteristics (11). The flow properties behind the shock are exactly the same as behind the faster of the original C_+ characteristics.

For the results presented in this thesis the calculation method used a further approximation to the assumption of weak shocks. When a C_+ characteristic catches a slower C_+ characteristic, the slower characteristic is removed and the original faster one is allowed to proceed normally. This is justified as the only error, for weak shocks, is in the speed of the characteristic:- it should be the average speed for both characteristics. The expected error is clearly very small. In fact, in almost all measurements and calculations referred to in chapter 3, there was no shock wave formation at all! A shock wave was shown to occur only in long (1.3 m) straight pipes coming from the exhaust port, for high speeds and loads for the motorcycle engine. Since completing the thesis, however, the final program is being very simply modified to precisely allow for weak shocks, that is, by using the correct average characteristic speed for the resultant finite disturbance.

2.6 INTERACTIONS BETWEEN C_+, C_- AND P CHARACTERISTICS

In an x - t diagram depicting the flow in a duct, P characteristics allow for entropy differences by themselves defining positions of discontinuous entropy changes. Equation (2.6) shows that also the P characteristics travel with the local particle velocity, and so mark

particle paths. As mentioned in section 2.3, the P characteristics effectively divide a constant cross-section duct into isentropic sections, for which virtually the only event in the x - t diagram is for C_+ and C_- characteristics crossing. Clearly, the determination of the x - t diagram within these sections is fairly simple. However, when a C_+ or C_- characteristic reaches the end of such an isentropic section, and passes a P characteristic, a more complex situation exists.

A section of an x - t diagram showing a C_+ characteristic passing a P characteristic is shown in the first diagram in figure (6). The correct final flow situation includes a reflected C_- characteristic, a transmitted C_+ characteristic with a different Riemann invariant, and the same P characteristic travelling with a different velocity. The exact final flow may be calculated using the knowledge that the pressures and velocities on either side of the P characteristic must be the same, and that the entropy in regions (1), (2) and (3) is s_1 in each case, while in both regions (5) and (4) the entropy must be s_5. The calculations used in the computer program to derive the final flow are described in detail in Appendix 3. The situation for a C_- characteristic passing a P characteristic is, of course, very similar and is not described.

In the computer program which plots the x - t diagram an important simplifying alteration is made. After the correct final values for the velocity, speed of sound, and so forth, are calculated using the method described in Appendix 3, these correct values are then inserted in the appropriate array spaces which describe all the existing characteristics. In relation to the first diagram in figure (6) the reflected C_- characteristic, is however, not created. This has the effect that when the next C_- characteristic meets the P characteristic, its transmitted component is exactly the same as if the original C_- reflection was in fact added. This may be explained by reference to

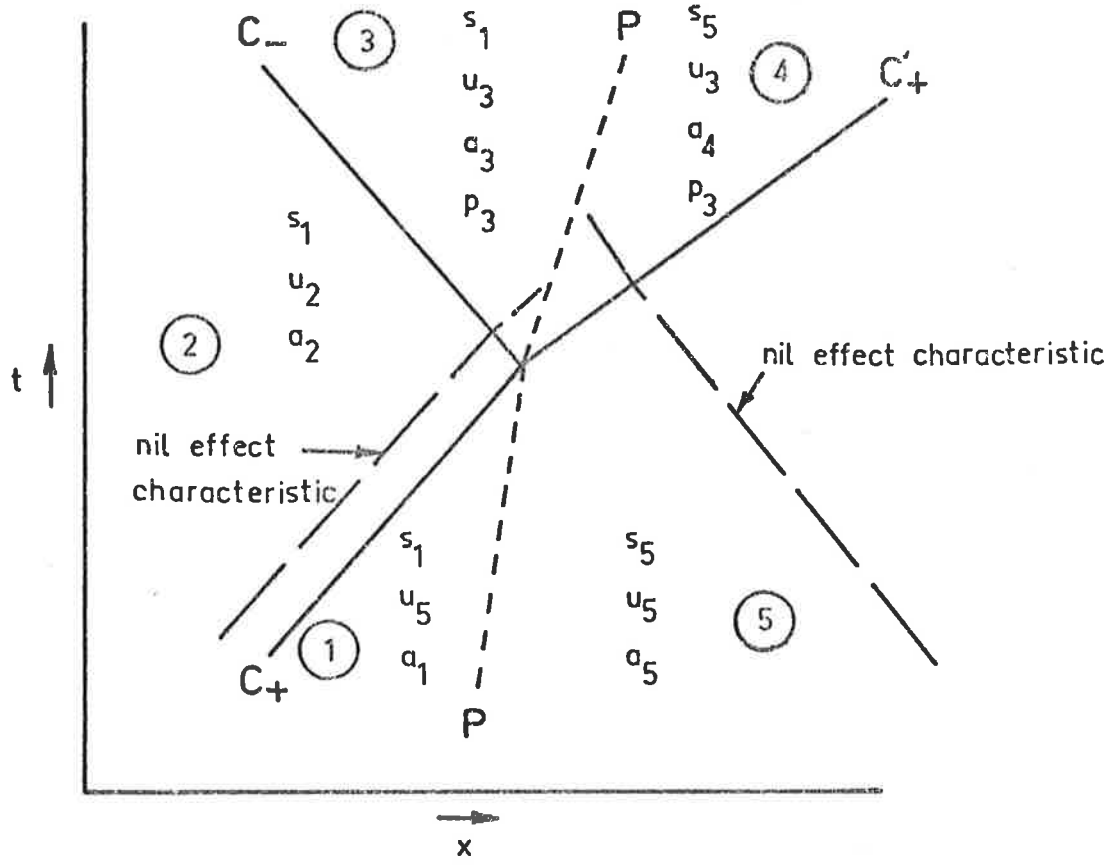

1/ INTERSECTION OF C_+, P CHARACTERISTICS

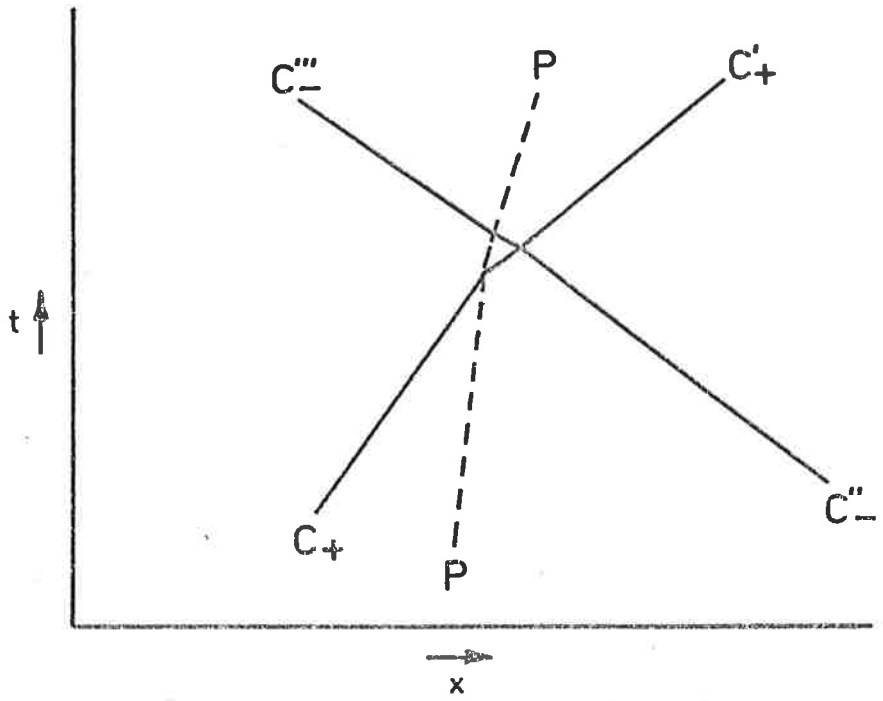

2/ INTERSECTION OF C_+, C_-, P CHARACTERISTICS AS COMPUTED

FIG.6 INTERACTIONS BETWEEN C_+, C_- AND P CHARACTERISTICS

the second x - t diagram in figure (6). When the C_+ characteristic passes the P characteristic there is a transmitted characteristic C_+' and a reflected C_- characteristic (not shown). The next left-facing characteristic to meet the P characteristic, C_-'', results in a transmitted component, C_-''', and a reflected component (not shown). Now, when the initial C_+ characteristic passes the P characteristic, the calculations described in Appendix 3, result in the final C_+' and P characteristics being correctly described, even though the reflection is not created in the x - t diagram. The flow existing after the next left-facing characteristic, C_-'', meets the P characteristic is solely determined by the correct description of these two characteristics. These characteristics are, of course, correctly known in the program. Therefore the resultant transmitted characteristic, C_-''', is correctly obtained by the calculation as in Appendix 3.

Clearly, if a method such as this were not used, there would very quickly be too many C_+ and C_- characteristics. The parts of the program which deal with the intersection between C_+ or C_- and P characteristics are in the main section of the program, in Appendix 6.

This deviation from the strictly correct method of computing an x - t diagram was found to be entirely acceptable with the number of characteristics usually used. Correct answers were always obtained when computing test cases for finite pressure waves meeting entropy discontinuities, as explained in section 2.3. With the computer program used to simulate various straight pipe engine exhaust systems, instability only occurred when very small numbers of C_+ and C_- characteristics were used (about 4, for some cases).

The method described above, for the simplification of the x - t diagram construction, is equally suitable with other types of discontinuities which result in a reflection and transmission from an incident characteristic. Reference is made to this in sections 2.10

and 5.1.

2.7 BOUNDARY CONDITIONS

The only boundary conditions considered in the analysis are:-

1. open exhaust port
2. closed exhaust port
3. open tailpipe.

In the x - t diagram, whenever a C_+ or C_- characteristic reaches one of these types of boundaries, a characteristic of opposite type is reflected. If the resultant flow is into the duct through the boundary, a P characteristic is also added.

2.7.1 Exhaust Port

The exhaust port is obviously the most important boundary as when it is open it matches the cylinder conditions to the gas flow in the exhaust pipe. This is ultimately responsible for the wave action and the resultant radiated exhaust noise. In the x - t diagram there are three events to be considered:-

1. C_- (or C_+) reaching open port
2. C_- (or C_+) reaching closed port
3. P reaching open port.

The last two events are simple. When a P characteristic reaches the open exhaust port, it is simply removed from the x - t diagram as it goes into the cylinder. In the computation, the only other change required is the updating of the entropy and speed of sound values for the gas in the exhaust pipe at the boundary between the cylinder and the exhaust pipe. Strictly, the entropy in the cylinder should be updated on the basis of this flow, but as this flow is very rare, the effect of not doing so is insignificant. Therefore, it has not been done, although to do so would be a relatively very simple change.

The calculations for the flow resulting as a C_- (or C_+) characteristic reaches the closed port are as given, for example, by Rudinger (10). For this case the flow velocity at the closed end is zero and the speed of sound, a, at this point is given from:-

$$\frac{a}{a_o} = \frac{\gamma-1}{2} Q_1 \qquad (2.11)$$

Where Q_1 is the Riemann invariant for the incident C_- characteristic. From equations (2.7) and (2.8), as the flow velocity is zero, the reflected C_+ characteristic has the same value for the Riemann invariant as the incident C_-. Clearly, if values of Q_1 increase for subsequent C_- characteristics reaching the boundary, so will the values of the Riemann invariants for the reflected characteristics. This explains the well known effect of a pressure wave being reflected as a wave of the same type from a closed end. This effect is observed in the measurements and calculations for straight exhaust pipes shown in section 3.2 and also in the sample x - t diagram calculation described in section 2.8.

The most important event, in an x - t diagram depicting exhaust gas flow, is a C_- (or C_+) characteristic reaching the open exhaust port. For this case the resultant flow is either inflow or outflow from the cylinder, which is either choked or unchoked at the port. In any case, a reflection will occur and, if there is outflow, a P characteristic is added. The detailed consideration of the flow through the exhaust port is presented in Appendix 4, but the following is a brief summary of the approach adopted.

The direction of the flow is dependent on the value of the Riemann invariant of the incident C_- characteristic, the cylinder conditions and the entropy of the gas in the duct near the exhaust port. As shown in Appendix 4, if the flow velocity at the exhaust port is

zero after a C_- characteristic reaches the port, the value of the Riemann invariant Q_1 for the characteristic is:-

$$Q_1 = \left(\frac{2}{\gamma-1}\right)\left|\frac{p_c(t)}{p_o}\right|^{\left(\frac{\gamma-1}{2\gamma}\right)} e^{\left(\frac{\gamma-1}{2\gamma R}\right)(s_d - s_o)} \qquad (2.12)$$

where s_d = entropy of gas in duct near port

$p_c(t)$ = cylinder pressure at time t

p_o, s_o = reference conditions.

If the value of the Riemann invariant of the C_- characteristic at the exhaust port is greater than that given by equation (2.12) inflow to the cylinder will occur (because this corresponds to a higher pressure in the duct than in the cylinder) and if less, outflow. In either case the final flow may be calculated using the equations for continuity of mass and energy, the equation for the Riemann invariant equation (2.8), and in addition, if there is outflow, an expression for the flow in terms of the cylinder conditions, i.e. equation (1) of Appendix 2. The determination of the flow in this way is complex and is considered in detail in Appendix 4. A listing of the subroutines FLWØUT and FLØWIN which perform these calculations is included in Appendix 6. Obviously the calculations are dependent on the cylinder conditions, the cylinder volume and the exhaust port area. These things have been considered in section 2.4 and in Appendix 2.

In terms of an x- t diagram for an engine exhaust system, as there is almost always outflow from the cylinder, virtually every time a C_- characteristic reaches the open exhaust port a P characteristic will be added. By the time the exhaust port closes, there would be an unmanageable number of these P characteristics present. It is clear that there can be a quite negligible reduction in computation accuracy if several of these characteristics are combined and replaced

by a single P characteristic. In the program, a subroutine is used which regularly reduces the number of these characteristics. When the subroutine is called, if there happen to be two adjacent P characteristics closer than a specified distance (typically 1cm) they are replaced by a single P characteristic. This is only done, of course, if there are no C_+ or C_- characteristics between them. The final P characteristic is placed mid-way between the initial two. The entropy values to the left and right of it are the same as those to the left of the left hand original and to the right of the right hand original, respectively. Of course, the velocity is the same for both initial and the final characteristics. The subroutine WVCLØS which performs this operation is listed in Appendix 6.

2.7.2 Tailpipe Outlet

At the tailpipe outlet boundary the duct flow is matched to the conditions in the atmosphere. The flow at the boundary is obviously very similar in principle to the flow through the exhaust port considered in section 2.7.1. There are two possible events in the x - t diagram which need to be considered:-

1. C_+ (or C_-) reaching open tailpipe
2. P reaching open tailpipe.

The second case is very simple and is similar to a P characteristic reaching an open exhaust port. As before the P characteristic is removed from the system and the entropy and speed of sound values for the flow at the boundary are updated.

The solution to the first event determines the velocity at the tailpipe outlet, and as mentioned in section 2.2 and shown in section 2.9 these velocity values determine the radiated sound. Again, the analysis is very similar to that for a C_- characteristic reaching an open exhaust port, but in this case the outlet area is fixed at the

full duct width and the atmospheric conditions remain the same.

When a C_+ characteristic reaches the open tailpipe, the existence of either inflow or outflow from the pipe may be established using a simplified form of equation (2.12), although the computer program achieves the same result indirectly. If the resultant flow is out of the duct, the speed of sound of the flow is dependent solely on the entropy level in the pipe, since the pressure is atmospheric. As the reference pressure level is (usually) atmospheric this speed of sound is given by:-

$$\frac{a}{a_o} = e^{(\frac{\gamma-1}{2\gamma R})(s_d - s_o)} \qquad (2.13)$$

(see, for example, Appendix 2 equation (20))

From equations (2.7) and (2.8), the Riemann invariant for the reflected C_- characteristic is then:-

$$Q_1 = (\frac{4}{\gamma-1})\, e^{(\frac{\gamma-1}{2\gamma R})(s_d - s_o)} - P_1 \qquad (2.14)$$

where P_1 = Riemann invariant of incident C_+ characteristic.

Clearly, from equation (2.14), for isentropic flow, changes in P_1 are associated with changes of opposite nature in Q_1. For this reason a positive pressure wave is reflected at the open tailpipe end as a negative wave. This is shown in the calculated examples in section 2.8 and in calculations and measurements discussed in chapter 3.

When the resultant flow is into the duct, the calculations are more complex and a P characteristic is added. For convenience, it is assumed that the flow enters the duct isentropically. The flow is determined using the energy equation, equation (2.7) using the known Riemann invariant of the incident characteristic, and by equating

pressures and velocities across the P characteristic. The detailed calculations are given in Appendix 5.

2.8 SAMPLE CALCULATIONS FOR STRAIGHT EXHAUST PIPES

It is now useful to consider sample calculations made using the method described in the preceding sections of this chapter. Firstly, a computed x- t diagram will be studied. As described below, the sample x- t diagram shows many of the features which have been mentioned in the foregoing sections.

Figure (7) shows a computed x- t diagram which simulates about two-thirds of one cycle in a straight pipe exhaust on a 2-stroke engine. The operating conditions assumed are an engine speed of 6000 r.p.m. and a pressure in the cylinder at E.P.O. of 7 atmospheres absolute. Of course, these values are a considerable exaggeration and were used purely to make the various events stand out. Also, for simplicity, only 12 initial C_+ and C_- characteristics were used. This small number of C_+ and C_- characteristics made it possible to leave all the P characteristics, created at the open exhaust port, in the x- t diagram without causing excessive complexity. The subroutine WVCLØS, as described in section 2.7.1, was set accordingly. For simplicity, figure (7) shows the paths of only two of the P characterisitcs.

The contact surface, between the gas initially at rest in the pipe and the hot exhaust gas, is shown by the first P characteristic coming from the open exhaust port. Section 2.2 mentioned that the motion of this P characteristic represents the path of the massless piston which may be considered as accelerating the flow. Figure (7) clearly shows how this characteristic speeds up and then slows down, as the mass flow rate from the cylinder rises and falls.

Now, section 2.3 mentioned that, usually, the initial value of entropy in the pipe is set equal to that in the cylinder at E.P.O.

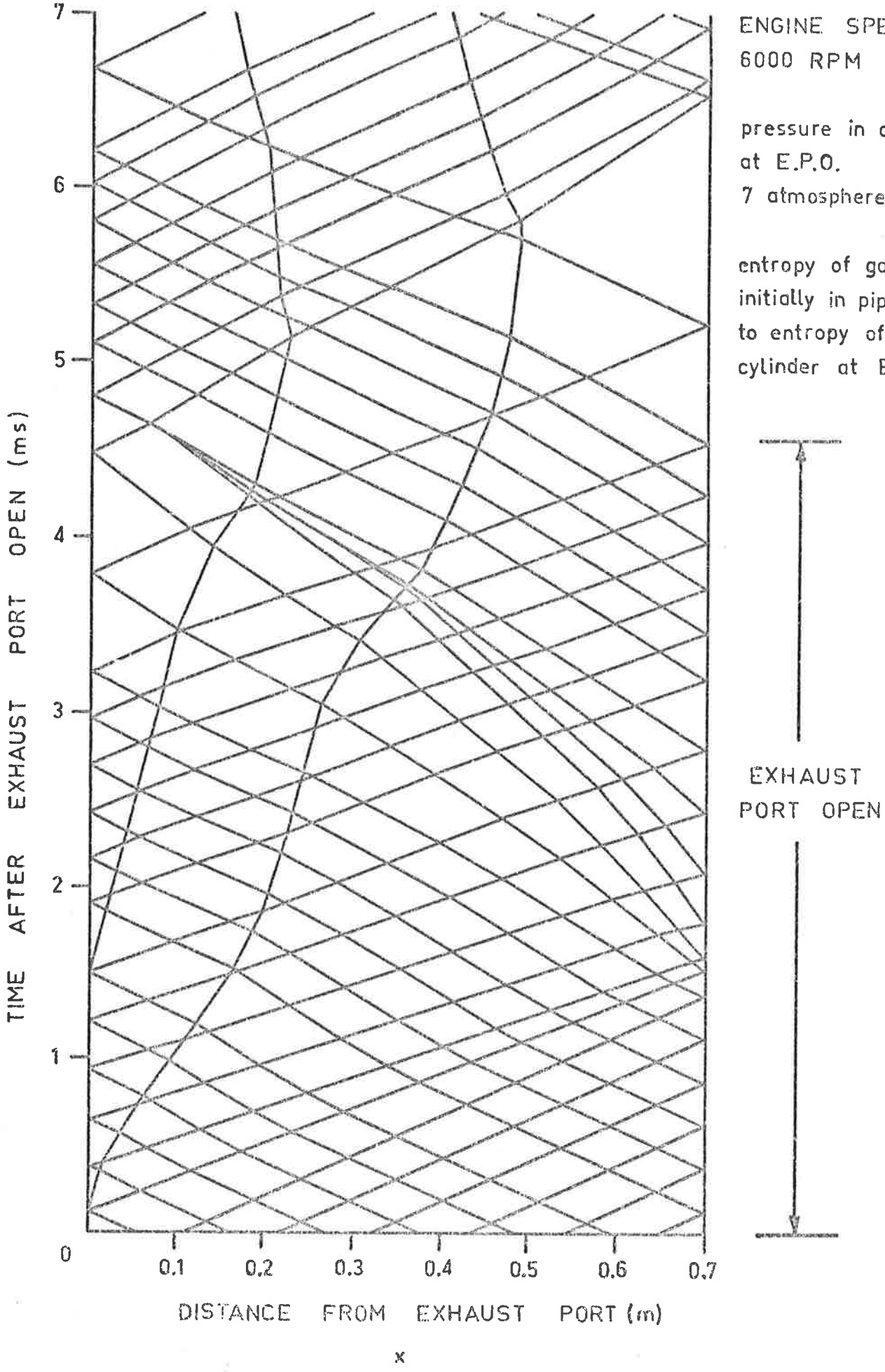

FIG. 7 COMPUTED x-t DIAGRAM FOR ENGINE WITH STRAIGHT PIPE EXHAUST

Furthermore, from section 2.2, as the shock strength at the port decreases and the crankcase gases cool the cylinder contents, the entropy of the outflowing gas becomes lower and lower. Ultimately then, the entropy of the gas exhausting into the pipe becomes lower than the value initially in the cylinder and pipe at E.P.O. The second P characteristic shown in figure (7) represents the path of the entropy discontinuity which separates regions with entropies just above and just below this initial level. It is interesting to note that nearly half of the exhaust gases have a lower value of entropy than the initial level in the cylinder, for this example.

The leading P characteristic obviously marks a large discontinuity in temperature levels. The C_+ and C_- characteristics would then be expected to slow down and speed up, respectively, on crossing it. This is quite clearly shown in figure (7). In fact, it is quite plain that the C_- characteristics speed up after crossing the first P characteristic and then gradually slow down as they pass into steadily cooler regions.

From the discussion of shock wave formation in section 2.5, it follows that a shock will form on the initial exhaust pulse if the duct is long enough. Certainly, figure (7) shows that the C_+ characteristics sent downstream when the exhaust port flow rate is rising do crowd together toward the end of the pipe. Although a shock wave does not form, the initial wavefront is clearly steepened. A shock does, however, form on the reflection of the rear of the initial wavefront from the tailpipe. In fact there are three occasions when a C_- characteristic catches a slower C_- characteristic. As mentioned in section 2.5, in each case the computer program simply removes the slower characteristic, in approximating the formation of a weak shock. (As mentioned in section 2.5, the program is being modified to give this weak shock its precise rather than approximate speed.)

The effects of pressure waves being reflected from the closed exhaust port and also from the tailpipe outlet were discussed in sections 2.7.1 and 2.7.2. When a pressure wave reaches the tailpipe outlet a reflected wave of opposite type is expected, whereas the closed exhaust port reflects a wave of the same type. Examples of both of these occurrences are seen in figure (7). The high pressure initial wavefront, distinguished by the crowding C_+ characteristics, is reflected from the tailpipe outlet as a low pressure wave. This is shown both by the way the reflected C_- characteristics fan out, and by the way these C_- characteristics accelerate the P characteristics downstream. A similar result is seen for the low pressure wave which is sent downstream when the exhaust port mass flow rate initially declines. On reflection from the tailpipe outlet, a high pressure wave results. The C_- characteristics representing this reflection crowd together and ultimately combine to form the shock which was discussed above. These reflected characteristics, as expected, slow down the P characteristics. A reflection of a wave from the closed exhaust port may also be seen. The low pressure initial reflection, coming from the tailpipe outlet, may be seen to be reflected from the now nearly closed exhaust port as another low pressure wave. This is clear, both from the way the C_+ characteristics continue to fan out, and by the way they now cause the gas to move back upstream.

It would appear from this discussion that the computation is correctly plotting the x - t diagram and it is interesting now to study an example of the more specific information that the calculation is intended to give. For example, the pressure wave development in a straight pipe exhaust system may be investigated. The necessary information may be taken progressively from the x - t diagram by determining the pressure behind every characteristic in the duct at successive instants of time. Figure (8) shows results obtained for a particular

case. This shows the distribution of pressure along the duct at successive times from E.P.O. to 5.5 milli seconds afterwards.

The calculation for figure (8) was performed for a different engine than that for figure (7), as it was considered preferable to test a variety of cases. The engine considered was again piston ported, although no provision was made for the crankcase (equivalent to zero transfer port area for all times). The operating conditions assumed were an engine speed of 3500 r.p.m. and a pressure in the cylinder at E.P.O. of 3.5 atmospheres absolute. The gas initially in the pipe was, of course, assumed to be at rest. This calculation required considerably more precision than the previous test case, so that the shape of the pressure waves would be well defined. Therefore, many more C_+ and C_- characteristics were included (about 60).

The calculated results are remarkably clear in showing certain phenomena. It may easily be seen how the initial wavefront steepens and very nearly forms a shock near the tailpipe outlet. This corresponds with the C_+ characteristics crowding together on the x - t diagram, as mentioned for the previous example. The following section reveals the considerable significance that this degree of wave steepening has on the resultant radiated sound.

As the initial pulse reaches the tailpipe outlet it is reflected, as expected from section 2.7.2, as a negative pressure wave. Then, as this reflection moves back upstream, it becomes markedly less steep. This clearly corresponds with the reflected C_- characteristics separating from each other, as seen in the x - t diagram, figure (7).

Obviously, when the reflected pressure wave reaches the exhaust port, the pressure near the port will be well below the atmospheric value. Such a low pressure wave may be used to improve the scavenging of the combustion products from the cylinder and improve the engine performance. This, then, is the basis of exhaust tuning phenomena.

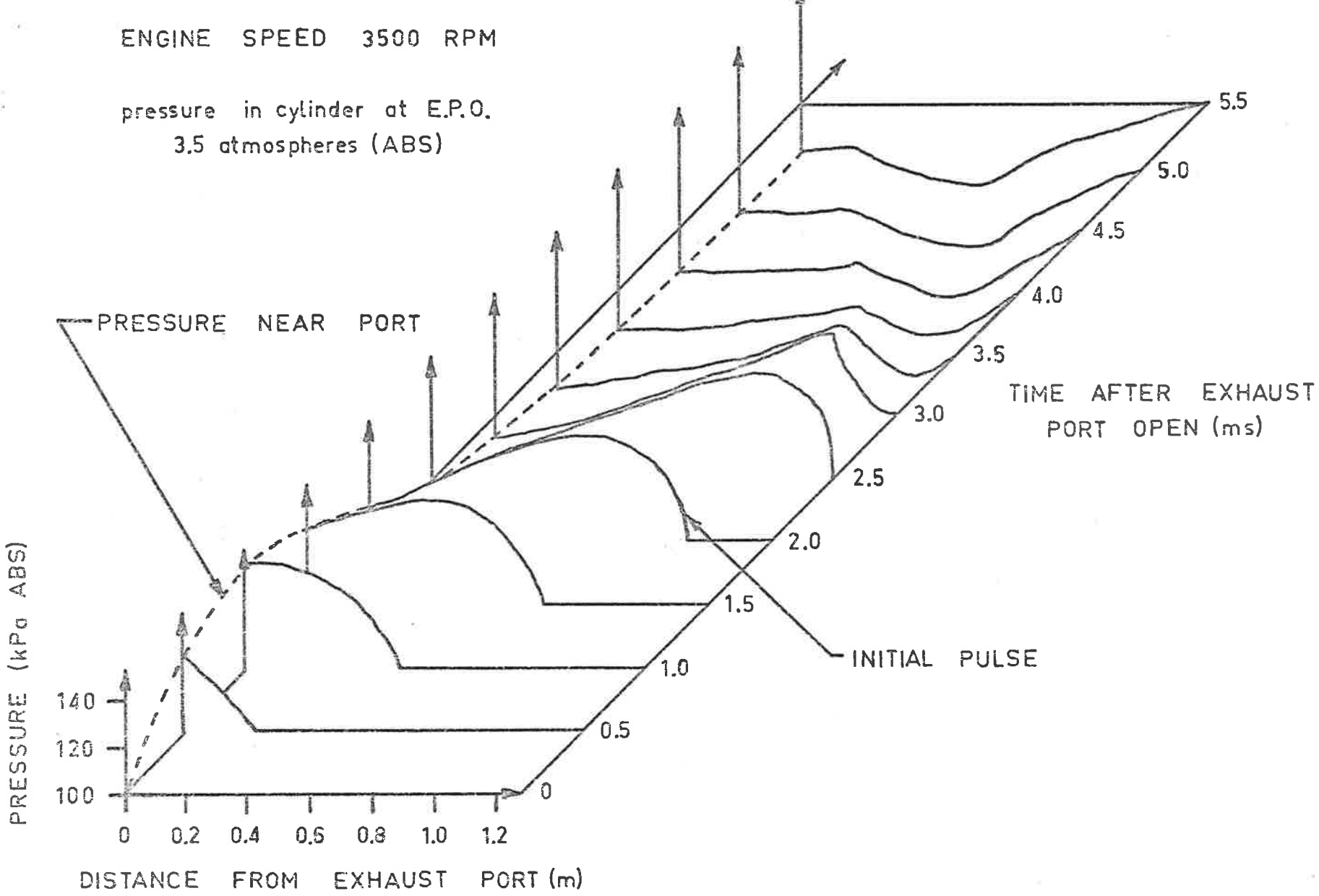

FIG. 8 COMPUTED PRESSURE WAVE DEVELOPMENT IN 1.3 m LONG STRAIGHT EXHAUST PIPE

From consideration of the above two examples it is clear that the calculation method appears to correctly account for the well known phenomena that would be expected to occur for unsteady compressible flow in a straight duct. Comparisons between measurements from actual engines and similar calculations are discussed in the next chapter.

2.9 RADIATED SOUND

The radiated sound from an engine exhaust system is directly dependent on the velocity values at the tailpipe outlet. As a quite adequate first approximation, which decouples the flow in the exhaust pipe from the radiated acoustic field, atmospheric pressure has been assumed as a boundary condition at the open end of the exhaust pipe in the calculation of the unsteady flow in the pipe itself. (A more exact boundary condition may be obtained by considering the near field of the radiated sound from a piston in a baffle but this is not warranted in the present study).

From the calculation of the unsteady flow in the pipe the velocity u(t) is obtained at the exhaust pipe outlet. If u(t) is slowly varying, by which is meant that $(\frac{du}{dt})_{max} << (\Delta u)_{max} \cdot \frac{c}{d}$ (i.e. $\omega.\frac{d}{c} << 1$), where d is the tailpipe diameter and c is the speed of sound, then the velocity potential in the far field, that is:-

$$\phi = -\int_{\substack{\text{exhaust pipe}\\ \text{outlet area}}} \frac{u(t-\frac{r}{c})}{2\pi r} \cdot d\eta\, d\zeta \qquad (2.15a)$$

(Where η,ζ are co-ordinates of a source element in the tailpipe outlet, and, if x,y,z are co-ordinates of the point in the far field, relative to axes based on the tailpipe outlet, then

$$r^2 = x^2 + (y-\eta)^2 + (z-\zeta)^2)$$

reduces to:-

$$\phi = - \frac{Au(t - \frac{r_o}{c})}{2\pi r_o}$$

(assumes the exhaust outlet is in an infinite baffle at $x = 0$)

where $r_o^2 = x^2 + y^2 + z^2$, the distance from source

A = area of tailpipe outlet.

The sound pressure $p = -\rho\phi_t$ is then:-

$$p(t) = \frac{\rho A}{2\pi r_o} \frac{du}{dt} (t - \frac{r_o}{c}) \qquad (2.15)$$

This is, of course, as for a simple monopole source, (see, for example, reference (13)).

For most of the acoustic frequencies of interest this is an adequate approximation, however, it may not be adequate where significant pulse steepening occurs at the leading edge of each exhaust pulse. For this case a step change in velocity may be considered for which equation (2.15a) is readily solved and the resulting step change in pressure at any distance R from the axis of the exhaust pipe is:-

$$\Delta p(t) \simeq \frac{\rho \Delta u(t - \frac{r_o}{c})\, c\, d}{2\pi R}$$

For such a step change in velocity, the width of this pressure pulse is $\frac{d\ R}{r_o c}$. For the comparisons with experiment presented in the following chapter the simple monopole solution (2.15) was used as it was found that the velocity at the exhaust pipe outlet, while often changing rapidly, giving rise to spikes in the acoustic pressure, did not change sufficiently rapidly for $(\frac{du}{dt})_{max} \cdot \frac{d\ R}{r_o c}$ to be greater than $\Delta u = u(t + \frac{d\ R}{r_o c}) - u(t)$, at the measuring station where $\frac{R}{r_o} \simeq \frac{1}{6}$. The

monopole source model was therefore used to compare with the measurements.

In the computer program, as mentioned in section 2.3, when a C_+ characteristic reaches the tailpipe outlet, the velocity value which is calculated, and the time of the event, are both stored in arrays. At the completion of each computed engine revolution, the radiated sound pressure cycle at a particular distance is calculated from these stored values using equation (2.15). A spectrum of the radiated noise is then obtained by a Fourier analysis of the cycle of pressure values. Finally the overall peak and r.m.s. sound pressure levels are calculated. These calculations are performed by the subroutines RMSCLC, VLDIFF, SPLCLC, RMSHRM, which are listed with the main program in Appendix 6.

It seems obvious from equation (2.15) that rapidly rising pressure waves greatly affect the radiated noise. This may be confirmed by a simple argument.

Consider that pressure waves of a certain amplitude but differing steepness reach the tailpipe outlet. Clearly, the steeper the wave the more rapidly the outlet velocity values will change. Hence, from equation (2.15), the steeper the wave, the greater is the radiated sound pressure. In terms of an x-t diagram, this means that if certain C_+ characteristics reach the tailpipe outlet bunched very close together, much more radiated noise will result than if they were far apart. This shows the importance of the pressure wave steepening which occurs in engine exhaust systems. Results of both calculations and measurements which exhibit the effects of such wave steepening are shown in chapter 3. Later, the effects of wave steepening on the suitability of the various theoretical approaches for muffler analysis are discussed in sections 4.4 and 4.5.

It is now clear that accurately following both wave steepening in the exhaust pipe and the fluctuation of velocity values at the tailpipe outlet is very important in determining the radiated exhaust noise. As mentioned in section 1.3, it was mainly these considerations which led to the form of calculation that was adopted.

2.10 SLOWLY VARYING AREA

The computation method, described in the preceding sections of this chapter, may only be used for studying simple straight pipe exhaust systems. Obviously, this is of limited use in closely studying exhaust noise in the more complex systems normally used on 2-stroke engines. As mentioned in section 2.3, the method was devised so that it could easily be extended to consider more complex systems. Below, it is shown how the method has been adapted to include ducts of slowly varying cross-section. Later, results shown in section 3.3 show how the improved method is successfully used to model tuned expansion chambers for high performance engines.

Ducts of slowly varying area may be accommodated in the one-dimensionalized analysis of section 2.1 fairly readily. As shown, for example, by Rudinger (10), the only one of the original conservation equations (2.1), (2.2) and (2.3) which needs to be modified is equation (2.1). The conservation of mass relation, for a varying area duct, becomes:-

$$\frac{\partial(\rho A)}{\partial t} + \frac{\partial(\rho u A)}{\partial x} = 0 \qquad (2.16)$$

where A = area of duct cross-section at a certain point.

Now, by combining equations (2.16), (2.2) and (2.3) in a way shown, for example, by Rudinger (10), the change in the Riemann invariant for C_+ and C_- characteristics passing along an isentropic region in a rigid duct with a gradually varying cross-section is:-

$$\Delta P_1 \text{ or } \Delta Q_1 = - \frac{au}{a_o} \frac{\partial \ln A}{\partial x} \Delta t \qquad (2.17)$$

That is, from equation (2.17), as a C_+ or C_- characteristic travels along the duct, the value of its Riemann invariant is continually modified according to the local flow conditions and rate of area change.

Several significant approximations are made, however, in the computer program which calculates the x - t diagram. Obviously it would be excessively complicated to update the values of the Riemann invariants for all the C_+ and C_- characteristics for each of the minute movements of the characteristics. Therefore, the value of a Riemann invariant is only updated just before the C_+ (or C_-) characteristic is about to meet either the exhaust port, tailpipe outlet, a P characteristic or a C_- (or C_+) characteristic. The normal calculations for the event are then performed using the new value of the Riemann invariant.

Further approximations involve the calculation of the change in the value of the Riemann invariant, using equation (2.17). It is assumed that the flow values, a and u, associated with a particular C_+ or C_- characteristic, have not changed since the previous event in the x - t diagram that the characteristic was involved in. Therefore, these values of a and u are used in equation (2.17). Also, these values determine the speed of the characteristic so, as the time expired since the last event is recorded, the position of the characteristic at the time of the last event it was involved in, may be found. Hence, the value of $\frac{\partial \ln A}{\partial x}$ is determined. As mentioned above, the value Δt, the expired time since the previous event the C_+ or C_- characteristic was involved in, is recorded in the program. This, of course, is the value used in equation (2.17). This value of time is stored in an array and is reset to zero, for the particular characteristic, after the calculations for the impending event are performed.

The method described above effectively treats the duct as having finite changes in area with the steps situated wherever a C_+ or C_- characteristic is involved in an event in the x - t diagram. Now, generally, whenever a C_+ or C_- characteristic reaches such a discontinuity in the duct, both transmitted and reflected characteristics will be present in the final flow. Clearly, the method described above does not add a reflection. This, then, involves the same modification as that mentioned in section 2.6, where a C_- reflection is not added when an incident C_+ characteristic passes a P characteristic. For the same reason as that given in section 2.6, namely that the next intersection between a C_- and the correct C_+ characteristic will give the correct C_- characteristic, this omission is quite acceptable.

Calculations of a conical segment of a spherical implosion for which there is an exact solution and calculations for a tuned expansion chamber, both discussed in section 3.3, show that the above-mentioned method is entirely adequate. In the calculations for the tuned expansion chamber, with 60 initial C_+ and C_- characteristics, occasionally the characteristics became sparsely separated in some of the 5 different segments of the exhaust system, however, the computation method retained stability with as few as 3 C_+ and C_- characteristics in a segment with a 20 times area change. Another good feature of the method is the computing time required. As extra calculations are performed only when major events occur in the x - t diagram, little additional time is required over that for a straight pipe. Tests showed that the time required to compute for the tuned expansion chamber was not greatly more than that for a similar length straight pipe.

The subroutines which perform the special calculations for a varying area duct, PQADIF and WAREU, are listed with the main program in Appendix 6.

2.11 SUMMARY

The calculation procedure which has been devised models the gas dynamics of the exhaust process and the resultant radiated noise for single cylinder 2-stroke engines with piston ports and crankcase scavenging. This has been achieved by matching the gas flow through the exhaust port to the resultant wave action in the exhaust system. The effects of the wave action at the tailpipe outlet have subsequently been used to determine the radiated noise.

To study the wave action, the method of characteristics for a one-dimensionalized flow in a duct was used. It was used in a way which was considered best suited to the determination of radiated sound. The calculation procedure uses a computer program to very accurately plot the paths of C_+, C_- and P characteristics on an x - t diagram which simulates the actual exhaust system. Typically 60 C_+ and C_- characteristics may be easily handled and the program has been run with 180 C_+ and C_- characteristics. (This produced a negligible improvement in accuracy over the 60 characteristics calculation). Exhaust systems which may be dealt with are simple straight pipes of any length, and ducts with any number of slowly varying area sections, also of any length. The inclusion of varying area sections involves little extra complication or loss of accuracy.

There has been a number of simplifications (basically numerical approximations) made which made it easier to plot the x - t diagram. These changes have been shown to be theoretically quite reasonable and from all the test cases run for which exact solutions are known, they appear to have overall a negligible effect on the accuracy of the predictions. (This, of course, is in contrast to the physical approximations, namely the omission of heat transfer and any viscous effects).

As mentioned in section 1.3, to study the noise resulting from the wave action, it was considered preferable to calculate

the actual wave diagram rather than adapting the method of Benson. Further comment may now be made on this.

The calculation method described in this chapter is usually operated with a fixed basic time interval of only 10^{-6} sec. This is clearly much smaller than the variable time interval used by Benson, which was usually never less than about 10^{-4} sec (implied from reference (3)). Obviously plotting the x- t diagram with a very small time interval allows for detailed resolution of the velocity at the tail-pipe. The arrival of C_+ characteristics, which are crowded together can be followed. There are many occasions for which the coarse time interval of 10^{-4} sec would be too long to correctly follow rapid changes in tailpipe velocity. For example, the initial pulse in the radiated sound pressure cycle from the motorcycle engine fitted with a tuned expansion chamber is barely 10^{-4} sec long (figure (19)).

More important than the time interval, however, is the ability of the calculation method to accurately follow wave steepening and shock wave formation. The considerable significance of wave steepening in influencing the radiated noise was discussed in section 2.9. Now, it is clear from the work in this chapter that the calculation method does, in fact, very accurately follow the wave steepening. The method of Benson however, involves using only a small number of fixed mesh points (typically 10) along the duct. It is obvious that such a limited number of fixed points will not resolve wave steepening to anything like the degree that following about 60 characteristics in an x - t diagram will.

To verify this assumption a comparison was made between a calculation obtained using the program described in this thesis, and a similar calculation performed by Dr. P.C. Baruah at the University of Manchester Institute of Science and Technology, using a standard program based on the analysis described by Benson. The calculations

were performed to simulate the first exhaust cycle for the same motorcycle engine as described in the following chapter, with the exhaust system consisting of a 1.3 m long straight pipe. The outputs selected for comparison were the instantaneous pressure values at a point in the pipe 1.12 m from the exhaust port. The inputs to the calculations were selected so that the formation of a weak shock, on the initial exhaust pulse, was to be expected. Figure (8(b)) shows the pressure values calculated by the two methods for the first 5 m secs after the exhaust port opens. It is very clear from the figure that the fixed mesh method of Benson has not adequately described the wave steepening and is also unlikely to predict with any accuracy the velocity derivative values at the tailpipe outlet, upon which the radiated sound pressure values depend. The large discrepancy between the two peak values is then not surprising since near the tailpipe outlet the pressure values from the initial positive pulse are combined with those from the soon arriving negative reflection.

The calculation method developed in this study was shown in section 2.8 to correctly exhibit the well known phenomena of compressible flow in a duct. The following chapter shows how well it models actual engine exhaust systems.

The listing of the main body of the computer program and the associated subroutines, which perform the calculations described above, is given in Appendix 6. The program, as listed, is arranged for simulating the motorcycle engine with a tuned expansion chamber exhaust.

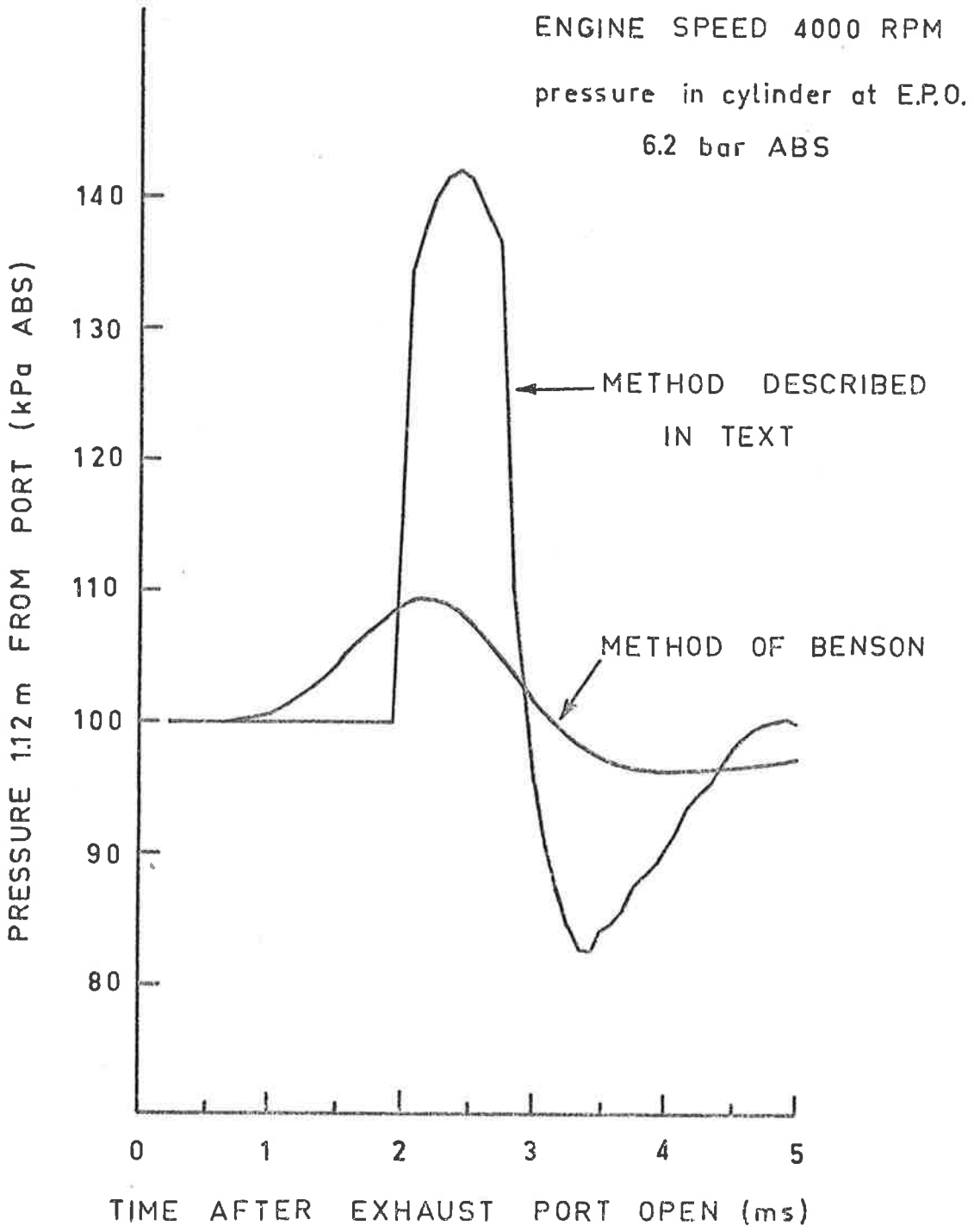

FIG. 8(b) COMPUTED PRESSURE WAVES IN 1.3 m STRAIGHT PIPE EXHAUST

CHAPTER 3

COMPARISON WITH EXPERIMENT AND KNOWN SOLUTIONS

3.1 EXPERIMENTAL CONSIDERATIONS AND EQUIPMENT

It was necessary to determine how well the calculation method described in chapter 2 modelled the events occurring in exhaust systems on actual operating engines. To do this, measurements were taken of various phenomena for a number of different exhaust systems. These measurements were then compared with calculations performed for the same systems. The results which are shown in this chapter indicate that the calculation method is very accurate indeed in describing the events relating to radiated exhaust noise.

To confirm the calculation technique, pressure measurements were taken at a number of positions inside several different exhaust systems. For each exhaust system the radiated sound for the same operating conditions (note exception mentioned below) was recorded at a certain point in the far field. Following section 2.9, the radiation was assumed to be hemispherical. Apart from confirming the calculation technique, as shown in this chapter, both measurements and calculations show aspects of the basic nature of exhaust noise for typical 2-stroke systems. This is particularly so in regard to the occurrence of wave steepening and the significance of the initial pulse.

Three exhaust systems were tested: a long straight pipe, a much shorter straight pipe, and a tuned expansion chamber, like those used to improve the performance of racing engines. The dimensions of these three systems, and the positions at which the pressure cycles inside the ducts were recorded, are shown in figure (9). All of the exhaust systems tested were mounted on the high performance, single

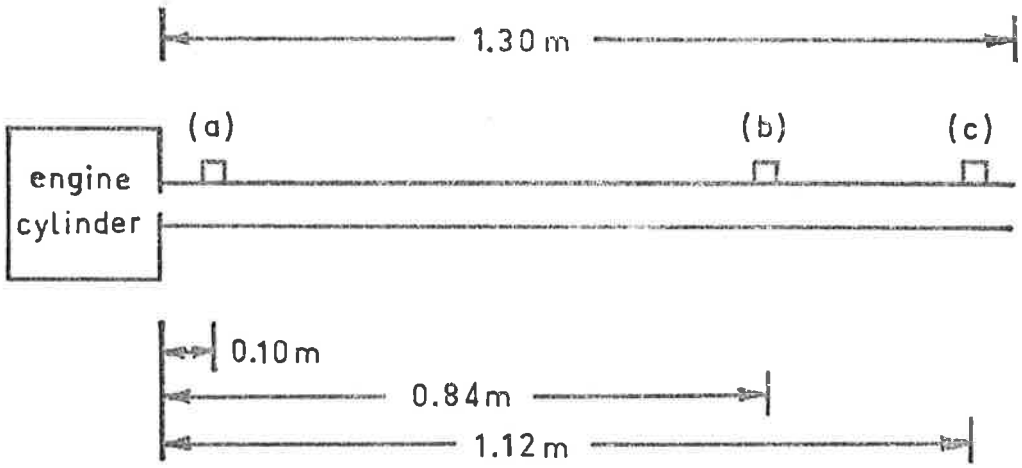

LONG PIPE

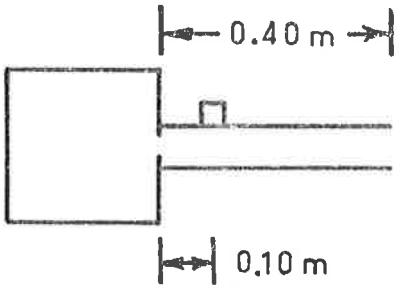

SHORT PIPE

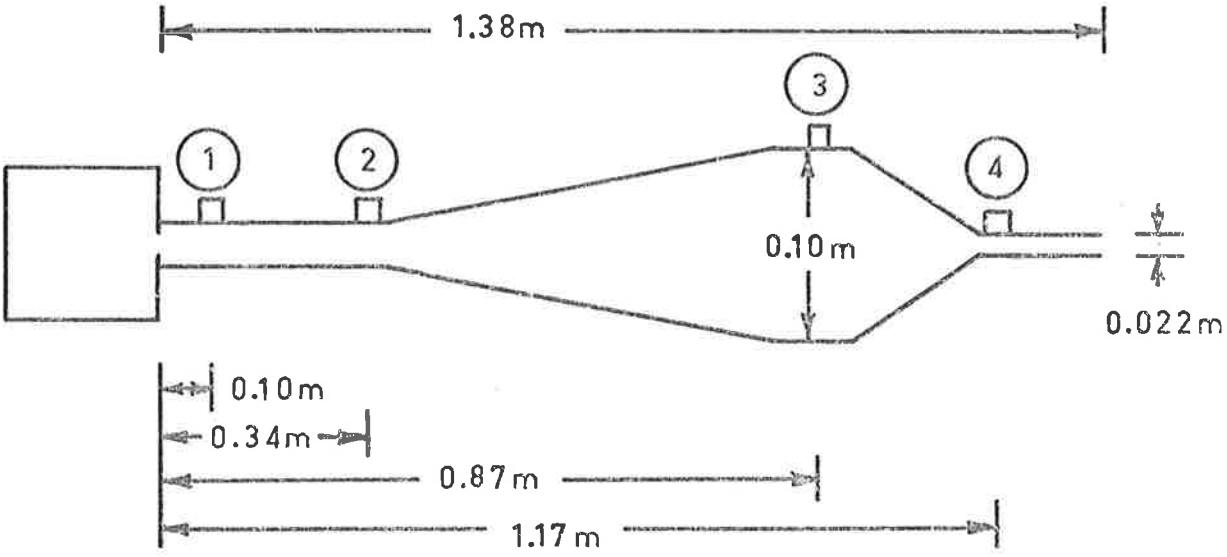

TUNED EXPANSION CHAMBER

long pipe, short pipe, first section of tuned expansion chamber all of diameter 0.04m

FIG. 9 EXPERIMENTAL EXHAUST SYSTEMS SHOWING MEASURING POSITIONS

cylinder, 125 cc 2-stroke Suzuki TS125 motorcycle engine described in Appendix 1.

The two straight pipes were used to test how well the basic computation method simulated the exhaust flow of varying entropy in a constant cross section duct. The long pipe was used to investigate the suspected nature of such long exhaust systems to steepen the initial exhaust pulse and possibly form a shock wave. This, of course, would reveal the ability of the calculation to correctly follow wave steepening and to correctly show the significance of such steepening in the radiated sound pressure cycle. In comparison, it was expected that the much shorter 0.4 m pipe would not allow wave steepening to anything like the same degree. A lower value of radiated noise was then expected to be both measured and calculated.

Use of the short 0.4 m pipe was also expected to confirm the ability of the computation to describe correctly all reflections of the initial exhaust pulse in different exhaust systems. Certainly, the shorter pipe would experience many more reflections of the initial pulse than would the 1.3 m pipe in a single engine cycle. For similarly small exhaust systems used on low performance engines (for example, lawnmowers, chain saws), this usually has the result that the higher order reflections, existing after one cycle, are of low magnitude. The longer exhaust systems used on high performance engines normally have much more significant residual reflections. It is, in fact, partly these residual reflections which cause the "tuning" phenomena. Thus, the ability of the calculation to correctly exhibit this and other aspects of exhaust tuning was thought to be important, not only because of its significance to the radiated noise. It seemed that a direct comparison with experiment with this in mind was important.

As mentioned in section 2.3, the effects of both heat loss through the pipe walls and viscous losses were not included in the

* The vibration sensitivity of the transducers was checked by placing them in blind holes close to their normal point of attachment and was found to be insignificant.

* The microphone was located 1m above the ground plane and the exhaust outlet was always ½m above the ground plane. The lowest frequency for destructive interference from ground reflection is then approximately 900Hz, although no account of such interference from ground reflection has been included in the analysis.

analysis. Certainly these effects would be greater in the longer 1.3 m pipe. Assuming these were the most significant omissions in the analysis, a comparison between the measured and calculated results was expected to show the significance of such omissions.

The experiments involving the tuned expansion chamber were performed to see if the calculation method correctly modelled the more complex situation of a slowly varying area duct. Also, as the tuned expansion chamber is nearly the same length as the 1.3 m pipe, it was possible to study any difference in the development of the initial exhaust pulse in the two systems.

As mentioned above, the experiments were all performed using a high performance, single cylinder, 125 cc motorcycle engine. A generator was used to provide constant known loads. Additional to the earlier mentioned exhaust pipe pressure and radiated sound measurements, the related engine cylinder pressure was recorded to supply the initial cylinder conditions for the calculation. Both the cylinder and exhaust pipe pressure measurements were obtained using quartz pressure transducers: Kistler type 7031 for the exhaust pipe and type 6005 for the engine cylinder. Each of the transducers was in a water-cooled housing. The resonant frequencies for the transducers in their housings were 10 kHz for type 7031 and 4 kHz for type 6005 (obtained from shock tube measurements). This response was adequate for the application of each one.* The measurements of radiated sound pressure were all taken in a free field, using a single microphone situated 5 m from the exhaust outlet.* Microphones used were B & K ½ inch type 4133 for the short pipe and tuned expansion chamber, and ¼ inch type 4136 for the 1.3 m pipe. The smaller microphone was used for the long pipe measurement as an especially fast rising pulse was expected. (The response time of the type 4136 microphone was less than 20μ sec).

The measurements involved, firstly, recording simultaneously

* The effects of flow turbulence and vena contracta, which reduce the effective port area, were to an approximate degree accounted for by assuming that the port areas were reduced by the "flow loss factor". That is, the effective area was assumed equal to 0.8 times the actual area.

pressure cycles in the cylinder and at one of the measuring points in the exhaust system, on a multiple beam oscilloscope. Thus, a particular exhaust pressure cycle was related to the pressure in the cylinder at E.P.O., for the same cycle. A sample measurement, for the short pipe, is shown in figure (10). The third pulse seen in the figure is a timing pulse which triggers the trace at precisely E.P.O. The measurement of the radiated noise in a free field environment necessitated separate recordings to be taken outdoors. As the operating conditions were the same as for the earlier measurements, it was simply assumed that the same cylinder and exhaust pipe pressures would exist. For the 1.3m pipe, the radiated sound pressure cycle was recorded directly on an oscilloscope, whereas for the other exhaust systems the radiated sound pressure was recorded on a tape recorder.

For consistency, all pressure measurements taken inside each of the three exhaust systems, and the radiated sound from both the short pipe and the tuned expansion chamber were obtained with the engine operating at 4000 r.p.m. under a fixed high load. This meant that the initial exhaust flow out of the cylinder was virtually the same for each of these cases. The radiated sound measurement for the 1.3m pipe was, however, taken with the engine running at 6000 r.p.m. with a low load. Of course, the correct calculation was made for each case.

The calculations were all performed using the correct measured values of initial cylinder pressure. As mentioned in section 2.3, an estimate of the temperature in the cylinder at E.P.O. was the only other initial condition required. In the subsequent computations the only departure from the method described in chapter 2 was to use a flow loss factor for the port areas of 0.8.* The following sections describe the results that were obtained. The significance of these

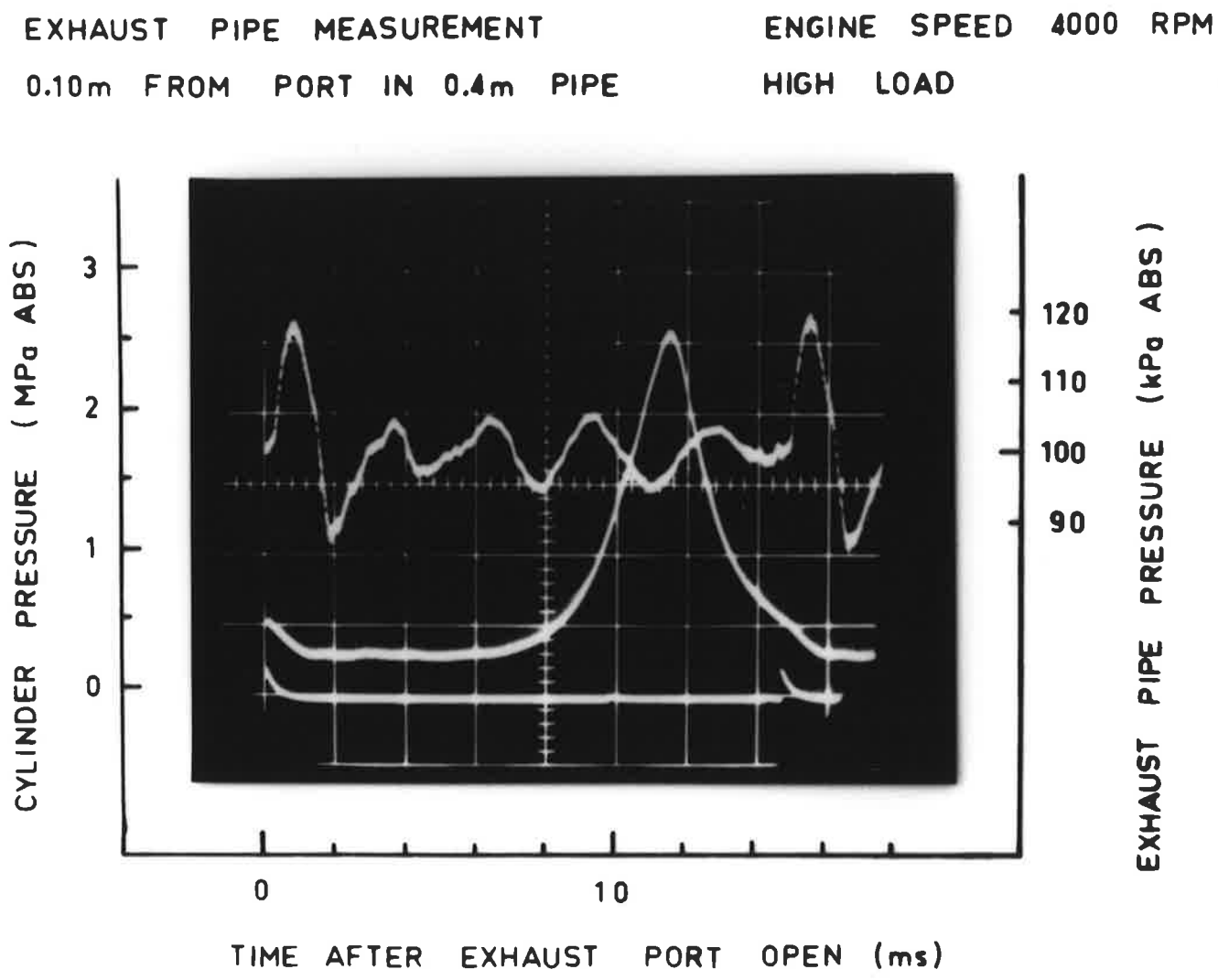

FIG. 10 SAMPLE CYLINDER AND EXHAUST PIPE PRESSURE MEASUREMENT

results in terms of the existing muffler theories is discussed in chapter 4.

3.2 STRAIGHT EXHAUST PIPE

3.2.1 Short Pipe

The results of measurements and calculations performed for the 0.4 m pipe are shown in figure (11). Traces (a) and (c) show the pressure cycles near the exhaust port and the radiated sound pressure cycles, respectively. These traces are, of course, for only one engine revolution. Trace (b) shows the computed cycle of velocity values at the tailpipe outlet from which the calculated radiated sound pressure cycle in (c) was derived. The calculations were obtained by running the computer program to simulate several (2) successive engine revolutions, after which a steady state situation was approached. At the start of the calculation the gas in the exhaust pipe was, of course, at rest.

Good agreement with measurement has been obtained for both the calculated cycle of pressure values near the port and the radiated sound pressure cycle. The calculated magnitudes of the initial and reflected pulses are shown in figure (11) to be very accurate, however, there is some error in the timing of the reflections. The cause of this lack of agreement in timing must be considered.

Possibly in view of the much closer detailed agreement found for the 1.3 m pipe and for the variable area pipe (discussed below), a main reason for the discrepancies is the fact that the initial region (i.e. in which the flow is far from one-dimensional), which is of the order of 2-3 diameters from the exhaust port, is a significant fraction (20%-30%) of the 0.4 m pipe length. Apart from this source of error, the other approximations made in the analysis, as mentioned in chapter 2, all add some small error. For example, the assumption that the new charge entering the cylinder is very rapidly mixed with the existing

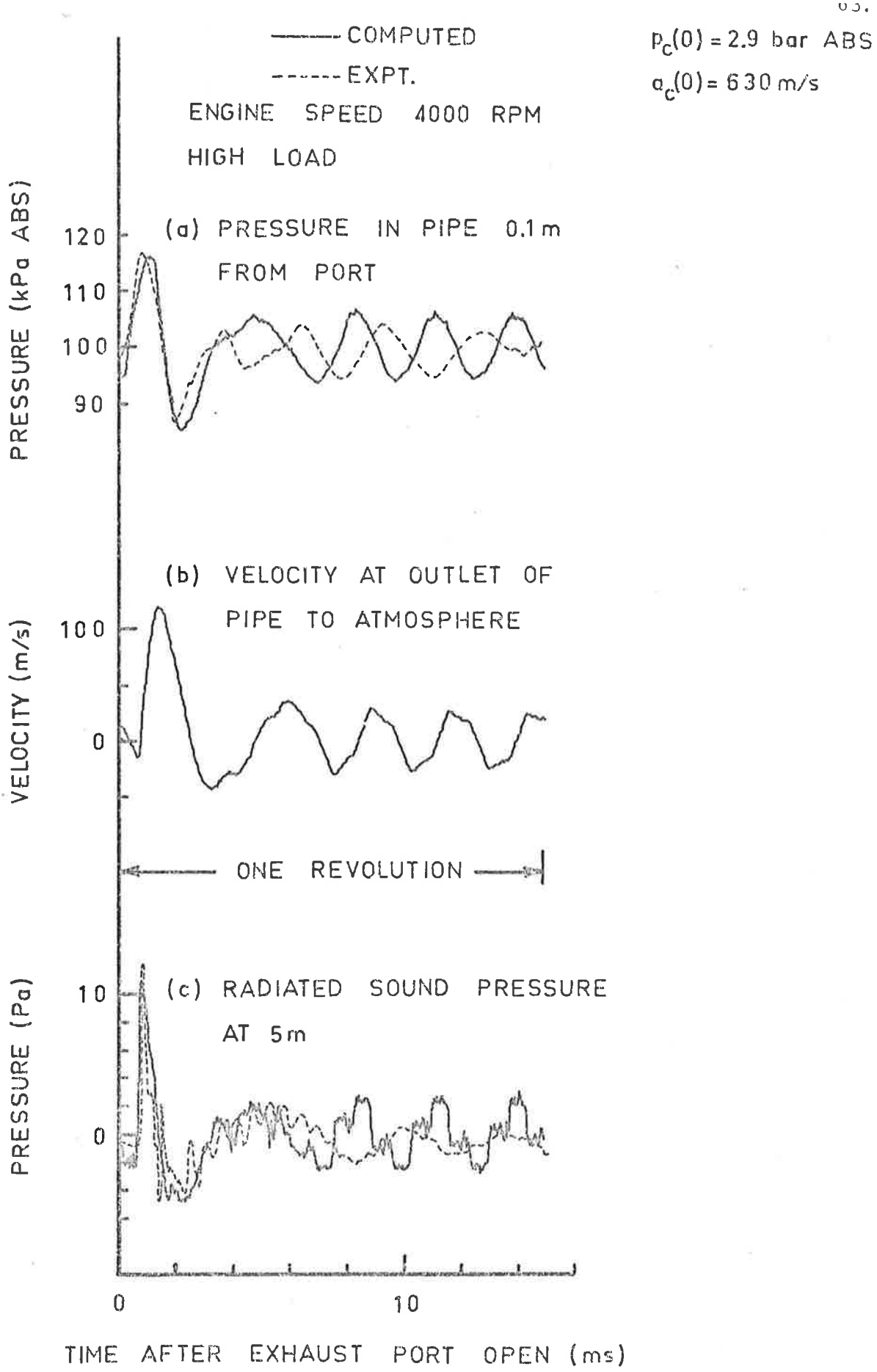

FIG.11 CALCULATIONS AND MEASUREMENTS FOR 0.4 m STRAIGHT PIPE EXHAUST

cylinder gas, is unlikely to be absolutely correct. The other factor which affects the agreement is the choice of gas temperature. In this context the inputs to the program must be discussed, as changes to these inputs will obviously affect the calculated result.

The computed results shown in figure (11) were obtained by setting the values of cylinder pressure and speed of sound at E.P.O. to 2.9 Bar absolute and 630 m/sec , respectively. The value of pressure was, of course, obtained from the cylinder pressure measurements. The value of the speed of sound was estimated on the basis of the expected temperature rise occurring in the cylinder as a result of the combustion. In obtaining the speed of sound value, the amount of fresh charge assumed to be admitted to the cylinder in each cycle was determined after taking into account the poor scavenging of the combustion products. Clearly, the speed of sound value is only a first estimate, and a slightly different value might equally well have been used. Figure (12) shows comparisons between the measurement used in figure (11)(a), for the pressure cycle near the exhaust port, and calculated traces obtained using values of speed of sound in the cylinder at E.P.O. of 670 m/sec and 590 m/sec (initial pressure unchanged). The difference between the agreement obtained in figure (11)(a) and that obtained in figure (12) shows the sensitivity of the calculation to such small changes in the speed of sound (temperature) of the exhaust. Somewhat better agreement in the location of the reflected waves for this and other calculations, may be achieved if the initial value of temperature is thus "adjusted". Of course, as shown in figure (12), the magnitude of the pressure waves is also changed by such temperature "adjustments".

Notable features shown in figure (11) will now be considered. The radiated pressure cycle is obviously dominated by the large magnitude peak, caused by the initial exhaust pulse. This is clear from both

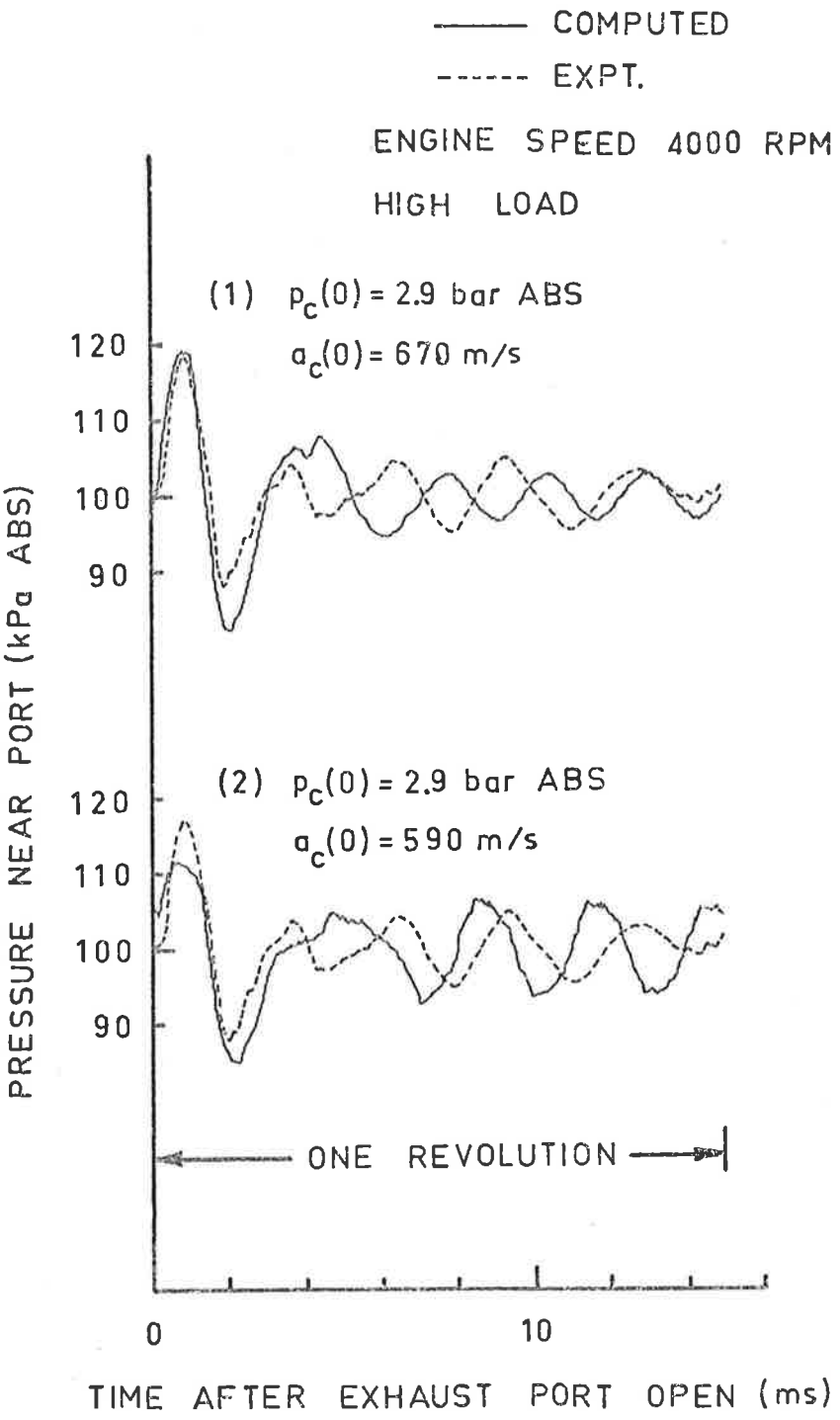

FIG.12 COMPUTED PRESSURE WAVES IN 0.4 m STRAIGHT PIPE

* The calculation was actually taken to a larger number of revolutions but there was no observed significant variation beyond the third revolution.

measured and calculated cycles. It is likely that the magnitude of the peak is influenced by the speed of opening of the exhaust port, rather than any possible wave steepening in the very short pipe. This is verified by the fact that the engine running at the same speed and load, with no pipe at all for the pulse to steepen in, radiated a pressure peak of nearly the same magnitude.

The calculated traces (b) and (c) show the interesting relation between the tailpipe outlet velocity and the resultant radiated noise. As explained in section 2.9, the cycle (c) is simply the derivative of the cycle (b).

A number of interesting features may be seen from both the measured and calculated pressure cycles near the port. It is clear that the initial pulse, a positive wave, is reflected from the open tailpipe outlet as a negative wave. This was expected, from the work in section 2.7.2. Also, the fairly low magnitude reflections remaining in the pipe at the commencement of the next cycle may be expected to not greatly influence the engine operation. It was, in fact, observed that the engine had no speed dependent tuning effects.

3.2.2 Long Pipe

Figure (13) shows both the measured and computed pressure cycles as obtained for the three positions indicated in figure (9) inside the 1.3m pipe. As for the short pipe, the calculated cycles were obtained after several (3) successive engine revolutions, and may be regarded as very near to the steady state solutions.*

Again, very good agreement is shown. The timing of both the initial and reflected pulses at all three positions, and the magnitudes of these pulses at the first two positions are indeed very accurately calculated. The discrepancy in the magnitudes at position (c), near the tailpipe outlet, is discussed in section 3.2.4.

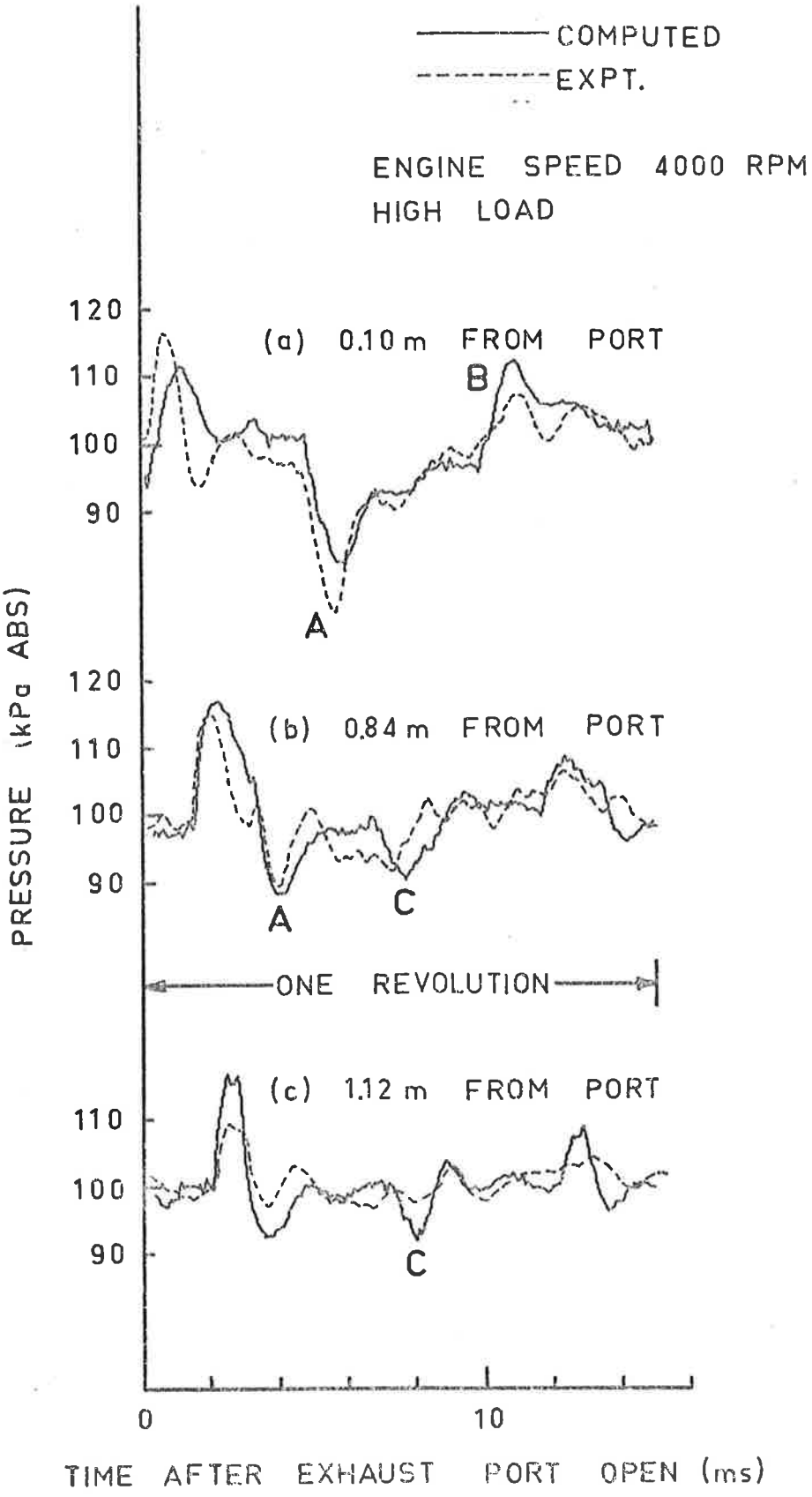

FIG. 13 PRESSURE WAVES IN 1.3 m STRAIGHT PIPE EXHAUST

In a similar manner as for the short pipe, the reflections of the initial pulse observed at each of the measuring positions, reveal noteworthy occurrences. At the positions 0.84 m and 0.10 m from the exhaust port, the reflection of the initial positive pulse from the tailpipe outlet (marked A in figure (13)) may be seen to be a negative wave travelling upstream. The reversed nature of such a reflection was anticipated in section 2.7.2. In fact, at measuring position (a), it may be seen that the negative reflection of the initial pulse is, in turn, reflected from the tailpipe outlet as a positive wave (marked B). This second reflection is seen arriving at position (a) about 11 milli seconds after E.P.O. As well as reflections from the tailpipe outlet, it is clear from both measurements and calculations at all positions that the first negative reflection is reflected off the nearly closed port as another negative wave (marked c). This behaviour was expected in section 2.7.1. On looking at the traces at all three positions, the progress of the initial pulse and the subsequent reflections is now obvious. Given the large magnitude of the resultant reflections seen to exist at the start of the next engine cycle, it would be expected that the engine operation would be fairly speed dependent. Such tuning effects, causing speed related erratic running, were observed.

A most important result seen in the pressure cycles in figure (13) is the ability of the calculation technique to adequately follow the steepening of the initial pulse along the pipe length. The significance of this steepening is obvious in influencing the radiated sound pressure cycle, as is discussed below. Better detail of the measurements and calculations which show the wave steepening may be seen in figure (14). The calculated pressure traces in figure (14) show the initial pulse steepening significantly on passing down the pipe. This, of course, corresponds with the C_+ characteristics on the

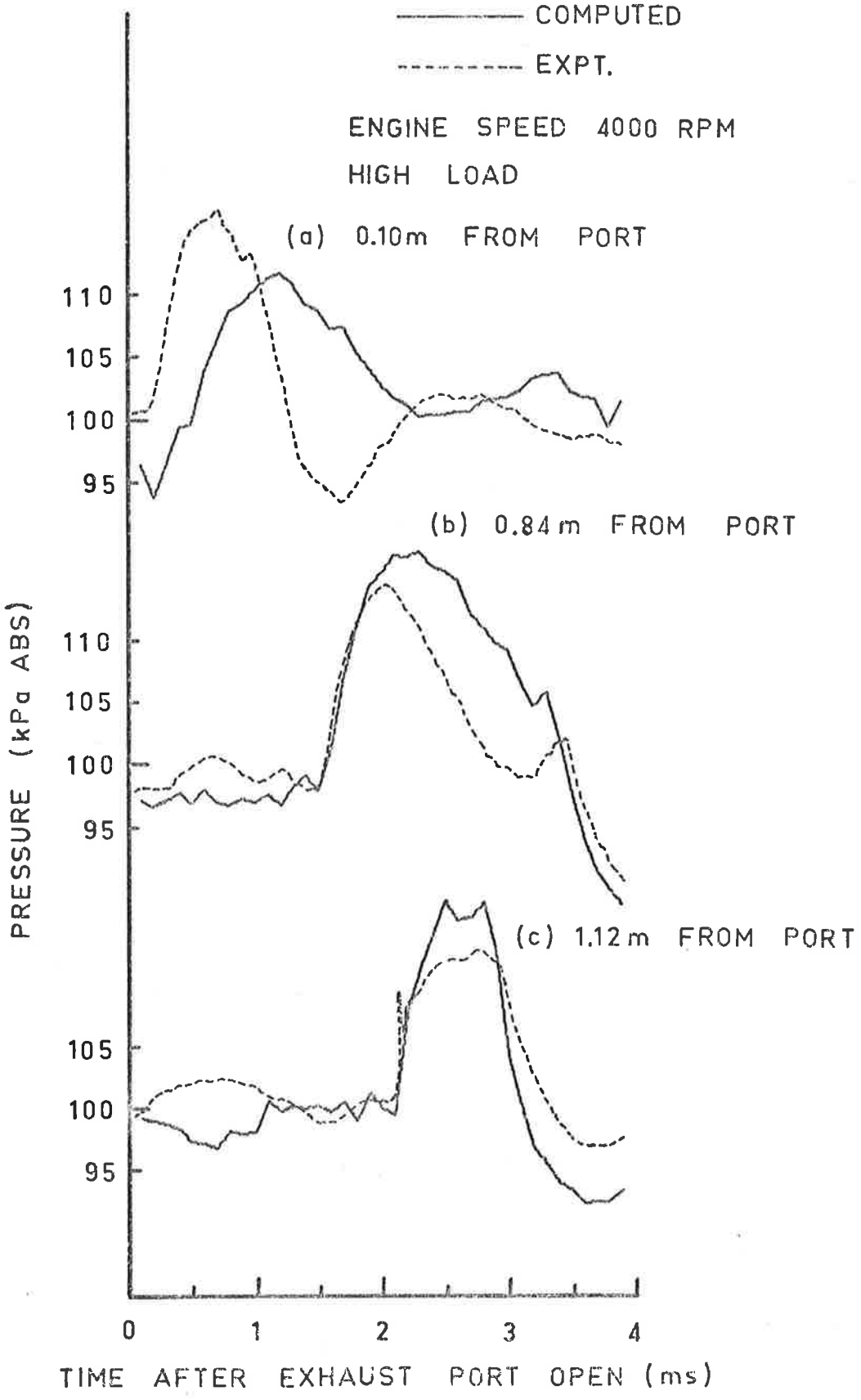

FIG. 14 INITIAL PULSE STEEPENING IN 1.3 m STRAIGHT PIPE EXHAUST

x - t diagram crowding together. Although not identical, the measured traces in figure (14) also show the steepening of the initial exhaust pulse. In fact, 1.12 m from the port, a shock wave of low strength has formed.

Now, it is clear that a given initial exhaust pulse will steepen much more in the 1.3 m pipe than in the 0.4 m pipe. Of course, measurements and calculations in figures (11) and (13) show this. From the discussion in section 2.9, it then follows that the sound pressure radiated, as the initial exhaust pulse reaches the tailpipe outlet, would be greater for the long pipe. Results in figures (15) and (11) show this to be the case. Figure (15) shows both measured and calculated radiated sound pressure traces for most of one revolution. Although the higher engine speed of 6000 r.p.m. and the lower load would change the shape of the initial pulse, it was not believed that there would be a great difference. In fact, the magnitude of the radiated sound pressure peak calculated by the same program run which gave the computed values for figures (13) and (14) was almost identical to the magnitude of the measured peak shown in figure (15). (Experimental difficulties prevented corresponding measurements at 4000 r.p.m. from being obtained). Therefore, the reason for the magnitude of the peak sound pressure radiated from the long pipe to be about double that for the short pipe is the effect of pulse steepening.

Figure (15) shows that, as for the short pipe, the calculated radiated sound pressure cycle closely simulates the measured trace. Again, both traces are dominated by the large peak, caused by the initial pulse. However, apart form the somewhat less significant effect of the first reflection of the initial pulse, there is little other specific agreement. The main peak is of much less duration than for the short pipe, being less than 2×10^{-4} seconds long. This is to be expected, as the steepened wave would rise very quickly. Certainly the calculated

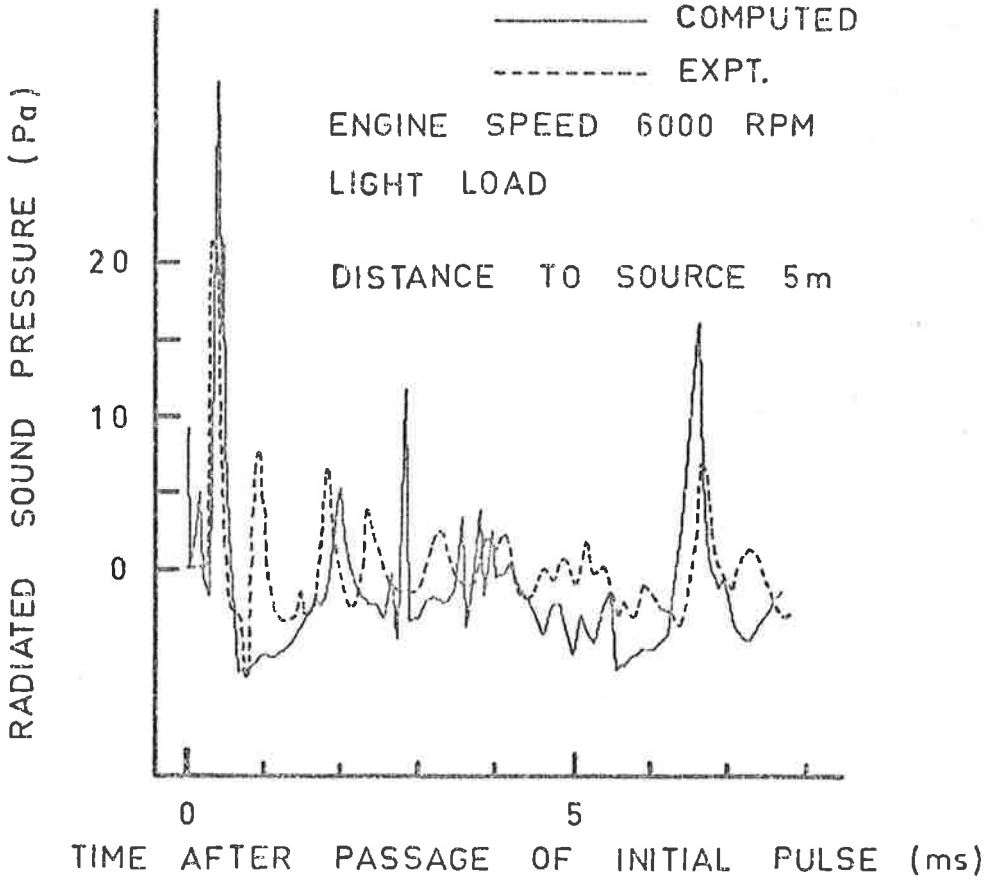

FIG. 15 SOUND RADIATED FROM 1.3 m STRAIGHT PIPE

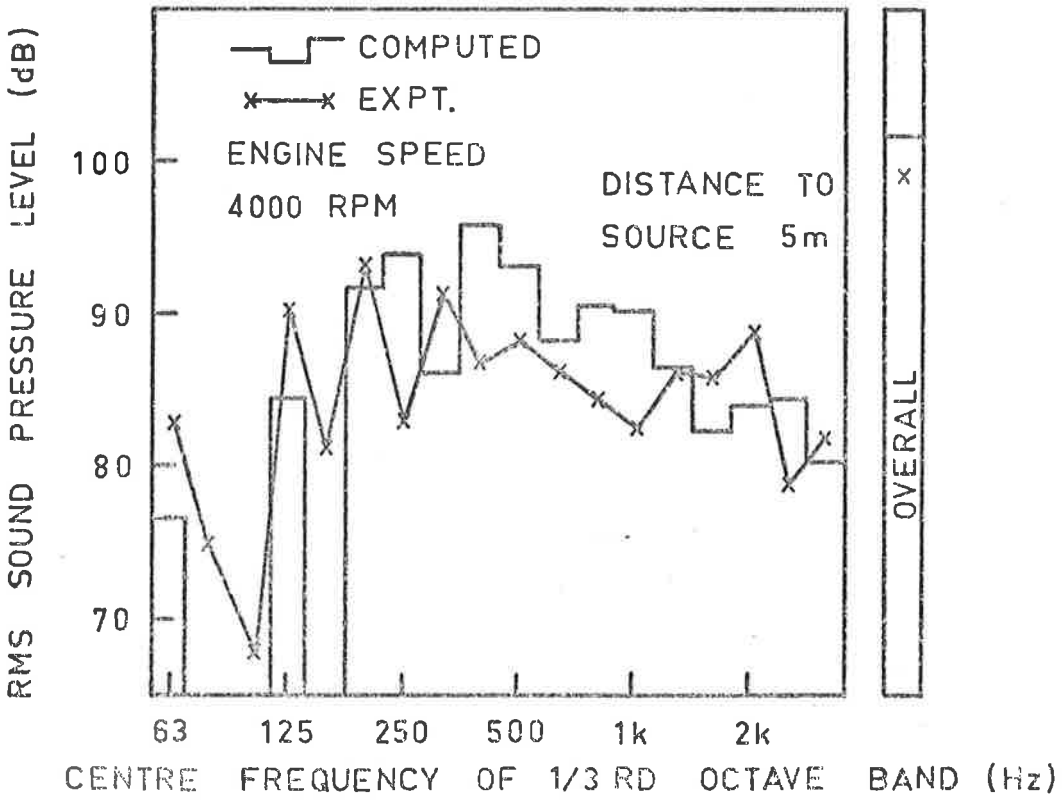

FIG. 16 THIRD-OCTAVE RADIATED NOISE FROM 0.4 m STRAIGHT PIPE

trace correctly shows the pulse duration.

3.2.3 Radiated Noise Spectrum

The calculated radiated sound pressure traces for the 0.4 m and 1.3 m pipes, in figures (11) and (15) showed generally good agreement with the measurements. It was, however, necessary to see how well the calculation method predicted the actual radiated noise as would be heard by an observer, in the far field. To do this the measured and calculated radiated sound pressure cycles for the short pipe, traces (a) in figure (11), were expressed as $\frac{1}{3}$rd octave spectra. The measured spectrum was actually obtained by analysing a tape recording using a $\frac{1}{3}$rd octave band filter. The calculated spectrum was derived from a Fourier anslysis of the pressure values for one engine cycle, with the values at the various harmonic peaks being added together in the appropriate $\frac{1}{3}$rd octave bands. Both spectra are unweighted.

The measured and calculated spectra, which were obtained, are shown in figure (16), together with the respective overall r.m.s. levels. Of course, the measured overall level was found directly, whereas the overall level for the calculated spectrum is simply the sum of the levels in the various bands. As may be seen, there is satisfactory agreement over most ranges of the spectrum, and for the overall levels as well.

3.2.4 Discussion

Results in the previous sections show that the calculation method may be used to predict the noise associated with straight pipe engine exhaust systems, of any length. The accuracy of the prediction that may be obtained by the method is shown by the way that both the overall level and the spectral content of the radiated noise from the 0.4 m pipe are closely described. The way in which the steepening of the initial exhaust pulse is adequately followed, and the consequent radiated sound pressure peak is closely predicted, indicate that the

method of following characteristics on an x - t diagram is the appropriate method of calculating the radiated sound pressure. Now, section 2.9 showed that the radiated noise may be determined from the fluctuation of velocity values at the tailpipe outlet. Clearly, the close relation between the measured and computed radiated sound pressure cycles shows that the calculation method used is sufficiently precise in obtaining these velocity values. While not of direct concern in this study, it is of interest to note the way the calculation method properly determines the wave action and the consequent exhaust tuning effects for the engine. This, of course, as discussed in chapter 1, is a prerequisite to obtaining the radiated noise.

Both measurements and calculations reveal that the expectedly steeper initial wave at the end of the 1.3 m pipe results in a greater radiated pressure peak. The measured radiated peaks were, in fact, 22 Pa for the long pipe and 12 Pa for the 0.4 m pipe. Certainly, these initial peaks contributed significantly in the overall radiated sound. Therefore, it is recommended that, to avoid wave steepening and the associated high radiated peak pressure, long straight pipes leading from individual exhaust ports should not be used. No doubt this explains the known advantage of having an intermediate muffler close to the engine in many automobile exhaust systems.

As mentioned in section 3.1, the calculation technique excludes the effects of both heat loss through the pipe walls and viscous losses. By now comparing measurements with calculations, for the two straight pipes, the significance of these omissions is shown below to be small.

A gradual heat loss along the 1.3 m pipe would cause pressure waves to travel through the pipe more slowly than as otherwise expected. However, as the timing of the reflected waves, as shown in figure (13), seems quite closely predicted, omitting the heat loss appears to be of minor importance. Also, the gradual reduction in temperature toward the

tailpipe outlet might be expected to change the shape of the pressure waves slightly, but again, the results shown in the traces (a) and (b) in figure (13) do not indicate any such large discrepancies. As explained below in this section, the poorer agreement in magnitude at the position 1.12 m from the port is, in fact, believed to be due to the heat loss, but as discussed later, it is not expected that the velocity values at the tailpipe outlet are in significant error.

The omission of viscous losses from the analysis would be expected to cause the higher order reflections of the initial pulse to be overestimated by the calculation method. This is shown to occur in the pressure cycle (a) in figure (11) and near the position marked B in trace (a) of figure (13). From the small magnitude of this error, this would not appear to be a crucial factor.

The poor agreement in magnitude between the measured and predicted pressure cycles near the open end of the long pipe is believed to be caused by the heat loss omission. With actual temperatures in the tailpipe lower than those calculated, as mentioned above, there would be small errors in timing and shape of the various arriving pressure waves in the computation. These errors would be accentuated for pressure cycle calculations near the outlet as, for a certain point in the duct, the pressure value would be the summation of a slightly inaccurate incident pulse and its reflection of opposite sign arriving at a slightly later time. The values of velocity at the tailpipe outlet on the other hand would then not necessarily be as far from measured values. In fact, the calculated radiated sound pressure trace in figure (15) is quite acceptable. This confirms that the omission of heat loss is justified as a first approximation. Simple modifications could be made to the program by approximating the heat transfer and incorporating it by relating it to a small change in entropy along the P characteristics, but this has not so far been considered necessary.

(In this case, assuming Prandtl number equal to 1 would allow the viscous heating, though small, to be included.)

3.3 SLOWLY VARYING AREA

3.3.1 Comparison with Known Solution

Before calculations and measurements were performed for the tuned expansion chamber shown in figure (9), it was considered necessary to check the changes to the computation method which were described in section 2.10. To do this, a calculation was performed for a varying area duct problem for which there was a known mathematical solution. The case considered was that of an initially weak shock travelling down a duct of decreasing area. In this instance, the strength of the shock was calculated by the computer program as the shock passed down the converging duct. Figure (17) shows the calculated shock Mach number obtained plotted against the diameter of the duct, for very large changes in duct cross-sectional area. The theoretically predicted curve in figure (17) was derived from Whitham's theory (11) in which the shock strength is related to the area. This particular theory was found by Whitham to give extremely accurate predictions of the shock strength for the imploding spherical shock (the Guderley problem) for which an exact solution exists. Clearly the calculation method follows very closely the result of Whitham up to a shock Mach number of nearly 2. The reason for the slight discrepancy appearing at Mach 2 is obviously the fact that the computer program approximates all shocks as being weak, as mentioned in section 2.5. From the results in figure (17), the calculation method certainly would be expected to be perfectly adequate to study engine exhaust systems. This follows as shocks in such systems will never have Mach numbers as high as 2.

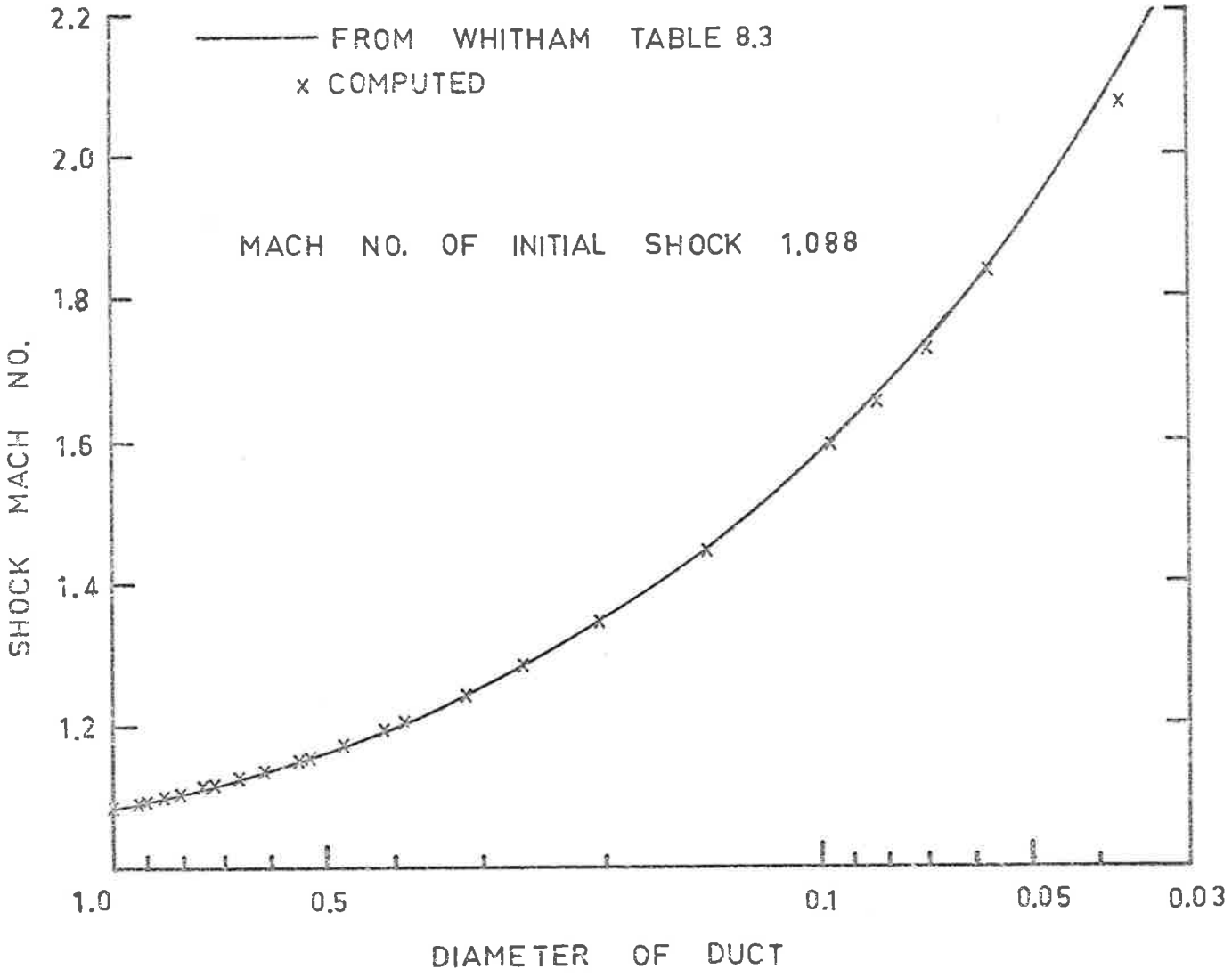

FIG. 17 SHOCK PROPAGATION ALONG DUCT OF DECREASING DIAMETER

3.3.2 Experimental Results for Tuned Expansion Chamber

In a similar manner as for the 1.3m straight pipe, a series of measurements and calculations were performed for the tuned expansion chamber shown in figure (9). As the pressure wave reflections in such a system were expected to be quite complex, it was not anticipated that the various phenomena would be as clear cut as in the case of the straight pipes. Therefore, as mentioned in section 3.1, the tuned expansion chamber was used primarily to test how well the calculation technique described such a slowly varying area duct.

Figure (18) shows the measured and computed pressure cycles obtained for the four locations in the tuned expansion chamber shown in figure (9). Again, as for the straight pipes, the calculated cycles were obtained after several (3) successive engine revolutions.

The agreement shown by the calculated traces in figure (18) is excellent, particularly at the first three positions. Both the timing and the magnitude of all the pressure pulses is very well predicted by the computation. A comparison between the agreement in figure (18) with that in figure (13) clearly shows that the calculation method is equally suited to studying either straight pipes or varying section ducts.

Certain interesting points may be seen by studying the pressure traces in figure (18). Obviously, it is no longer possible to readily follow the development of the initial and reflected waves, as for the 1.3m straight pipe. However, the fact that the calculation method so accurately predicts the pressure cycles at points (1), (2), (3) and even (4), when there are such pronounced differences between each of these points, of itself seems to justify the computation method used.

The exhaust tuning effects, for which a tuned expansion chamber is used in the first place, are determined by the cycle of pressure values near the exhaust port. Clearly, the good agreement between the

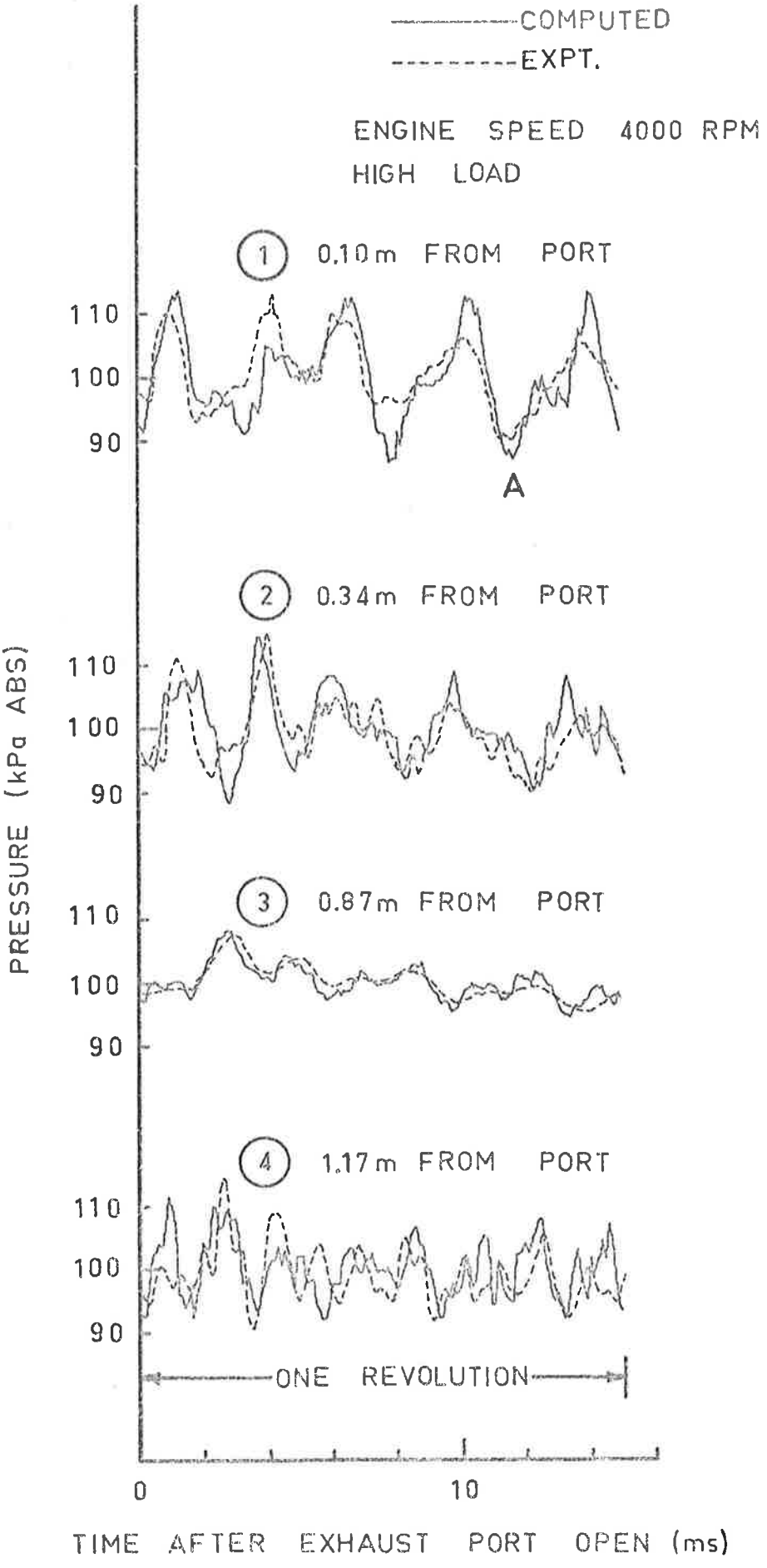

FIG. 18 PRESSURE WAVES IN TUNED EXPANSION CHAMBER

pressure cycles at the position 0.10 m from the port indicates that such tuning phenomena are correctly described by the calculation. These tuning effects will now be considered, based on the author's observations.

For a 2-stroke engine with a tuned expansion chamber, the exhaust tuning is achieved by correctly timing the arrival of basically three pressure waves at the open exhaust port. These pressure waves may be seen reaching the port in both the calculated and measured pressure cycles in trace (1) in figure (18). The significance of these pressure waves is described below.

Shortly after the exhaust port opens it is desirable to have a negative pressure wave arriving at the port, so that the exhausting of the cylinder may be achieved as quickly and completely as possible. This pressure wave is reflected back towards the port from the initial positive pulse, as the pulse moves into the gradually expanding area section shown in the diagram of the tuned expansion chamber in figure (9). This negative wave is shown in figure (18) to reduce the pressure at the port for the period between about 2 and 4 msecs after E.P.O. Following the negative wave, it is desirable to have a high pressure wave, caused by the reflection of the initial pulse in the area contraction, to reach the port just before E.P.C. This has the effect that some of the fresh charge which has gone into the exhaust pipe is forced back into the cylinder, causing a slight supercharging in the cylinder. This positive wave is shown in trace (1) of figure (18) to reach the port about 4 msecs after E.P.O. Finally, it is desirable to have the exhaust port open on the next engine cycle just after a low pressure wave has reached the port. It is clear from both measured and calculated values in trace (1) of figure (18) that the pressure is, in fact, low when the exhaust port opens again.

Obviously, the pressure cycle near the exhaust port will not greatly change in shape with higher engine speed:- it will be more or

or less a truncated form of the trace (1) in figure (18). Therefore, as the pressure at point A in trace (1) of figure (18) is very low, the engine would be expected to run very well at a speed (about 5000 r.p.m.) for which the exhaust port opens near point A in the cycle. Also, from figure (18), it appears that the exhausting and supercharging effects would be optimised at this speed. In fact the engine was observed to run very well at about 5000 r.p.m.

By studying the development of the initial exhaust pulse, at each of the four locations, it is clear that wave steepening is not greatly evident. It is described later, in section 4.3, how the large increase of area, near position (3), reduces the tendency of such wave steepening. Both measurements and calculations do show, however, some degree of steepening of the initial pulse as it passes from position (3) to position (4), in the very narrow tailpipe.

The radiated sound pressure cycles, as measured and calculated are shown separately in figure (19). As in the case of the straight pipes, both cycles in figure (19) are dominated by a peak resulting from the initial exhaust pulse. The magnitudes of these peaks are much less than for the 1.3 m straight pipe for reasons mentioned in section 3.3.4. Clearly, the calculation closely simulates the measured peak in both magnitude and duration. The duration of the measured peak, as for the long straight pipe, is only about 10^{-4} seconds. Apart from the peak, the calculation does not closely follow the details of the rest of the measured radiated sound pressure cycle, however, the form of the trace is certainly very similar. Correspondingly, the $\frac{1}{3}$rd octave band spectrum of the radiated noise is closely predicted (section 3.3.3).

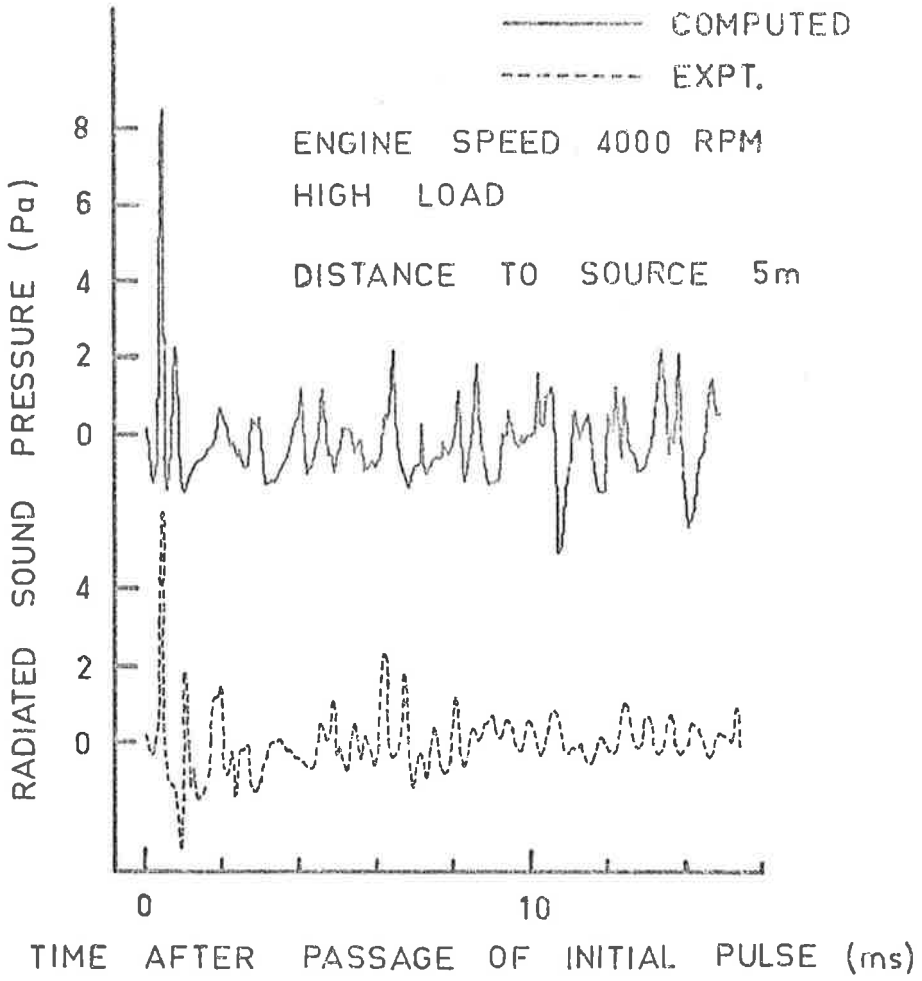

FIG. 19 SOUND PRESSURE CYCLE RADIATED FROM TUNED EXPANSION CHAMBER

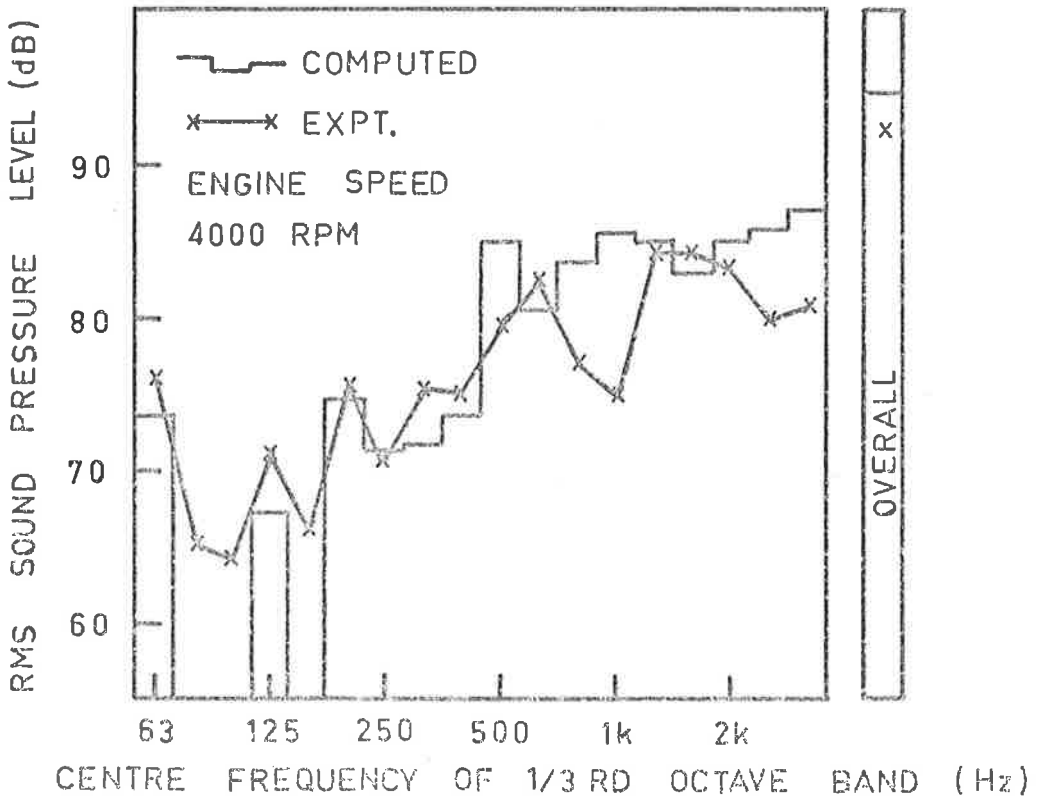

FIG. 20 THIRD-OCTAVE RADIATED NOISE FROM TUNED EXPANSION CHAMBER

3.3.3 Radiated Noise Spectrum

In a similar manner as described in section 3.2.3, for the 0.4m pipe, the computed and measured unweighted $\frac{1}{3}$rd octave radiated noise spectra for the tuned expansion chamber were obtained. These are both shown in figure (20) together with the overall r.m.s. levels. As is shown, the agreement between the spectra is generally excellent, with a noticeable error only in a small region near 1 kHz. The overall r.m.s. level is accurately predicted as well. The good agreement obtained over the spectrum indicates that the small errors in the timing of the minor pulses in the calculated radiated sound pressure trace had little effect.

3.3.4 Discussion and Summary

The very good results shown for the study of the test case in section 3.3.1, indicated that the method developed to model slowly varying area ducts would be as accurate as the basic method that describes straight pipes. The results of calculations and measurements performed for the tuned expansion chamber confirm this. In fact, the correspondence of some of the values, as shown in the preceding sections, is quite remarkable. In particular, the pressure cycles at positions (1), (2) and (3) inside the tuned expansion chamber and the spectrum of radiated noise are all quite accurately computed. Again, as for the straight pipes, the precise prediction of the magnitude and duration of the very short peak in the radiated sound pressure cycle shows the benefit of computing the x - t diagram in the manner described in chapter 2. Once more, the value of a small time interval and close determination of the velocity values at the tailpipe outlet is clear. It may then be expected that any differently shaped gradually varying area expansion chamber may be studied as easily, with the same accuracy.

As for the straight pipes, the good agreement between measure-

ments and calculations shows that the omission from the analysis of heat loss through the pipe walls and viscous losses is quite reasonable. Certainly, results in figure (18) clearly show that any errors caused by a lack of damping are slight. The effects of heat loss, however, need some explanation, as in the case of the 1.3 m straight pipe.

The pressure cycles at position (4), in the tuned expansion chamber, are shown in figure (18) to exhibit the similar lack of agreement as in figure (13) for the position (c), in the straight pipe. As for the 1.3 m straight pipe, it is believed that this effect is caused by the heat loss along the exhaust system. Such an effect would be similar for both systems as they are nearly the same length. It is then expected that the calculation for the tuned expansion chamber would have small errors in timing of the arrival of pressure waves at the tailpipe outlet. Obviously, this explains the discrepancies between the traces for position (4), as shown in figure (18). Such timing errors would also cause similar errors of timing for the minor pulses in the radiated sound pressure cycle. This may, in fact, be seen to occur by comparing the measured and computed radiated sound pressure traces in figure (19). It seems likely that these errors do not greatly affect the overall radiated noise and this view is supported by the excellent agreement between the measured and calculated radiated $^1/_3$rd octave band spectra in figure (20). Thus neglecting the heat loss again seems to be an acceptable approximation.

By following the development of the initial pulse in the tuned expansion chamber, it is obvious that wave steepening is much less evident than in the long straight pipe. Now, the engine was running at the same speed and load when pressure measurements were taken inside each of the exhaust systems. Therefore, the initial pulses, measured at the position nearest to the exhaust port, would be expected to be very similar for both the 1.3 m pipe and the tuned expansion chamber.

The same applies for the calculated traces. Traces shown for positions (1) and (a) in figures (18) and (13), respectively, show in fact very similar initial pulses. However, at positions (3) and (b), which are both about the same distance from the exhaust port, the initial pulse in the tuned expansion chamber is much less steep. This difference in steepness is obviously caused by the increase in cross-sectional area. The increasing cross-sectional area has the effect of reflecting the pressure wave back upstream as a negative wave, thus weakening the pulse. Correspondingly, wave steepening (characteristics crowding together) does not occur to the same extent as it does for the 1.3 m straight pipe. It is consequently no surprise that the magnitude of the peak in the radiated sound pressure cycle is much less for the tuned expansion chamber than for the long straight pipe. The measured peak values were 6 Pa (4000 r.p.m., high load) and 22 Pa (6000 r.p.m., low load), respectively.

Although the experiment was not carried out, the calculated peak SPL for the 1.3 m pipe for the same engine conditions (4000 r.p.m. and high load) as used for the tuned expansion chamber experiment, was 20 Pa, which is not greatly different from the measured value at 6000 r.p.m. This, of course, is the calculated value corresponding with the results shown in figure (13). Given the accuracy of the predicted pressure cycles for the engine speed of 4000 r.p.m., in figures (13) and (18), and the agreement between predicted and measured radiated sound pressure cycles in figure (19), the above comparison between the two measured peak levels validly makes the point. Therefore, this difference in wave steepening, and in the resultant radiated peak level confirms the belief, stated in section 3.2.4, that long straight pipes following individual exhaust ports, should be avoided if possible.

Finally, several features of the sound radiated from each of the three experimental exhaust systems may be observed. The radiated

sound pressure cycle for each of the systems is dominated by a large magnitude peak caused by the initial exhaust pulse. This may be expected to be the case for many exhaust systems used on small 2-stroke engines, particularly when an exhaust manifold is not used. Clearly, the large peak affects the peak sound pressure level, whereas the lower magnitude fluctuations, caused by wave reflections, will significantly affect the r.m.s. level and the spectrum shape. The next chapter reveals the significance of these and other facts in determining the suitability of the various existing muffler theories.

CHAPTER 4

COMPARISONS WITH OTHER THEORETICAL APPROACHES

The description of the calculation method in chapter 2 and its use in determining the sound radiated from an engine exhaust system, in chapters 2 and 3, revealed certain types of non-linear behaviour in exhaust systems. In particular, pulse steepening was shown to be very significant. Also, it is clear from section 2.7.1 that the sound source, the exhaust port, may not be described in a simple way. Following the work which has been described in previous chapters, it is now possible to comment on the suitability of the existing muffler and exhaust noise theories, in light of these non-linear effects and other facts. As mentioned in section 1.2, the existing theories include the lumped and distributed linear impedance methods and the single pulse approach. The following sections show that each of these methods has a number of limitations. As is shown below, most of these limitations may be overcome by using the computation method of chapter 2, as the limitations are properly taken into account.

4.1 ENGINE SOURCE IMPEDANCE

As mentioned in section 1.2, both the lumped and distributed element analyses usually require simplifications to be made concerning the engine exhaust noise source impedance. Normally the sound source is approximated as being either a pressure source (voltage source in terms of the electrical analogy) of zero impedance, or a volume velocity source (a current source) of infinite impedance. Clearly, there is a large difference between these extreme values. The use of one approximation or the other is justified by the fact that the

impedance of the exhaust system is either very much greater or less than the sound source, as is explained below.

The nature of the source impedance may, in fact, be deduced from considerations of the previous chapters.

As the release of the cylinder gas through the exhaust port is the cause of the wave action in the exhaust system, it is clear that this fluctuating flow at the exhaust port is the ultimate sound source. Obviously when the port first opens and the pressure ratio exceeds the critical pressure ratio (approximately 1.8), the port acts as an infinite impedance current source, since the mass flux which forms the initial pulse is unaffected by the exhaust system. The source impedance, for the formation of the initial exhaust pulse, will then be virtually infinite for all frequencies. The period during which this critical pressure ratio is exceeded is very small, however, and the results of chapter 3 show that this initial exhaust pulse is by no means responsible for all of the radiated sound. As mentioned in section 3.3.4, the many reflections of the initial exhaust pulse in the exhaust system are responsible for significant fluctuations in the radiated sound pressure cycle. As these fluctuations have some effect on the overall r.m.s. level and the spectrum shape, the conditions at the exhaust port when these reflections of the initial pressure pulse are themselves reflected from the exhaust port back to the tail-pipe, are significant. That is, the port could be either open or closed. Clearly, the overall source impedance will vary for different speeds and loads, as the reflected pressure waves will reach the exhaust port at different times in the cycle. Thus for 2-stroke single cylinder engines, treating the sound source as an infinite impedance current source is perhaps a good first approximation in some instances, but it does appear from the present work that, in general, the fluctuating flow at the exhaust port is too dependent on the exhaust system

itself for it to be usefully idealized as a current or voltage source.

Some analyses, however, require a value of the source impedance acting at a manifold outlet, downstream of the exhaust ports. This is usually the case with multi-cylinder engines, as for practical purposes the source may be regarded as being at the manifold outlet. In such instances, the current sources at the ports (infinite impedances), acting on the very low impedance manifold, create a sound source at the manifold outlet very much like a pressure source (i.e. a zero impedance voltage source). This approximation is valid at low manifold impedance, that is with a large volume, and at high frequencies, but not so high for the manifold to cease to act like a lumped impedance. The greatest errors are then expected at some high frequencies for which wave effects would occur in the manifold. Also, for reasons mentioned earlier in this section, the precise source impedance at the manifold outlet may change with varying engine operating conditions because of wave action in the manifold and in the coupling exhaust system. That is, the impedance of the exhaust system is not likely to be large compared with the manifold at either all frequencies or operating conditions.

Following the simple derivations of the sound source impedance given above, it is interesting to note the values used in other studies. For muffler designs for small 2-stroke engines, Watters et al (7) used an infinite source impedance. This is clearly in line with the argument presented earlier in this section. For the source impedance at the outlet of a manifold, Sreenath and Munjal (14) suggested using the impedance of the volume of the manifold. Again, this is a reasonable approach. Also for manifold sources, Alfredson (9) recognised the existence of an "exhaust driving signal" for a particular engine and manifold combination. That is, he treated the outlet of the manifold as a voltage source. Rather than use approximate values, some

researchers (for example, reference (15)) have attempted to measure the source impedance using exhaust systems on operating engines. As would be expected from the explanation given above, the source impedances thus obtained are likely to be complex and to vary with changing engine operating conditions and different exhaust systems.

From the above, it is clearly difficult to arrive at a simple expression for the sound source impedance to be used with linear muffler theories. The use of an infinite value for the source impedance of an exhaust port is the only simplification which may be recommended with any degree of certainty. Obviously, the calculation technique described in chapter 2 would not encounter any of these difficulties. The calculation correctly allows for the sound source effects at all times by accurately adding a C_+ reflected characteristic when an incident C_- reaches the exhaust port.

Apart from the source impedance, the lumped and distributed element approaches have other errors which are described in the following sections.

4.2 LUMPED ELEMENT THEORY

The lumped element theory is often applied to small muffler systems, as used on 2-stroke engines. For such systems the assumption that the impedance of each of the elements acts at a point is reasonably accurate. This is true, of course, only when the element lengths are much less than the wavelength of the frequency of interest.

The theory may easily be used in the study of Helmholtz resonator type mufflers. For example, Watters et al (7) used the lumped element approach with expectedly good low frequency results in describing a cavity - tailpipe type muffler on a 2-stroke engine. As mentioned in the previous section the correct assumption of an infinite source impedance was used.

Most small mufflers used on 2-stroke engines are, however, not of the type for which the simple linearized lumped element theory may be readily applied. Many mufflers are of the orifice - cavity - tail-pipe type, in which there is some kind of restriction leading to the volume. The two basic forms of mufflers are shown in figure (21). The inlet restriction is used, often simply because experience has shown that the sound reduction achieved is greater with it in place. The explanation for this, of course, is partly that it reduces the magnitude of the initial mass flux pulse. Whereas the cavity - tailpipe muffler may be designed to operate nearly linearly, the behaviour of the inlet restriction, in the alternative design, is wholly non-linear. This is discussed further in Part 2 section 9.2.

Larger mufflers used on motorcycles are actually often of the simple cavity - tailpipe type, but in these cases the lumped element theory is again inadequate. Of necessity, motorcycle exhaust systems are much longer. Therefore, the lumped impedance assumption is in error for all but the very low frequencies.

Thus as is generally well known, the lumped element theory is only an approximate approach valid if at all for only part of the frequency range. This is because, firstly, the systems studied often include orifices, which have been shown (for example by Bies and Wilson (16)) to behave non-linearly at the sound pressure levels which are widely known to exist in mufflers. Secondly, the tubes and volumes used exhibit wave effects at high frequencies.

The calculation method described in chapter 2 appears to be a much better approach. As discussed in section 5.1, both a restriction and an area discontinuity may be easily included in the characteristic calculation described in this work.

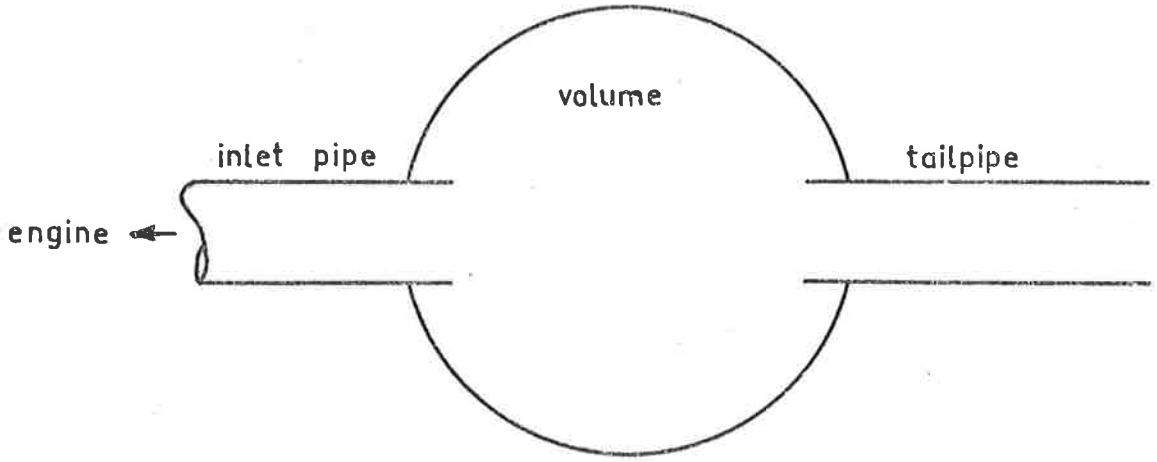

CAVITY - TAILPIPE MUFFLER

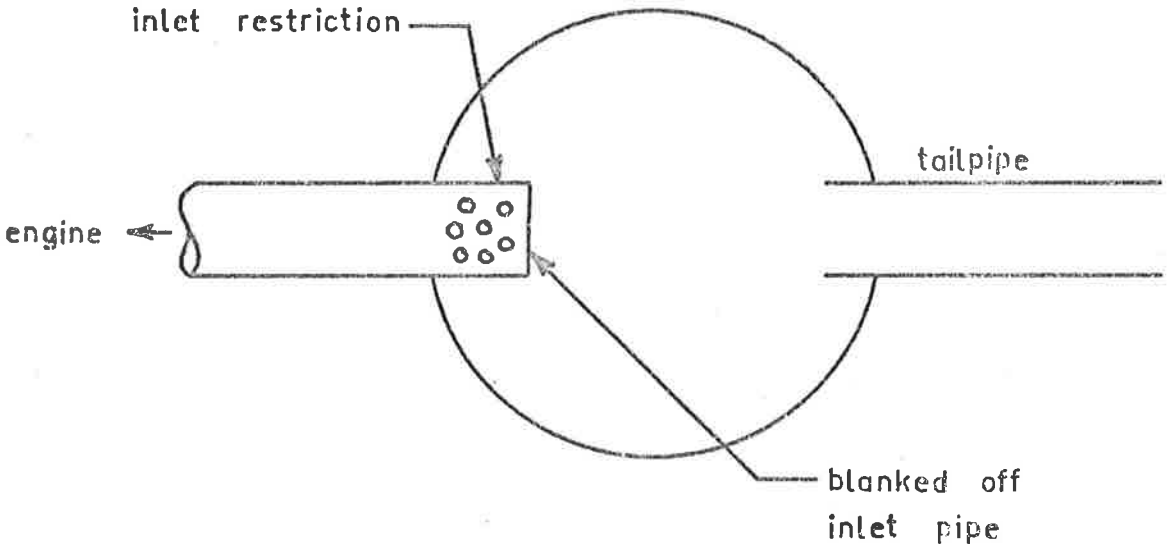

ORIFICE - CAVITY - TAILPIPE MUFFLER

FIG. 21 MUFFLER TYPES FOR SMALL 2-STROKE ENGINES

4.3 WAVE STEEPENING EFFECTS

Before the distributed element and single pulse theories are considered, it is first necessary to summarize the wave steepening effects which have been made evident in this study. These steepening effects will be shown in the next sections to impair the accuracy of both the single pulse and distributed impedance approaches.

Wave steepening was described briefly in section 2.2 and calculated examples were shown in section 2.8. Measurements and calculations indicating the steepening of the initial exhaust pulse in the 1.3 m straight pipe were shown in figures (13) and (14).

Now, as described in section 2.9, the radiated sound pressure from an engine exhaust is determined by the fluctuating velocity values at the tailpipe outlet. It was shown that a steeper pressure pulse gives rise to faster rising velocity values at the tailpipe which cause a greater magnitude radiated sound pressure pulse. This was clearly shown by the greater magnitude pressure peak radiated from the long pipe than from the short pipe (see section 3.2) - 22 Pa as against 12 Pa . In these cases the reason for the large difference in the peak values was overwhelmingly the wave steepening in the greater length.

The effects of wave steepening were also shown by the results for the tuned expansion chamber discussed in section 3.3.4. The tuned expansion chamber is about the same length as the 1.3 m straight pipe, but the steepness of the initial pulse in the former was much less. The magnitude of the radiated pressure peak was measured at 6 Pa as against 22 Pa for the long pipe. As mentioned in 3.3.4, this large difference is due to the reflections sent back upstream from the initial pulse as it moves into the increasing duct area. The steepening is virtually stopped in the larger diameter section as the area increase causes the magnitudes of the pressure and velocity in the

initial pulse to be much lower. In terms of an x - t diagram the particle velocity, u, is reduced and the speed of sound, a, more closely approaches the stagnation value, so that the velocities of all the C_+ characteristics, given by u+ a, become very much the same. Thus the characteristics no longer catch up with each other.

It is well known that the magnitude of the sound pressure peak radiated from a tuned expansion chamber may be reduced by having the tailpipe intrude into the large diameter section. The radiated sound is then less as the initial pressure wave reaching the tail-pipe outlet is of lower magnitude and is not as steep.

The effects of wave steepening in increasing the magnitude of the radiated sound pressure peak, in a non-linear way, are now clearly significant. The calculation method as devised in chapter 2, obviously describes such wave steepening fairly accurately. Of course, the distributed element and single pulse theories do not.

4.4 DISTRIBUTED ELEMENT THEORY

The distributed element analysis is usually applied to large muffler systems, for which the element lengths are long in comparison with a wavelength. Such muffler systems are often placed downstream of a manifold on a multi-cylinder engine. As explained in section 4.1, the nature of the source impedance at a manifold outlet is uncertain. The source impedance is likely to be either very low, or complex. For this reason, the use of the distributed element theory may involve a source impedance error as the theory is often used in cases when the source impedance is hard to define.

The other main source of error is obviously the neglection of wave steepening effects, which is unavoidable in the linearized approach. These steepening effects were described in the previous section as being sometimes very significant and it is clear that they

will be important if peak flow velocities in the exhaust system are high and/or the pipe lengths are long. The possibility of serious source impedance and wave steepening errors at high engine speed or high engine load therefore limits the applicability of any distributed element theory.

Alfredson (9), however, obtained good results using the distributed element theory to describe complex mufflers comprised of a lot of quarter wave filters. Comment must now be made on these results. Alfredson did not encounter any significant wave steepening errors for several reasons. Firstly, the mufflers were placed downstream of the engine manifold, where sound pressure levels are usually lower than in the straight pipes downstream of individual ports on small 2-stroke engines. Secondly, in much of the experimental work there was an initial expansion chamber between the manifold and the test section. This was probably sufficient to reduce the steepening effects and to reduce the amplitude of the pressure pulses entering the muffler being tested. As mentioned in section 4.1, Alfredson effectively used the assumption of a pressure source of zero impedance, at the manifold outlet. This was probably justified as the work was done on an approximately 200 h.p. multi-cylinder diesel engine with exhaust manifolds. The low impedance of the manifolds, possibly combined with the also low impedance of the initial expansion chamber, would then account for the good agreement obtained using a zero source impedance.

It would then appear that the distributed impedance approach may be sufficiently accurate to describe mufflers which are placed downstream of well defined sound sources, provided long straight pipes are not used. The method is, however, likely to give poor results when modelling long exhaust systems on 2-stroke engines, as wave steepening is certainly going to occur.

The basic method described in chapter 2 clearly avoids both the non-linear sound source impedance and wave steepening errors and would seem a more satisfactory approach in general for studying muffler systems. In particular, the method appears suitable for studying muffler systems for single cylinder 2-stroke engines and for multi-cylinder engines with long pipe manifolds. Of course, the analysis needs to be extended to include things such as step changes in area (and branches for multi-cylinder engines) so that quarter wave filters and other components may be included. The possibility of such extensions is considered in section 5.1.

4.5 SINGLE PULSE METHOD

The single pulse method studies the strength of a shock representing the initial exhaust pulse as it passes down the exhaust system. It is assumed that, the lower the strength of the shock at the tailpipe, the lower is the radiated noise from such an exhaust system when it is used on an actual engine. This method has two sources of error.

Firstly, radiated sound pressure cycles are not solely comprised of the peak caused by the initial exhaust pulse. Measured radiated pressure cycles for the short pipe, long pipe and tuned expansion chamber (figures (11), (15), (19)) each show a large magnitude spike, with minor peaks from the subsequent reflections of the initial exhaust pulse in the exhaust system. These minor fluctuations would influence the r.m.s. level and the spectrum shape of the radiated sound, as mentioned in section 3.3.4. The relative effects of the initial peak and these minor fluctuations would obviously be different for different muffler systems.

Secondly and mainly, the single pulse method is in error as wave steepening is disregarded. The assumption is made that the

initial pulse has already steepened to become a shock. This analysis would be appropriate if the initial pulse quickly steepened up. However, measurements and calculations, some of which are shown in chapters 2 and 3, indicate that shock wave formation only occurs at the end of long straight pipes coming from an individual port, and then, at least for the engines used and the typical exhaust pipe diameters, only rarely.

It is simple to show how the single pulse method may be used to draw unreasonable conclusions. For example, a shock will not change in strength in passing down a long straight pipe. The single pulse approach would then indicate that the sound pressure cycles radiated from both short and long straight pipe exhaust systems should have equal initial peaks. This was shown in section 3.2 to be quite wrong. As another example, consider the tuned expansion chamber. A shock, on passing down a small angle conical expansion followed by a similar contraction to the same area again, will have virtually the same strength. Therefore, from the single pulse method, the expansion chamber tested, as shown in figure (9), should not have radiated a substantially lower sound pressure peak value than a simple long straight pipe; experimentally it certainly did, for the reasons given in sections 3.3.4 and 4.3. In fact, shock strength is only effectively weakened by such an expansion followed by a contraction if the area changes are step discontinuities.

It is clear that only the full non-linear results, as may be obtained from an x - t diagram, will readily describe the above and other events accurately. The use of the method described in chapter 2 is then completely justified once the relevant descriptions of particular muffler elements are included in the analysis.

CHAPTER 5

EXTENSIONS AND CONCLUSIONS

5.1 EXTENSIONS OF ANALYSIS

It is believed that the method described in chapter 2 for studying the noise radiated by exhaust systems could be readily extended to consider many more complex practical systems. Any extensions would first require the consideration of a number of extra boundary conditions for the duct flow. None of these boundary conditions is likely to be more complex than those already considered, certainly not as complex as the open exhaust port boundary. Boundary conditions which may be considered include, for example:-

1. step changes in duct area
2. resistance in duct (e.g. orifice)
3. quarter wave filter (extended inlet or outlet from step change in duct area).

Each of these three boundary conditions may be considered as the junction between separate x - t diagrams, with the appropriate matching calculations performed whenever characteristics reach the discontinuity. The first two types of boundary conditions, however, may each simply be considered as being part of the one main x - t diagram. To illustrate the required technique, the calculations which would describe the flow existing after a C_+ characteristic reaches an area discontinuity will now be considered, briefly.

The x - t diagram describing the flow is shown in figure (22). For simplicity the final flow is assumed to be isentropic. The incident C_+ characteristic, on reaching the step change in area, gives

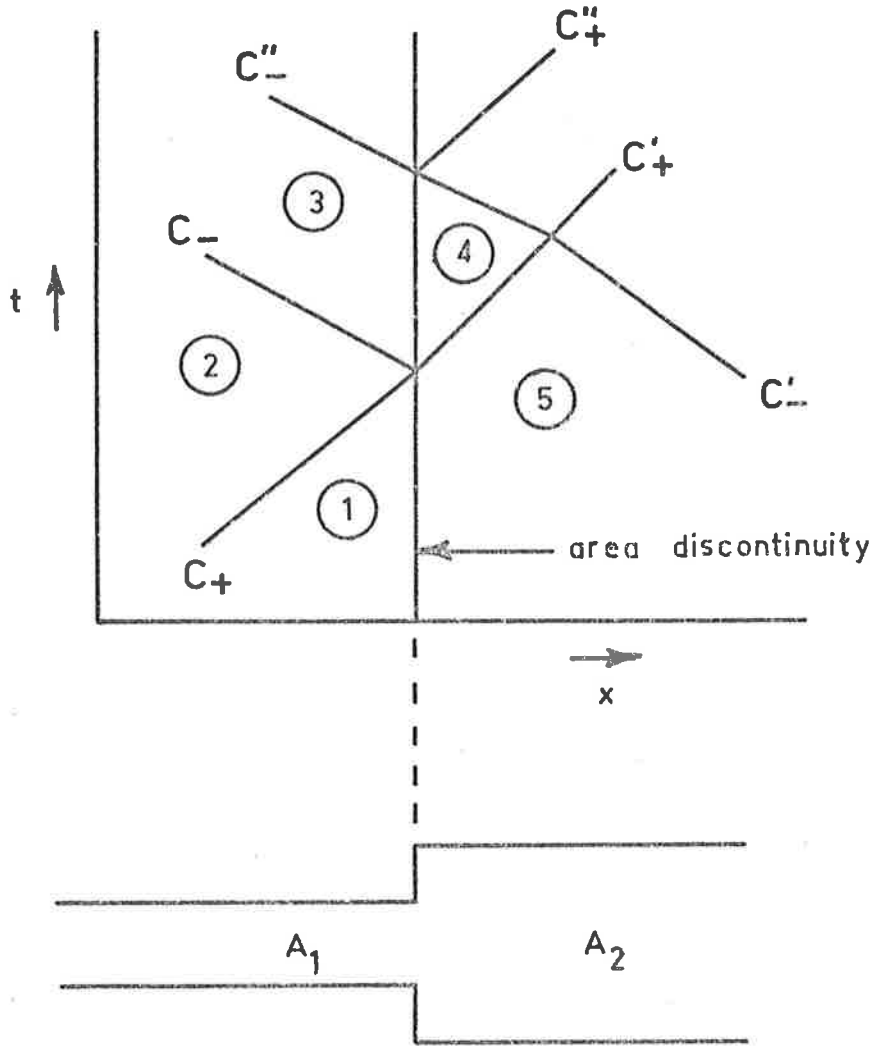

FIG. 22 C_+ CHARACTERISTIC MEETING AREA DISCONTINUITY FOR ISENTROPIC FLOW

rise to a reflected C_- characteristic and a transmitted characteristic, C_+' , with a different Riemann invariant. Now, the area discontinuity itself may be considered in the program as a "special characteristic". That is, the information regarding its position, area ratio, the local value of entropy, the speeds of sound and the velocities of the flows to either side of the area change, may all be held in the same arrays which contain the information describing the C_+, C_- and P characteristics. The value of a certain variable in one of the arrays would easily distinguish between the C_+, C_- and P characteristics and the area discontinuity.

When the incident C_+ characteristic reaches the area discontinuity, the final flow would be calculated in a subroutine, the transmitted characteristic, C_+' , would be correctly allowed for, and the description of the flow existing near the area change, in regions (3) and (4) in figure (22), would be placed in the appropriate array spaces describing the discontinuity. This is similar to the method used in the program, as shown in sections 2.3 and 2.6, to allow for a C_+ characteristic passing a P characteristic. The area discontinuity is then analogous to the entropy discontinuity of section 2.6. As discussed in section 2.6, the reflected C_- characteristic need not be created in the program. Briefly, this may now be seen in figure (22), as when the next left-facing characteristic, C_-' , reaches the area discontinuity, the description of the transmitted component, C_-'' , is dependent only on the correct description of the current conditions at the boundary and the description of the characteristic C_-' , itself. Clearly, the transmitted characteristic C_-'' will be correctly found.

The same basic method may be used to incorporate a resistance boundary in the duct into the calculation. For the case of a quarter wave filter, and for multiple branching in general (which would need

to be included to study multi-cylinder engines) extra separate duct sections would be required, resulting in a more complex program.

For all cases, the applicability of the method depends on the one-dimensional approximation, that is L/D>>1. However, the quite good results for the short pipe suggest that the method may still give useful results if L/D is as low as perhaps 4. Of course, this basic limitation will also be true for any other method as each of the lumped and distributed impedance and single pulse methods requires some approximation for what would be a complex two-dimensional unsteady flow in any element for which L/D is not >>1.

5.2 CONCLUSIONS

The use of the method of characteristics, by computing the x - t diagram in the way described in chapter 2, has been shown to be a highly satisfactory means of studying the operation and radiated noise for 2-stroke engine exhaust systems. The method is obviously equally suitable for 4-stroke engines. The method has successfully been used to accurately model both the development of the initial exhaust pulse in an exhaust system and the spectrum of the sound radiated. Of particular merit is the way the method closely follows both wave steepening and the resultant rapid changes in velocity at the tailpipe outlet. Straight pipes of variable length and slowly varying area ducts have both been considered.

It is expected that the method could readily be extended to analyse many muffler systems, for example, those including quarter wave filters and expansion chambers with step changes in area.

This method of exhaust system analysis clearly has advantages over the simple lumped element theory and is an improvement on the distributed impedance model for two reasons. Firstly, wave steepening is correctly allowed for and secondly the precise sound source impedance

is included at all times. The method is also clearly better than the single pulse approach.

Consideration has been given to the similar previous uses of the method of characteristics which studied engine operation, only. These have been found unsuitable for radiated noise studies as very fine resolution of the events at the tailpipe outlet is required. The method developed in this study provides this.

PART II: AN INVESTIGATION OF THE NOISE SOURCES IN A ROTARY LAWNMOWER

INTRODUCTION

The work presented in this section gives details of an investigation of the noise source characteristics of a typical 2-stroke engine rotary lawnmower. This type of machine was initially selected for study because of local community concern about the high noise levels from these machines and correspondingly a local manufacturer's concern to reduce this noise. Initially, a detailed series of experiments was performed to see which of the four basic noise sources, that is, the mechanical, fan or cutter blade, exhaust and inlet noises were significant. It was soon found that the inlet noise was the least significant and this source was not investigated further.

Following these preliminary investigations, each of the basic noise sources was investigated in turn with the intention of finding the precise nature of the noise. Mechanical noise, in particular, was investigated thoroughly. Finally, on the basis of the findings, recommendations are made for design changes. The expected noise reductions to be obtained are given in some cases.

It must now be mentioned that it was not intended to design a quiet lawnmower or to recommend design changes to meet certain proposed and existing legislation, but rather the intention of the study was simply to investigate the noise sources and their characteristics in a general manner. As a result of this, many of the findings are applicable to similar kinds of machinery. Certainly the noise levels from the test lawnmower were studied with legal noise limits in mind, however, this was done mainly to show the magnitude of the problem in this case. The recommendations for design improvements are then not made with any absolute limit in mind for the lawnmower.

CHAPTER 6

NOISE SOURCES ON THE LAWNMOWER

The type of lawnmower used was the Simpson-Pope rotary 2-stroke, pictured in figure (23). A brief list of specifications appears in Appendix 7. This lawnmower is a cheaper variety of the rotary type, with no special noise provisions except an exhaust muffler. This is unlike some models from other manufacturers, which have a partial or complete cover over the engine. The mower is a walk-behind type, that is, it is not self propelled, and the starting is by a pull rope.

6.1 POSSIBLE SOURCES OF NOISE

Preliminary measurements of noise made at the operator position showed that the overall noise level was high and it was the opinion of the operator that the noise was objectionable. At the low engine speed of 2700 r.p.m. the overall sound pressure level was 94 dBA re $2 \times 10^{-5} N/m^2$, whereas at 3400 r.p.m. the level was 98 dBA. In reference (17) it is stated that the 1970 noise control goal for lawnmowers set out by the National Industrial Pollution Control Council of the U.S. Department of Commerce, at the position of the operator, was 92 dBA sound pressure level at a typical high operating speed (about 3400 r.p.m.). Obviously the test engine considerably exceeds this limit.

It is clear that a greater understanding of the lawnmower noise problem was required, and the aim of the project was to provide this. In order that a proper study of the noise making processes could be made, it was first necessary to classify the various noises produced by the mower as being attributable to one of the four main sources listed in table 6.1.

FIG. 23 TEST LAWNMOWER

Table 6.1 : Noise Sources for Rotary Lawnmower

INLET NOISE
EXHAUST NOISE
MECHANICAL NOISE
FAN OR CUTTER BLADE NOISE

The inlet noise is that coming from the air inlet of the engine, the exhaust noise is that coming from the exhaust outlet of the muffler, the fan or cutter blade noise is caused by the passage of the cutter blades through the air, and the mechanical noise includes all remaining sources. Strictly, the mechanical noise should refer to noise radiated from the vibrating parts of the engine, but it includes the fan noise caused by the centrifugal cooling fan which blows cooling air over the cylinder fins. Trivial noise sources such as the cutter blades striking the grass have not been considered.

A detailed investigation was made of mechanical noise, in as much as which of the many components were significant, and results are shown in chapter 7. Detailed studies were also made of the cutter blade noise and the exhaust noise and results are shown in chapters 8 and 9. The investigations of inlet noise were only of a preliminary nature, however. The conclusions reached in chapters 7, 8 and 9 lead to the recommended design changes given in chapter 10.

Results shown in the remainder of this chapter consist of measurements which indicate the comparative significance of the four various sources on the test lawnmower. The measurements given are then compared with those obtained in other studies and the overall levels are compared with existing and projected legal limits. Following this, it is then possible to see generally the nature of the noise problem for the specific test lawnmower.

6.2 MEASUREMENT CONSIDERATIONS

When an investigation of this type is made, one must consider what type of measurement is required. For instance, measurements could relate to the near sound field, in fact at the operator's ear, or the far sound field as noticed by a distant observer. At low frequencies there will be a difference in these two measurements, not simply related to the greater distance, in that sound levels in the near field (closer than a wavelength to the source) are in general not simply related to those radiated in the far field. Also one must consider the possibility of the sound radiation being directional. It was considered that measurements of sound power would be the most useful, as once this is known the sound pressure level may be deduced, assuming no near field effects and no directionality.

Generally, the obtaining of sound power measurements necessitated the use of the reverberation chamber at the University of Adelaide. The determination of sound power in such a chamber will now be briefly considered.

In a reverberation chamber, it is necessary to find the mean square sound pressure level at an adequate number of fixed positions and find the space average thereof. For frequencies well above that corresponding to the lowest order modes of the room, Beranek (reference (1), figure 6.5) shows that with a rotating sound diffuser in a reverberation room, 3 microphones are adequate for an 80% probability of ± 1 dB accuracy. For the measurements described below, a single microphone traversing diagonally across the room was used to achieve space averaging.

When the sound pressure level is measured and the reverberation time recorded, the sound power level may be determined from the following relation (see, for example, reference (1) P. 150):-

$$L_w = \overline{L}_p + 10 \log V - 10 \log T_{60} + 10 \log (1 + \frac{S\lambda}{8V}) - 13.5 \text{ dB} \qquad (6.1)$$

where L_w = sound power level dB re 10^{-12} watt

$\overline{L}_p$ = space average mean square sound pressure level dB re 2×10^{-5} N/m^2

V = volume of test room, less source m^3

T_{60} = reverberation time, with source sec.

λ = wavelength of sound m

S = area of all boundary surfaces in room m^2

Such measurements are valid for $\lambda < \lambda_g$ where

$$\lambda_g = (\frac{V}{4})^{1/3}$$

here $V = 180$ m^3 so that $\lambda_g = 3.56$ m. Corresponding to this λ_g is a frequency of 96 Hz. Measurements above 100 Hz have therefore been regarded as accurate.

Beranek also states (p. 148, reference (1)) that if the source is usually floor mounted, this should be done in the reverberation room and this was done for most measurements, with the lawnmower on the floor of the chamber.

For all measurements the method used to determine the reverberation time was to record the decay of random noise, and then analyse the recording for each $1/3$ octave band.

Some exhaust noise measurements were also made outdoors, that is under free field conditions. It was believed necessary to measure the exhaust noise in this way, so that the level at the first harmonic (at a frequency of typically 50 Hz) could be determined accurately. If the radiation is omnidirectional, under these conditions (as expected for exhaust noise), a value of sound power may be determined. For hemispherical radiation of sound, in a free field, the sound pressure

level and sound power level are related by the following equation, as is well known:-

$$L_w = L_p + 20 \log r + 8 \text{ dB} \qquad (6.2)$$

where r = distance to source m

In order to obtain meaningful noise measurements two engine speeds were chosen for a full series of tests: 2700 r.p.m. and 4000 r.p.m. The former engine speed was considered to be a typical low operating speed and the latter was considered as the maximum operating speed to be used. Some measurements were also made at 3400 r.p.m. In reference (18), in which contributions from the various noise sources were also investigated, the only mention of engine speed is in relation to the measurement of cutter blade noise, when 3600 r.p.m. was used. In reference (17) it is stated that for tests relating to U.S. noise legislation, the speed used should be the one giving the highest noise level in normal high speed operation. Speeds used in tests referred to in reference (17) vary from 3200 to 3600 r.p.m., so that for the test mower some noise levels at 3400 r.p.m. are interpolated between the measured values at 2700 and 4000 r.p.m. for comparison.

Comment should be made, also, on the S.A.E. test procedure referred to in reference (17), as of necessity there are major differences between the S.A.E. procedure and the measurement methods used in this study. The S.A.E. method was not used for this study as the main concern was with the noise contributions from the various sources rather than the overall level. The S.A.E. procedure calls for a free field test in which the sound source traverses a path 23 feet (7m) from a microphone, with a ground covering of synthetic turf (for uniformity) between the source and the microphone. Rudd and Bender (17) state that ± 3 dBA variation is noticed with different types

of ground surface. In all tests done in this study, so that no errors would arise from using different surfaces, hard ground surfaces were used, both outdoors and in the reverberation chamber.

So that the measurements shown in later sections of this chapter may be seen in relation to proposed legal noise limits, some description of these limits is now given.

Proposed noise legislation for South Australia, taken from current Tasmanian legislation (see reference (19)), allows 77 dBA sound pressure level for power lawnmowers, measured at a distance of 7.5 meters. This then, for omnidirectional sources, corresponds to 102.5 dBA sound power. This legislation closely follows current U.S. legislation as described in reference (17). For example, for lawnmowers manufactured after 1st January 1975 the Chicago City Ordinance level at 23 feet (7 metres) was 77 dBA sound pressure level, and after 1st January 1978 the level was 72 dBA. It is possible that noise legislation in various countries differs slightly from the American and the proposed South Australian legislation, so that care must be exercised in interpreting results given in this study.

6.3 RESULTS OF MEASUREMENTS

Before detailed investigations of each of the four noise sources listed in table 6.1 were made, it was necessary to determine the contribution that each made to the total sound power radiated. It was mentioned earlier how the reverberation room was used. The general measurement technique consisted of isolating each noise source in turn in the reverberation room and measuring the sound power at several speeds. For mechanical noise, inlet noise and cutter blade noise it was anticipated that variations of noise with the regularity of the engine firing would be small, and in fact this was found to be the case. However, while the noise from these sources was steady and unrelated to whether

* If the engine fired on every 2nd revolution with the same peak cylinder pressure as when firing continuously, the sound power is halved, that is, 3dB less. As the engine fired even less often the total effect was roughly approximated by subtracting 4.5dB.

the engine fired on each revolution, the exhaust noise varied greatly. Therefore, the way in which the overall level of exhaust noise was determined must now be considered.

6.3.1 Exhaust Noise Measurement

In normal operation, when not actually cutting grass, the engine does not fire on every revolution, although, of course, it does when under load and cutting thick grass. For this study it was considered that the exhaust noise coming from the muffler outlet with the engine running with no load would effectively describe the exhaust noise from a lawnmower in typical use. As a study was made of the muffler action (see chapter 9), thereby requiring regular firing of the engine, measurements which were made at 2700 and 3400 r.p.m. were, in fact, obtained with a load on the engine. Therefore, to obtain a value for the exhaust noise radiated by the engine when it fires less often than even every second revolution, 4.5 dB was subtracted from the measured value obtained with load.*

To then obtain the total sound power radiated from the muffler outlet at 2700 and 3400 r.p.m., it was considered preferable to take free field measurements as the level at the first harmonic (at 50 Hz for 3000 r.p.m.) could then be accurately obtained, and as problems with exhaust fumes might be avoided. All noise sources apart from the exhaust were silenced by using a very effective acoustic cover, with the muffler placed on the end of a short pipe which just protruded through the cover. Due to experimental difficulties at the higher engine speed of 4000 r.p.m., however, a similar measurement could not be obtained. An exhaust noise measurement at 4000 r.p.m. was subsequently made by running the engine in the reverberation chamber. For this experiment the inlet noise was piped out, the cutter blades were removed and the mechanical noise was minimised by placing the engine on an isolated space frame. Therefore only the mechanical noise from the basic engine was included

in this measurement. No load was used on the engine.

6.3.2 Sound Power from Different Sources on Lawnmower

As mentioned above, the inlet, mechanical and cutter blade noises were each measured separately in the reverberation chamber.

The inlet noise was obtained by running the engine outside the chamber and by piping the inlet noise through the walls into the chamber. The mechanical noise was obtained with the engine running inside the chamber but with the inlet and exhaust taken outside using flexible pipes (cutter blades removed for this test). For each of the mechanical and inlet noises no load was used on the engine as these noises were found to be largely independent of load. To determine the cutter blade noise, a very quiet electric motor was used to drive the blades in their normal housing. Finally, the exhaust noise was determined as described above.

The results obtained for the test lawnmower are presented in table 6.2 together with those quoted by Rudd and Bender (17) and as obtained by Sperry and Sanders (18). Results for the test lawnmower are linear, as are those of Sperry and Sanders, whereas those from Rudd and Bender are A-weighted. In table 6.2 the value for the mechanical noise at 3400 r.p.m. for the test lawnmower is interpolated between measurements at 2700 and 4000 r.p.m. All other values are from actual measurements.

Even considering that the results quoted in reference (17) are A-weighted, it is clear that the test mower is significantly noisier for each source considered. The cutter blade noise and mechanical noise will later be shown (see figures (24)(a) and (b)) to peak in the mid-frequency region, where the A-weighting has little effect. Therefore from the levels given in table 6.2, using figures (24)(a) and (b) as well, the mechanical and cutter blade noises for the test mower may be shown

Table 6.2 : Levels of Noise from Different Sources

(sound power re 10^{-12} watt)

	TEST MOWER	TEST MOWER	TEST MOWER	FROM(18)	FROM(17)
source	2700 r.p.m.	3400	4000	3600	3400
INLET	88dB(linear)	-	-	86.5dB(linear)	- dBA
EXHAUST	102	103	104	100.5	97.5
MECHANICAL	96	99	102	95.5	92.5
FAN OR CUTTER BLADE	101	106	110	94.5	97.5
COMPUTED TOTAL	105.2	108.3	111.5	102.4	101.5

to be about 6 dB greater than those reported by Rudd and Bender (17) (see table 6.3).

A direct comparison may be made between the results from the test mower and the results of Sperry and Sanders (18), which refer to a Briggs and Stratton Corporation model 6B-HS four-stroke mower. For each of the inlet, exhaust and mechanical noises the test mower is about 2 to 3 dB noisier, but for cutter blade noise the test mower is over 11 dB noisier. However, in reference (18) it is stated that all the measurements were taken with the mower on a simulated grass surface, so that the true differences will be somewhat less. In addition, it is implied in reference (18) that the measurements of cutter blade noise were taken when the blade system was not enclosed in the mower housing. For reasons mentioned in chapter 8 it is certain that this method underestimated the cutter blade noise by at least several dB.

It is concluded, therefore, that the test mower produces a moderately higher level of noise than indicated in the other two studies,

when overall levels are considered. Much of this may be attributed to the noise from the cutter blades.

6.3.3 Narrow Band Spectra

As a preliminary to more detailed measurements of the various noise sources on the test lawnmower, it is interesting to look at the spectra of sound power radiated from the different sources at both 2700 r.p.m. and 4000 r.p.m.

The exhaust noise spectrum at 2700 r.p.m. is obtained from the free field measurement, which was recorded when a load was placed on the engine. As mentioned in section 6.3.1, so that the overall level would approximate that from a lightly loaded engine, 4.5 dB was subtracted across the whole measured spectrum to obtain the spectrum shown in figure (24)(a). The exhaust noise spectrum for 4000 r.p.m. is taken directly from the reverberation room measurement described in section 6.3.1. This spectrum then consists of a composite of the exhaust noise and the mechanical noise from the bare engine. By comparison with the mechanical noise spectrum alone it is clear for which frequencies the exhaust noise is greater.

The spectra of sound power for all the other sources are obtained from the reverberation room measurements. In all cases, the necessary corrections have been made for the different reverberation times and the different microphones used.

The narrow band spectra of the different sources, adjusted to read sound power in dB re 10^{-12} watts, are shown in figure (24)(a) for 2700 r.p.m. and in figure (24)(b) for 4000 r.p.m. The filter used was a B & K type 2107, set to a constant 6% bandwidth. As such, the spectra must be interpreted carefully, as the exhaust noise, for example, is composed of harmonic peaks, with very little noise between these peaks, as was shown in chapter 1. The filter bandwidth gives the false

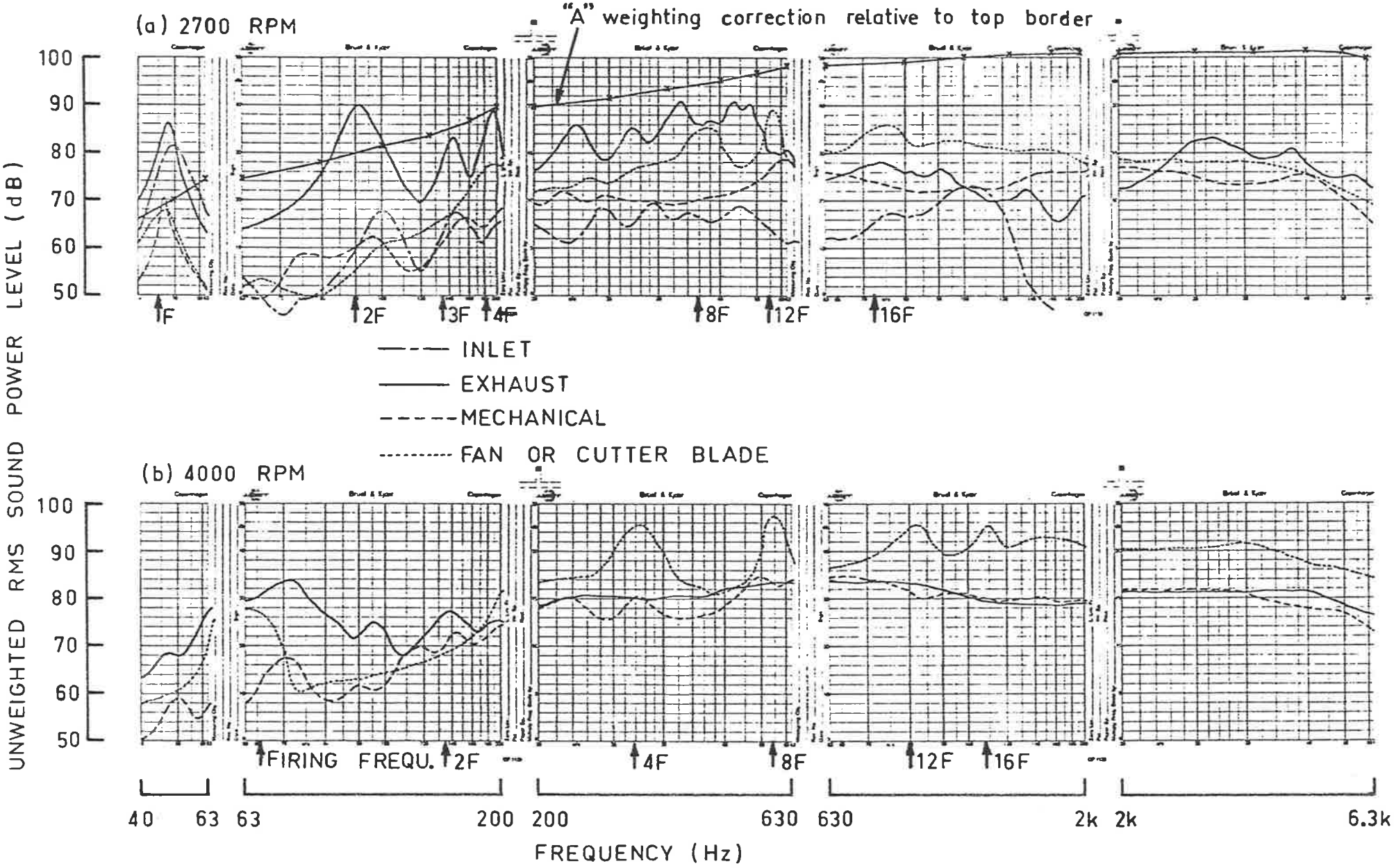

FIG. 24 NARROW BAND SPECTRA OF NOISE SOURCES ON LAWNMOWER

impression of high levels between such peaks. Also, with a 6% bandwidth filter it is not possible to distinguish beyond about ten harmonics, so that broad band noise is not necessarily indicated by a flat mid and high frequency spectrum.

Both figures (24)(a) and (b) give linear measurements, which do not represent the way the human ear hears the noise. It is preferable to refer to the A-weighting scale, which approximates the response of the human ear to sound levels such as an observer (or operator) would be subjected to. The necessary correction to obtain an A-weighted profile is taken from reference (1), table 4.1, and is shown in figure (24)(a) displayed about the uppermost border of the trace. It is left to the reader to make a mental subtraction.

On the A-scale, at 2700 r.p.m., the cutter blade noise is the major source, but with the exhaust noise dominating in the regions up to 500 Hz and above 2.5 kHz.

At 4000 r.p.m. the levels of all noise sources have increased considerably, however, the cutter blade noise has gone up about 10 dB and dominates the A-weighted spectrum. At this speed the levels of exhaust noise (which included the mechanical noise from the bare engine) and mechanical noise are very similar, for some regions. This suggests that possibly the mechanical noise was greater than the exhaust noise for these frequencies.

These results differ slightly from those of Clark and Williams (20) in which the mechanical noise dominated from 500 Hz to 10 kHz and muffled exhaust noise from 25 Hz to 500 Hz. However, if the test lawnmower had less cutter blade noise the results would be roughly similar.

A similar comparison may be made between the results for the test mower and the results of Sperry and Sanders (18). Their measure-

ments showed a much lower (by about 10 dB) cutter blade noise, and had exhaust noise dominant to 500 Hz and mechanical noise dominant above 500 Hz.

6.4 NOISE REDUCTION REQUIREMENTS

Preliminary remarks relating to the noise reduction requirements will now be made so that the magnitude of the problem of reducing the noise from the different sources on the lawnmower to acceptable levels will be clear. Below, only a rough guide to the specific reductions required for the individual noise sources will be given, however, as this work is more concerned with the general investigation of the noise source characteristics than in designing a lawnmower to meet certain regulations.

For the purposes of briefly assessing the noise reduction required to meet the proposed local legislation, the S.A.E. measurement method (see reference (17)) is assumed to apply. A test speed of 3400 r.p.m., and part load conditions are also assumed.

Table 6.2 gives unweighted sound power levels. By now applying A-weighting corrections to the linear spectra of figures (24)(a) and (b), from the values in table 6.2 the following A-weighted overall levels are estimated (table 6.3). The measurements of Rudd and Bender are again included for comparison.

It is clear from table 6.3 that the mower as tested will need a noise reduction of at least 3.5 dBA, corresponding to a test on a hard surface, to achieve the proposed South Australian limit of 102.5 dBA at 3400 r.p.m. Even if the cutter blade noise is entirely eliminated, it may be seen that the remaining mechanical and exhaust noise totals 102.3 dBA. Therefore, the minimum requirement to meet this legislation, is a significant reduction in both cutter blade noise and exhaust noise.

Table 6.3 : Levels of Noise from Different Sources

(sound power re 10^{-12} watt, A-weighted)

	TEST MOWER	TEST MOWER	TEST MOWER	FROM(17)
source	2700r.p.m.	3400	4000	3400
INLET	80dBA	-	-	-
EXHAUST	98	100	102	97.5
MECHANICAL	96	98.5	101	92.5
FAN OR CUTTER BLADE	99	103.5	108	97.5
COMPUTED TOTAL	102.6	105.9	109.7	101.5

Of course, to meet the 1978 Chicago City Ordinance limit, which is 5 dB lower than the local limit, the overall reduction required is at least 8.5 dB. This would require the noise levels from all sources on the test lawnmower to be significantly reduced.

6.5 NOISE REDUCTION METHODS

Chapters 7, 8 and 9 on mechanical noise, cutter blade noise and exhaust noise cover detailed investigations of these noise sources and Chapter 10 shows possible methods of noise reduction, however, it is now useful to briefly look at past attempts at lawnmower noise reduction. Rudd and Bender (17) considered the benefit to be gained using currently known noise reduction techniques and the expected cost involved. The noise reduction techniques they suggest are:-

1. using the best available muffler
2. reducing engine speed by 500 r.p.m.

3. using an acoustic engine enclosure and isolating the engine from the base frame
4. using the best available quiet cutting blade.

These solutions are generally expensive and have rarely, to date, been used. The reason is doubtless the cost and/or the unacceptable compromise of either performance or maintainability. It was believed, therefore, that a more fundamental understanding of the noise making processes could lead to solutions which reduced the generation of noise at the sources. This was the motivation for the work described in the following chapters.

CHAPTER 7

MECHANICAL NOISE

7.1 SIGNIFICANCE OF MECHANICAL NOISE

For the test lawnmower, the mechanical noise was shown in chapter 6 to be less significant than the exhaust and cutter blade noise, although on the A scale at 3400 r.p.m., it is only 1.5 dB less than the exhaust noise. It was shown from table 6.3 that to meet the proposed South Australian legal limit, a reduction of several dB in mechanical noise would probably be required. In fact, if the cutter blade noise is reduced significantly and the exhaust noise reduced by 2-3 dB , then mechanical noise would dominate. In the sound power spectra shown in figures (24)(a) and (b), it is clear that to reduce the mechanical noise overall, a reduction in the range from 500 Hz to 5 kHz is required.

As the mechanical noise then needs to be reduced by several (about 3) dB in the region 500 Hz to 5 kHz to meet the proposed local limit, it may seem appropriate to use a cover over the engine, lined with absorbent material. However, this approach assumes that mechanical noise cannot otherwise be reduced and also ignores the possibility of more restrictive legislation. A machine cover is an added complexity to be avoided if possible, as engine cooling must be provided for, and ready maintenance would be difficult. So that more might be understood about mechanical noise, a detailed study was made of the possible sources of radiation and the causes of excitation. It is expected that the findings shown below would relate to many similar types of machinery with small petrol engines.

7.2 POSSIBLE SOURCES OF MECHANICAL NOISE

There is a number of possible sources on the lawnmower from which sound classified as mechanical noise may radiate. The basic engine consists of the two halves of the crankcase, together with the cylinder and head (see figure (23)). Each of these parts may be a significant contributor and so may be the cooling fins, which are integral with the cylinder and head. The engine is bolted to the base frame, which is a large sheet metal covering over the cutter blades; it clearly contributes to the noise. Attached to the crankshaft under the base frame, is the cutter blade mounting plate, which is another large surface made of sheet metal which may again radiate significant noise. Attached to the top of the crankshaft, under the small engine cover, is the combination flywheel - magneto - cooling fan. This may produce noise from its fan action as it blows cooling air over the engine fins. The small engine cover itself may be a source of noise. The lawnmower has an optional grass catching attachment, but this was not used on any of the tests and is not shown in figure (23).

It is unlikely that any other part of the mower would contribute to the mechanical noise, so the possible sources to be investigated are as listed below in table 7.1.

Table 7.1 : Possible Mechanical Noise Sources on Lawnmower

1. crankcase, cylinder and head (basic engine)
2. cooling fins
3. base frame
4. cutter blade mounting plate
5. engine cover
6. flywheel - magneto - fan.

Before the significance of the above sources is discussed it is first necessary to consider the causes of the excitation which set the mower into vibration. The importance of the noise sources listed in table 7.1 is considered in section 7.7.

7.3 POSSIBLE CAUSES OF EXCITATION

The vibration of the engine may be considered to be the response of the structure to various exciting forces. If the sources of the excitations may be identified, there is the possibility of reducing the mechanical noise at the point of excitation.

In all, there are four possible sources of excitation, and these are shown listed in table 7.2 and are described in the following sections. It will be shown in section 7.4 that impact noise is the most significant.

Table 7.2 : Possible Sources of Mechanical Excitation

1. gas pressure force
2. inertia forces from reciprocating motion
3. impact noise
4. bearing noise.

7.3.1 Gas Pressure Force

In an internal combustion engine an obvious source of fluctuating forces is from the gas pressure force, exerted by the compressed and ignited charge of gas contained in the cylinder. The lawnmower engine has crankcase compression as well, caused by the underside of the piston, but this will not be as great as that occurring above the piston, because of the higher compression ratio and the increase in pressure on the firing of the charge. The gas pressure force will act on the cylinder walls, on the cylinder head and, through the connecting rod,

on the main bearings. It has been shown (reference (21)) that the main source of vibration from this force is through the big end bearing of the connecting rod. The cylinder pressure, over one engine cycle, acting on the piston area then constitutes the gas pressure force, and examples of the cylinder pressure are shown in figure (25). Figure (25)(a) shows a pressure measurement for a typical load setting of the lawnmower engine, with timing markings showing T.D.C., E.P.O., B.D.C. and E.P.C. Figure (25)(b) shows a pressure measurement for a very heavy load on the engine and figure (25)(c) shows a non-firing compression followed by a firing stroke. Figure (25)(c) is typical of the normal part load operation of the engine.

The cylinder pressure diagrams in figure (25), which relate directly to the gas pressure force, may be Fourier analysed to give a spectrum of harmonics covering the audio range. An example of such a spectrum is shown in figure (26), which is derived from the pressure trace in figure (25)(b), and is taken to the 20th harmonic. Such spectra show high levels of pressure at low harmonics and decreasing levels at successively higher harmonics, extending through the whole audio range (see references (21), (22) and (23)).

7.3.2 Inertia Forces from Reciprocating Motion

Another possible source of excitation of the structure is from the inertia forces related to the unbalanced reciprocating mechanism.

The reciprocating motion of the piston is not purely sinusoidal, and this may be seen from figure (27) by considering the piston displacement, x. The piston displacement may be expressed in terms of the crank angle, θ, and the con-rod angle, ϕ, and this is done in equation (7.1). This kind of analysis is as described, for example, in chapters 11 and 12 of reference (24).

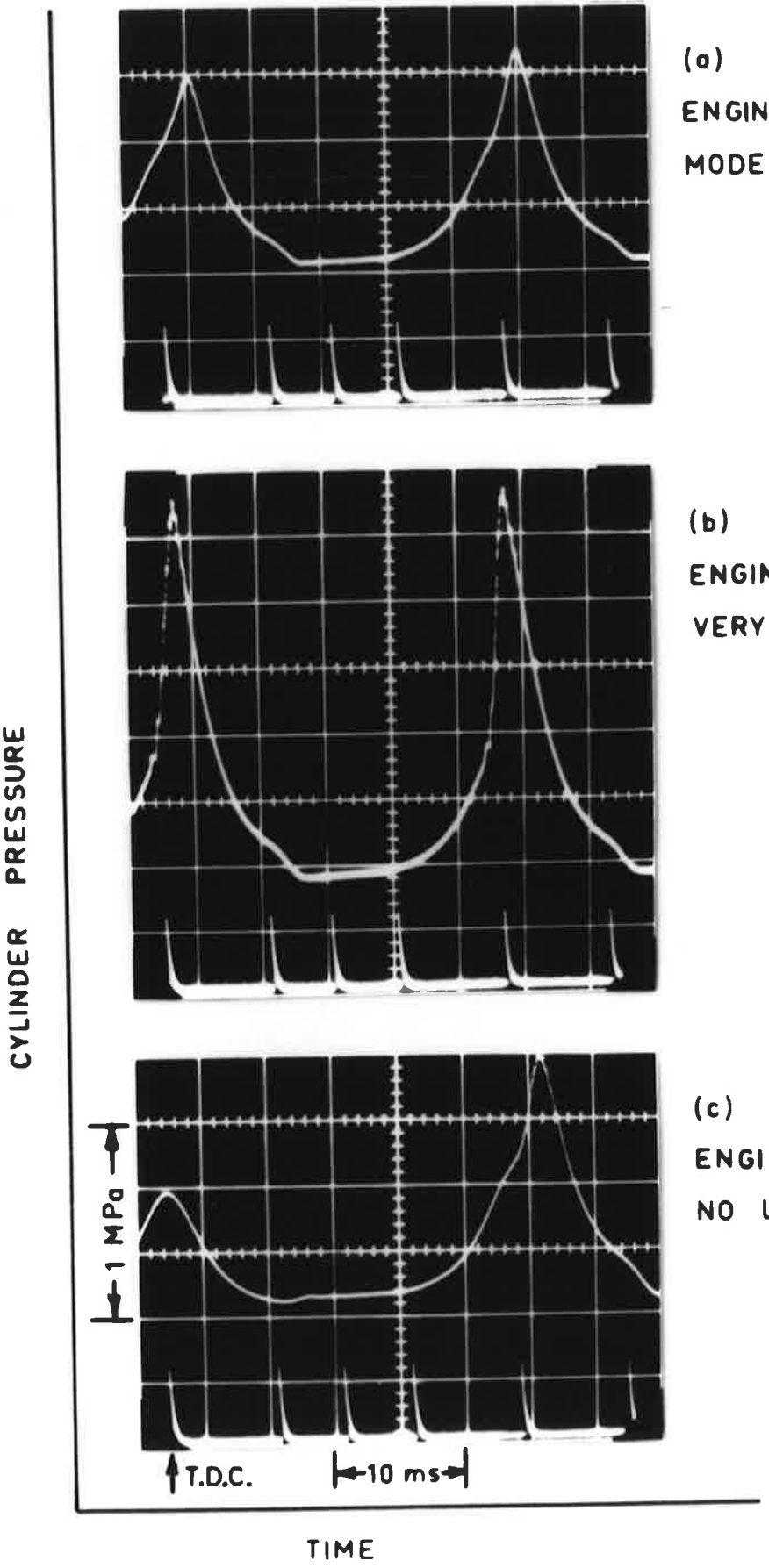

FIG. 25 CYLINDER PRESSURE MEASUREMENTS

Derived from trace (b) of Fig. 25

Values shown are harmonics

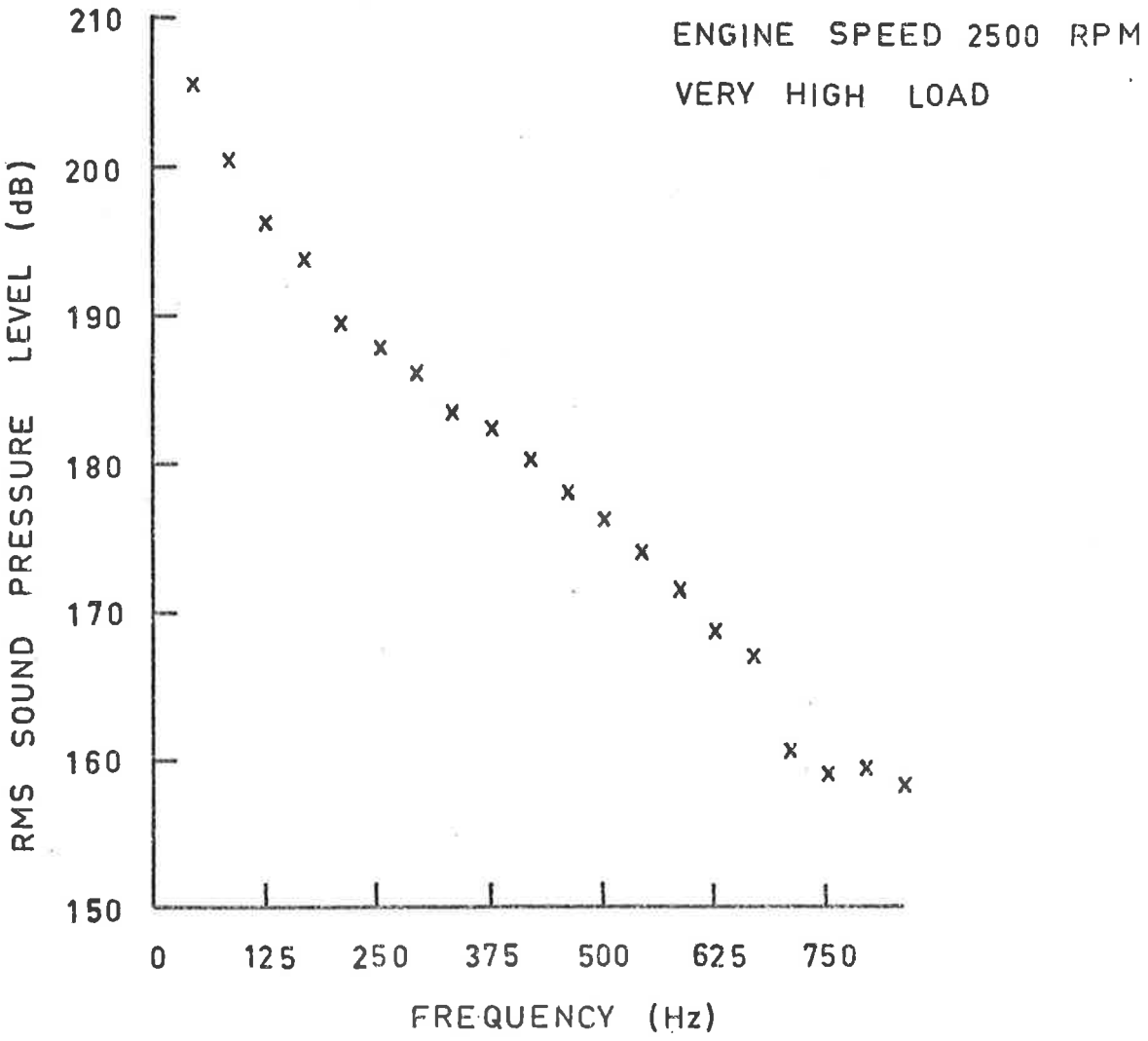

FIG. 26 CYLINDER PRESSURE SPECTRUM

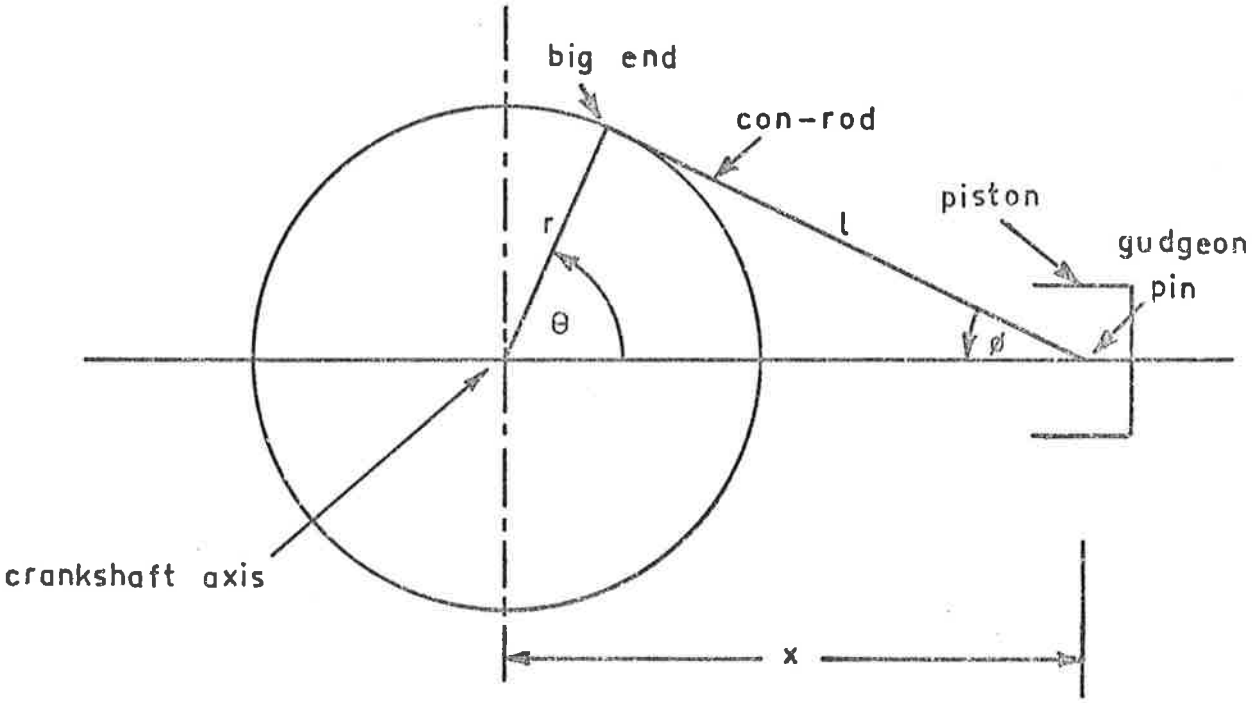

FIG. 27 SLIDER - CRANK MECHANISM

$$x = r\cos\theta + \ell\cos\phi \tag{7.1}$$

ϕ may be expressed in terms of θ

$$\cos\phi = [1 - q^2\sin^2\theta]^{\frac{1}{2}} \tag{7.2}$$

where r = crank radius

ℓ = con-rod length

$q = r/\ell$ con-rod obliquity

θ = crank angle

ϕ = con-rod angle.

Using equations (7.1) and (7.2) the piston displacement x may be expressed by an expansion series in $\sin\theta$ terms. This expansion series leads to an expression for piston acceleration d^2x/dt^2, from which a series of harmonics of the inertia force exerted at the gudgeon pin may be found. The series derived for the acceleration is in terms of harmonics of the crank angle θ, that is, in terms of $\cos\theta$, $\cos2\theta$, $\cos4\theta$, $\cos6\theta$, etc. For piston acceleration only even terms after $\cos\theta$ appear. The eighth harmonic, for example, which corresponds to 334 Hz for 2500 r.p.m. is shown below.

$$a = -\omega^2 r\left(\frac{64}{q}\left[\frac{5q^8}{2^{14}} + \frac{5.7q^{10}}{2^{16}} + ...\right]\cos8\theta\right) \tag{7.3}$$

where a = 8th component of piston acceleration

ω = speed of rotation of crankshaft.

From this, the force exerted at the gudgeon pin by the piston mass may be found, and similar forces will act on the crankshaft and cylinder sides when the inertia of the con-rod is considered. The inertia forces related to the reciprocating mechanism may obviously be calculated accurately and, for a fixed engine speed, the forces are, of course, not related to the engine load.

7.3.3 Impact Noise

In order that an engine may operate, the parts which move in relation to each other must have adequate clearances at the locations of relative motion. Regardless of the surface layer of lubricant covering all parts, when forces reverse or change direction, parts which have relative motion will move to take up the clearances between them. The resulting impact, from the relative motion across such a clearance, causes what is referred to as impact noise.

The conventional reciprocating internal combustion engine has clearances between the piston and cylinder, at the small end of the con-rod (gudgeon pin), at the big end of the con-rod and at the crankshaft bearings. It is unlikely that significant impacts occur at either the crankshaft bearings or the gudgeon pin (very small clearance here), so that these two possibilities will be disregarded. However, the occurrence of big end knock (big end impact) and piston slap (piston impact on cylinder) will be considered in detail. In the sections that follow, an "axial" direction is parallel to the line of the piston reciprocating motion, and a "sideways" direction is perpendicular to the cylinder wall.

Big End Knock

From a consideration of the slider-crank motion, as shown in figure (27), it may be seen that there are a number of forces acting at the big end. These are from: the gas pressure force on the piston (axial), the inertia force of the piston and gudgeon pin (axial) and the inertia force from the motion of the con-rod (axial and sideways).

It may be shown (using the analysis of section 7.3.2) that the magnitudes of the inertia forces, from the motion of the piston and gudgeon pin and also from the axial motion of the con-rod, have maxima at T.D.C. and B.D.C. and change sign (pass zero) at about 90° after

T.D.C. and B.D.C. However, for the inertia forces from the sideways motion and the rotation of the con-rod, the events are offset by 90°.

In general, if either the sideways inertia force, or the resultant axial force, at the big end, is relatively large while the other changes sign, there is little possibility of big end knock. This is shown by figure (28)(a), in which one component force changes sign while the other is large, and the relative movement is small compared to the diametral clearance. (The big end bearing on the test lawnmower engine is actually a roller type, however, the above is still true). If, however, one force changes sign while the other is relatively small, big end knock may occur, as shown in figure (28)(b). As the axial forces are usually much larger than the sideways forces, big end knock may then occur whenever the resultant axial force changes sign. Also, as the con-rod rocking force (sideways and rotation forces) changes sign at T.D.C. and B.D.C., big end knock may only occur, from this change of force, at T.D.C. when the gas pressure and inertia forces, by chance, balance.

Piston Slap

Piston slap occurs when the resultant sideways force on the piston changes sign, making the piston move to, and hit, the other side of the cylinder. The resultant sideways force on the piston consists of a component from the con-rod rocking motion, and the sideways component from the resultant axial piston force, caused by the con-rod inclination.

When the angle of the con-rod inclination, ϕ, shown in figure (27), changes sign as the engine passes T.D.C. and B.D.C., the sideways component of the force on the piston due to a compressive or tensile force in the connecting rod (required to balance the axial forces) also changes sign. It is clear too that the sideways force

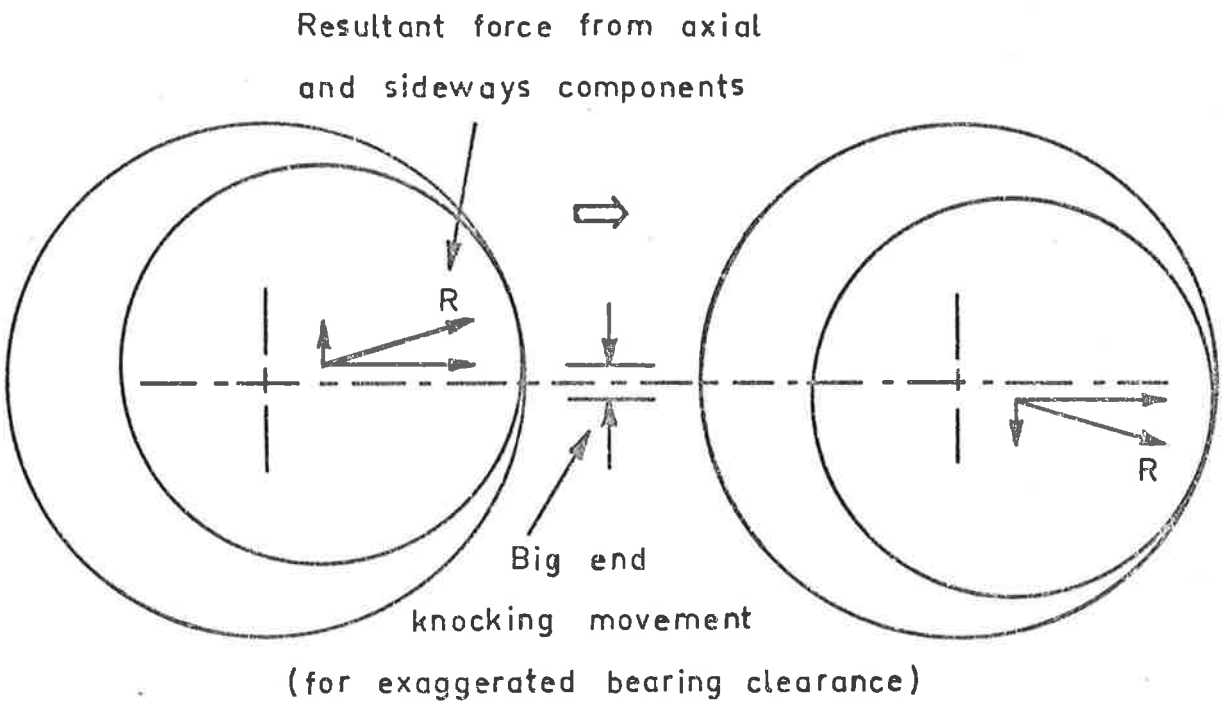

(a) WHEN CONSTANT FORCE COMPONENT IS LARGE

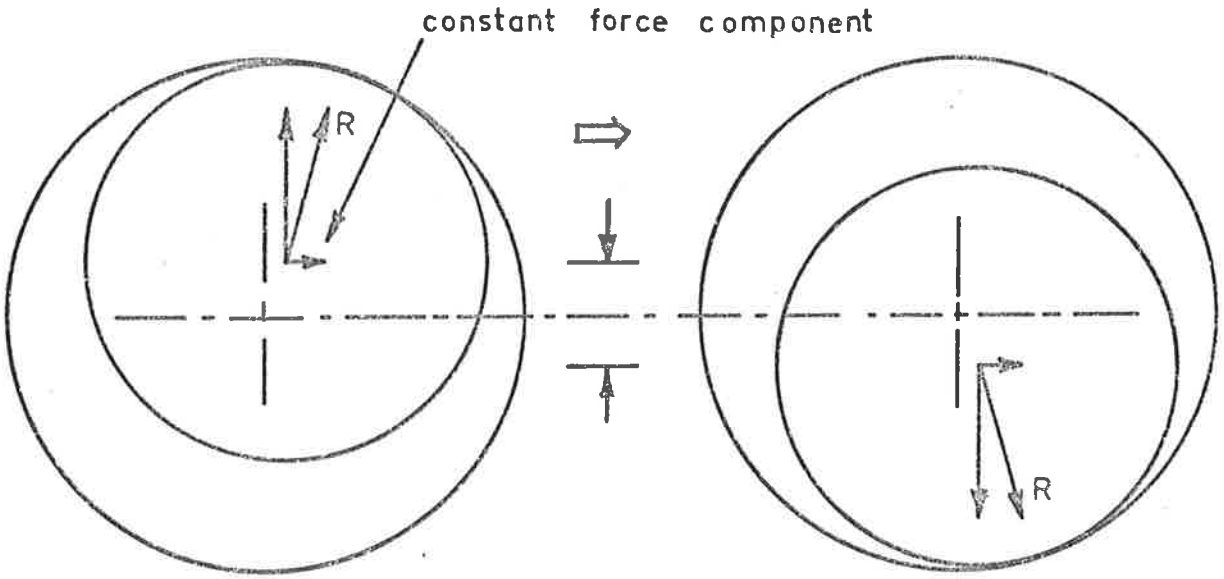

(b) WHEN CONSTANT FORCE COMPONENT IS SMALL

FIG. 28 BIG END KNOCK

on the piston due to the inertia of the con-rod against the rocking motion also changes sign at T.D.C. and B.D.C., so that, as both force components will rarely be equal and opposite, piston slap will occur. In fact, the sideways force resulting from the balance of the axial forces on the piston will almost always be far larger than the force due to the rocking motion of the con-rod, so that the former may be considered as the sole cause of the piston slap. This form of piston slap, resulting basically from a constant axial force and changing con-rod angle, will be referred to as type 1. Various forms of piston slap type 1 are shown in figure (29).

At positions other than T.D.C. and B.D.C., that is, for any θ of the crankshaft other than zero or π, the resultant sideways force on the piston will also change sign if the resultant axial force changes sign. For the lawnmower engine, the only part of the engine cycle for which this is possible is on the compression stroke. This may be explained simply.

Measurements and calculations (see table 7.3) show that for all practical engine speeds at T.D.C. the gas pressure force is always larger than the opposing piston inertia force. The piston is then forced downwards. At 90° after T.D.C., at which time the gas pressure force is still large, the inertia force changes sign and thereafter acts in the same direction as the gas pressure force (downwards). At 90° before T.D.C. the piston inertia force changes sign again (to act upwards), but as the gas pressure force is then very small, the resultant axial force changes sign. The resulting piston slap from this cause will be referred to as type 2.

In the rare event of the resultant axial force being zero at T.D.C., piston slap will result, as at this point the con-rod rocking force changes sign.

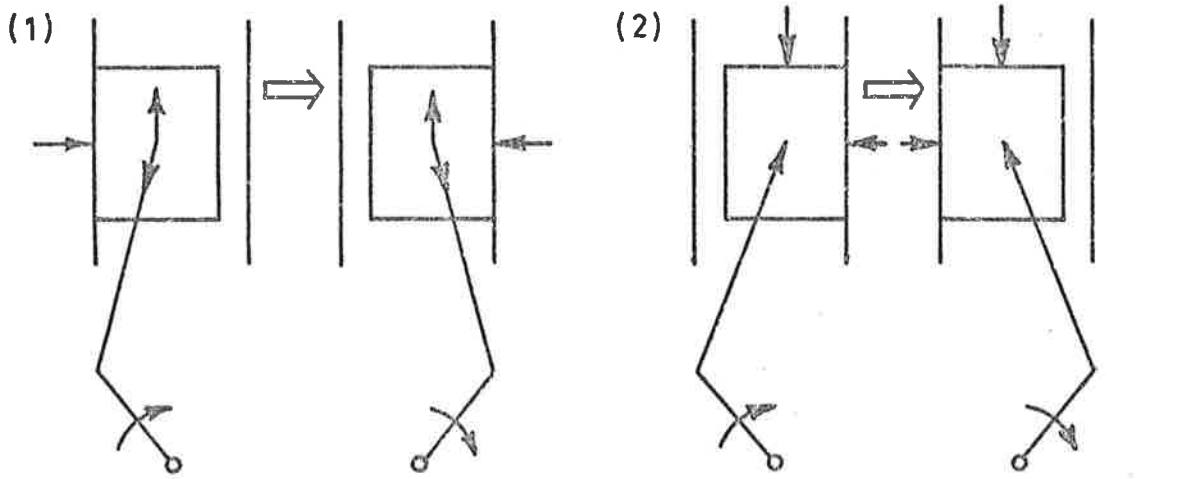

INERTIA FORCE DOMINANT NEAR T.D.C., SHOWING BALANCE OF FORCES

GAS PRESSURE FORCE DOMINANT NEAR T.D.C.

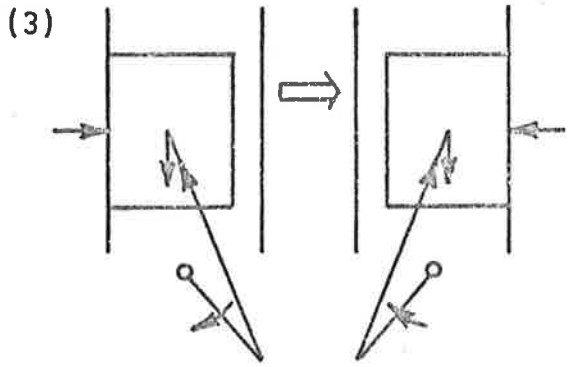

INERTIA FORCE DOMINANT NEAR B.D.C.

FIG. 29 PISTON SLAP TYPE 1

7.3.4 Bearing Noise

The final source of excitation is the vibration of the structure caused by the engine bearings. Such vibration is that associated with the operation of ball and roller bearings caused by the rotation of the balls or rollers in their housings. The lawnmower engine has a roller type big end bearing and also has roller type bearings in both the upper and lower crankcase halves, to locate the crankshaft.

7.4 SIGNIFICANCE OF CAUSES OF EXCITATION

Gas Pressure Force

Grover and Lalor (22) state that for small diesel engines, the gas pressure force is the main exciting force for the mechanical noise. However, for the lawnmower engine, the cylinder pressures are much lower (150 psia as against 1000 psia), so that the gas pressure force may not be the most important. Also the rate of pressure rise during the burning of the charge is much less for a petrol engine, than for a diesel engine (reference (22)), so that again it seems likely that the gas pressure force is not dominant.

It has been found (references (21), (22) and (23)) that at constant speed the levels of the harmonics of cylinder pressure spectra in the range from about 300 Hz and above are determined by the rates of pressure rise on ignition, so that if the mechanical noise is pressure dependent, a significant rise would be expected with a faster rising pulse. In figure (25) it may be seen that the rate of pressure rise does vary with load, however, in measurements of a preliminary nature no increase in mechanical noise was observed with increasing load. The mechanical noise, in fact, was observed to be remarkably constant, in that it did not fluctuate with the intermittent firing of the engine. Figure (25)(c) shows cylinder pressures for a non-firing stroke followed by a firing stroke, and in fact, during light

load running typical of the lawnmower not cutting grass, the non-firing strokes were more frequent. If the gas pressure force is significant, for the mechanical noise to remain constant during such uneven running, the damping of the vibrational modes would have to be very small. This may be demonstrated by a simple example.

For a vibration to decay noticeably in one engine revolution, the amplitude must be halved (say). For a speed of 3000 r.p.m. there are 20 milli secs/rev and at 2000 Hz there is ½ milli sec/cycle, giving 40 cycles at 2 kHz per engine rev.

The logarithmic decrement, Λ, for decay is given by:-

$$\Lambda = \ell n \frac{A_n}{A_{n+1}}$$

$$= \frac{\pi}{Q} \qquad (7.4)$$

from P. 196 reference (25) where

A_n = maximum excursion for reference cycle

A_{n+1} = maximum excursion for following cycle

Q = quality factor

Therefore, from equations (7.4), for the amplitude at 2 kHz to be halved in one revolution, $Q = 182$. Actual measurements taken from the engine, for vibration at about 2 kHz (taken from figures (30)(b) and (c)) reveal a quality factor Q of about 60, which is small enough to cause a noticeable decrease in vibration in one revolution.

In light of this and the earlier evidence, it is very unlikely that the gas pressure force is the main cause of the excitation.

Inertia Forces from Reciprocating Motion

For reasons given above, it is unlikely that the gas pressure

force is the most significant source of the excitation. From the analysis given in section 7.3.2, the relative magnitudes of the gas pressure force and the inertia force may now easily be seen.

Using equation (7.3), the 8th harmonic of the inertia force exerted at the gudgeon pin by the motion of the piston, may be found. For the lawnmower engine, at 2500 r.p.m., this force is 4×10^{-4} N. This may now be compared with the 8th harmonic of cylinder pressure force. Assuming the corresponding pressure level to be 172 dB (from a cylinder pressure spectrum corresponding to a light load), a cylinder pressure force of 16 N is obtained. Obviously, even for a very light load (low pressure) and high engine speed (high piston acceleration) the gas pressure force is far larger at the 8th harmonic (334 Hz at 2500 r.p.m.). It is not likely that the situation will be different for higher frequencies as the inertia terms become smaller as well as the gas pressure terms. Therefore, it is clear that the inertia forces caused by the reciprocating motion will have no relation to the radiated mechanical noise.

Impact Noise

It was originally believed that the main source of the excitation was either the gas pressure force or the impact noise. As described below, it was easily shown that the impact noise was by far the more significant of the two, and, in fact, was responsible for almost all the mechanical noise.

The gas pressure force excitation of the structure, caused by the rapid pressure rise on ignition, is further shown in the following simple experiment to have no relation to the mechanical noise. An accelerometer (B & K type 4329) was firmly attached (screwed) to the engine crankcase and a pressure transducer (Kistler sparkplug type) was placed in the engine cylinder. The engine was run with

various loads and the outputs from the pressure transducer and the accelerometer were observed on a dual beam oscilloscope. A number of the oscilloscope traces so obtained are shown in figure (30). It may be noted here that only traces (30)(a), (d), (h) and (i) were obtained with a load on the engine. A typical measurement with load, shown in figure (30)(a) clearly shows that there is no relation between engine firing and the mechanical excitation. In fact the excitation mainly comes in bursts which are obviously related to impacts. This is vastly different from the situation for an automotive diesel engine (reference (22)) in which the gas pressure force is dominant and piston slap is of secondary importance.

As will be shown in section 7.5.2, for the test engine, the impacts are caused by piston slap. This has considerable significance, as the gas pressure cycle is then rather irrelevant, and special designs to slow down the burning of the charge would be totally useless. The dominance of piston slap for the lawnmower engine is no doubt partly due to the relatively large clearance between the piston and the cylinder (0.007 inches or 0.18 mm). This clearance is typical for small two and four stroke engines that are not particularly designed for high performance nor specially designed to have small clearances. For other such engines, therefore, piston slap is also likely to be dominant.

Bearing Noise

The experiments with the accelerometer and pressure transducer, mentioned above, show that the impacts are the dominant sources of excitation, however, they also show that there is possibly a background level of vibration caused by the bearings at high engine r.p.m. This may be interpreted from figures (30)(a) and (d) for example. It is expected that the big end bearing provides most of the bearing noise. It is

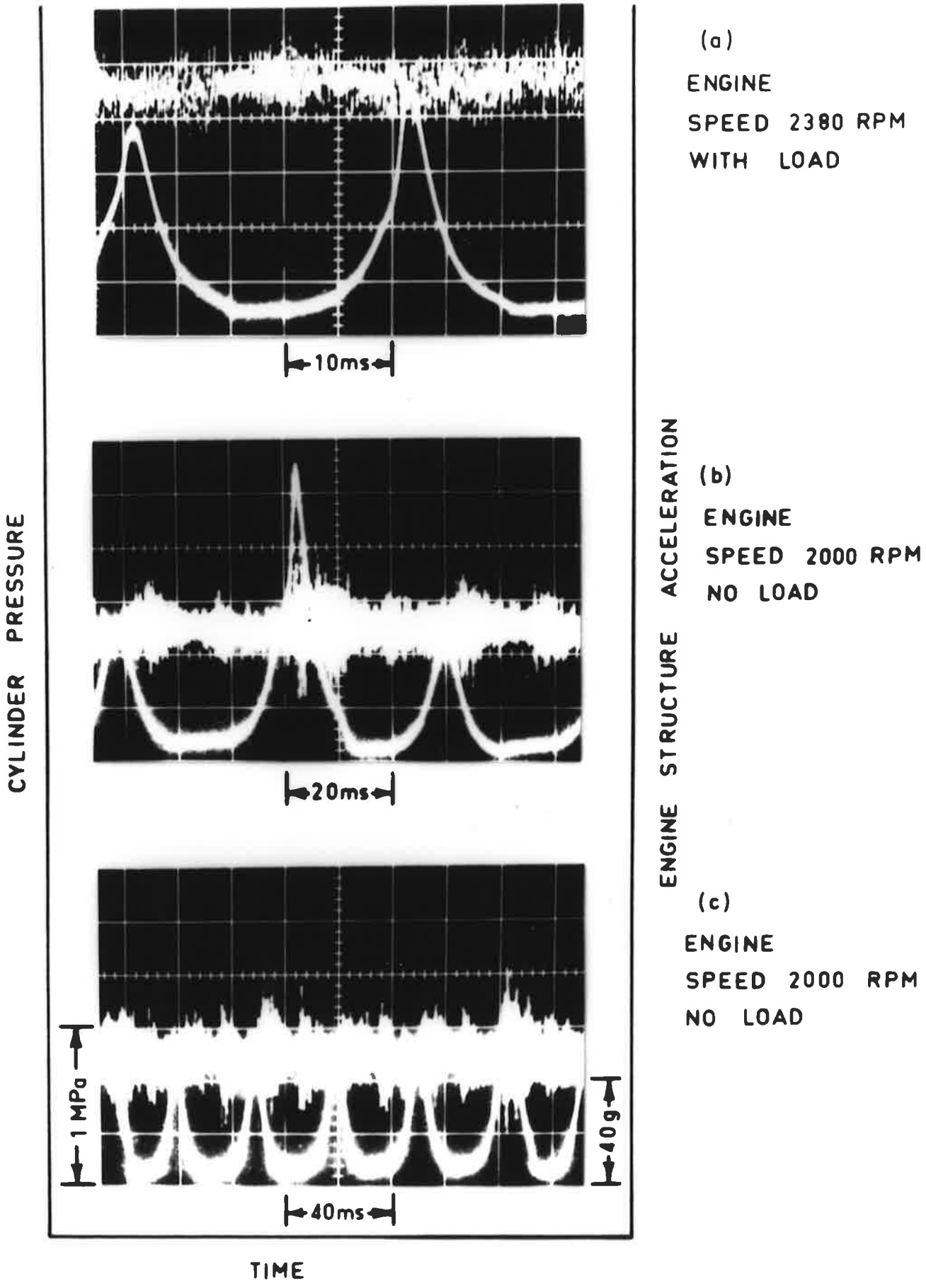

FIG. 30(a,b,c) CYLINDER PRESSURE AND ENGINE STRUCTURE ACCELERATION

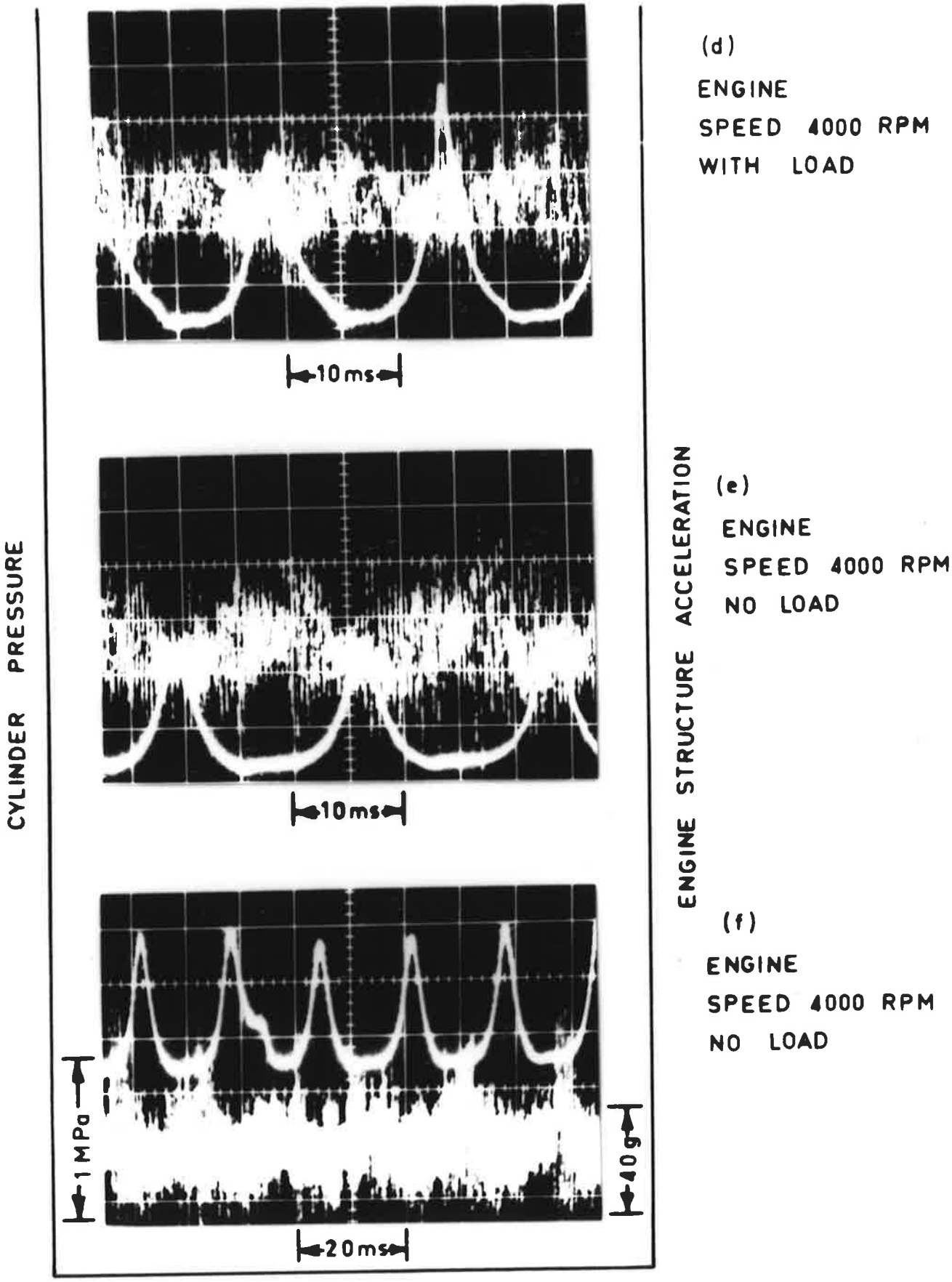

FIG. 30 (d,e,f) CYLINDER PRESSURE AND ENGINE STRUCTURE ACCELERATION

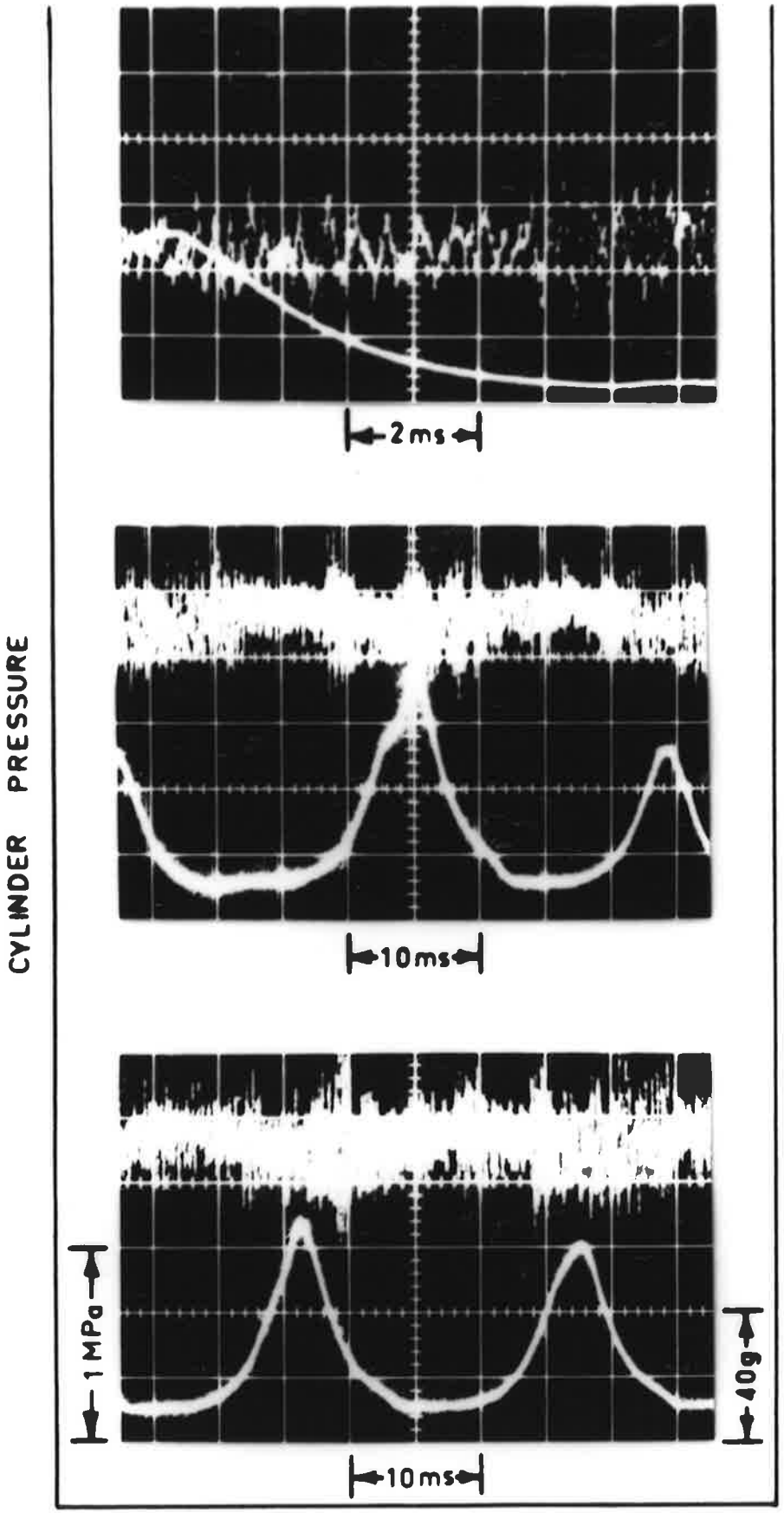

FIG. 30(g,h,i) CYLINDER PRESSURE AND ENGINE STRUCTURE ACCELERATION

interesting to note however that the dominant vibrational frequency of the engine is about 2 k - 4 kHz (from figure (30)(g)), whereas the roller rotational frequency in the big end bearing is about 500 Hz at 4000 r.p.m. The irregularities in the accelerometer traces at high engine speed could, of course, result from the different vibrational modes of the structure decaying, after an impact, at different rates. The existence of bearing noise is then by no means certain.

7.5 IMPACT NOISE

As the impacts from the reciprocating motion have been shown to be the most significant source of excitation to the engine structure, all aspects of impact noise must be considered in detail. It will be proven in section 7.5.2 that piston slap type 1, as described in section 7.3.3, is the dominant impact which occurs. This type of piston slap is determined by the forces on the piston at both T.D.C. and B.D.C., so that a study will first be made of the resultant axial force on the piston (in the direction of piston motion), as the engine passes T.D.C. and B.D.C.

7.5.1 Resultant Axial Force on Piston

As shown in section 7.3.2, the piston acceleration resulting from the reciprocating motion, may be expressed as a series of harmonics of the crank angle θ. In considering the total acceleration, it is sufficiently accurate to consider only the first two terms, so that the piston acceleration may be given by:-

$$a = - w^2 r(\cos\theta + \frac{4A_2}{q} \cos 2\theta) \qquad (7.5)$$

where $$A_2 = \frac{q^2}{2^2} + \frac{q^4}{2^4} + \frac{15q^6}{2^9} + \frac{35q^8}{2^{11}} + \ldots.$$

a = piston acceleration

for the lawnmower engine:-

$$r = 2.65 \times 10^{-2} m$$

$$q = 0.253$$

$$\frac{4A_2}{q} = 0.257$$

From equation (7.5) it may be seen that the magnitude of the piston acceleration has maxima at crank angles of 0, π (at T.D.C. and B.D.C.). It is clear that the magnitude at T.D.C. is greater than that at B.D.C., by a factor of 1.69.

At 2000 r.p.m., measurements of the gas pressure force are derived from figure (30)(b), for both firing and non-firing at T.D.C., and at 4000 r.p.m., from figure (30)(d) (third cycle) and figure (30)(f). Generally on firing strokes the gas pressure force will be greatest slightly after T.D.C., however, this small delay will be ignored. When the engine passes B.D.C. it will be assumed that the gas pressure force is zero.

The effective mass of the piston, used to determine the inertia force acting at the gudgeon pin, is taken as the piston mass (124 gms), gudgeon pin mass (31 gms) and $\frac{1}{3}$ of the con-rod mass (43 gms) (198 gms total). The resulting calculated and measured inertia and gas pressure forces at the gudgeon pin, at T.D.C. and B.D.C. for 2000 and 4000 r.p.m. are shown in table 7.3. In table 7.3 a positive sign indicates that the force acts in a direction opposite to the inertia force.

Table 7.3 : Axial Forces on Effective Piston Mass

(Newtons)

2000 r.p.m.

	T.D.C. Non-Firing	B.D.C.	T.D.C. Firing
Inertia Force	- 290	- 170	- 290
Gas Pressure Force	1490	0	3600
RESULTANT	1200	- 170	3310

4000 r.p.m.

	T.D.C. Non-Firing	B.D.C.	T.D.C. Firing
Inertia Force	-1160	- 690	-1160
Gas Pressure Force	1490	0	2720
RESULTANT	330	- 690	1560

7.5.2 Relative Significance of Big End Knock and Piston Slap

The identification of the dominant exciting force is of critical importance, as any recommendations of design changes will be based on such knowledge.

To determine the source of the excitation, as mentioned earlier, the lawnmower engine was run with a sparkplug incorporating a Kistler pressure transducer, and with a B & K type 4329 accelerometer mounted on the side of the crankcase. The outputs of both instruments were simultaneously displayed on a dual beam oscilloscope, in a manner used by Grover and Lalor (22) so that the relation between engine operation and exciting forces could be seen. About half of the measurements, to which reference is made below, were made without a load on the engine.

There are several types of impacts possible, during an engine

cycle, which are termed either big end knock or piston slap, and descriptions of these were given in section 7.3.3.

For both firing and non-firing strokes at 2000 r.p.m., it appears that piston slap type 1 causes the impacts at T.D.C. For non-firing strokes, for example, at 2000 r.p.m., it is shown in table 7.3 that the gas pressure force at T.D.C. of 1490 N is much larger than the opposing piston inertia force of 290 N. Therefore, the resultant axial force will clearly not change sign just after the engine passes T.D.C. Therefore, it is clear that the impact occurring shortly after T.D.C. at 2000 r.p.m., as shown in figures (30)(b) and (c) for both firing and non-firing strokes, is not piston slap type 2. Also, as the inertia forces at the big end are only about 25% greater than at the piston and are therefore much less than the gas pressure force, the impact is not big end knock resulting from a change in sign of the axial force. It may be shown that the sideways inertia force at the big end, caused by the con-rod rocking motion, will change sign at T.D.C. (and B.D.C.), however, the large resultant axial force will prevent the occurrence of slack and the resulting big end knock. Obviously the impact which occurs near T.D.C. at 2000 r.p.m. must be piston slap type 1.

At B.D.C., at 2000 r.p.m., the gas pressure force on the piston is negligible, so that the resultant force on the piston may be assumed equal to the inertia force of 170 N. As the inertia force is approximately constant for some time after B.D.C., it is clear that the impact occurring shortly after B.D.C., as shown in figures (30)(b) and (c), takes place before the resultant axial piston force changes sign. Therefore, the impact near B.D.C. is neither due to piston slap type 2 nor due to big end knock resulting from a change in sign of the axial force. There may be some doubt as to whether the impact at B.D.C. is piston slap type 1 or big end knock resulting

from the con-rod rocking force, however, calculations performed using the methods described in section 7.6 suggest that it is piston slap type 1. These calculations, based on the assumption that the piston slap type 1 occurs, predict reasonably accurately the relative magnitudes of the accelerations of the engine structure at T.D.C. and B.D.C., and the time delay of the impacts from T.D.C. and B.D.C. The results of the calculations for 2000 r.p.m. are shown below in table 7.4, in which they are compared with measured values, taken from figures (30)(b) and (c).

Table 7.4 : Piston Slap Type 1, 2000 r.p.m.

	T.D.C. Non-Firing	B.D.C.	T.D.C. Firing
RESULTANT AXIAL FORCE ON PISTON	1200 N	-170 N	3310 N
TIME DELAY TO IMPACT			
CALCULATED	1.5 m secs	2.9 m secs	1.1 m secs
MEASURED	2 m secs	3 m secs	1.5 m secs
RELATIVE ACCELERATION			
CALCULATED	1.92	1	2.69
MEASURED	1.4	1	1.9

At 4000 r.p.m. the situation is significantly different, as shown by figures (30)(d), (e), (f) and (g). Whereas at 2000 r.p.m. the accelerations are more or less regular, at 4000 r.p.m. there appears to be a high level of background noise from the bearings, and also similar gas cycles are seen to cause different accelerations (figures (30)(e) and (f)).

In table 7.3 it is shown that, at T.D.C. for a non-firing stroke at 4000 r.p.m., the gas pressure force of 1490 N nearly balances the piston inertia force of 1160 N. At the big end, the total inertia

force of about 1600 N more closely balances the gas pressure force, and this would cause slack at the big end. As the con-rod rocking force at the big end changes sign at T.D.C., big end knock would be expected, however, no such regular excitation occurs. It is, therefore, unlikely that either type of big end knock is significant at either 2000 or 4000 r.p.m., so that their occurrence will no longer be considered.

The only large regular excitation at 4000 r.p.m. occurs slightly after B.D.C., and for similar reasons as those given earlier for the impacts near T.D.C. and B.D.C. at 2000 r.p.m., this must be piston slap type 1. These impacts are clearly shown in figure (30)(f). For firing strokes, such as shown in figure (30)(d) (engine running with a heavy load), the resultant force on the piston at T.D.C. is now large, so that piston slap type 1 would be expected soon after T.D.C. This is clearly shown in figure (30)(d), in which there is a significant excitation soon after T.D.C. which does not occur for non-firing strokes (figure (30)(f)). Further verification of the significance of piston slap type 1 at 4000 r.p.m. is shown in table 7.5, in which the calculations were performed as for table 7.4. The time delay of the piston slap from B.D.C. is taken from the first cycle in figure (30)(e), and the acceleration magnitudes averaged from a number of cycles are shown relative to the impact at B.D.C. at 2000 r.p.m. The values for the firing stroke at T.D.C. are taken from the third pulse in figure (30)(d).

At high speed, for the lawnmower engine, the inertia force is large, so that when it changes sign 90° before T.D.C., thereby causing the resultant axial force to also change sign (see section 7.3.3), there is the possibility of piston slap type 2 occurring. Piston slap type 2 appears to be shown as an impact just before T.D.C.

Table 7.5 : Piston Slap Type 1, 4000 r.p.m.

	T.D.C. Firing	B.D.C.
RESULTANT AXIAL FORCE ON PISTON	1560 N	-690 N
TIME DELAY TO IMPACT		
CALCULATED	1.1 m sec	1.4 m sec
MEASURED	-	1.5 m sec
RELATIVE ACCELERATION		
CALCULATED	2.64	2.00
MEASURED	2.5	2.5

in some cycles at 4000 r.p.m. (in figures (30)(d) and (f)), however, the large impact from the piston slap type 1 at B.D.C. possibly obscures it. Figures (30) (h) and (i), for an engine speed of 3000 r.p.m., do, in fact, show the piston slap type 2 quite clearly. As expected, the impact is shown occurring shortly before T.D.C. Furthermore, the cycle shown in figure (30)(i) shows the piston slap type 1 as impacts just after T.D.C. and B.D.C. Generally, as the level of performance and speed of an engine increases, piston slap type 2 becomes increasingly significant due to the large inertia force, however, for the normal operation of the lawnmower engine, piston slap type 1 clearly dominates.

From the above discussion it may be seen that piston slap is the dominant source of excitation of vibration for the lawnmower engine. It would be expected that piston slap would, similarly, be dominant in many small engines.

7.6 CALCULATION OF PISTON SLAP RESPONSE

The piston slap considered below, previously referred to as type 1, is that which results near T.D.C. and B.D.C., when the sign of the con-rod angle of inclination changes. This was shown in the previous section to be the significant source of excitation, for the lawnmower engine. From a simple consideration of the events occurring near T.D.C. and B.D.C., the motion of the piston may now be described by a series of equations, and the acceleration response of the structure may be estimated.

Motion of Piston

In order that the motion of the piston, after T.D.C. and B.D.C., may be described, certain simplifying assumptions will be made. Firstly, it will be assumed that the piston slap occurs soon after passing T.D.C. or B.D.C. This will imply that the angle of inclination of the con-rod is fairly small (crank angle less than about 20°), so that the con-rod may be regarded as having constant sideways and angular velocity, that is, with an acceleration of zero. The assumption is shown to be valid at 2000 r.p.m. by figures (30)(b) and (c) in which the impact occurs no more, in fact, than about 20° after either T.D.C. or B.D.C.

A second assumption, which is less accurate, is that the resultant axial force on the piston is constant before piston slap. Again, an inspection of figures (30)(b) and (c) shows that the gas pressure does not diminish greatly before the piston slap impact, and as the inertia forces are nearly sinusoidal they will be even more nearly constant.

Near either T.D.C. or B.D.C. the motion of the big end may be regarded as entirely in a sideways direction relative to the direction of piston motion. The speeds of rotation of the con-rod and the

crankshaft, will then be related by the lengths of the con-rod ℓ and the crank radius r:-

$$\omega_1 = \frac{r}{\ell}\omega$$

$$= q\omega \qquad (7.6)$$

where ω_1 = speed of rotation of con-rod

ω = speed of rotation of crankshaft

For a constant resultant axial force on the piston, F, it may be seen that the sideways component of the force, which is responsible for the piston slap, will vary linearly with the con-rod angle of inclination, provided that the angle is small. It is obvious that this sideways force may be expressed as:-

piston slapping force = F tanϕ (if rocking couple is ignored)

where $\phi = \phi(t)$ = con-rod angle of inclination

F = resultant axial force on piston.

For small ϕ, this may be expressed as:-

piston slapping force = $F\phi(t) = F\omega_1 t$

$$= Fq\omega t \qquad (7.7)$$

where t = time after T.D.C. or B.D.C., that is, after $\phi = 0$.

Thus the acceleration of the effective piston mass m after $\phi = 0$, in moving the distance x towards the opposite cylinder wall is:-

$$\ddot{x} = \frac{Fq\omega t}{m}$$

So that, as $x = 0$, $\dot{x} = 0$ at $t = 0$:-

$$\dot{x} = \frac{Fq\omega t^2}{2m}$$

$$x = \frac{Fq\omega t^3}{6m}$$

Therefore, the time for the piston to travel from one side of the cylinder to the other is given by:-

$$\text{time after T.D.C. or B.D.C. to impact} = \left(\frac{6sm}{Fq\omega}\right)^{1/3} \qquad (7.8)$$

where s = piston clearance on diameters

m = effective mass of piston (piston and gudgeon pin and $\frac{1}{3}$ mass of con-rod).

The momentum of the piston on impact may then easily be described by:-

$$\text{momentum of piston on impact} = \tfrac{1}{2}(36\, Fq\omega s^2 m^2)^{1/3} \qquad (7.9)$$

It may be shown for a particular engine that the initial acceleration level (on the effective cylinder side wall mass) caused by the piston slap, varies linearly with the momentum of the piston on impact. This was verified by the comparison between the acceleration amplitude calculations, which were obtained using this assumption, and the measurements taken on the side of the crankcase. It is seen from tables 7.4 and 7.5 that the calculated acceleration values have the correct relative magnitudes. In general, the accuracy of the analysis described above may be seen by comparing all the measured and calculated values shown in tables 7.4 and 7.5. The agreement obtained is quite satisfactory.

Nature of Impact

In order that the magnitude of the initial acceleration level of the cylinder wall may be crudely estimated, the nature of the impact of the piston on the cylinder wall must be considered.

The situation in both the piston and cylinder, for the duration of the initial impact, may be described by a consideration of the stress waves generated at the area of contact. The actual wave pattern will consist of a complex combination of longitudinal, bending and shear waves, however, the bending waves will be assumed to occur alone, for simplicity.

After the piston hits the cylinder wall a bending wave travels through the piston and slows it down and another wave accelerates the cylinder in the direction in which the piston was moving originally. When the bending wave has travelled to the opposite side of the piston, the entire mass of the piston will have lost momentum to the cylinder. The mass of the piston will usually be much less than the mass of the cylinder downstream of the bending wave in the cylinder (about $1/15$ th for the lawnmower engine), so that the piston will have lost nearly all of its original momentum at this point. In practice other parts of the engine will be affected as well and the total mass absorbing the momentum will be referred to as the effective cylinder side wall mass. The force acting at the contact surface is defined as the rate of transfer of momentum to the cylinder, and this may be seen to be determined by the rate of advance of the bending wave in the piston. To a rough approximation the force may be regarded as constant until the bending wave travels to the opposite side of the piston.

As shown above, the time for the momentum transfer may be estimated, and it is clear that this is the same no matter how large the resultant axial force F on the piston and no matter what the speed of the engine. Clearly, for a constant coefficient of restitution

on impact, the initial acceleration of the effective cylinder side-wall mass will scale linearly with the initial momentum of the piston. A crude estimate of the initial acceleration may now be made assuming a coefficient of restitution of 1.

For a plate, the bending wave speed may be expressed in terms of the longitudinal wave speed:-

$$c_B = c_L \left[\frac{(2\pi)^2}{12} \frac{t^2}{\lambda^2} \right]^{\frac{1}{2}} \qquad (7.10)$$

where c_B = bending wave speed

c_L = longitudinal wave speed

t = thickness of plate

λ = wavelength of disturbance.

For the relevant bending wave, the wavelength, λ, is half the circumference of the piston or cylinder. From (7.10) it then follows that the bending wave speed may be assumed roughly equal to the longitudinal wave speed. It may then be shown that at 2000 r.p.m. with a resultant force F of 1200 N at T.D.C., the force at the contact surface is 5 kN. Assuming a value for the effective cylinder side-wall mass of 5 kgm, the acceleration level on this mass, following impact, is then about 100 g. Actual measurements, on the side of the crankcase gave 23 g peak amplitude, and for other cases considered the error was about a factor of 3. As the accelerometer was placed partway down the crankcase skirting and not on the side of the cylinder, agreement with experiment is remarkably good. This further supports the basic conclusion that the mechanical noise is determined by piston slap.

7.7 VIBRATION RESPONSE AND SOUND RADIATION

The response of the structure of the assembled lawnmower to

the exciting forces described above will be to vibrate in various modes, each with different damping and each with different sound radiation characteristics. To determine which parts of the mower efficiently radiate sound, comparison tests were done with the mower running with a particular noise source present and then with the mower either with the source removed or silenced. The sound sources considered are listed in table 7.1. All experiments were conducted in the reverberation chamber with the blades removed from the cutter blade mounting plate, the exhaust and inlet carried outside through flexible pipes and no load on the engine. The no load condition was used for convenience, and because as mentioned earlier, the noise did not seem to vary with load, was very regular regardless of engine firing, and anyway this would best represent noise from an operating lawnmower.

The contribution to the noise from the engine base frame was determined by substitution of the frame with one which was constructed of angle iron and rubber-isolated from both the engine and the floor. The apparatus is shown in figure (31), although the cutter blade mounting plate was not removed as in the photo. At 2700 r.p.m. the sound level overall (linear) was 1.5 dB less without the base frame and at 4000 r.p.m. the sound level was 4.5 dB less. It could be concluded, therefore, that the base frame is a significant noise source. This was further shown by an experiment in which a small sound absorbing box, lined in fibre wool, was placed over the engine which was rigidly mounted on the still exposed standard frame. The box worked well with the silent frame but did not with the standard frame, even at high frequencies, so that the standard frame must have contributed much of the noise.

The contribution from the cooling fins was determined by running the engine on the silent frame alternatively with a normal cylinder and head, and with a cylinder and head with no fins.

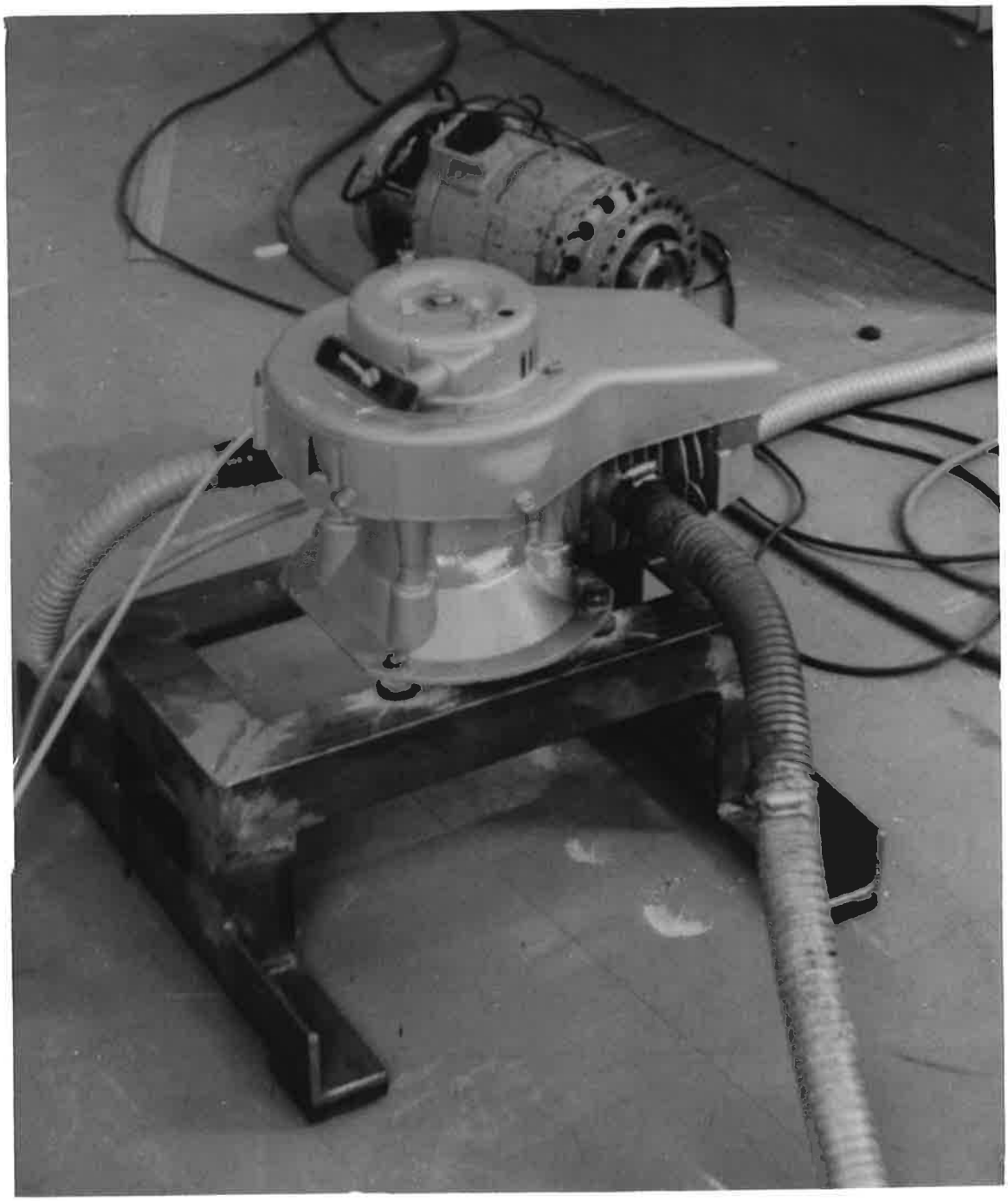

FIG. 31 LAWNMOWER ENGINE ON SILENT FRAME

At 2700 r.p.m. there was no overall difference but at 4000 r.p.m. there was 4.5 dB more noise without the fins. It may be concluded that the cooling fins on the engine do not radiate significant noise, and in fact add significant rigidity and mass.

The significance of each of the cutter blade mounting plate (shown in figure (32)), the small engine cover (shown on top of the engine in figures (23) and (31)) and the engine cooling fan (located underneath the engine cover) was found by simple comparison tests to be small.

At the end of the series of experiments the engine consisted only of the cylinder and head and crankcase. As the total mechanical noise reduction for the bare engine compared to the complete mower was only 3 dB at 2700 r.p.m., it is clear that the crankcase, cylinder and head are the major sources of radiated sound apart from the engine base frame.

7.8 CONCLUSION

The most important finding of the investigation of mechanical noise on the lawnmower is the identification of the major source of the excitation as being piston slap. By using reasonable simplifying assumptions, the slapping motion of the piston across the cylinder clearance was described analytically. By making further assumptions about the nature of the impact of the piston on the cylinder wall, the acceleration response of the cylinder wall was estimated. Measurements obtained in a series of experiments verified the analytical methods used.

The sound power radiated by each of the individual sources of mechanical noise was studied. It was found that the basic engine and the base frame were about equally significant, with contributions from the other sources being of lesser importance. The findings relating

to both the sound radiation characteristics and the phenomenon of piston slap lead to suggested design alternatives, and these are described in chapter 10.

CHAPTER 8

CUTTER BLADE NOISE

8.1 INTRODUCTION

In the past, little work has been devoted to rotary lawnmower cutter blade noise although that of Sperry and Sanders (18) is an example. Much work has been done concerning axial flow fans, although, of course, not specifically relating to lawnmower blades. The effects of most aspects of fan noise have been investigated and in many cases the spectrum levels can in fact be accurately predicted (for example, Mugridge and Morfey (26)).

On the test lawnmower, the cutter blades are mounted on the edges of a large disc, as shown in figure (32). The disc is bolted to the bottom of the crankshaft and the blades are enclosed by the engine base frame (see figure (23)), to which the grass catcher is attached (the grass catcher was not used in this study). The function of the blades is to provide an upward airflow to raise the grass for cutting, to cut the grass and blow the clippings into the catcher. It has been shown in experiments that both the existing cutter blade system and also an earlier model cutting system (from the same manufacturer) induce the same sort of air flow under the blade cover (engine base frame). This flow for the existing cutting system is illustrated in figure (33). The blade lift imparts on upward motion, relative to the blades and disc, with a downward motion near the drive shaft completing the flow path. The whole flow shown in figure (33) rotates about the drive shaft in the housing above the blade disc, in the same direction as the blade disc. The flow has a somewhat smaller

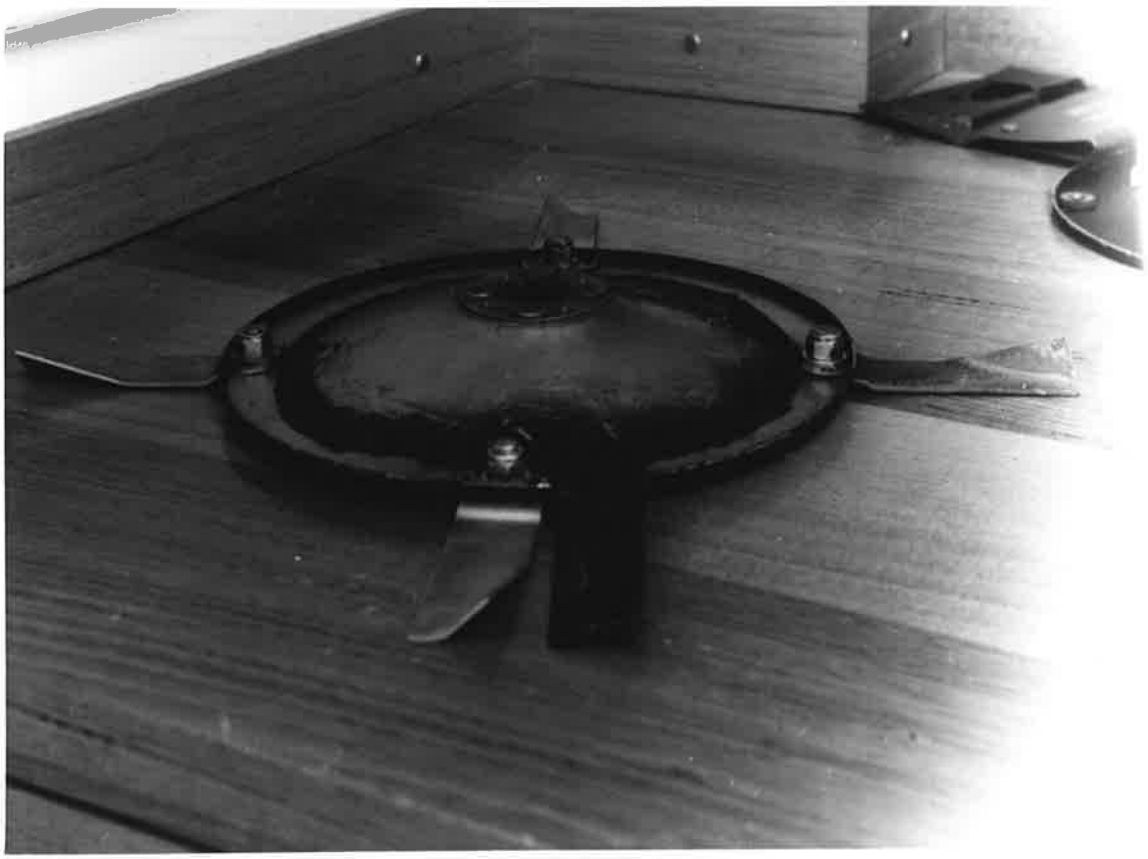

FIG. 32 BLADE DISC WITH CUTTER BLADES ATTACHED

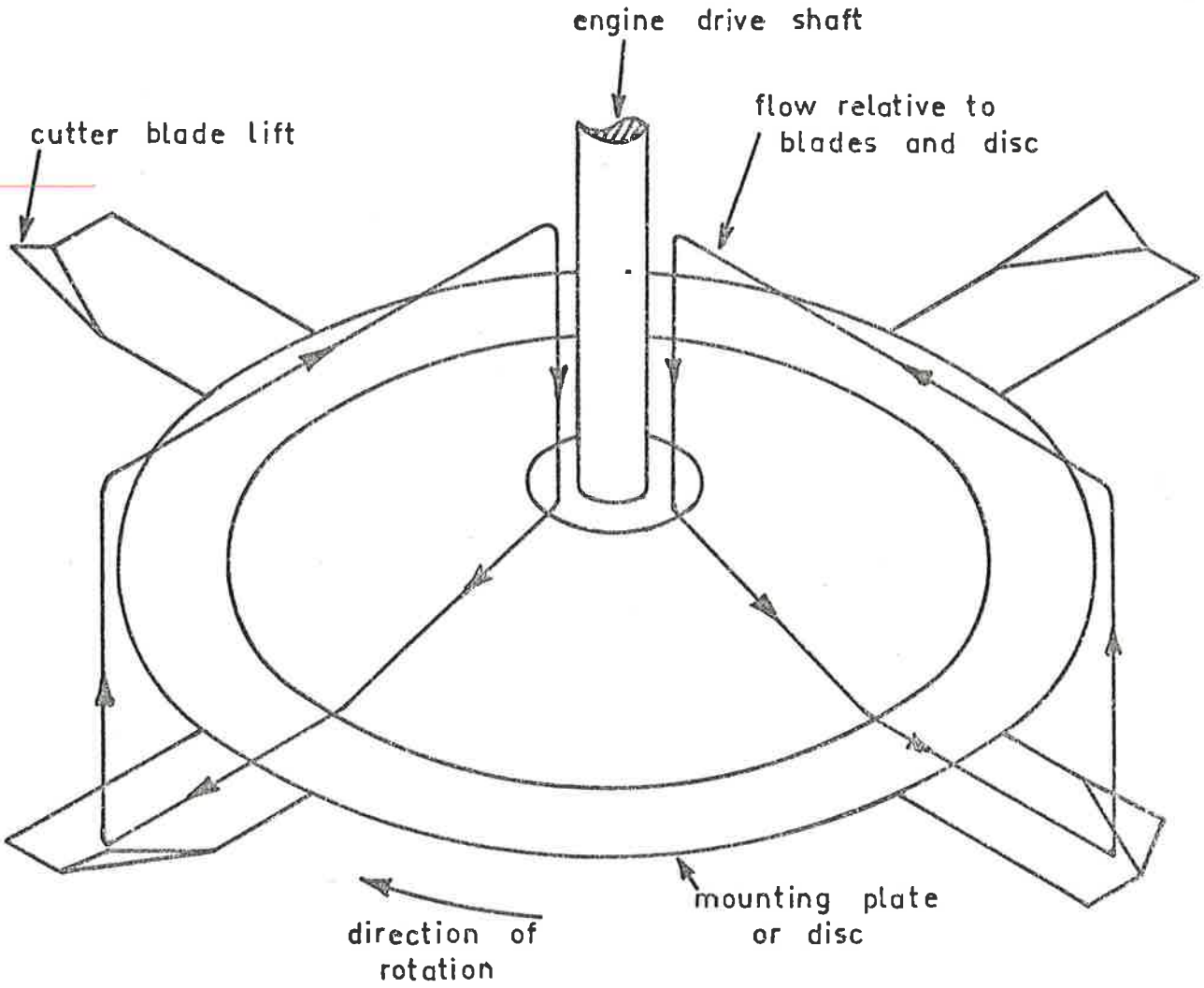

FIG. 33 FLOW PATTERN INDUCED BY BLADES UNDERNEATH COVER

rotational velocity than the disc, so that it then still has a large rotational velocity relative to the housing. As the catcher duct is the only outlet to the atmosphere for the centrifugal flow, the air and the entrained grass clippings flow into the catcher through this outlet. Measurements show that the flow velocity through this outlet may be, in fact, as high as nearly 20 m/sec. The catcher, which has a mesh covered air outlet, then collects the clippings by acting as a part settling chamber - part sieve.

Two sets of apparatus were used for the experiments performed in this study. The sound power measurements used in chapter 6 were obtained by running a lawnmower, with the engine replaced by a silent electric motor drive, in the reverberation chamber, with the mower wheels on the floor (no catcher used, catcher flap closed). The height of the blades above the ground is adjustable, however, only one height was used for the measurements as the effect of different heights was found to be negligible.

Further measurements of sound power radiated, as well as all of the flow investigations, were carried out on a separate apparatus. Most of these latter tests were carried out in collaboration with Mr. G. A. Lines as part of a final year undergraduate project. These experiments, again performed in the reverberation chamber, involved using an electric motor driving the cutter blades and disc, housed in a simulated blade cover. The simulated blade cover was constructed of transparent perspex, as was the simulated ground surface, with the apparatus being mounted nearly 2 metres above the reverberation chamber floor. Figure (34) shows this apparatus with the cutting system from the test lawnmower, although not in the reverberation chamber, and with the simulated ground surface removed. Several experiments were performed to see whether the two sets of equipment

FIG. 34 SECOND APPARATUS FOR MEASURING CUTTER BLADE NOISE

radiated the same noise with the same blade systems, and in fact, only a ± 1 dB difference was observed (see figure (35)).

At 3400 r.p.m. the blade tip speed and Mach number for the standard test cutting system are as shown below:-

blade tip speed = 82.3 m/sec

blade tip Mach number = 0.24.

This speed is typical of all lawnmowers as most have a cutting width the same as the test lawnmower (0.46 m or 18 inches).

8.2 SIGNIFICANCE OF CUTTER BLADE NOISE

In table 6.3 it was shown that for the test lawnmower the cutter blade noise is the main noise source at 2700, 3400 and 4000 r.p.m., being 1 dBA, 3.5 dBA and 6 dBA above the exhaust noise, respectively. Interpolating from the spectra shown in figures (24)(a) and (b) to a speed of 3400 r.p.m., the cutter blade noise dominates the spectrum from above about 300 Hz, so that a reduction of cutter blade noise would, in effect, reduce the overall noise at that speed.

Cutter blade noise levels measured by Sperry and Sanders (18) and as referred to by Rudd and Bender (17) were shown in tables 6.2 and 6.3 to be significantly less than those obtained for the test lawnmower engine. As the method described in chapter 6 was believed to very accurately measure the sound radiated by the test lawnmower cutter blades, and as cutter blade systems used by other Australian manufacturers do not appear to be radically different than the test system, some comment must be made on the much lower levels observed in the other studies. It is believed that these differences may partly be due to the cutting system on the test lawnmower and certainly, to some extent, related to the different measurement methods used.

As a preliminary measurement to determine the difference

with another cutting system, a 2 bladed cutting system from another manufacturer was tested on the rig shown in figure (34). The noise level was actually 2 dB greater than with the standard system from the test mower. No experiment was performed to determine the effect of a different housing, however, it was observed that for the cutting system on the test lawnmower, the noise was reduced by 8 dB by removing the whole blade enclosure shown in figure (34). This indicates that the blade enclosure is very significant.

In the measurements made by Sperry and Sanders (18) (see table 6.2) the level of blade noise at 3600 r.p.m. was 94.5 dB(linear) sound power compared to 106 dB(linear) sound power for the test lawnmower at 3400 r.p.m. The method used by Sperry and Sanders to determine blade noise was however significantly different to that used in this study in that the cutter blade system was placed in a reverberation chamber such that it was some distance from any obstruction to the flow. That is, the cutter blades were not operated in their normal flow environment, in the base frame housing in the vicinity of a flat surface (the floor), so that, as the housing was mentioned above as having a large effect , the results of Sperry and Sanders significantly underestimated the total noise. Therefore, in comparison, the test lawnmower cutting system may not be all that much noisier than that tested by Sperry and Sanders.

From the above it is clear that the cutter blade noise is a serious problem for the test lawnmower, and must be reduced if the overall level is to be reduced. It is not as clear, however, how great the cutter blade noise for the test lawnmower is in comparison with that for lawnmowers tested by other researchers but from the results presented in tables 6.2 and 6.3, it appears that cutter blade noise is always a major noise source for rotary lawnmowers.

8.3 POSSIBLE SOURCES OF CUTTER BLADE NOISE

Axial flow fan noise research (for example, references (26), (27) and (28)) shows that the sources of fan noise are the rotating steady pressure profile on the blades, the fluctuating blade forces and vortex shedding.

The noise radiated by the steady pressure profile on the system of blades, as they rotate, is often significant for low speed fans with few blades. However, this source will normally be significant only when the inlet flow to the blades is very steady, with no steady crossflow or turbulence, unlike the situation for lawnmower cutter blades. With a symmetrical blade pattern, the fundamental frequency is the blade passing frequency, however, the radiated sound power level from this source drops as the harmonic order becomes higher (reference (28)). As the measured spectra of the lawnmower blade noise (see figures (24)(a) and (b)) show that the levels at the higher blade passing harmonics are large, and also as the inlet flow to the blades is obviously not steady, it is clear that the rotating steady pressure profile is not a significant noise source.

Mugridge and Morfey (26) state that for fan noise at subsonic blade speeds, which applies to all lawnmower cutter blades, the sources are either dipole in nature or quadrupole in nature. Dipole sources are associated with fluctuating forces on objects (in this case the blades) and quadrupole sources are usually associated with the noise from turbulent fluid flow far from boundaries (vorticies in mixing regions). Figure (35) shows the variation in the overall sound power level, measured in the reverberation room using each of the two sets of apparatus, from 700 r.p.m. to 4000 r.p.m., together with a line representing the variation of noise from a dipole source. It is clear that the cutter blade noise is basically dipole in character, which indicates that the fluctuating force on the cutter blades

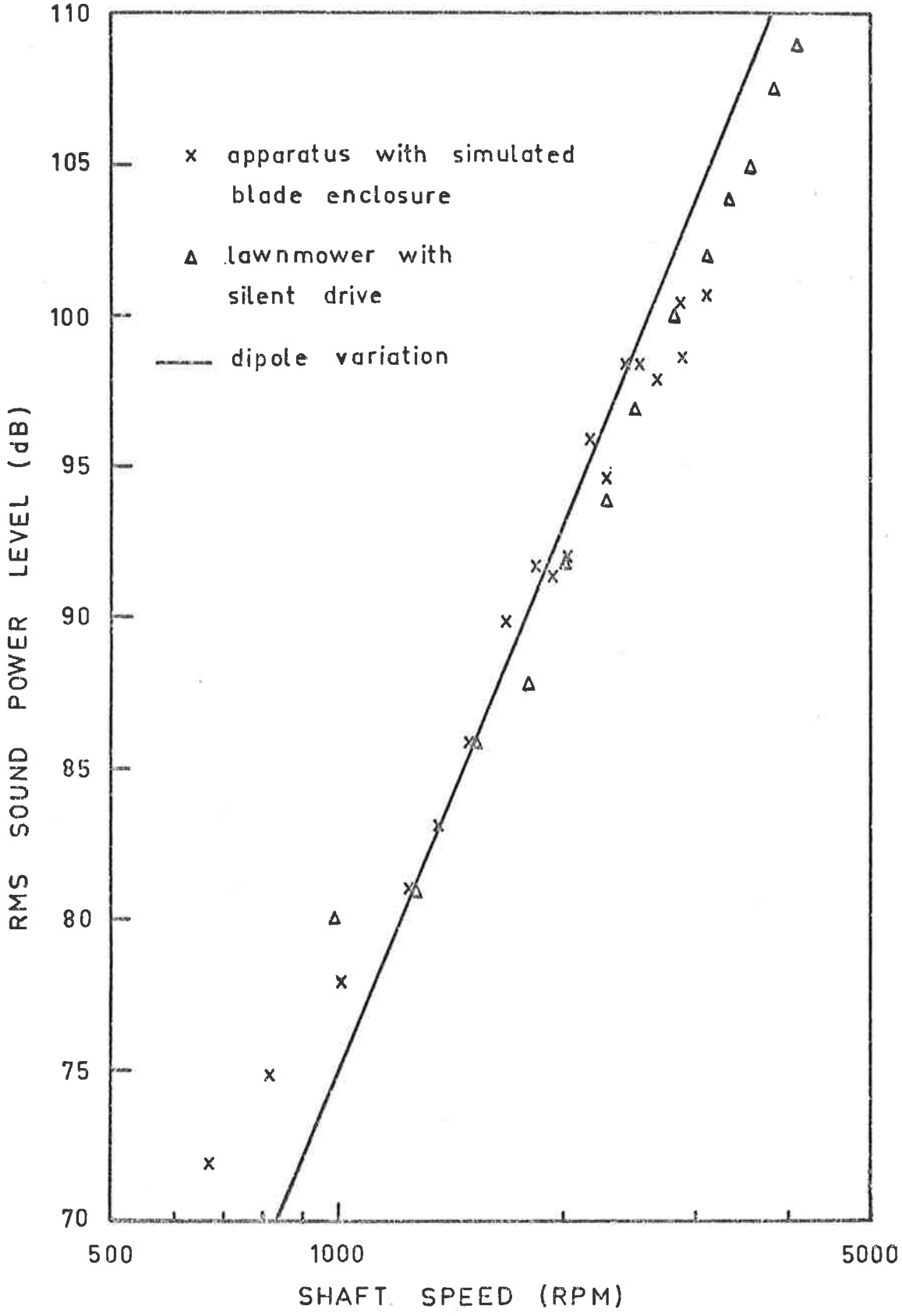

FIG. 35 CUTTER BLADE NOISE VARIATION WITH SPEED

is the main source of the radiated noise.

Generally, it would be expected that the fluctuating blade forces and resultant noise would scale with the mean blade forces, that is, with the blade lift and drag and the amount of air pumped. This was found to be the case. As the blade lift angle was reduced to zero, with a corresponding decrease in the mean blade force and the air flow, so the radiated sound power level was found to be reduced. These results are shown in table 8.1.

Table 8.1 : Variation of Sound Power with Blade Lift

(dBA re 10^{-12} watt, 2700 r.p.m.)

(cutter blades in apparatus of figure (34) with simulated ground surface)

BLADE UPLIFT ANGLE	Lw
45°	99
15°	95
10°	93
0°	90

As shown in table 8.1 there was a considerable amount of noise even with flat blades. This was obviously because the blades were poor aerofoils and still created significant turbulent wakes.

8.4 FLUCTUATING BLADE FORCES

Now that the cutter blade noise has been conclusively shown to be caused by the fluctuating forces on the blades, it is interesting to consider the source of these fluctuating forces.

The fluctuating force on a given blade may result from either the fan inflow conditions or from the wake caused by the blade itself. Fluctuating blade forces resulting from the variation of fan inflow conditions may be due to :- (e.g. from references (26) and (27))

1. Upstream turbulence which becomes part of the fan inflow.
2. Taking inflow which is made up of part of the fan's own turbulent wake which has been recycled.
3. An uneveness in the circumferential velocity field caused by irregularities in the blade housing.
4. Turbulence resulting from the direct wake flow of a preceding blade. Such a wake flow may include a tip vortex, trailing edge vortex as from a stalled aerofoil, spanwise flow variation vortex (mainly at blade base on blade mounting disc) caused by differences in flow in a radial direction (reference (26)).

Fluctuating blade forces resulting from the flow past the blade itself may be due to:-

5. A steady frequency modulation, not at the blade passing frequency, caused by, for example, blade vibration.
6. Boundary layer turbulence near the surface of the blade.
7. Turbulence resulting from the wake of the blade itself, as in (4) above.

By performing a few simple experiments and by making reasonable assumptions all but causes (4) and (7) above were initially dismissed as being insignificant in this study. These considerations are given below. Ultimately, the fluctuating forces on a blade, caused by the blade's own wake, were shown to be the source of the cutter blade noise.

The effect of upstream turbulence (cause 1) was easily shown to be negligible. It was found that with the apparatus shown in figure (34), the addition or removal of a large flat surface simulating the floor had no measurable effect on the radiated sound power. With the simulated "floor" removed there would have been effectively

no turbulence in the fan inflow, yet the noise was not diminished.

For similar reasons as given for cause (1), the recycling of the turbulent wake of the fan (cause (2)) may clearly be disregarded. There is obviously no significant effect caused by these sorts of inflow conditions.

Several experiments showed that significant irregularities in the blade housing (cause (3)) also had a negligible effect on the sound power radiated. Firstly, it was found that the placement of a flow directing "splitter" plate near the inlet of the catcher duct did not affect the noise. This "splitter" plate was 5 cm by 13 cm in size and was located only 1 cm above the blade tips and was similar to that used in some lawnmowers to deflect the flow into the catcher duct. Secondly, it was found that there was no change in the noise when the cutter blade mounting disc was moved slightly, relative to the blade housing. Both of these changes were expected to affect the circumferential velocity field but they certainly had no effect on the sound power radiated.

Barry and Moore (28), to whom Morfey (27) makes a reference in his review article, state that if blade vibration is significant then the spectrum of radiated sound will have peaks at frequencies other than the blade passing harmonics. Clearly in the cutter blade noise spectra shown in figures (24)(a) and (b) only peaks at the blade passing harmonics are present (apart from peaks at the shaft speed). Therefore cause (5) is insignificant.

Finally, the effect of boundary layer turbulence (cause (6)) may readily be dismissed as insignificant in comparison with the obviously much greater effect of the wake turbulence of the stalled blades (cause (7)).

It now remains to be determined whether the fluctuating forces on a blade are caused by the blade's own wake, or by the inter-

action of the blade on the wake of the preceding blade. Reference may now be made to the experiments of Sperry and Sanders (18) as these involved using a blade system of the same overall diameter and running at a similar speed as used for the test lawnmower system.

With a blade system consisting of a flat bar $\frac{1}{8}$ inch thick, 2 inches wide and 18 inches long, the noise level obtained, which could be attributed to mainly the wake turbulence of a preceding blade, was as high as from a conventional cutting system (for measurements in reference (18) blades were far removed from objects). Various changes to the blades, such as sharpened edges and forward leaning angle significantly reduced the sound (by sharpening the trailing edge on a flat bar, Sperry and Sanders reduced noise above 2 kHz by 15 dB). This was presumably because of the effect on separation and the corresponding size of the wake that subsequently interacts with the next blade. However, when lift was introduced on the blades these effects were nullified as the following blade no longer immediately passed through the preceding blade's wake. It has been found (reference (27)) that in one case a 1° angle of attack, for a rotor system, reduced noise noticeably, as the blade wake was swept downstream. As it could be assumed that the lawnmower cutter blades must have at least some lift, it is concluded that noise resulting from the direct interaction between a blade and the wake turbulence of a preceding blade (source (4)) may be disregarded for well designed blade systems (i.e. in those cases in which there is some lift and not simply drag on the blade).

Therefore, the fluctuating forces on a blade, for the currently used test system and probably for all rotary lawnmower cutting systems, are caused by the action on the blade of the blade's own turbulent wake. This may now explain why the noise level was 8 dB greater (as mentioned

earlier) with the housing in place around the blades than with the housing removed. The slight pressure differential between the air on either side of the cutter blade mounting disc, with the housing in place, causes an increase in the mean blade force which effectively, through its effect on the blade wake, increases the fluctuating blade forces and the noise. (That is, the effect of the housing is to increase the apparent angle of attack over the cutter blades, thereby increasing the drag and possibly the lift).

8.5 CONCLUSION

There was a number of significant findings in the study of the cutter blade noise. Firstly, the noise was found to be dipole in nature and obviously dependent on the fluctuating forces on the cutter blades. These fluctuating forces, and consequently the noise, were found to scale roughly with the mean blade forces and the amount of air pumped. The presence of the blade housing was then found to have a significant effect as it caused a pressure differential to exist across the blades and the mounting disc, thereby increasing the mean drag and lift forces on the blades and, correspondingly, the noise.

The fluctuating blade forces on each blade were found to be determined by the blade's own turbulent wake and did not result from a number of other possible sources including interaction with the wake of the preceding blade.

The findings reached lead to several suggested design alternatives and these are considered in chapter 10.

CHAPTER 9

EXHAUST NOISE

The following sections concerning exhaust noise are by no means as detailed as in the preceding chapters which describe the mechanical noise and the cutter blade noise, as part 1 of the thesis has covered to a great extent the source and characteristics of exhaust noise in single cylinder, piston ported 2-stroke engines. The work described below then only covers those aspects which directly relate to the operation of the lawnmower muffler. Of course, the action of the lawnmower muffler is very similar to the action of similar small mufflers on 2 and 4-stroke engines and common features may be identified.

9.1 OPERATION OF LAWNMOWER MUFFLER

The lawnmower muffler used in this study is shown in position on the lawnmower in figure (23) and projections of it are shown in figure (36)(a). The muffler consists of a receiving volume with an orifice as an outlet to the atmosphere and with four slits in the inlet pipe coming from the engine acting as an inlet restriction. There is also a shroud around the inlet slits which forces the flow to reverse direction. This muffler is then of the orifice - cavity - tailpipe type as is shown in figure (21) and as mentioned in section 4.2.

The operation of the lawnmower muffler was investigated by taking measurements of the radiated sound pressure cycle, coming from the muffler outlet, and by taking pressure measurements inside the main volume of the muffler, with both types of measurements relating to the same operating conditions. To determine the insertion loss of

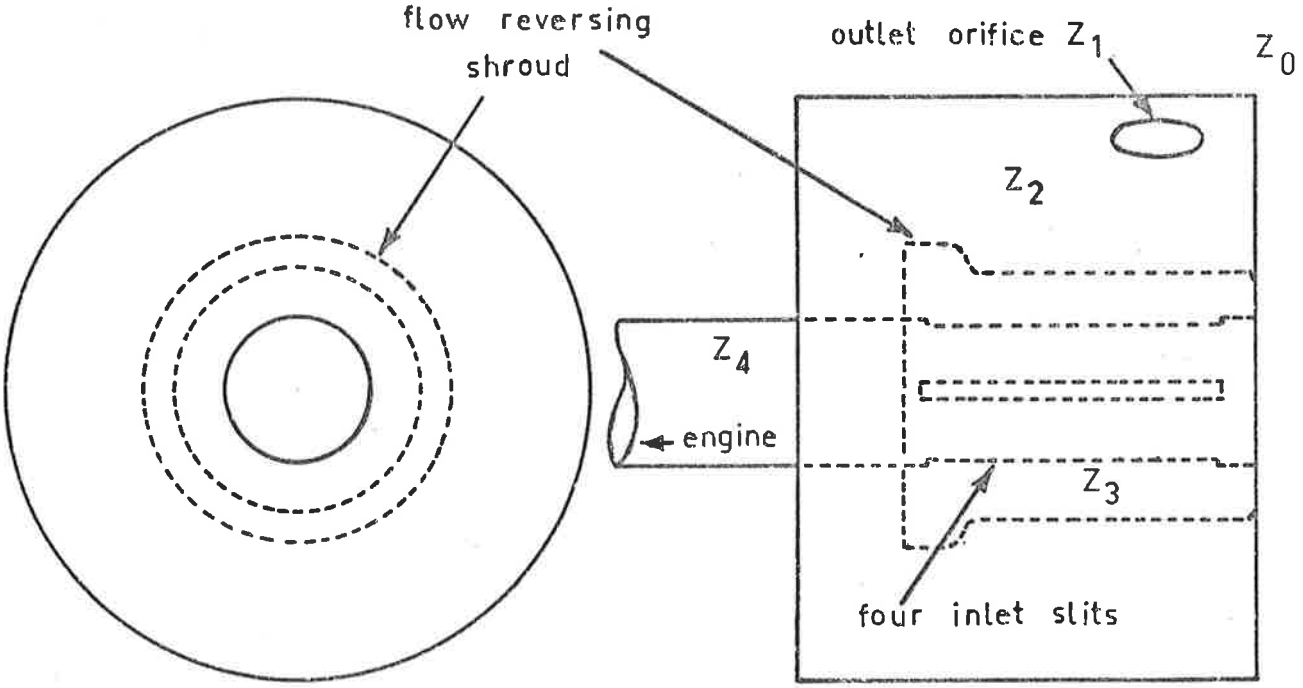

(a) LAWNMOWER MUFFLER

SCALE: 3/4 FULL SIZE

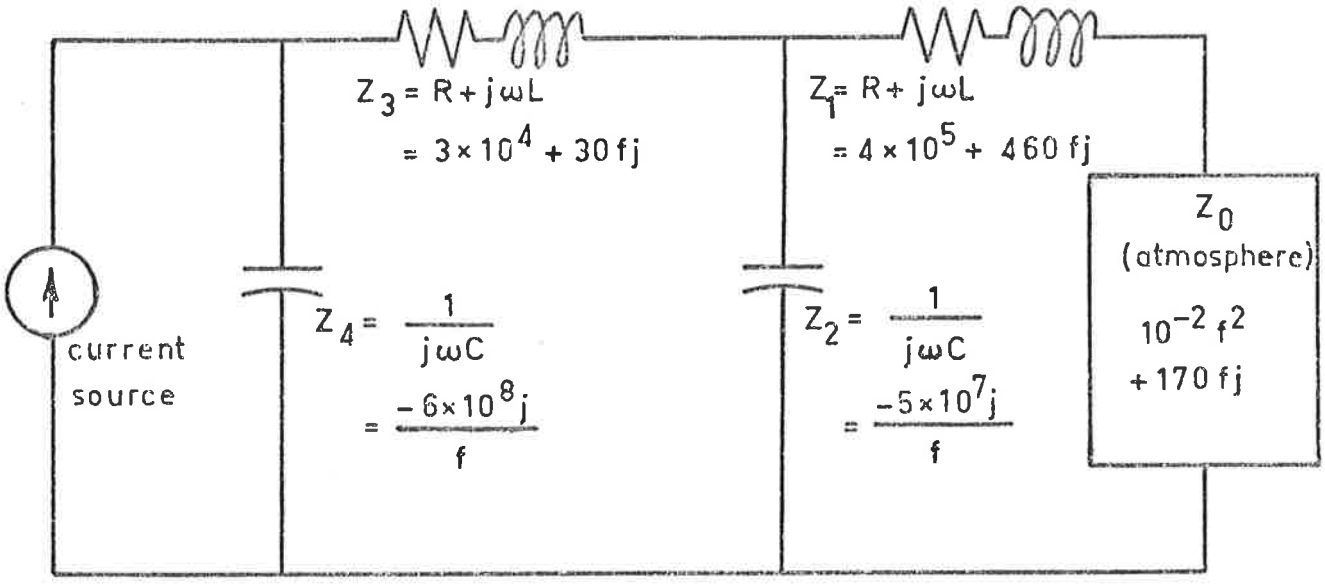

f = frequency in Hz

(b) ANALOGOUS CIRCUIT WITH IMPEDANCES IN DIMENSIONS $kg.m^{-4}.s^{-1}$

FIG. 36 LAWNMOWER MUFFLER

the muffler, the muffler was alternately placed on and then removed from the exhaust outlet of the engine, with the engine modified so that the noise from all the other sources was greatly reduced.

The pressure measurements taken inside the muffler volume were obtained using a Kistler quartz pressure transducer type 640/601 B which was placed inside a water-cooled housing. The resonance frequency of the transducer in the housing was 4 kHz (obtained from shock tube measurements), which was considered adequate.

The measurements of radiated sound were taken in a free field environment (outdoors) at a distance of 3.7 m from the source, using a B & K type 4131 (1 inch) microphone and a Nagra 4.2 tape recorder. The background noise for these measurements of radiated sound pressure was checked by running the engine with the exhaust noise silenced by an extremely large muffler, and was found to be at least 10 dB below the levels being measured in all frequency bands from 40 Hz to 10 kHz.

Sample measurements of both the radiated sound pressure from the muffler outlet, and the pressure in the muffler volume, are shown together in figure (37). In each case slightly more than one engine cycle is shown. As described below, certain interesting features may be observed in these pressure traces.

From the radiated sound pressure cycle in trace (a) of figure (37) it is clear that, although still significant, the peak resulting from the initial pulse is not as great in relation to the other fluctuations as it was in the cases for all the exhaust systems used on the motorcycle engine. This is clear from the way the initial peak greatly dominates the radiated sound pressure cycles in figures (11), (15) and (19). This is partly due to the fact that pulse steepening does not occur in the short muffler system, and because the muffler has

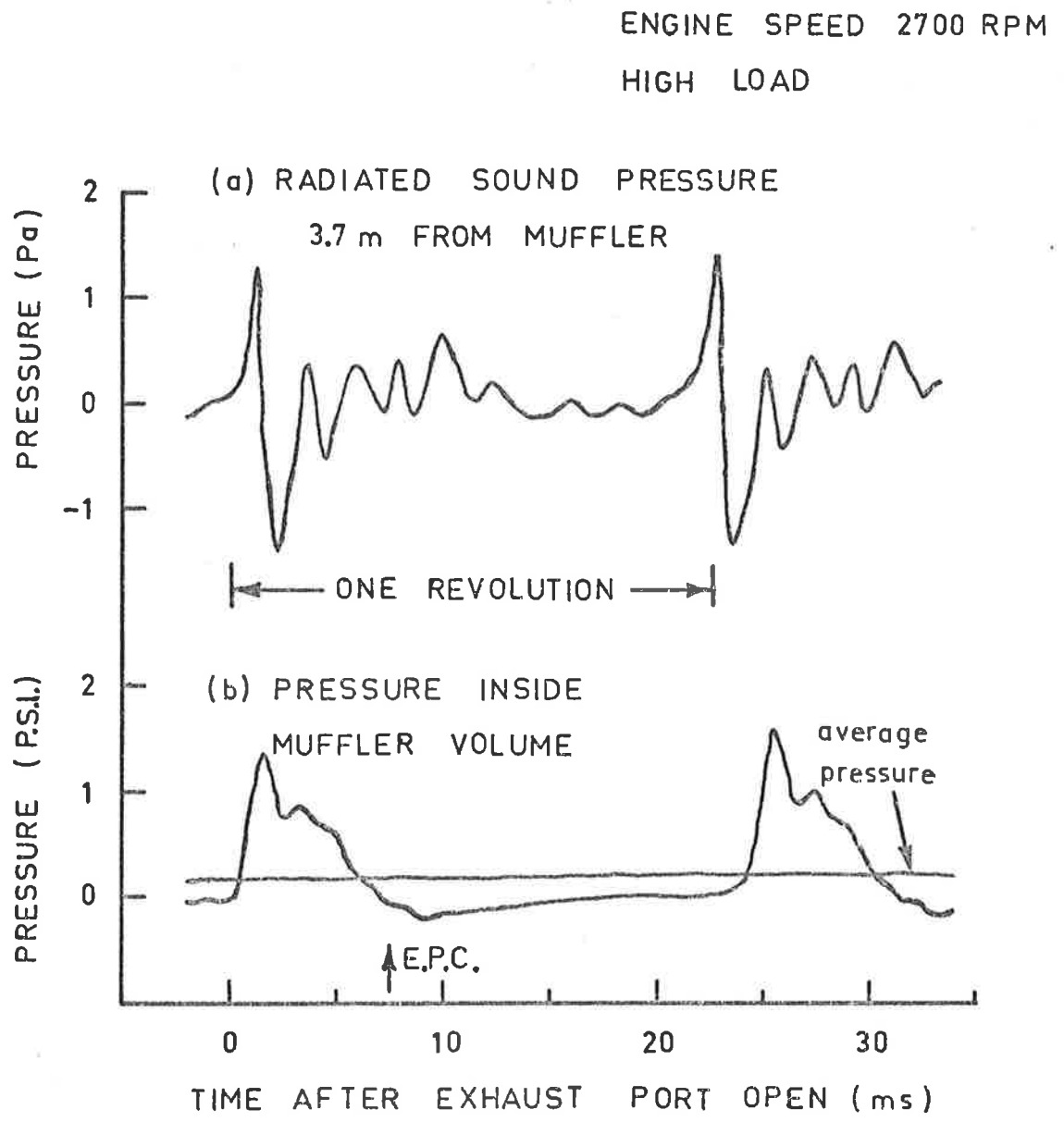

FIG. 37 OPERATION OF LAWNMOWER MUFFLER

a considerable volume expansion which the other systems do not have.

Apart from the initial peak, the most noteworthy feature of the radiated sound pressure cycle from the lawnmower muffler is the series of oscillations occurring at a frequency of about 420 Hz (2.35 milli seconds per cycle). These oscillations are obviously the response of the Helmholtz resonance of the muffler volume and the outlet orifice to the excitation from the initial pulse. In fact, a calculation showed that, for hot exhaust gas, the resonance frequency of the volume and orifice combination, for the lawnmower muffler, was 360 Hz.

Measurements taken inside the lawnmower muffler volume show a noticeably different pressure cycle. In trace (b) of figure (37) the only readily discernable event is the rapid filling of the volume by the exhausting charge of gas, and then the gradual release of the gas through the outlet orifice. From figure (37)(b) it almost appears that the release of gas from the volume is in some way related to the time for which the exhaust port is open, however, this is just a coincidence. Measurements taken at higher speeds, for which the exhaust port is open for a shorter time, show that the time for the exhausting of the muffler volume is the same (about 8 milli seconds) as at 2700 r.p.m. Such a constant exhausting time would, in fact, be expected as the gas release from the volume, through the outlet orifice, would be very crudely at an exponentially decreasing rate, with a certain time constant. Certainly, the release of gas over only about $\frac{1}{3}$ of the engine cycle is not desirable, as is mentioned later in section 10.3. As well as the gradual release of gas, it is clear from trace (b) of figure (37) that, inside the muffler volume, there are a few minor fluctuations of pressure caused by the abovementioned Helmholtz resonance effect. The effect of the resonance is much more noticeable in the radiated sound pressure cycle as, of course, the radiated sound pressure is related to, effectively, the derivative of the velocity values at the outlet

and not the absolute values (see section 2.9). In fact a calculation was performed to verify that the magnitude of the radiated sound pressure fluctuations, shown in figure (37)(a), was related to the pressure fluctuations observed in the muffler volume (figure (37)(b)) at the Helmholtz resonance frequency of about 420 Hz. By assuming the sound source to be a simple monopole, the peak to peak muffler pressure fluctuation which would cause the measured radiated sound pressure fluctuation of about 1 Pa (peak to peak) was calculated to be 0.22 psi. This is clearly very near to the measured values shown in trace (b) of figure (37).

In trace (b) of figure (37), the horizontal line superimposed on the measured cycle shows the average reading of the pressure transducer, obtained by using an R-C averaging circuit. This trace was obtained so as to positively identify the base level pressure, existing for most of the cycle, as the atmospheric pressure. To check this, average back-pressure measurements were taken at the pressure transducer locating position in the muffler volume by using a water filled manometer. As these measurements showed a value of 6.5 inches of water or 0.24 psi, and as the average pressure line in figure (37)(b) is also about 0.25 psi above the base level, it is then clear that the base level is, in fact, the atmospheric value.

The measurement shown in figure (37)(b) then indicates that the lawnmower engine operates normally with an actual level of back-pressure of about 1½-1 psi when the engine is exhausting the cylinder gas. This shows clearly that a measurement of average back-pressure for such an engine and muffler combination should be interpreted carefully, as an average measurement is obviously not straightforwardly related to the value acting during the exhausting process.

It is interesting to note that the inlet slits did not substantially increase the back-pressure acting at the exhaust port. In fact,

the manometer experiments showed that the average back-pressure was the same upstream of the slits as it was downstream. This fact is significant as it means that such an inlet restriction may always be used on small cavity mufflers, and, from what follows in the next section, may be used with good effect. (The total area of the inlet slits was, in fact, slightly larger than the inlet pipe).

From the results described above, it is clear that a cavity muffler acts by being rapidly filled with the exhaust gas charge and then by more gradually releasing the charge to the atmosphere. Also, it is clear that the radiated sound pressure cycle consists of an initial peak, the strength of which is clearly related to the size of the cavity volume, followed by the Helmholtz resonance type fluctuations of the cavity volume and tailpipe outlet.

So that some further insight may be found into the operation of the lawnmower muffler, it is now interesting to see how well the lumped element linear theory describes the muffler's action. As is shown below, the lumped element theory is, in fact, useful at low frequencies, as was anticipated in section 4.2.

9.2 USE OF LINEAR MODEL

In light of the satisfactory results obtained by, for example, Watters et al (7), in describing the behaviour of small mufflers using lumped element theory, a similar linear model for the lawnmower muffler was made.

In figure (36)(a) it may be seen that the lawnmower muffler may be regarded as a resistance + inductance (inlet orifices) - capacitance (volume) - resistance + inductance (outlet orifice) system. Also the small volume upstream of the inlet slits may be regarded as a small capacitance. For reasons which were given in section 4.1, the sound source impedance may be regarded as infinite (current source).

The analogous electrical circuit representing the muffler is shown in figure (36)(b), complete with the computed values of the analogous lumped impedances of the various components. These impedances are based on the well known linear relations (for example, as in reference (13)). In figure (36)(b) the atmospheric impedance, Z_o, is the radiation impedance on a piston radiator in an infinite baffle (from, for example, Morse (13)).

From the diagram of the analogous circuit it may be seen that the impedance for each of the elements may be found for various frequencies and the action of the circuit may be determined. By calculating the ratio between the current passing through Z_o, the atmospheric impedance, for the complete circuit, to the current passing through Z_o for the circuit which would simulate an engine with no muffler, the insertion loss of the muffler may be found. Also, by studying the effect of Z_4, the impedance of the inlet tube capacitance, the beneficial effect of the inlet slits may be seen. The insertion loss of the muffler, as calculated for audible frequencies using the values from figure (36)(b), is shown in figure (38) together with the measured insertion loss obtained at two engine speeds. Of course, at low frequencies the measured insertion loss is plotted only at precise harmonics, as it is for these frequencies that the 6% bandwidth analyser distinguishes the discrete harmonics. To illustrate the action of the various muffler components, the effects in the analogous circuit at several frequencies are investigated below.

50 Hz

At about 50 Hz, which corresponds to the firing frequency of the engine at 3000 r.p.m., Z_3 and Z_o are small, Z_2 is twice Z_1, so that most current flows through Z_1 and Z_o, the atmospheric impedance. (Of course, for this frequency Z_4 is so large that it may be neglected).

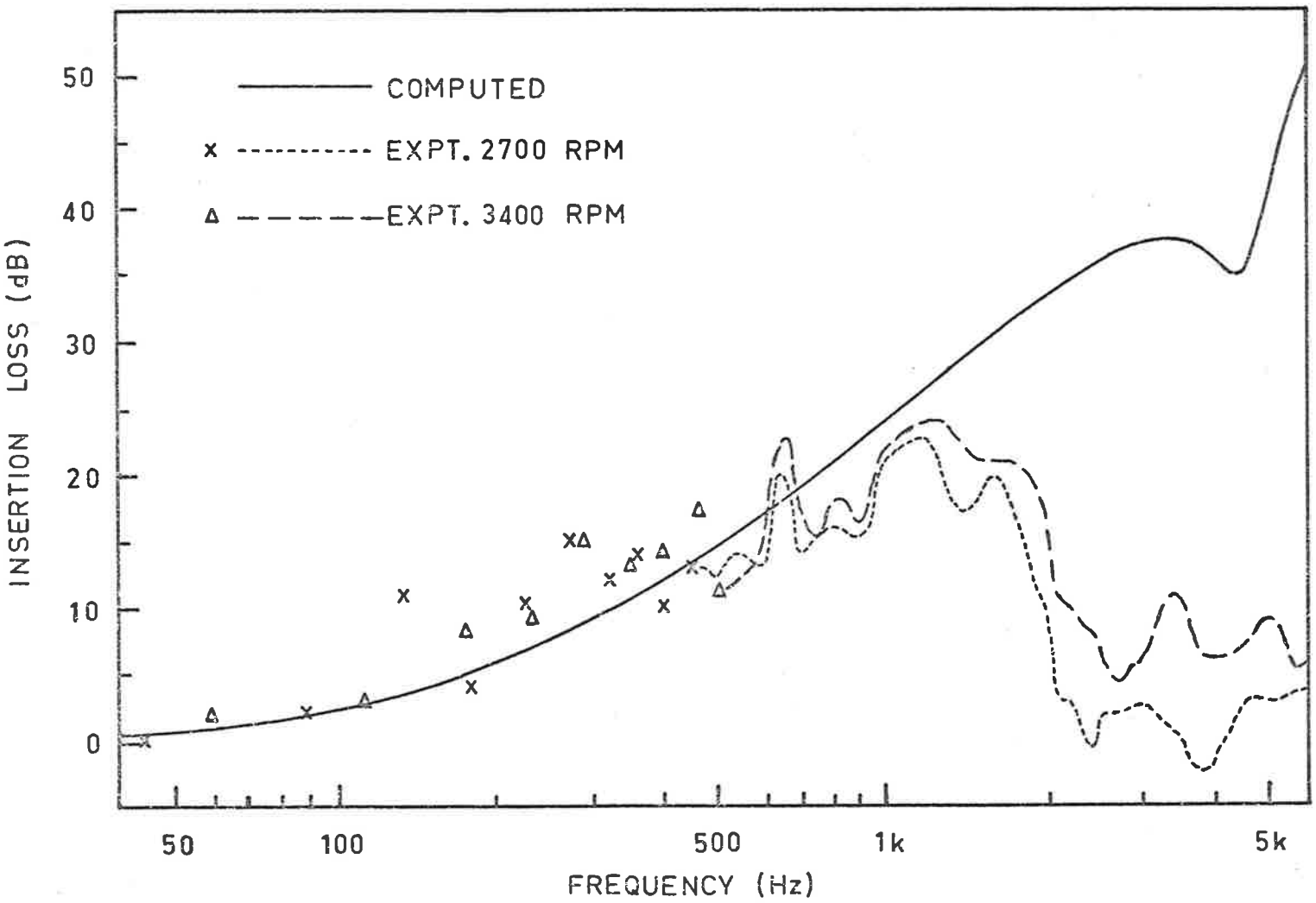

FIG. 38 INSERTION LOSS FOR LAWNMOWER MUFFLER

If the muffler is removed, the exhaust system then consists of a very short pipe and the entire current from the source goes through the atmospheric branch. The resulting computed insertion loss at 50 Hz is then clearly very low, at about 1 dB. This is in very good agreement with the measured values of 0 dB and 2 dB (for the two engine speeds) obtained at the firing frequency as shown in figure (38).

100 Hz

At 100 Hz, Z_4 may again be considered so large that open circuit may be assumed at this point. At this frequency Z_2 for the large capacitance is now roughly of the same magnitude as Z_1 and Z_o. As shown in figure (38), the computed insertion loss is about 2 dB. This still agrees favourably with the measured values of 2 dB and 3 dB at the second harmonic.

500 Hz

Again Z_4 may be considered very large in comparison with all other values. The computed insertion loss here is about 15 dB (current reduced by factor of about 6), as most current is shunted through the capacitance of the large volume. Once more, the measured insertion loss as shown in figure (38) is very near to the calculated value.

For progressively higher frequencies, the computed insertion loss continues to rise as the large capacitance shorts out the atmospheric branch. However, wave action occurs in the muffler at higher frequencies as the lumped impedance analogy breaks down, with the result that the measured insertion loss is much less than the computed trace suggests. This is shown in figure (38) in which the measured insertion loss becomes very low after about 2000 Hz. In fact, the dimensions of the muffler given in figure (36)(a) show that cross-modes would be expected at about this frequency.

Benefit of Inlet Slits

Regardless of how poorly the lawnmower muffler acts at high frequencies, it would be even less effective if not for the presence of the inlet slits which provide the restriction leading to the muffler volume. This was proven in a simple experiment and is discussed below in relation to the simple electrical analogy model.

A muffler was constructed with a larger volume than used on the original lawnmower muffler and, although it had a similar outlet orifice, the muffler did not have a restriction leading to the volume. Experiments showed that it was greatly inferior to the standard muffler, in silencing the lawnmower engine exhaust noise. This is obviously because the effect of the slits is to reduce the sharpness in the velocity rise at the tailpipe, that is, they greatly reduce high frequency radiated sound. Even though the linear theory was shown above to be decidedly inaccurate at high frequencies, the action of the inlet slits may now be crudely explained using such theory. This is considered below.

Research into the action of orifices at high sound pressure levels (for example by Ingard and Ising, as referred to in reference (1)) shows that at high peak velocities the impedance is mainly resistive and is non-linear. Generally, the impedance increases with increasing particle velocity. Now, the values of impedance for the resistances shown in figure (36)(b) are calculated using the quite low average velocity values. Clearly the resistance shown for the inlet slits is greatly underestimated. Therefore, at high frequencies and for high peak velocities, the impedance presented by the small capacitance Z_4 will be lower than that from the resistive part of Z_3. This will mean that the impedance Z_4 will then short circuit the rest of the system, so that an increased insertion loss is caused. This then corresponds, roughly, with the abovementioned measurements.

Therefore, from the above, lumped element theory is seen to be adequate in describing the muffler behaviour up to at about 1 kHz and may be used to give a simplified explanation of the beneficial effect of the inlet slits. In section 10.3, lumped element theory is used to design an improved muffler of the orifice - cavity - tailpipe type for the lawnmower engine.

CHAPTER 10

RECOMMENDATIONS FOR ALTERNATIVE DESIGN

Following the work described in the previous chapters of the second part of this thesis, recommendations are now made for a number of design alterations which, if implemented, would be expected to result in lower noise levels to be radiated from the test lawnmower. Of course, as mentioned earlier the investigations of the various noise sources on the lawnmower were made in a general manner, so that many of the recommendations given below are readily applicable to other similar types of machinery, in particular those powered by small 2 and 4-stroke engines.

10.1 MECHANICAL NOISE

The possible methods of mechanical noise reduction for the lawnmower are: reduction of excitation; reduction of vibration response and sound radiation; isolation of the source by the use of covers. The first of these methods is considered below in substantial detail.

10.1.1 Reduction of Excitation

It was shown in chapter 7 that the major source of the excitation of the lawnmower structure was from piston slap, with bearing noise possibly being a minor source at high speeds. Using the results of the analysis of piston slap type 1 in section 7.6, the effects of various design changes on the radiated sound pressure levels may then be found. First, however, the relation between the acceleration levels in the engine structure and the radiated sound pressure, must be considered.

[Note: In the remainder of section 10.1 the term "radiated sound pressure" is taken to mean the r.m.s. radiated sound pressure.]

For a periodic impulsive excitation of a multi-vibrational mode structure the radiated sound pressure at any frequency is, of course, proportional to the acceleration of the structure at that frequency, where the acceleration is measured at any point. Also, clearly, equal isolated impacts result in the same acceleration levels and radiated sound pressure. For an internal combustion engine, for equal piston impacts, the acceleration levels of the structure and the resultant radiated noise do not, however, remain the same at different engine speeds. This is considered briefly below.

For equal impacts, if the decay period is longer than the period between the impacts (which, from figure (30), appears to be the case), then it may be shown that the r.m.s. velocity (and acceleration) of the structure will scale with the square root of the frequency of impacts N. This may be seen, crudely, by considering firstly the average increment in energy due to an impact I, that is:-

$$\Delta E = mv\Delta v + \tfrac{1}{2}m\Delta v^2$$

$$= Iv + \tfrac{1}{2}\frac{I^2}{m}$$

Therefore,
$$\langle \Delta E \rangle = \tfrac{1}{2}\frac{I^2}{m} \qquad (10.1)$$

where $I = m\Delta v$, the impulse.

Thus for N impacts per unit time, the energy supplied (for impacts occurring at not precise periods) is given by:-

$$\tfrac{1}{2}N\frac{I^2}{m}$$

The energy lost per cycle of the vibrating system depends

on the damping ratio and is $4\pi\zeta E$, where E is the energy in the system. Thus, in unit time, the energy lost is approximately given by:-

$$4\pi\zeta . \tfrac{1}{2} m \overline{v^2} . f_n$$

where f_n = resonant frequency.

Since the energy supplied must equal the energy lost $\overline{v^2} \propto N$. Therefore, in terms of sound pressure, it is clear that:-

$$\text{sound pressure radiated by equal impacts} \quad \propto \quad \omega^{\frac{1}{2}} \qquad (10.2)$$

where ω = speed of rotation of crankshaft.

In order to reduce the excitation of the structure from conventional piston slap, a large number of design alternatives may be used. Some of the changes are readily applicable to the existing lawnmower, whereas, others would require major design changes. Such major design changes involve the use of significantly different engine layouts. Another method, to reduce the excitation, is to change the form of the piston slapping motion. The benefit to be had from each of these alternatives is considered in the following sections.

10.1.2 Initial Design Alternatives

It was shown in section 7.5 that the dominant force on the piston at B.D.C. is always the inertia force, whereas, at T.D.C. for firing strokes it is always the gas pressure force. An expression for the inertia force at B.D.C. may now be substituted into equation (7.9). From section 7.5 the inertia force at B.D.C. may be assumed equal to the first harmonic, with rough accuracy. Therefore:-

$$F = -m\omega^2 r \qquad (10.3)$$

Substituting for F in equation (7.9) gives:-

momentum of piston on impact = $\frac{1}{2}(36\, r\, q\, \omega^3 s^2 m^3)^{1/3}$ (10.4)

when inertia force dominates

Using equation (10.4) the momentum of the piston on impact at B.D.C. depends upon:-

obliquity of con-rod, q

engine crankshaft speed, ω

piston clearance, s

effective mass of piston, m

crank radius, r

In addition, using equation (7.9) at T.D.C., the momentum again depends on the resultant axial force F, which in this case consists largely of the gas pressure force.

If it is assumed that only the above variables change, then since the acceleration level of the structure is proportional to the piston momentum at impact, the radiated sound pressure varies as the piston momentum as given in equations (7.9) and (10.4) multiplied by $\omega^{\frac{1}{2}}$ (from relation (10.2)). The feasibility of obtaining a worthwhile noise reduction by reducing each of the above variables will now be considered below.

Gas Pressure Force Dominant

As the high gas pressure force at T.D.C. is essential to the operation of the engine, a reduction of piston momentum on impact caused by a reduction in the gas pressure force is not possible. Also, from equation (7.9), it may be seen that when the gas pressure force is dominant at T.D.C., the radiated sound pressure is relatively insensitive to changes in either the gas pressure force F or the con-rod obliquity q (momentum proportional to the $\frac{1}{3}$ rd power of these variables). Therefore little will be gained by reducing these even if it is possible to do so. Similarly, the advantage gained by a small speed reduction is small, since from equations (7.9) and (10.2)

it may be found that reducing the speed from 3400 r.p.m. to 2900 r.p.m. gives only a 1 dB reduction in radiated sound power.

Inertia Force Dominant

Equations (10.4) and (10.2) show that when the inertia force is dominant, the radiated sound pressure varies with crankshaft speed such that:-

$$\text{radiated sound pressure} \propto \omega^{3/2} \tag{10.5}$$

In this case the proposed speed reduction from 3400 r.p.m. to 2900 r.p.m. may be shown to give a 2 dB reduction in the radiated sound power, so that again little will be gained especially as engine power would be reduced.

Reduced Piston Clearance

It may be seen from equations (7.9) and (10.4), that the relation between the radiated sound pressure from impacts at both T.D.C. and B.D.C., and the diametral clearance, is given by:-

$$\text{radiated sound pressure} \propto s^{2/3} \tag{10.6}$$

From the manufacturer's drawings, the cold clearance for the piston is 0.007 inches (0.18 mm) which, as is well known, is typical for the piston and cylinder materials used. Using the relation (10.6), it may be shown that a reduction of piston clearance to 0.004 inches would cause a sound power reduction of over 3 dB. This reduction in clearance, for the standard piston, would seem to be impractical as the original piston was found to expand sufficiently, under heavy load conditions, to seize in the bore. This high degree of expansion occurred in the area of the gudgeon pin bosses, as a result of the higher local heat transfer, and is common for plain pistons as is well known. However, using the standard piston, the clearance may be reduced, if the piston is machined slightly oval as is commonly done to compensate for the greater expansion near the gudgeon pin bosses.

It may be mentioned that considerable research has been done recently to achieve a reduced piston clearance, for example, by using expansion controlled pistons (as mentioned in reference (22)). The possibility of using any such piston modifications is not considered in this thesis, but it is clear from relation (10.6) that there is much to be gained by a greatly reduced clearance.

Reduced Piston Mass

From equations (7.9) and (10.4) it may be seen that the relations between the radiated sound pressure and the effective piston mass are:-

$$\text{radiated sound pressure (gas pressure force dominant)} \propto m^{2/3} \qquad (10.7)$$

$$\text{radiated sound pressure (inertia force dominant)} \propto m \qquad (10.8)$$

For the lawnmower engine, the effective mass of the piston was composed of the piston itself (124 gms), the gudgeon pin (31 gms) and $\frac{1}{3}$ the mass of the con-rod (43 gms). It then follows from relations (10.7), (10.8) that if the effective piston mass is reduced from 198 gms to about 150 gms, the radiated sound pressure will be reduced by about 1.7 dB and 2.5 dB, respectively. The piston used in the existing engine is of an aluminium alloy, whereas the con-rod and gudgeon pin are of cast iron and steel, respectively. If suitable lightweight materials are available for these parts, a useful sound power reduction of several dB would be obtained.

Split Skirt Piston

The above considerations assume that the impact takes place over a fixed time Δt, so that the acceleration of the cylinder scales with the momentum of the piston on impact. As shown in section 10.1.1,

the acceleration also depends on the number of impacts per second. In addition, for fixed momentum on impact the instantaneous acceleration scales with $\frac{1}{\Delta t}$, where Δt is the duration of impact. Thus increasing Δt has a direct effect on reducing a pressure pulse corresponding to this initial acceleration of the structure. Depending, however, on the modes excited by this longer duration impact and their Q, the net effect on the sound power radiated due to a longer impact may or may not be significant. (for $\Delta t \ll$ than the resonance period, the subsequent vibration is independent of Δt). Clearly, if Δt becomes comparable with the period of the characteristic modes excited, increasing Δt will reduce the acceleration response. Thus a slotted piston skirt, as is sometimes used in automotive engines, will increase Δt and for the above reasons this may reduce the sound power radiated since Δt may then be of the same order as the period of the resonant vibration.

Increased Cylinder Mass

It is clear from section 7.6 that the initial acceleration of the engine structure following impact is inversely proportional to the effective cylinder side wall mass. The acceleration may therefore be decreased by increasing the mass of the cylinder wall or fins. At the same time, increasing the mass by increasing the cylinder wall thickness will increase the frequency of vibration and indeed the net effect may be to increase the sound radiated due to an improved radiation ratio. Thus care is required in considering the effects on the sound radiated of modifying the cylinder. A larger mass and a lower stiffness will reduce the resulting acceleration of the cylinder and the corresponding sound pressure.

10.1.3 Piston Tilt

The analysis of piston slap, considered so far, has assumed that piston slap occurs as described in section 7.3.3, that is, with

the gudgeon pin having traversed the clearance s before impact. If the piston is made to move in a tilting motion, as described by figure (39), and as is commonly done in production engines, it may be seen that the effective travel of the centre of the piston (at the gudgeon pin) is halved. The expectation of a lower sound power radiated is verified by the following analysis.

Near T.D.C. the motion of the piston will be as shown in figure (39)(a) and the forces acting, as shown in figure (39)(b). The assumptions made in section 7.6, of constant resultant axial force F and small crank angles, will again be made. It will also be assumed for convenience that the centre of mass of the piston coincides with the geometric centre and that the gudgeon pin is offset from the centre of the piston by an eccentricity e (see figure (39)(b)).

From figure (39)(b) it may be seen that for the time period considered the torque on the piston as a function of time is:-

$$Fe - Fq\,\omega t\,\frac{r_p B}{2}$$

where t = time from T.D.C. (or B.D.C.)

e = eccentricity of gudgeon pin

r_p = ratio of piston skirt length to bore

B = bore

From a certain crank angle before T.D.C. and until the same angle after T.D.C., it may be seen that the tilting torque Fe will be the greater, causing a tilting motion toward the left hand side of the cylinder. It is clear that the final tilting to the left hand side of the cylinder, as shown in the 3rd diagram of figure (39)(a), does not commence until the time past T.D.C. at which the tilting torque Fe is less than the varying torque. It may be shown that this time, t_1, is given by:-

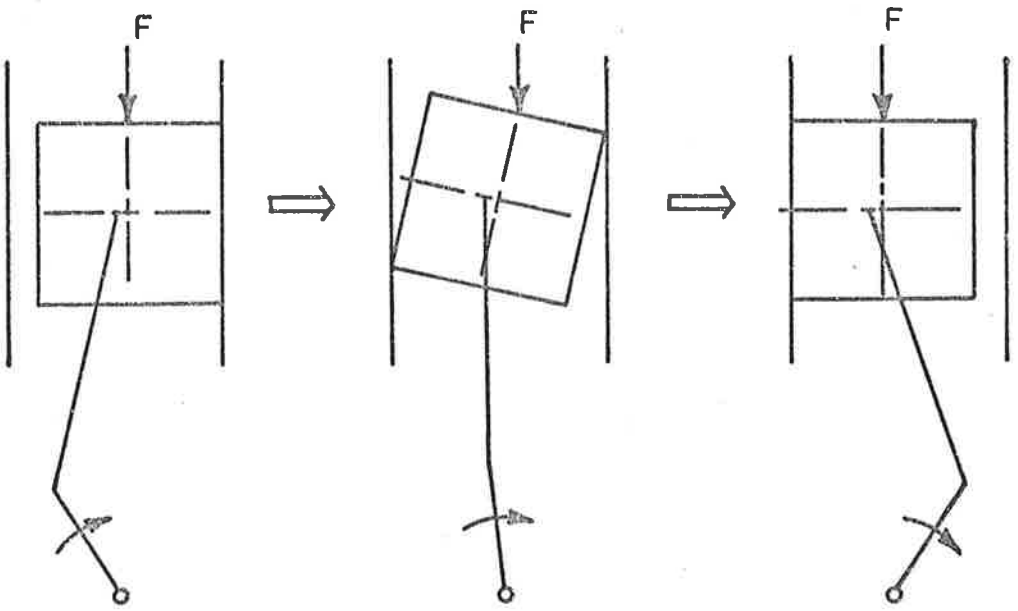

(a) MOTION OF TILTING PISTON NEAR T.D.C.
WITH GAS PRESSURE FORCE DOMINANT

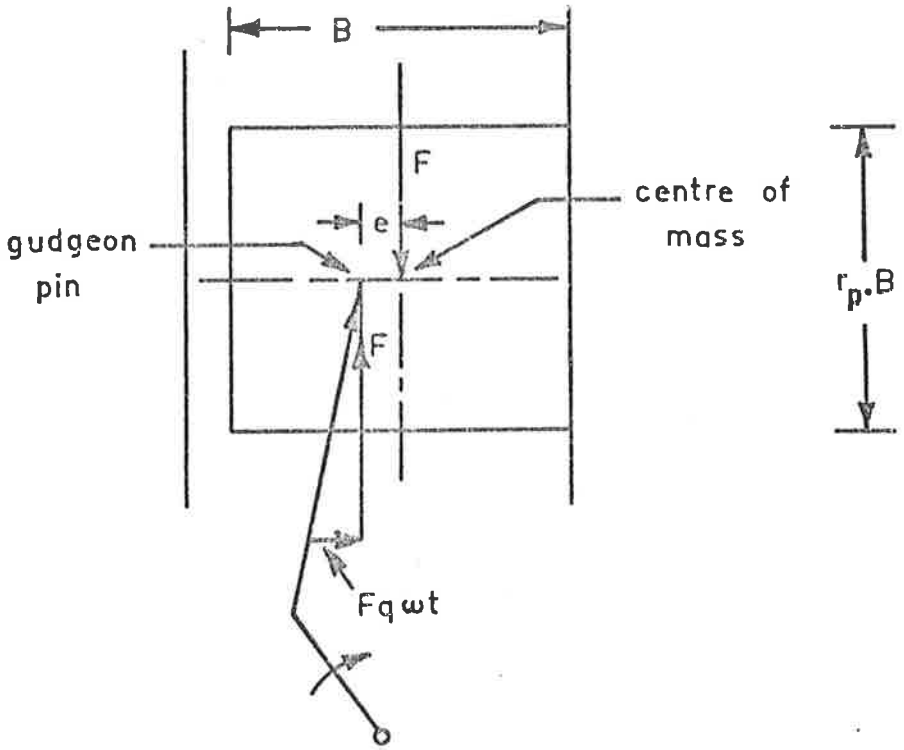

(b) FORCES ON TILTING PISTON NEAR T.D.C.

FIG. 39 PISTON TILT WITH OFFSET GUDGEON PIN

$$t_1 = \frac{2e}{r_p B q \omega} \qquad (10.9)$$

From a consideration of the forces acting on the piston, during the tilting motion, an expression for the sideways distance travelled by the piston centre may be found:-

$$x(t_2) = \frac{F r_p^2 q \omega t_2^3}{6m(4K^2 + r_p^2)} \qquad (10.10)$$

where t_2 = time from start of piston tilting

$x(t_2)$ = distance travelled by piston centre

K = ratio of radius of gyration of piston mass to bore

m = effective piston mass.

The corresponding equation for a normal piston, in a slapping motion, from section 7.6 is:-

$$x(t) = \frac{F q \omega t^3}{6m} \qquad (10.11)$$

where t = time after start of piston slapping motion (after T.D.C.)

$x(t)$ = distance travelled by piston centre.

Using equations (10.10) and (10.11), assuming that the impact for the tilting piston occurs before T.D.C. (or B.D.C.), it may be shown that the ratio of the radiated sound pressure from the engine with a tilting piston, to that radiated from a standard engine is:-

$$\text{ratio of radiated sound pressures for tilting: slapping} = \left[\frac{r_p^2}{4(4K^2 + r_p^2)}\right]^{1/3} \left[\frac{8K^4}{r_p^4} + \frac{4K^2}{r_p^2} + 1\right]^{1/2} \qquad (10.12)$$

It may also be shown that if the tilting is to be completed exactly at T.D.C. or B.D.C., when inertia forces dominate, the ratio of the required eccentricity to the bore is given by:-

$$\frac{e}{B} = \sqrt[3]{\frac{3 s r_p q^2 (4K^2 + r_p^2)}{8r}} \qquad (10.13)$$

where r = crank radius

s = piston clearance

For the lawnmower engine, the value of $\frac{e}{B}$ from equation (10.13) is 6.2×10^{-2}. From equation (10.12), assuming values of K and r_p of $\frac{1}{3}$ and 1.0, respectively, the ratio of the sound pressure radiated by the impact from tilting, to that from normal slapping is 0.69. Now from equations (10.9) and (10.10), if the tilting is to finish exactly at T.D.C. (or B.D.C.) for a value of q of 0.253, the tilting will start about 28° before T.D.C. (or B.D.C.). Therefore, as the second tilting motion, as shown in diagram 3 of figure (39)(a), will not start until 28° after T.D.C., the resulting acceleration from this impact will be less than from that near T.D.C., as the resultant force is much less when the impact occurs. It may be seen, that the expected benefit from placing the gudgeon pin eccentric in the piston, will be at least about 2 dB reduction in radiated sound power.

10.1.4 Alternative Engine Layout

It is of interest to now briefly consider alternative engine layouts, particularly larger engines operating at lower speeds, the use of a greater bore to stroke ratio and engines with increased numbers of cylinders. It is assumed that all prospective engines must deliver the same power, drive the cutter blade mounting plate directly from the crankshaft and drive the cutter blades with the

same peripheral velocity. From the point of view of mechanical noise, as caused by piston slap type 1, the effects were predicted crudely by simple scaling arguments.

Lower Engine Speed

If a larger engine with a lower crankshaft speed produces the same power with the same mean effective pressure, the swept volume clearly varies inversely with the speed. For geometrically similar engines, the variation of the engine speed ω with the bore (diameter) B is:-

$$\omega \propto B^{-3} \tag{10.14}$$

Also, it is clear that the following relations are true:-

effective piston mass	$m \propto B^3$	(10.15)
gas pressure force	$F \propto B^2$	(10.16)
piston clearance	$s \propto B$	(10.17)
crank radius	$r \propto B$	(10.18)

Using the relations (10.14) to (10.18) it may be simply shown that, whether either the gas pressure or inertia forces dominate, the sound power radiated depends only weakly on B. If gas pressure forces dominate (that is, for impacts after T.D.C.):-

$$\text{radiated sound pressure} \quad \propto B^{-1/6} \propto \omega^{1/18} \tag{10.19}$$

If inertia forces dominate:-

$$\text{radiated sound pressure} \quad \propto B^{-3/2} \propto \omega^{1/2} \tag{10.20}$$

Relations (10.19) and (10.20) show that a larger, slower engine is marginally quieter but offers no practical advantage.

Greater Bore to Stroke Ratio

If the bore to stroke ratio is increased by increasing the bore and decreasing the stroke to give the same swept volume, again only a small practical advantage may be had. In terms of engine bore B, it may be shown that:-

radiated sound pressure (gas pressure force dominant) $\propto B^{-2/3}$ (10.21)

radiated sound pressure (inertia force dominant) $\propto B^{-1}$ (10.22)

Multiple Cylinders

By using more than the usual single cylinder, whilst retaining the same bore to stroke ratio and engine speed, it may be shown that no practical advantage at all is gained. This is, basically, because the penalty of increased numbers of impacts offsets the benefit of reduced piston momentum at each impact.

10.1.5 Alternative Methods

On the test lawnmower there is some scope for achieving a noise reduction by means of reducing the vibration response. This may be done by using vibration isolation and by attaching parts together at the points of maximum stiffness.

Vibration isolation could be applied to the various parts which are attached to the basic engine, and for the test lawnmower this includes the base frame, the cutter blade mounting plate and the engine cover. If the isolation was very effective, from the results of section 7.7, a reduction of at least 3 dB overall, could be achieved.

Generally vibration response is reduced if parts are attached together at the points of maximum stiffness. For the test lawnmower engine, it may be seen from figures (23) and (31) that the base frame

and the engine cover, both, are attached to the crankcase at the furthest extremities of thin surfaces, that is at points of minimum stiffness where vibration would be at a maximum.

Enclosures

The use of enclosures or covers is a method by which the sound radiated by a structure or surface is prevented from reaching the far field. For the lawnmower such a cover could be used to enclose the basic engine itself. A cover of this type was constructed for simple experiments.

The cover was constructed with a lining of 1½ inch thick fibre wool and would have been expected to greatly reduce high frequency sound, particularly above about 2 kHz. When used as a cover over the engine on the silent frame, with the cover very effectively vibration isolated, an overall reduction of 5.5 dB was achieved, with an 8 dB reduction over 650 Hz. When the vibration isolation of the cover was reduced, however, to the level expected for a production engine, the overall reduction was much less as the cover was then radiating low frequency engine vibrations better than the standard mower. The sound reduction achieved in these experiments was expected to be the maximum possible with the particular lining material as the engine base frame, which is a proven noise source, was not in place under the engine. Therefore, given the disappointing overall sound reduction and the fact that proper engine cooling must be provided, the use of an engine enclosure is not recommended.

10.1.6 Summary

The work described in the preceding sections shows that considerable reductions in mechanical noise from the lawnmower may be obtained by reducing the excitation through minimizing piston slap. To a lesser extent some worthwhile benefit is to be had by isolating

the engine from the base frame. For the test lawnmower, the expected reductions of sound power radiated as a result of certain modifications are given below in table 10.1. If some of the modifications are used simultaneously, of course, their effects are cumulative.

Table 10.1 : Reduction of Mechanical Noise

	MODIFICATION	REDUCTION IN DB
1	Piston clearance 40% less*	3
2	Lightweight con-rod	2
3	Offset gudgeon pin	2 (approx)
4	Engine isolated from frame	3

Many of the above modifications are expected to have direct applications with other machines powered by small 2 and 4-stroke engines.

* [Reduction of the piston clearance is conceivable by improved quality control in relation to selective fitting, also possibly by the use of a more sophisticated design incorporating, for example, machining of the pistons to a slightly oval shape.]

10.2 CUTTER BLADES

Following the investigation of cutter blade noise described in chapter 8, recommendations are made below for alternative designs of the cutting system. If the suggestions are implemented, it is expected that there would be a significant reduction in the noise radiated by the cutting system on the test lawnmower, although the magnitude of the expected reduction is not given.

In chapter 8 it was shown that the fluctuating forces on the cutter blades are responsible for the cutter blade noise. Moreover,

it was shown that the cause of the fluctuating force on a blade was the action of the blade's own turbulent wake. Generally, the fluctuating blade forces may be expected to scale with the mean blade force, that is, with the blade lift angle and the amount of air pumped by the blades. Therefore if the amount of air required to be pumped by the cutter blades may be reduced, so will the fluctuating blade forces and the resultant noise from them be reduced. As shown below, a reduction in the amount of air needed to be pumped by the cutter blades may be accomplished by either optimizing the flow in a conventional type of cutting system, or by having a separate fan acting as the main air pump whilst also having blades to cut the grass.

10.2.1 Conventional Cutting System

With a conventional cutting system, such as that used on the test lawnmower, the driving force producing the flow is provided by the cutter blades themselves. That is, there is an inseparable link between the fan action and the cutting action. From the point of view of noise control this is not desirable as it is difficult to control the noise while maintaining the cutting action and the removal of the grass clippings. This disadvantage leads to the recommendations given in the next section concerning separate fan and cutting systems.

For the conventional cutting system, however, it is obvious that to reduce the noise it is necessary to improve the quality of the air flow so that the aerodynamic forces on the blades for a given air flow may be a minimum. That is, if the channelling of the flow into the catcher duct is optimized, the necessary blade lift angle to provide the required air pumping may be reduced along with the noise. In fact, even if the blades are unaltered, improved channelling itself is likely to reduce the mean blade forces.

The air flow into the catcher duct on the test lawnmower

cutting system was investigated by taking velocity profiles across the duct width near the duct inlet (at a fixed height above the base of the mower). In all such measurements separation and subsequent flow reversal near the upstream wall of the catcher duct indicated that the flow was far from optimized. It is then obvious that the noise level would be reduced if a volute shaped inlet to the catcher is used, as well as a somewhat smaller blade angle. In fact, such a volute shaped blade housing has been used successfully on some other makes of lawn-mowers (for example, Victa) for some time.

Apart from these changes it seems unlikely that any other design change could reduce the noise while maintaining the grass cutting and grass catching action. Of course a slower engine speed or blade tip speed has a very pronounced effect on the noise (figure (35)) as the noise is dipole in character. However, as it is generally accepted (for example, reference (17)) that an adequate cutting speed for blunt blades is 80 m/sec (about 3000 r.p.m. for 18 inch cutting diameter), a reduced speed will not be regarded as an adequate solution.

10.2.2 Separate Fan and Cutting System

As mentioned above, it is preferable to have a separate fan and cutting system as the amount of air required to be pumped by the blades may then be reduced, thereby reducing the noise from the blades. Of course having separate air pumping and cutting systems may be combined with the recommended changes given above.

A separate fan and cutting system as described below is, as yet, not completely proven in practice, however, mention of it is made in this thesis as a significant noise reduction is conceivable through its use.

To ascertain the airflow which must be provided by the air pump and the blades, respectively, the nature of the flow in the blade

housing for the test lawnmower cutting system was investigated using visualization techniques. The flow pattern found, is described in section 8.1 and shown in figure (33). It was clear that the airflow which must be provided by the blades is that which is sufficient to raise the grass for cutting and to raise the clippings into the swirling flow above the blade disc. The blades, however, need not provide the driving force behind the radial flow, outwards from the centre of the blade disc, nor for the centrifugal flow relative to the housing. There is some uncertainty regarding the actual action of blades in cutting grass, that is, whether the air flow they provide is sufficient for the removal of the clippings or whether they are required to hit the clippings, so giving them an upward as well as tangential velocity. It has been assumed that the airflow, itself, is adequate.

Therefore, so that the fluctuating blade forces and the subsequent noise might be minimized, a centrifugal air pump was devised to provide the majority of the flow (radial and centrifugal) with a small blade lift angle used to raise the grass. The air pump, as shown in figure (40), was mounted immediately above the blade disc. As the flow velocity at the cutter blade tips was greater than in the air pump, the noise from the air pump was expected to be much less than from the blades. In fact, the noise from the cutting system with the blades with a 10° lift angle was no greater whether the air pump was installed or not. Experiments showed that the noise radiated by the cutting system consisting of the air pump and the 10° lift blades was 6 dB less than from the standard system on the test mower, although the peak flow velocity was found to be only about 60% of that required. However, it is expected that a similar air pump could be made to provide a sufficient air flow without significantly adding to the noise provided by the blades themselves.

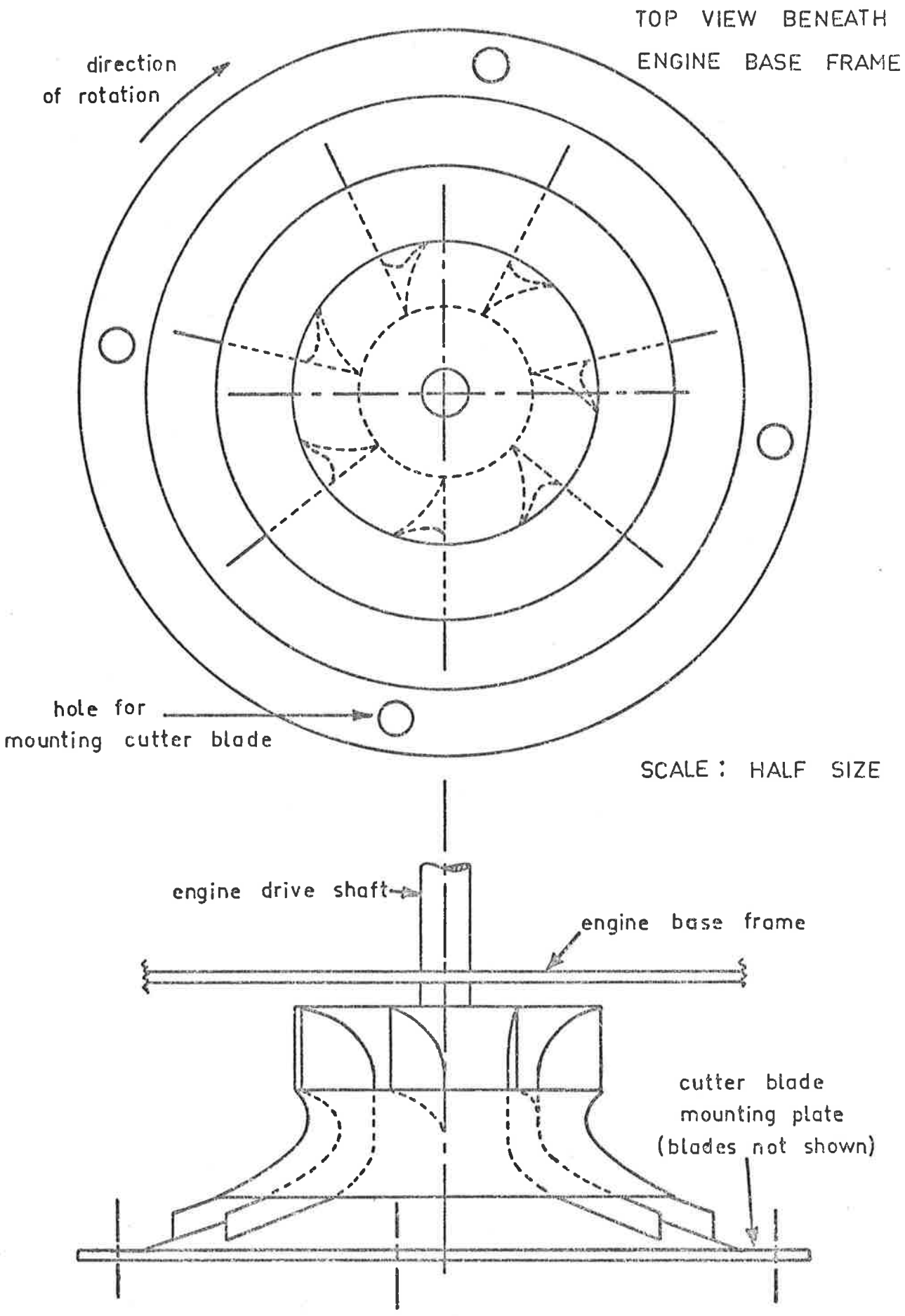

FIG. 40 CENTRIFUGAL AIR PUMP
FOR CUTTING SYSTEM

10.3 EXHAUST NOISE

The measurements of insertion loss for the lawnmower muffler, shown in figure (38), indicate that there is a definite need to increase the low frequency attenuation. Figure (38) shows, in fact, that the sound at the first two harmonics of the firing frequency is almost totally unaffected by the standard muffler. This poor low frequency insertion loss is obviously related to the rather too rapid release of gas from the muffler volume described in section 9.1. As well as improving the low frequency attenuation, it is necessary to maintain the good mid frequency insertion loss and to make improvements above about 2 kHz. These requirements are then the basis for the recommendations given below. In section 10.3.1, modifications to the standard type of muffler are considered and in section 10.3.2, the possible benefit from a different port shape is briefly studied.

10.3.1 Design Improvements for Muffler

It was shown in section 9.2 that the linear muffler analysis as used, for example, by Watters et al (7) was adequate for cavity mufflers for frequencies below about 1 kHz. Therefore, suggestions for improvements to the existing lawnmower muffler, to increase the attenuation at low frequencies, will be based on this analysis. Modification of the existing lawnmower muffler is, of course, a simple solution but it is not necessarily the ultimate means of silencing the exhaust. An alternate solution using a varying area pipe designed by the method of part 1 may be cheaper and less bulky and provide a greater insertion loss. Such methods were not considered here, however.

Watters et al (7) showed that the insertion loss of a cavity muffler is greater when the firing frequency of the engine is above the volume - orifice (or tailpipe) resonance. This means that if the resonance frequency is made lower for a fixed engine speed, the gas

takes longer to exhaust out of the muffler chamber. It is preferable that the exhausting be extended somewhat beyond one engine cycle. Therefore the resonance for the lawnmower muffler needs to be reduced to about 45 Hz, as this would extend the exhausting over 1 cycle at 3000 r.p.m. Calculations mentioned in section 9.1 show the resonance for the existing muffler to be at about 360 Hz, whereas measurements of the radiated sound pressure cycle described in the same section suggest that it may be nearer 420 Hz. The resonance frequency then needs to be reduced by a factor of about 8.

It may be shown that:

$$f_o \propto \sqrt{\frac{D^2}{V\ell}} \quad \text{reference (7)} \qquad (10.23)$$

where f_o = resonance frequency

D = tailpipe diameter

V = cavity volume

ℓ = tailpipe length

f_o will be reduced by a factor of 8 if:

D constant

V x 3 (10 cm diameter x 23 cm length)

ℓ x 21 (tube of 25.5 cm length)

(The original equivalent tube length for the orifice was taken as approximately the orifice diameter).

A muffler of the above dimensions would be bulky but not unacceptable. Such a muffler would be similar to the muffler no. 2, which Watters et al tested on a 2-stroke engine, except that the volume for the proposed design is twice as large. As Watters obtained satisfactory values of back-pressure during the cylinder exhausting (no more than 1 psi above atmospheric) it would be expected that the

proposed design would be quite adequate in this regard.

Wave action may be expected to occur at high frequencies. The first pass band of the tailpipe would be expected at about 1 kHz. Such wave action may be attenuated by the use of quarter wave or other types of filters incorporated into either the cavity volume or tailpipe. When the engine is operating at speeds above the basic resonance frequency, the sound pressure level in the tailpipe will not be as great as in the cavity, as the tailpipe is shorted out by the low impedance cavity volume. Therefore linear theory may be used to adequately design any tailpipe filters.

Finally, as the inlet slits, which form the inlet restriction to the standard muffler volume, were shown in section 9.2 to be beneficial in reducing middle and high frequency noise, they may be retained.

10.3.2 Alternate Port Shape

It was mentioned in chapter 1 that variations is the mass flow rate through the exhaust port of an engine into the exhaust system result in the wave action and the subsequent exhaust noise. Now the wave action would obviously be less if the release of the exhaust gas through the port was more gradual, so that the higher harmonics of the initial pulse could be reduced while the lower harmonics would be relatively unaffected. This would then be expected to result in a considerable reduction in the high frequency radiated noise.

To briefly check the advantage to be gained, a simplified pulse shape for the exhaust cycle was assumed to be sent down an exhaust system of infinite length (no reflections). The fraction of a cycle occupied by the pulse shape was allowed to vary and the resulting pressure cycle at a point in the exhaust pipe was Fourier analysed. For the pulse shape, a single period cosine curve of 13 kPa peak amplitude was used since the actual initial pulse appeared to take, very roughly, this form (see figure (2)). It was assumed that

no pulse steepening would occur. The pressure cycle is shown in figure (41)(a).

Now, with the pressure peak held constant at 13 kPa the fraction of the engine cycle occupied by the pulse was set to 1/15 th, 1/22 nd, 1/30 th and respective cycles were analysed to the 40 th harmonic (2 kHz at 3000 r.p.m.) and results are shown in figure (41)(b). For the actual engine, such a variation in pulse width would be accompanied by a change in peak amplitude, however, general trends are correct. For a variation of pulse width from 1/15 th to 1/30 th there is about a 15 dB difference at the 40 th harmonic, however the low frequency noise for the long pulse is 6 dB greater. Even when the pulse width is 1/22 nd as compared to 1/30 th of a cycle, a difference of over 10 dB is seen at the 40 th harmonic.

It is clear, therefore, that careful design of the port shape (for 2-stroke engines with piston operated ports) or valve lift rates (for 4-stroke engines with poppet valves) is essential, and a possible high frequency noise reduction may be achieved by ensuring that the exit mass flux from the engine does not occur too rapidly. This sort of consideration is impractical for high speed, high performance engines, but for slower speed engines there may be benefits in designing the port (or cam profile) so that the rate of increase in port area with crank angle is relatively slow. Obviously the effects could be studied in detail by the application of the program developed in part 1. It was not pursued further here.

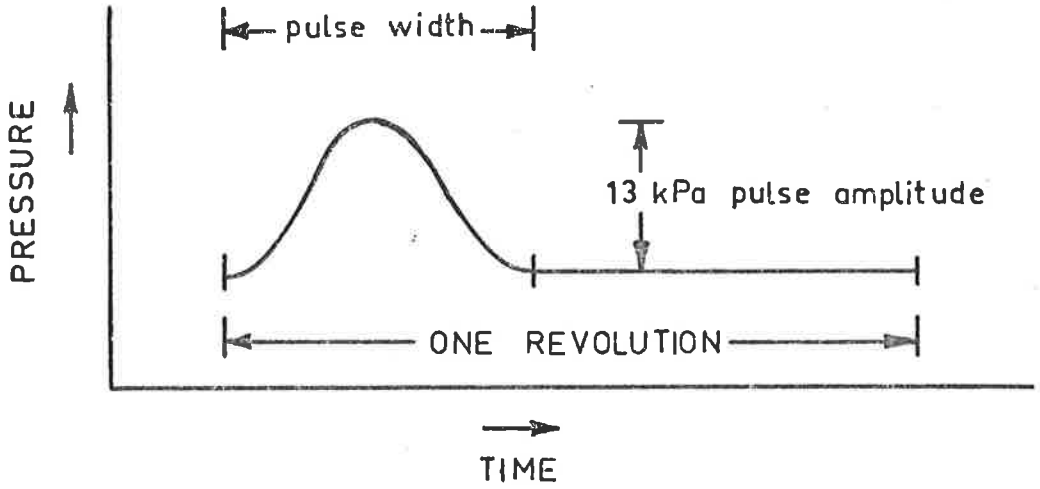

(a) PRESSURE AT POINT IN EXHAUST PIPE, WITH SIMPLIFIED PULSE

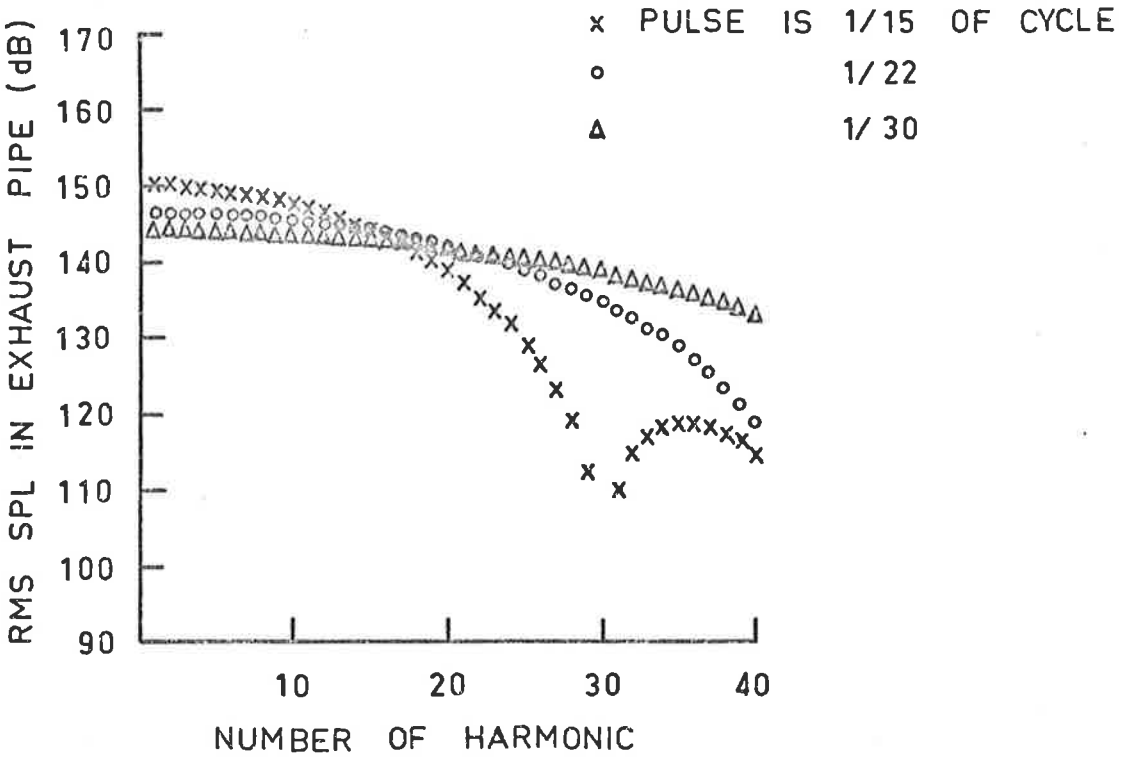

(b) SPECTRUM OF SOUND IN EXHAUST PIPE

FIG. 41 ALTERNATIVE PULSE SHAPE

CHAPTER 11

CONCLUSION

The investigation made into the basic noise sources of the lawnmower showed conclusively the relative significance of each of the sources. It was found that each of the mechanical, cutter blade and exhaust noises was significant in the overall radiated noise level with cutter blade noise being particularly dominant at high speed. Generally, the exhaust noise was greatest at low frequencies with the cutter blade and mechanical noise being greatest at the middle and high frequencies. Clearly, if any overall noise reduction is to be achieved, and it was shown that there needs to be a reduction to meet proposed legislation, then the noise from each of the above sources must be reduced.

The studies of each of the basic noise sources showed that in each case considerable reductions of noise from the lawnmower are possible, without having to use undesirable alternatives such as a slower operating speed, an engine cover or a highly restrictive muffler. In making these studies, various interesting features of each of the main noise sources were found and in some cases the results were expected to have wider application to similar types of machinery powered by small 2 and 4-stroke engines.

The mechanical noise, for example, was conclusively shown to be caused by piston slap. A very detailed analysis of mechanical noise, including a theoretical discussion of piston slap, showed that by making various changes to the engine the piston slap and the resultant mechanical noise could be significantly reduced.

The cutter blade noise was found to result from the fluctuating forces on the cutter blades caused by the action of the blades' own turbulent wakes. It was found that the best possibilities for reduction of this noise lay in either using an improved blade housing or by using a separate fan and cutting system.

In investigating the exhaust noise it was found that the very small existing muffler acted in a predictable way if described by simple linear acoustics and equivalent electrical impedances. Correspondingly a much more effective muffler could be designed by reducing the resonant frequency of the cavity and tailpipe, that is, by simply increasing the volume of the cavity and increasing the tailpipe length. The dimensions would still be relatively small compared with acoustic wavelengths of interest, so that for this case this simple theory will be adequate. It seems likely, however, that a variable area, longer exhaust muffler making use of the methods of part 1 could be designed to provide a much greater insertion loss than the present muffler and possibly an equally acceptable or better design solution than the simple increase in cavity volume just described.

It is expected that many of the recommended alterations could be made to the existing lawnmower with a resultant significant reduction in the radiated noise. Most of the recommendations do not involve very expensive changes apart from the admittedly high tooling costs involved.

APPENDIX 1

MOTORCYCLE ENGINE SPECIFICATIONS

The engine used is from a Suzuki TS 125 model motorcycle. The engine is a single cylinder air cooled 2-stroke type, is crankcase scavenged and has piston operated ports. Lubrication is provided by the "posi-force" system:- a system in which a regulated supply of fresh oil is force fed to various locations in the engine. Ignition is by flywheel magneto.

BASIC DIMENSIONS

compression ratio	6.7 : 1
bore x stroke	56 x 50 mm (2.20 x 1.97 in)
swept volume	123 cc (7.5 in^3)
crankcase compression ratio	1.3 : 1
maximum power	13 h.p. at 7,000 r.p.m.
maximum torque	1.36 kg-m (9.8 lb-ft) at 6,500 r.p.m.
ignition timing	21 - 23° BTDC

PORT TIMING

Inlet	open	70°	BTDC
	close	70°	ATDC
Exhaust	open	98°	ATDC
	close	98°	BTDC
Transfer	open	116°	ATDC
	close	116°	BTDC

APPENDIX 2

CYLINDER AND CRANKCASE CONDITIONS

1. MASS FLOW RATE IN TERMS OF CYLINDER CONDITIONS

The mass flow rate out of the cylinder may be expressed in terms of the cylinder conditions, the exhaust port throat area and a flow parameter C(t). The parameter C(t) is constant for choked flow and for subsonic flow is related to the pressure ratio between the reservoir (cylinder) and the throat static pressure (equal to static pressure just downstream of the port). The derivation of C(t) is considered in section 2 of this appendix.

Thus $$\dot{m}(t) = C(t)\,\rho_c(t)\,a_c(t)\,A(t) \qquad (1)$$

where $\dot{m}(t)$ = mass flow rate as function of time

$\rho_c(t)$ = density in cylinder

$a_c(t)$ = sonic velocity in cylinder

$A(t)$ = area of exhaust port open

from (1)

$$\dot{m}(t) = \rho_c(t)\,V_c(t)\,\frac{C(t)\,a_c(t)\,A(t)}{V_c(t)}$$

where $V_c(t)$ = volume of cylinder

Therefore, if $$\lambda(t) = \frac{C(t)\,a_c(t)\,A(t)}{V_c(t)} \qquad (2)$$

since $$M_c(t) = V_c(t)\,\rho_c(t) \qquad (3)$$

$$\dot{m}(t) = \lambda(t)\,M_c(t) \qquad (4)$$

where $M_c(t)$ = total mass in cylinder.

Now $$M_c(t) = M_c(o) - \int_o^t \dot{m}\, dt$$

Therefore, substituting for $M_c(t)$ in (4):-

$$\dot{m}(t) = \lambda(t)\,[M_c(o) - \int_o^t \dot{m}\, dt\,] \qquad (5)$$

It is now necessary to obtain a general solution to this equation for $\dot{m}(t)$. Differentiating (5) with respect to t:-

$$\frac{d}{dt}\,[\frac{\dot{m}(t)}{\lambda(t)}\,] = -\frac{\dot{m}(t)\,\lambda(t)}{\lambda(t)}$$

Now integrating gives:-

$$\int_o^t \frac{d[\frac{\dot{m}(t)}{\lambda(t)}\,]}{\frac{\dot{m}(t)}{\lambda(t)}} = -\int_o^t \lambda(t)\, dt$$

$$\ln\,[\frac{\dot{m}(t)\,\lambda(o)}{\lambda(t)\,\dot{m}(o)}\,] = -\int_o^t \lambda(t)\, dt$$

Taking exponentials:-

$$\frac{\dot{m}(t)}{\lambda(t)} = \frac{\dot{m}(o)}{\lambda(o)}\; e^{-\int_o^t \lambda(t)dt} \qquad (6)$$

From (5), at $t = 0$:-

$$\dot{m}(o) = \lambda(o)\, M_c(o)$$

Therefore, substituting for $\dot{m}(o)$ in (6) gives:-

$$\dot{m}(t) = \lambda(t)\, M_c(o)\; e^{-\int_o^t \lambda(t)\, d(t)} \qquad (7)$$

This is the required general solution for the mass flow rate $\dot{m}(t)$.

Equation (2) shows that $\lambda(t)$ has the dimensions of $[\text{time}]^{-1}$, so that $\lambda(t)$ is then the reciprocal of a characteristic time required to exhaust the cylinder.

2. FLOW PARAMETER

The flow parameter, C(t), as described in section 1 of this appendix, will now be derived. Obviously this flow parameter must be known for both outflow and inflow through the cylinder exhaust port. Similarly, a value of the flow parameter must be known for flows between the crankcase and the cylinder. There are two general flow cases which must be considered:- choked flow and subsonic flow. In all cases the flow is considered to be isentropic from the source of the flow (cylinder, crankcase or exhaust pipe) to the throat (exhaust port or transfer ports), with a loss in total pressure occurring as the flow leaves the throat. Furthermore, for subsonic flow, it is assumed that the throat static pressure is equal to the downstream static pressure (in either the cylinder, crankcase or exhaust pipe). The form of the flow parameter then follows quite simply from the energy equation, as it is assumed that the flow is adiabatic. As an example, the flow parameter for a flow from the cylinder to the exhaust pipe will be obtained.

Figure (1) shows the flow situation considered. The mass flow rate from the cylinder may be expressed in terms of the conditions in the exhaust port:-

$$\dot{m}(t) = \rho_p\, A(t)\, u_p$$

that is,

$$\dot{m}(t) = \rho_p\, A(t)\, M_p\, A_p \qquad (8)$$

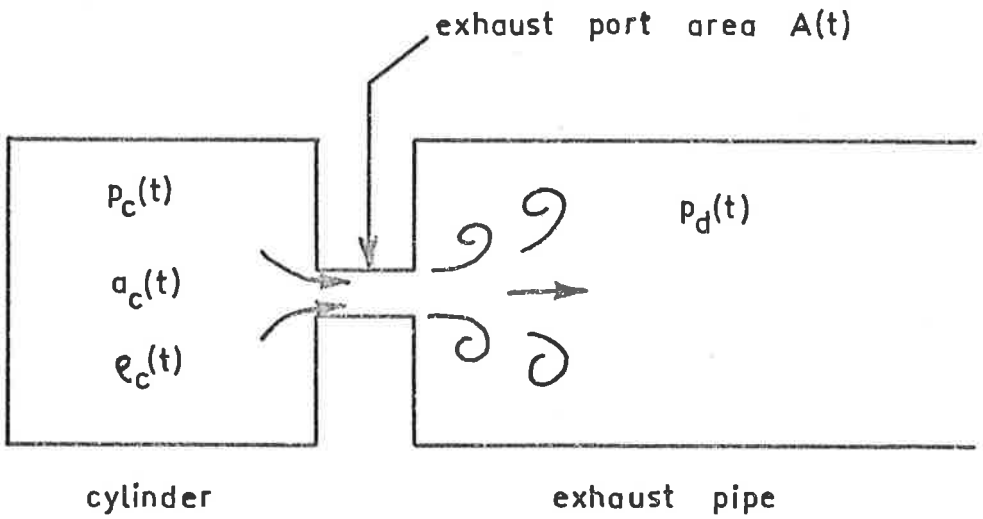

FIG.1 OUTFLOW FROM CYLINDER

where subscript "p" refers to the flow in the exhaust port area A(t).

M_p = flow Mach number in port.

Now, as mentioned above, the flow is adiabatic from the cylinder to the exhaust port. Therefore, the constant energy relation gives:-

$$u_p^2 + \left(\frac{2}{\gamma - 1}\right) a_p^2 = \left(\frac{2}{\gamma - 1}\right) a_c^2(t) \qquad (9)$$

on rearrangement:-

$$\frac{a_c(t)}{a_p} = \left[1 + \left(\frac{\gamma - 1}{2}\right) M_p^2 \right]^{\frac{1}{2}} \qquad (10)$$

As the flow is isentropic to the exhaust port, the cylinder conditions are also the stagnation conditions for the flow in the port. Therefore, using isentropic relations, from equation (10) a relation in terms of density is obtained:-

$$\frac{\rho_c(t)}{\rho_p} = \left[1 + \left(\frac{\gamma - 1}{2}\right) M_p^2 \right]^{\left(\frac{1}{\gamma - 1}\right)} \qquad (11)$$

Therefore, substituting for a_p and ρ_p in equation (8), using relations (10) and (11), gives:-

$$\dot{m}(t) = \rho_c(t)\, a_c(t)\, A(t)\, M_p \left[1 + \left(\frac{\gamma - 1}{2}\right) M_p^2 \right]^{-\frac{(\gamma+1)}{2(\gamma-1)}} \qquad (12)$$

The solution for choked flow now follows directly from (12), as $M_p = 1$ for this case. Hence, for choked flow:-

$$\dot{m}(t) = \left(\frac{2}{\gamma + 1}\right)^{\frac{(\gamma+1)}{2(\gamma-1)}} \rho_c(t)\, a_c(t)\, A(t) \qquad (13)$$

Therefore, from equation (1) of this appendix, for choked flow the value of the flow parameter C(t) is given by:-

$$C(t) = \left(\frac{2}{\gamma+1}\right)^{\frac{\gamma+1}{2(\gamma-1)}} \tag{14}$$

Now, a relation between the cylinder pressure, $p_c(t)$, and the static pressure in the port, p_p, may be obtained in a similar manner as equation (11):-

$$\frac{p_c(t)}{p_p} = \left[1 + \left(\frac{\gamma-1}{2}\right) M_p^2\right]^{\frac{\gamma}{\gamma-1}} \tag{15}$$

For choked flow in the port $M_p = 1$ and the following relation is obtained from (15):-

$$\frac{p_c(t)}{p_p} = \left(\frac{\gamma+1}{2}\right)^{\frac{\gamma}{\gamma-1}} \tag{16}$$

Now, for flow which is barely sonic in the port, as for general subsonic flow, the static pressure in the port, p_p, is assumed equal to the static pressure in the exhaust duct, $p_d(t)$. Therefore, it is clear that for choked flow to occur in the exhaust port

$$\frac{p_c(t)}{p_d(t)} > \left(\frac{\gamma+1}{2}\right)^{\frac{\gamma}{\gamma-1}} \tag{17}$$

with the value of C(t) for such choked flow given by (14).

For $1 < \frac{p_c(t)}{p_d(t)} < \left(\frac{\gamma+1}{2}\right)^{\frac{\gamma}{\gamma-1}}$ there is subsonic flow out of

the exhaust port. The value of M_p in equation (12) is now not known, but the solution may be obtained by taking advantage of the relation (15), as for subsonic flow p_p is assumed equal to $p_d(t)$. On thus obtaining relations for M_p in terms of $p_c(t)$ and $p_d(t)$ from (15), and substituting in equation (12), the following expression may be found for the mass flow rate:-

$$\dot{m}(t) = \left(\frac{2}{\gamma-1}\right)^{\frac{1}{2}} \left(\frac{p_c(t)}{p_d(t)}\right)^{-\left(\frac{\gamma+1}{2\gamma}\right)} \left[\left(\frac{p_c(t)}{p_d(t)}\right)^{\left(\frac{\gamma-1}{\gamma}\right)} - 1\right]^{\frac{1}{2}} \rho_c(t)\, a_c(t)\, A(t) \qquad (18)$$

Therefore, for subsonic outflow from the cylinder

$$C(t) = \left(\frac{2}{\gamma-1}\right)^{\frac{1}{2}} \left(\frac{p_c(t)}{p_d(t)}\right)^{-\left(\frac{\gamma+1}{2\gamma}\right)} \left[\left(\frac{p_c(t)}{p_d(t)}\right)^{\left(\frac{\gamma-1}{\gamma}\right)} - 1\right]^{\frac{1}{2}} \qquad (19)$$

The flow parameters to be used for flows between the cylinder and crankcase and also for inflow from the exhaust pipe to the cylinder will now be considered. For any case of choked flow, the flow parameter is, of course, given by equation (14). For subsonic flows between the cylinder and the crankcase, the stagnation conditions are obviously the conditions existing inside the higher pressure volume. The static pressure in the transfer ports is assumed to be the same as the pressure in the lower pressure volume. The flow parameter may then be found directly using equation (19) with the relevant values of pressure.

In the case of subsonic inflow to the cylinder through the exhaust port, the pressure in the port is, of course, assumed equal to the cylinder pressure. The upstream stagnation pressure is now

unknown but it is calculated from the known values of static pressure, flow velocity and speed of sound in the exhaust duct using equation (15). In the program the flow in the exhaust duct is, of course, known as each new exhaust port flow is determined before the cylinder and crankcase conditions are updated. The flow parameter for this case then simply follows from equation (19).

In the computer program, the flow parameter is calculated in the subroutine MASSEX, which is listed in Appendix 6.

3. ENTROPY IN CYLINDER AND CRANKCASE

As a result of a flow between the cylinder and the crankcase through the transfer ports, the entropy in the lower pressure volume must be updated. This entropy change is caused, firstly, by the loss of total pressure of the inflowing gas, and secondly, by the mixing of the original gas with the incoming charge. Of course, the entropy level in the higher pressure volume is constant as it is assumed that all outflow occurs isentropically up to the transfer ports.

To obtain the solution the inflow process is arbitrarily broken up into several simple steps, for each of which the entropy change may be found. It will always be assumed that any inflow only adds a small amount of mass, and so, changes the conditions in the lower pressure volume only slightly.

It is assumed that the gas first enters the lower pressure volume as if a balloon is placed at the exit of the transfer ports. That is, the inflowing gas comes to rest with the same total pressure as the original gas, without yet mixing with it. As the inflow barely changes the conditions in the volume, the flow may be regarded as constant. Therefore, since the flow is adiabatic, it may be assumed that the stagnation temperature of the gas entering the volume is the same as the upstream stagnation value. That is, the temperature of the

gas inside the balloon is equal to that inside the higher pressure volume. At the end of the flow period the balloon is considered to burst, allowing the gases of equal pressure but different temperature to completely mix.

The entropy change in the lower pressure volume, is then calculated by first computing the change caused by the inflowing gas before it mixes with the original gas, and then finding the entropy change following the mixing of the gases. This latter calculation is performed in a similar manner to that in the examples given in sections 1.8 and 1.9 of reference (12). For convenience the same symbols will be used as in reference (12) where possible.

The flow situation considered is shown in figure (2). The diagram showing the second stage of the flow shows the conditions for the higher pressure volume and for the original gas in the lower pressure volume as unchanged. This is approximately correct after a small finite flow. Once the entropy change is determined, the final conditions in both volumes including the correct effects of the mass transfer are, of course, calculated. Clearly, the analysis is adequate for small amounts of mass transfer, such that $M_1 \ll M_2$.

Firstly, the extensive entropy change $S_A - M_2 s_2$, caused by by the inflowing gas before it mixes with the original gas, must be found. Now, generally, an entropy change may be expressed in terms of temperature and pressure differences, as given by equation (1.43c) in reference (12):-

$$s - s_1 = C_p \ln\frac{T}{T_1} - R \ln \frac{p}{p_1} \qquad (20)$$

where entropy values are intensive.

Considering regions (1) and (3) of figure (2), it then follows that the extensive entropy of the mass M_1 in region (3) is

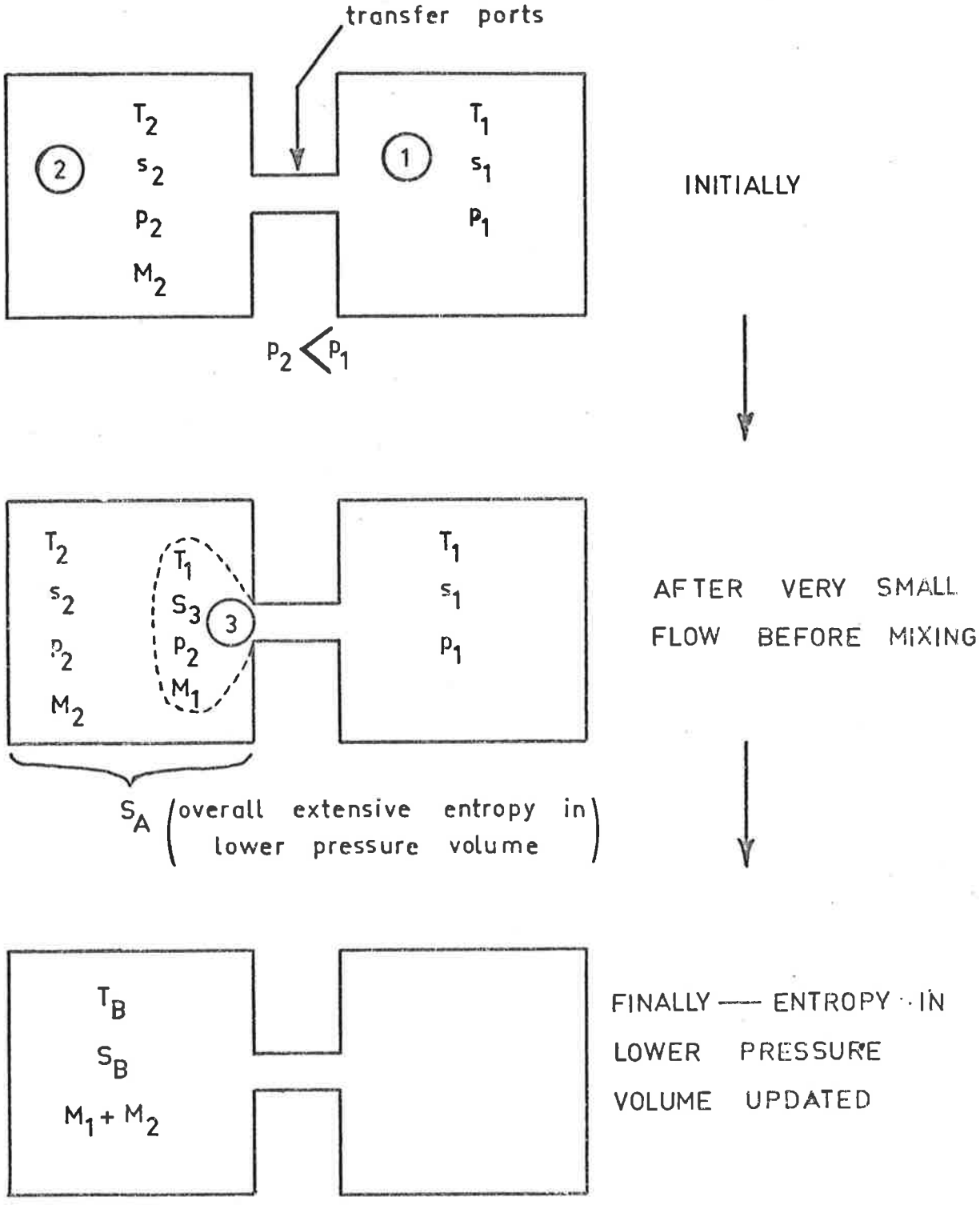

FIG. 2 GENERALIZED FLOW BETWEEN CYLINDER AND CRANKCASE

given by:-

$$S_3 = M_1 s_1 - RM_1 \ln \frac{p_2}{p_1} \tag{21}$$

The slight compression of the original gas in the lower pressure volume before the mixing has been assumed isentropic. Therefore the value given by S_3 is then equal to the total change in the extensive entropy in the lower pressure volume, before mixing. That is:-

$$S_A - M_2 s_2 = M_1 s_1 - RM_1 \ln \frac{p_2}{p_1} \tag{22}$$

Now the entropy change $S_B - S_A$, following mixing, must be determined. As discussed in section 1.9 of reference (12), this entropy change may be determined by considering the processes by which the gas in the final mixed state may be reversibly returned to the unmixed state. These processes will be described briefly. First, the mixed gas is partitioned according to the ratio M_1/M_2. The mass M_2 is then reversibly heated (or cooled) to temperature T_2 and the mass M_1 likewise to temperature T_1. Obviously, the pressures in the partitioned regions are no longer the same. The final step involves moving the partition slowly to the low pressure side while reversibly transferring heat to or from both regions to keep the temperatures constant at T_1 and T_2. The entropy changes are then straightforwardly found for each of the two steps, as shown in reference (12). The extensive entropy changes for this reverse process are given below.

For the first step:-

$$\text{entropy change} = - M_1 C_v \ln \frac{T_B}{T_1} - M_2 C_v \ln \frac{T_B}{T_2} \tag{23}$$

For the second step:-

$$\text{entropy change} = - M_1 R \ln \frac{T_B}{T_1} - M_2 R \ln \frac{T_B}{T_2} \tag{24}$$

The change in extensive entropy values $S_B - S_A$ may now be found from (23) and (24). Firstly, the temperature T_B may be expressed in terms of the initial conditions, as in equation (1.33b) of reference (12):-

$$T_B = \frac{M_1T_1 + M_2T_2}{M_1 + M_2} \tag{25}$$

Therefore, from equations (23), (24) and (25):-

$$S_B - S_A = M_1C_p \ln\left[\frac{M_1T_1 + M_2T_2}{T_1(M_1 + M_2)}\right] + M_2C_p \ln\left[\frac{M_1T_1 + M_2T_2}{T_2(M_1 + M_2)}\right] \tag{26}$$

The total change in intensive entropy in the lower pressure volume is now given by (26) + (22) divided by the total final mass $M_1 + M_2$:-

$$\frac{S_B}{M_1+M_2} - X.s_2 = Y.s_1 - R.Y \ln\frac{p_2}{p_1} + Y.C_p \ln\left[Y + X\frac{T_2}{T_1}\right] + X.C_p \ln\left[Y\frac{T_1}{T_2} + X\right] \tag{27}$$

where $$X = \frac{M_2}{M_1 + M_2}$$

$$Y = \frac{M_1}{M_1 + M_2}$$

The values for X and Y may be given in terms of the $\lambda(t)$ term which was introduced in section 1 of this appendix. From equation (4) of this appendix, $\lambda(t)$ for the lower pressure volume is given by:-

$$\lambda(t) = \frac{\dot{m}(t)}{M(t)} \tag{28}$$

where $\dot{m}(t)$ is the mass flow rate out of the volume (a negative quantity in this case).

Now, if Δt is the length of the time for which it is assumed the flow occurs, then:-

$$\lambda(t)\,\Delta t = \frac{\dot{m}(t)\,\Delta t}{M(t)} \tag{29}$$

In terms of the values given in figure (2) it is then clear from (29) that:-

$$\frac{M_1}{M_2} = -\,\lambda(t)\,\Delta t \tag{30}$$

The negative sign, of course, appears as $\lambda(t)$ is negative for a flow into the lower pressure volume.

The terms X and Y given for equation (27) may now be expressed in terms of $\lambda(t)$, using the approximation that M_1/M_2 is small. If a term, A, is introduced such that:-

$$A = \lambda(t)\,\Delta t \tag{31}$$

Then $X = 1 + A$

$Y = -\,A(1 + A)$

Therefore, for a flow from the crankcase to the cylinder, for example, the new value for the intensive entropy in the cylinder, $s_c(t)$, may be given in terms of the original cylinder and crankcase conditions. From (27):-

$$\text{New } s_c(t) = -A(1+A)s_{cr}(t) + R.A(1+A)\,\ell n\frac{p_c(t)}{p_{cr}(t)}$$

$$+ (1+A)s_c(t) \text{ (old value)}$$

$$- A(1+A)C_p\,\ell n\left[\frac{(1+A)T_c(t)}{T_{cr}(t)} - A(1+A)\right]$$

$$+ (1+A)C_p\,\ell n\left[1+A - \frac{A(1+A)T_{cr}(t)}{T_c(t)}\right] \qquad (32)$$

where subscript c refers to cylinder conditions

subscript cr refers to crankcase conditions

A is given by equation (31).

To complete the solution, the value of $\lambda(t)$ for the cylinder must be known for the flow from the crankcase to the cylinder. Obviously, $\lambda(t)$ for this flow is not given by equation (2) of this appendix. The correct value of $\lambda(t)$ may be easily found by equating the inflow to the cylinder with the outflow from the crankcase.

Now, the mass flow rate from the cylinder is given by equation (4) of this appendix:-

$$\dot{m}(t) = \lambda(t)\,M_c(t)$$

that is,
$$\dot{m}(t) = \lambda(t)\,V_c(t)\,\rho_c(t) \qquad (33)$$

where, of course, both $\dot{m}(t)$ and $\lambda(t)$ are negative for the case at hand.

The mass flow rate out of the crankcase is the same as $-\dot{m}(t)$ from equation (33). Therefore, using equation (1) of this appendix:-

$$\dot{m}(t) = -C(t)\,\rho_{cr}(t)\,a_{cr}(t)\,A_{tr}(t) \qquad (34)$$

where $A_{tr}(t)$ = area of transfer ports open.

Hence, by equating the values for $\dot{m}(t)$ in equations (33) and (34) and substituting for the density values in terms of pressure and speed of sound, the value of $\lambda(t)$ for the cylinder may be found:-

$$\lambda(t) = - \frac{C(t)\, a_c(t)\, A_{tr}(t)}{V_c(t)} \times \frac{p_{cr}(t)\, a_c(t)}{p_c(t)\, a_{cr}(t)} \qquad (35)$$

This value of $\lambda(t)$ is then used in equation (32).

In the computer program, the calculations to determine the $\lambda(t)$ terms and the entropy changes for the cylinder and crankcase, are performed in subroutine MASSEX.

4. PORT AREAS AND CYLINDER AND CRANKCASE VOLUMES

The cylinder and crankcase volumes and the exhaust and transfer port areas, at a particular time after the exhaust port has opened, are calculated very accurately. The piston motion is considered as simple harmonic motion with a correction for the con-rod obliquity. In figure (3) the exact distance of the piston from the cylinder head is given by:-

$$x = - (\ell \cos\phi - r \cos\theta) + k \qquad (36)$$

where k = constant

An approximate expression, assuming S.H.M. is:-

$$x = - (\ell - r \cos\theta) + k$$

The correction term for the con-rod obliquity is therefore $\ell(1 - \cos\phi)$, which is small but is included in the analysis. The value of $\cos\phi$ may be found in terms of θ, the angle from bottom dead centre (B.D.C.):-

$$\cos\phi = (1 - q^2 \sin^2\theta)^{\frac{1}{2}} \qquad (37)$$

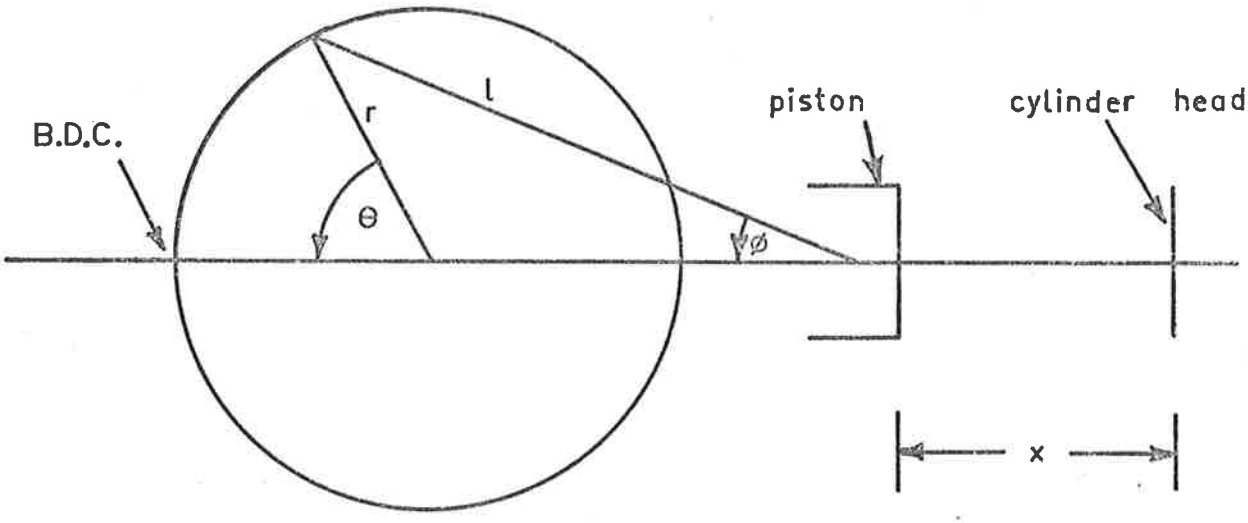

FIG.3 MOTION OF PISTON IN CYLINDER

where $q = \frac{r}{\ell}$ = con-rod obliquity.

The determination of the cylinder volume as a function of time is then straightforward, and is given by:-

$$V_c(t) = \frac{V_{sc}}{R_c - 1} + \frac{V_{sc}}{2} + \frac{V_{sc}}{2}\cos\theta + \ell b(1 - \cos\phi) \qquad (38)$$

where V_{sc} = swept volume in cylinder

R_c = compression ratio in cylinder

b = area of cylinder bore

$$\theta = \frac{2.\pi.t.RPM}{60} - \frac{X_c.\pi}{180}$$

where t = time after E.P.O. seconds

RPM = engine speed r.p.m.

X_c = angle between E.P.O. and B.D.C., degrees.

In equation (38), the last term is the correction for the con-rod obliquity. This correction is subtracted from a similar relation for the crankcase volume:-

$$V_{cr}(t) = \frac{V_{scr}}{R_{cr} - 1} + \frac{V_{scr}}{2} + \frac{V_{scr}}{2}\cos\theta - \ell b(1 - \cos\phi) \qquad (39)$$

where V_{scr} = swept volume in crankcase

R_{cr} = compression ratio in crankcase

The determination of the exhaust port and transfer port areas is slightly more complex. It is assumed that both types of ports, both piston operated, are rectangular in shape, and are fully open at B.D.C. The exhaust port will first be considered.

With reference to figure (3) and equation (36), if the width of the exhaust port is w, the open area is given by:-

$$A(t) = \ell w \cos\phi_{EPO} - \ell w \cos\phi$$

$$- r w \cos\theta_{EPO} + r w \cos\theta \qquad (40)$$

where ϕ_{EPO}, θ_{EPO} are the values for ϕ and θ at E.P.O.

Now, if the area of the fully open exhaust port is B, then at B.D.C., $A(t) = B$, $\phi = 0$, $\theta = 0$. Therefore, on substitution in (40):-

$$r w = \frac{B}{(\frac{1}{q}\cos\phi_{EPO} - \cos\theta_{EPO} + 1 - \frac{1}{q})}$$

Therefore,

$$A(t) = \frac{B(\cos\theta - \cos[\frac{X_c.\pi}{180}] + \frac{1}{q}\cos\phi_{EPO} - \frac{1}{q}\cos\phi)}{(1 - \cos[\frac{X_c\pi}{180}] + \frac{1}{q}\cos\phi_{EPO} - \frac{1}{q})} \qquad (41)$$

A very similar result may be obtained for the transfer port area.

A listing of the subroutine AREAVL, which performs these calculations in the computer program, is given in Appendix 6.

APPENDIX 3

C_+ CHARACTERISTIC PASSING P CHARACTERISTIC

The calculations used to describe the flow existing after a C_+ characteristic passes a P characteristic are considered below. Reference is made to the first diagram in figure (6) in chapter 2.

As shown in figure (6), the final flow situation in the x - t diagram includes a reflected C_- characteristic and a transmitted characteristic, C_+' , which is different from the incident C_+. The P characteristic proceeds with a different velocity. All that is required to determine the final flow is the complete description of the initial C_+ and P characteristics. Obviously, this information is included in the x - t diagram. The values required in terms of figure (6) are then:-

for P: s_1

u_5

a_1

s_5

for C_+: s_1

u_2

a_2

$$P_1 = \left(\frac{2}{\gamma - 1}\right) \frac{a_2}{a_o} + \frac{u_2}{a_o}$$

As mentioned in section 2.6, the final flow is obtained using the fact that pressures and velocities on either side of the P characteristic must be the same, and that the entropies are the same in all regions

to each side of the P characteristic. The values shown in figure (6) have been simplified using these facts.

As the pressures in regions (3) and (4) are the same, from the expression of entropy in terms of temperature and pressure, equation (20) of Appendix 2, the following is true:-

$$\frac{a_4}{a_3} = e^{\frac{\gamma-1}{2\gamma R}(s_5 - s_1)} \tag{1}$$

Similarly, for regions (1) and (5):-

$$\frac{a_5}{a_1} = e^{\frac{\gamma-1}{2\gamma R}(s_5 - s_1)} \tag{2}$$

Suppose another C_+ characteristic, with the same Riemann invariant as the initial incident one, follows behind the initial C_+ characteristic. This may be termed a nil effect characteristic. Its path is shown in figure (6) by a long dashed line. Clearly, it will not alter the flow in any way and will pass into region (3) with an unchanged Riemann invariant. This Riemann invariant, the same as for the initial C_+ characteristic, is then given by:-

$$P_1 = \left(\frac{2}{\gamma-1}\right)\frac{a_3}{a_o} + \frac{u_3}{a_o} \tag{3}$$

If a C_- characteristic, which does not alter the flow, approaches the P characteristic, as shown in figure (6) by the other long dashed line, a similar relation is obtained. Here, the Riemann invariant may be expressed in terms of velocity and speed of sound in regions (4) and (5). Hence:-

$$\left(\frac{2}{\gamma-1}\right)\frac{a_5}{a_o} - \frac{u_5}{a_o} = \left(\frac{2}{\gamma-1}\right)\frac{a_4}{a_o} - \frac{u_3}{a_o} \tag{4}$$

In the above set of four equations a_4, a_3, a_5, u_3 are the only unknowns, so that the solution may be obtained. For example, a relation may be found to solve a_4:-

$$a_4 = \frac{P_1 + (\frac{2}{\gamma-1}) \frac{a_1}{a_o} e^{\frac{\gamma-1}{2\gamma R}(s_5 - s_1)} - \frac{u_5}{a_o}}{(\frac{2}{\gamma-1}) \left[e^{\frac{\gamma-1}{2\gamma R}(s_1 - s_5)} + 1 \right]} \qquad (5)$$

The remainder of the solution is straightforward.

APPENDIX 4

FLOW THROUGH OPEN EXHAUST PORT

The calculations used to describe the flow existing after a C_- characteristic reaches an open exhaust port are given below. The final flow is either inflow or outflow from the cylinder, in which the flow at the port is either sonic or subsonic. Naturally, before the calculation proceeds the nature of the flow must be known with, initially, the direction being determined. The flow direction may conveniently be found by first considering the general case for inflow and then the particular case of zero inflow. The flow direction is considered in section 1.1.

1. INFLOW TO CYLINDER

The x - t diagram shown in figure (1) describes the event. The incident C_- characteristic is reflected as a C_+, and as there is inflow, a P characteristic is not created. The final flow is determined using steady flow relations and by assuming that the flow, as shown in the second diagram in figure (1), is adiabatic and isentropic from the full duct area A_d to the port area A(t). For both sonic and subsonic flows, it is then assumed that the only loss in total pressure is that which occurs when the flow enters the cylinder. For subsonic flow, it is further assumed that the static pressure in the port is equal to the cylinder pressure. This is no longer true when the flow in the port is sonic, but then, the flow may be determined since the speed of sound at this point is equal to the flow speed. As a simplification, only subsonic flows in the main duct are considered.

In conjunction with the above assumptions, the only other

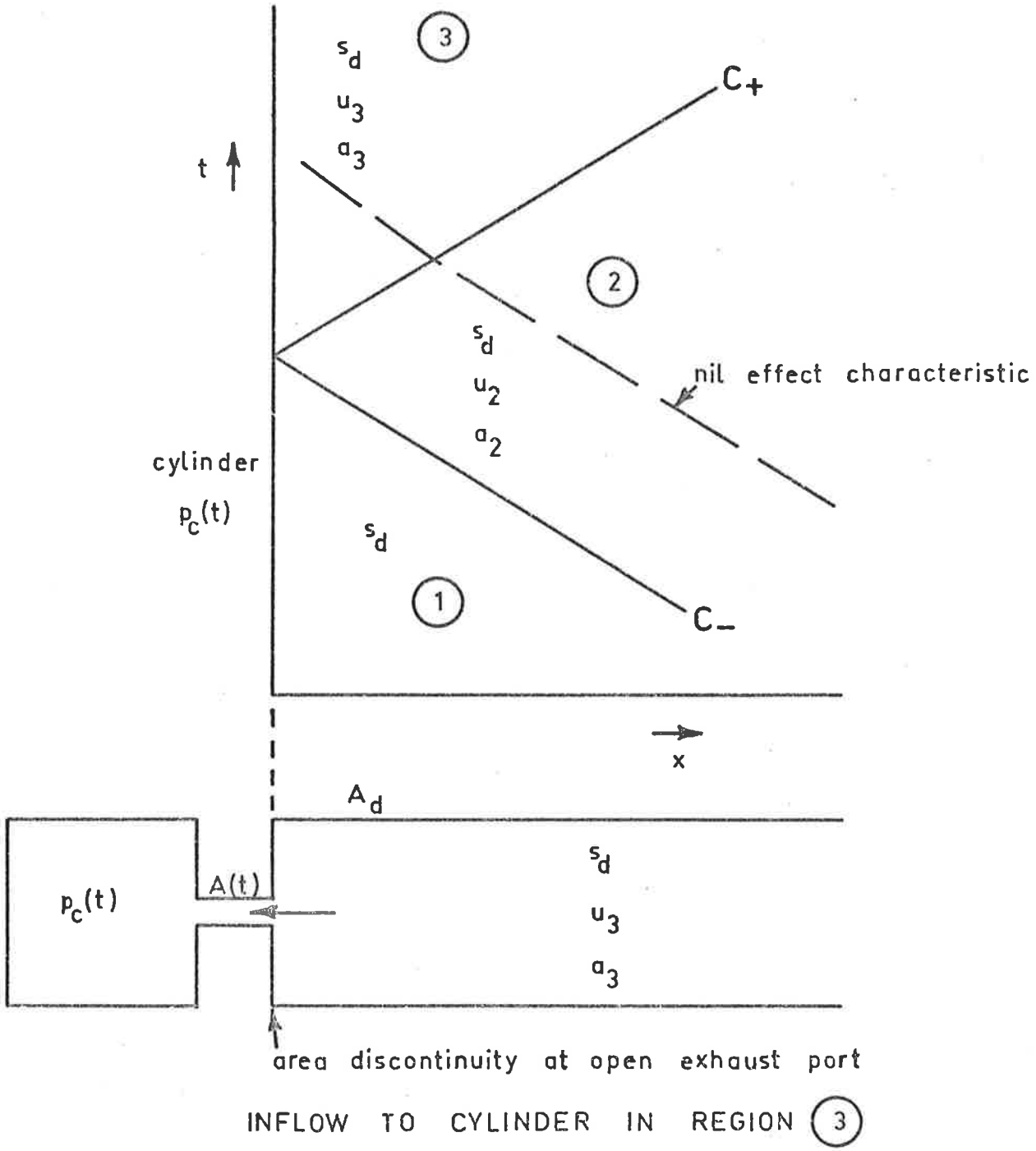

FIG.1 C− CHARACTERISTIC CAUSING INFLOW TO CYLINDER

information needed to obtain the final flow is a description of the incident C_- characteristic, the cylinder pressure, and the areas of the duct and the exhaust port. As in figure (1), these values are:-

for C_-: s_d

u_2

a_2

$Q_1 = (\frac{2}{\gamma-1}) \frac{a_2}{a_o} - \frac{u_2}{a_o}$

for cylinder: $p_c(t)$

duct area: A_d

port area: $A(t)$

As mentioned in section 2.7.1 the final flow is calculated using the equations of continuity of mass and energy and equation (2.8), as well as relations from the above-mentioned assumptions. Obviously some different relations are obtained for sonic and subsonic cases. For both types of flow the assumption of adiabatic, isentropic flow across the area discontinuity at the port introduces the area values into the equations. The relations which may be applied irrespective of whether the flow in the port is sonic or not will be obtained first.

As the flow in the second diagram in figure (1) is adiabatic, the energy equation may be written for the flow from the duct to the port:-

$$u_p^2 + (\frac{2}{\gamma-1}) a_p^2 = u_3^2 + (\frac{2}{\gamma-1}) a_3^2 \qquad (1)$$

where subscript "p" refers to the flow in the exhaust port area, A(t).

Similarly, the equation for continuity of mass flow becomes:-

$$\rho_p A(t) u_p = \rho_3 A_d u_3$$

Now, as the flow is assumed isentropic, this equation may be written as:-

$$a_p^{(\frac{2}{\gamma-1})} A(t)\, u_p = a_3^{(\frac{2}{\gamma-1})} A_d\, u_3 \qquad (2)$$

If, as in Appendix 3, a nil effect C_- characteristic is assumed to pass from region (2) to region (3) in the x - t diagram, the Riemann invariant for this characteristic is given by:-

$$Q_1 = (\frac{2}{\gamma-1})\frac{a_3}{a_o} - \frac{u_3}{a_o} \qquad (3)$$

where Q_1, of course, is the same as the Riemann invariant for the incident C_- characteristic.

Clearly, the set of equations (1) to (3) is appropriate for a flow which is either sonic or subsonic at the exhaust port. These equations have four unknowns:- u_p, a_p, u_3 and a_3. One more equation, based on the earlier assumptions given about the flow is then required to fix the solution. As the limiting case of infinitesimal inflow is zero flow, the final relation which is required to establish the flow direction, is one which applies to subsonic inflow. This may be obtained from the assumption that the static pressure in the port, for subsonic flow, is equal to the cylinder pressure. Substituting cylinder pressure into the equation for the speed of sound in the port in terms of pressure and entropy, then gives:-

$$a_p = a_o(\frac{p_c(t)}{p_o})^{(\frac{\gamma-1}{2\gamma})} e^{(\frac{\gamma-1}{2\gamma R})(s_d - s_o)} \qquad (4)$$

(see Appendix 2 equation (20))

Using equations (1) to (4), for a known incident C_- character-

istic, a solution for subsonic inflow may be found, as is shown in section 1.3. The following sections 1.1 and 1.2 use the four equations to determine, first, the flow direction, and second, whether there is sonic inflow at the port. Equation (4) shows already that if there is subsonic inflow, then the value of a_p depends only on the cylinder pressure and the entropy in the duct. This has special significance, as is shown in the following sections dealing with inflow.

1.1 DIRECTION OF FLOW

The direction of the flow resulting as a C_- characteristic reaches the open exhaust port may be determined by studying the case of infinitesimal inflow to the cylinder. As mentioned in the previous section, this flow is subsonic, so that equations (1) to (4) apply.

For infinitesimal inflow, $u_p \to 0$ and $u_3 \to 0$. From equation (1), then $a_3 \to a_p$. Also from equation (3):-

$$(\frac{2}{\gamma-1}) \frac{a_3}{a_o} \to Q_1' = (\frac{2}{\gamma-1}) \frac{a_p}{a_o}$$

where Q_1' = value of Riemann invariant for zero flow.
Substituting for a_p in the above equation from equation (4) then gives:-

$$Q_1' = (\frac{2}{\gamma-1}) (\frac{p_c(t)}{p_o})^{(\frac{\gamma-1}{2\gamma})} e^{(\frac{\gamma-1}{2\gamma R})(s_d - s_o)} \qquad (5)$$

This is then the same as equation (2.12).

When inflow occurs, clearly $u_p > u_3$ as the area at the exhaust port is smaller than the duct. It follows from equation (1) that, as a_p is fixed for subsonic inflow, then:-

$$a_3 > a_p$$

Therefore:- $$\left(\frac{2}{\gamma-1}\right)\frac{a_3}{a_o} > \left(\frac{2}{\gamma-1}\right)\frac{a_p}{a_o} = Q_1'$$

Then, using the expression for the Riemann invariant in equation (3), as u_3 is negative, it is clear that:-

$$\text{for inflow} \quad Q_1 > Q_1'$$

Similarly, using relations for infinitesimal outflow, it may be shown that $Q_1 < Q_1'$ if outflow exists. The calculations for outflow are described in section 2 of this Appendix.

1.2 NATURE OF INFLOW

Given that inflow to the cylinder occurs after a C_- characteristic reaches the open exhaust port it must be established whether the inflow is sonic or subsonic at the port, before the final calculations may be done. The nature of the flow may be determined by considering the case of an inflow which is barely sonic. For this flow, both sonic and subsonic relations may be applied. Now, the special relation obtained for subsonic flow is equation (4). Clearly, a relation for sonic flow is now required so that, by using both together, the case of barely sonic flow may be determined.

A relation for sonic flow in the port may easily be obtained by substituting for $u_p = a_p$ in equations (1) and (2), as is shown below. Substituting for u_p in equation (1) gives:-

$$\left(\frac{\gamma+1}{\gamma-1}\right) a_p^2 = u_3^2 + \left(\frac{2}{\gamma-1}\right) a_3^2 \qquad (6)$$

Similarly, from equation (2):-

$$a_p^{\left(\frac{\gamma+1}{\gamma-1}\right)} A(t) = a_3^{\left(\frac{2}{\gamma-1}\right)} A_d \, u_3 \qquad (7)$$

Now, using equations (6) and (7) the case of barely sonic inflow may be found by substituting the value of a_p from equation (4). However, it is more convenient at this stage to eliminate a_p from equations (6) and (7) and arrive at a relation in terms of u_3 and a_3 which is applicable for barely sonic flow as well as greatly choked flow. Therefore, using equations (6) and (7), the following relation in M_3^*, the Mach number M_3 corresponding with sonic flow in the exhaust port, is finally obtained:-

$$M_3^* = \left(\frac{2}{\gamma+1}\right)^{\frac{\gamma+1}{2(\gamma-1)}} \frac{A(t)}{A_d} \left[1 + \left(\frac{\gamma-1}{2}\right) M_3^{*2} \right]^{\frac{\gamma+1}{2(\gamma-1)}} \qquad (8)$$

Equation (8) may be solved by iteration. In the computer program, for two different ranges of area ratio, different iterations are performed. For each case, the starting value of M_3^* for the iteration is derived from equation (8) after appropriate approximations have been made.

Limiting sonic flow may now be considered. The solution may be obtained if the value for a_p for subsonic flow, from equation (4), is combined in either equations (6) or (7) with the value for M_3^* calculated from equation (8). Suppose equation (7) is used. Rearranging and substituting for a_3 in terms of M_3^* and u_3 leads to an expression for u_3:-

$$u_3 = - M_3^{*\left(\frac{2}{\gamma+1}\right)} \left(\frac{A(t)}{A_d}\right)^{\left(\frac{\gamma-1}{\gamma+1}\right)} a_p \qquad (9)$$

The negative value for u_3 is, of course, taken as the flow is into the cylinder. Equation (9) may now be solved as M_3^* is known and a_p, for this barely sonic inflow, is fixed by equation (4). Once u_3 is found in equation (9), a_3 follows from the known Mach number.

Therefore, with a similar approach to that used in section 1.1, choked inflow through the exhaust port may be shown to occur when:-

$$Q_1 > \left(\frac{2}{\gamma-1}\right)\frac{a_3}{a_o} - \frac{u_3}{a_o}$$

where Q_1 = Riemann invariant of incident C_- characteristic

a_3, u_3 are as obtained above for barely sonic inflow.

Now that the nature of the inflow is determined, the calculations for both sonic and subsonic flow may be considered.

1.3 SUBSONIC INFLOW

Section 1 showed that when subsonic inflow to the cylinder occurs, the final flow may be obtained from equations (1) to (4). These equations may be solved by an iteration procedure. Details of this procedure follow.

Using equation (2), a relation for u_p may be found. This relation may then be substituted for u_p in equation (1) and the following relation for a_3 is then obtained:-

$$a_3 = a_p \left| \left(\frac{A(t)}{A_d u_3}\right)^2 \left(\frac{2}{\gamma-1}\right)(a_3^2 - a_p^2) + \left(\frac{A(t)}{A_d}\right)^2 \right|^{\left(\frac{\gamma-1}{4}\right)} \qquad (10)$$

Also equation (3) may be used to get an expression for u_3 in terms of a_3:-

$$u_3 = \left(\frac{2}{\gamma-1}\right) a_3 - a_o Q_1 \qquad (11)$$

The iteration procedure is then as follows:-

As mentioned earlier, for subsonic inflow, a_p may be found from equation (4). Then, using known values of a_p, A_d, $A(t)$ and good

estimates for u_3 and a_3, a value of a_3 is obtained from equation (10). Using this value of a_3 in equation (11), a new value of u_3 is found and the procedure starts again. The basic iteration proved to be unstable. This was overcome by simply using as the next estimate for each of u_3 and a_3 a weighted average of the previous value and the new estimate. A series of checks is employed to ensure that a_3 and u_3 are within possible bounds. Also, this and all other iterations are self terminating, in that they keep going until the answers are to a required accuracy. After this, when u_3 and a_3 are finalized, the remainder of the solution is simple.

1.4 CHOKED INFLOW

When choked inflow to the cylinder occurs, the continuity equations, equations (1) and (2) of course still apply. Section 1.2 showed that these equations lead to the result that the flow Mach number in region (3) is fixed for a given area ratio $A(t)/A_d$. Now, using the already calculated value of M_3^* from equation (8), and the known value of the Riemann invariant of the incident C_- characteristic, the solution may be obtained from equation (3). The value of u_3 is then:-

$$u_3 = \frac{-a_o Q_1}{(\frac{2}{\gamma-1})\frac{1}{M_3^*} + 1} \qquad (12)$$

The calculation of a_3 and then P_1 for the reflected C_+ characteristic is then simple.

The subroutine which performs all the calculations for inflow to the cylinder is FLØWIN, which is listed in Appendix 6. The test to determine the direction of the flow is, of course, performed in the main program before subroutine FLØWIN may be called.

2. OUTFLOW FROM CYLINDER

The analysis given below for outflow from the cylinder is very similar to that given in the preceding sections for inflow. Wherever possible the same assumptions are used.

The following sections describe the calculations used to determine the final outflow existing after a C_- characteristic reaches the open exhaust port. An x - t diagram describing the flow is shown in figure (2). The incident C_- characteristic is reflected as a C_+ and as outflow occurs a P characteristic is added. The occurrence of outflow will be assumed. That is, the value of the Riemann invariant of the incident C_- characteristic will be assumed to be less than Q_1' as in equation (5) of this appendix.

Now, the flow through the port may be either sonic or subsonic. Obviously, before the calculation proceeds it must be known which occurs. This nature of the outflow and then the form of the calculations required are both dependent on the assumptions which are made concerning the flow. As for inflow, the final situation is determined using steady flow relations and by assuming that the flow is isentropic from the cylinder to the port area A(t) and adiabatic throughout. For subsonic flow, it is also assumed that the static pressure in the exhaust port is equal to the static pressure, $p_d(t)$, in the duct just downstream of the port. That is, the flow is assumed to enter the duct from the port as if from a square edged orifice, as shown in the second diagram in figure (2). For choked flow, a system of shocks is situated somewhere between the port area A(t) and the duct area A_d. For simplicity, only subsonic flows are assumed to exist in the main duct.

As well as the above assumptions, the only other information needed to obtain the final flow is a description of the incident C_- characteristic, the cylinder conditions and the areas of the duct and

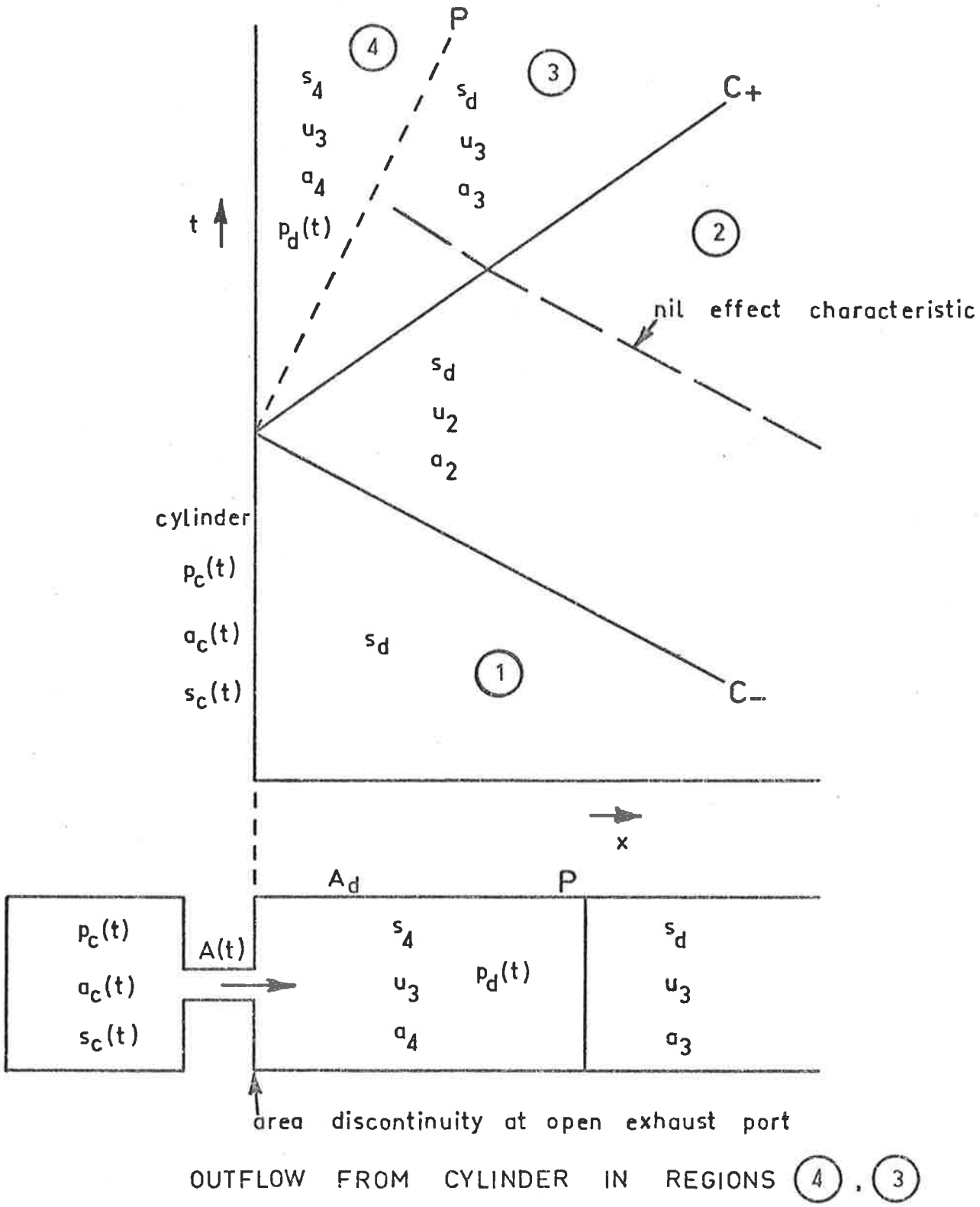

FIG. 2 C- CHARACTERISTIC CAUSING OUTFLOW FROM CYLINDER

the exhaust port. As in figure (2), these values are:-

for C_-: s_d

u_2

a_2

$$Q_1 = \left(\frac{2}{\gamma-1}\right)\frac{a_2}{a_o} - \frac{u_2}{a_o}$$

for cylinder: $p_c(t)$

$a_c(t)$

$s_c(t)$

duct area: A_d

port area: $A(t)$

As mentioned in section 2.7.1, the final flow may be calculated using the equations of continuity of mass and energy, equation (2.8) and an expression of the flow in terms of the cylinder conditions, i.e. equation (1) of Appendix 2. These equations may be obtained from the above-mentioned assumptions and also from the fact that the pressures and velocities either side of the P characteristic are the same. The area ratio between the exhaust port and the exhaust pipe enters the problem through the expression for conservation of mass.

First, the relations which apply irrespective of whether the flow in the exhaust port is choked or not will be considered. Then these will be used together with special relations to solve the case of a flow which is barely sonic in the port. This limiting case will mark the changeover point from which, for lower values of the Riemann invariant, choked flow will be assumed. Ultimately, as for inflow, an expression will be arrived at which will determine, from the value of Q_1, whether the flow is subsonic or choked.

As the whole flow is adiabatic, the constant energy equation for the flow from the cylinder to region (4), in the x - t diagram in

figure (2), gives:-

$$u_3^2 + \left(\frac{2}{\gamma-1}\right) a_4^2 = \left(\frac{2}{\gamma-1}\right) a_c(t)^2 \qquad (13)$$

If, as in Appendix 3, a nil effect C_- characteristic is assumed to travel behind the incident characteristic from region (2) to (3), the following is true:-

$$Q_1 = \left(\frac{2}{\gamma-1}\right)\frac{a_3}{a_o} - \frac{u_3}{a_o} \qquad (14)$$

where Q_1 is the same as the Riemann invariant of the incident C_- characteristic.

Now, as the pressures in regions (3) and (4) on either side of the entropy discontinuity are the same, a_4 may be expressed in terms of a_3 and the respective entropy values in the regions:-

$$a_4 = a_3 \, e^{\left(\frac{\gamma-1}{2\gamma R}\right)(s_4 - s_d)} \qquad (15)$$

(see Appendix 2 equation (20)).

The fact that the velocities in regions (3) and (4) are also the same, has already been incorporated in the values shown in the x - t diagram in figure (2).

Clearly, equations (13) to (15) are true for both sonic and subsonic flows in the port. There are four unknowns:- u_3, a_3, a_4, s_4. Therefore, only one other relation is required for a complete solution. This is provided by the expression for mass flow through the port in terms of the cylinder conditions, equation (1) of Appendix 2. Equating the exhaust port mass flow to that in region (4), then gives:-

$$C(t)\,\rho_c(t)\,a_c(t)\,A(t) = \rho_4\,A_d\,u_3$$

Therefore, substituting for the density values in terms of pressure and speed of sound gives:-

$$\frac{C(t)\, p_c(t)\, A(t)}{a_c(t)} = \frac{p_d(t)\, A_d\, u_3}{a_4^2} \qquad (16)$$

where $C(t)$ = flow parameter.

This equation does not yet enable the complete solution to be obtained as it includes the unknown pressure in region (4), $p_d(t)$. However, equation (16) is very convenient for considering the case of barely sonic flow, as is shown in section 2.1. The complete solution may be obtained by substituting for $p_d(t)$ in (16) using the relation (20) of Appendix 2 for the region (4) and the cylinder conditions:-

$$p_d(t) = p_c(t)\left(\frac{a_4}{a_c(t)}\right)^{\left(\frac{2\gamma}{\gamma-1}\right)} e^{-\frac{(s_4 - s_c(t))}{R}} \qquad (17)$$

Now, using equations (13) to (17), the complete solution for either choked or subsonic flow at the port may be found once the value of $C(t)$ is known. This result is in contrast with that obtained for inflow, as in the above analysis, details of the flow in the port itself have not been considered.

As shown in section 2 of Appendix 2, the value of $C(t)$ is known and fixed for choked flow at the port, but for subsonic flow it is dependent on the pressure ratio between the cylinder gas and the gas in region (4). This pressure ratio is, of course, not directly known but is implied in equation (17).

It must now be known whether the flow in the port is choked or subsonic. This is determined by the approach given in the next section.

2.1 NATURE OF OUTFLOW

Once it is known that outflow occurs, the nature of the outflow may be determined by considering the case of a flow which is barely sonic in the exhaust port. This is similar to what was done for inflow. This flow situation is then the limiting case of subsonic flow for which choked flow relations might equally well be applied. Consideration of this flow situation will enable it to be known whether the flow resulting from a particular C_- characteristic reaching the port is either choked or subsonic at the port.

For this case of subsonic flow which is barely sonic, the final result may now be obtained using the relations (13) to (17), of course, and the assumptions which have been made earlier, concerning both sonic and subsonic flow.

Now, for barely sonic flow, the value of C(t) in equation (16) is the same as the value given by equation (14) of Appendix 2. Also, for sonic flow in the port, as the flow comes adiabatically and isentropically from the cylinder, there is a fixed relation between the reservoir (cylinder) pressure, $p_c(t)$, and the static pressure in the throat (port) as is well known. As the flow is still just subsonic as well, this value of pressure in the port is equal to the static pressure, $p_d(t)$, in region (4) of the duct. Therefore:-

$$p_d(t) = p_c(t)\left(\frac{2}{\gamma+1}\right)^{\frac{\gamma}{\gamma-1}} \qquad (18)$$

Therefore, substituting for C(t) from equation (14) of Appendix 2, and for $p_d(t)$ from (18) into equation (16) gives:-

for barely sonic outflow

$$\frac{A(t)}{a_c(t)}\left(\frac{\gamma+1}{2}\right)^{\frac{1}{2}} = \frac{A_d u_3}{a_4^2} \qquad (19)$$

The conditions to cause barely sonic outflow may now be obtained simply from equations (13) and (19) as these only have u_3 and a_4 as unknowns. An expression for u_3 is then found:-

for barely sonic outflow

$$u_3 = a_c(t)\left|\left(\frac{2}{\gamma-1}\right) + \left(\frac{2}{\gamma+1}\right)\left(\frac{1}{\gamma-1}\right)^2\left(\frac{A_d}{A(t)}\right)^2\right|^{\frac{1}{2}} - a_c(t)\left|\left(\frac{2}{\gamma+1}\right)\left(\frac{1}{\gamma-1}\right)^2\left(\frac{A_d}{A(t)}\right)^2\right|^{\frac{1}{2}} \qquad (20)$$

Now, to obtain the value of the Riemann invariant, Q_1, for which the flow in the port is barely sonic, the value of a_3 must be known.

The pressure in region (3) is the same as $p_d(t)$. Therefore, substituting for $p_d(t)$ using equation (18), it follows from the expression for speed of sound in terms of pressure and entropy (equation (20) of Appendix 2) for region (3) and the cylinder, that:-

for barely sonic outflow

$$a_3 = a_c(t)\left(\frac{2}{\gamma+1}\right)^{\frac{1}{2}} e^{\left(\frac{\gamma-1}{2\gamma R}\right)(s_d - s_c(t))} \qquad (21)$$

Therefore, using a similar argument to that given in section 1.1 of this appendix, choked outflow through the exhaust port may be shown to occur when:-

$$Q_1 < \left(\frac{2}{\gamma-1}\right)\frac{a_3}{a_o} - \frac{u_3}{a_o}$$

where Q_1 = Riemann invariant of incident C_- characteristic

a_3, u_3 are as obtained for barely sonic outflow from equations (21) and (20).

Now that the outflow has been found to be either choked or subsonic, the calculations for each case may be considered.

2.2 SUBSONIC OUTFLOW

In section 2 of this appendix it was shown that for either choked or subsonic outflow from the cylinder, the final flow may be obtained from equations (13) to (17). It is shown below how the subsonic flow is then obtained.

Now, for subsonic flow which is isentropic and adiabatic from the cylinder to the port, equation (19) in Appendix 2 showed an expression of C(t) in terms of $p_c(t)/p_d(t)$. Using equation (20) of Appendix 2, $p_c(t)/p_d(t)$ may itself be expressed in terms of the entropy and speed of sound values in region (4) and in the cylinder, as in equation (17). On thus substituting for C(t) in equation (16), using equation (15) as well, the following is obtained:-

$$a_4^4 a_3^2 X = a_c(t)^2 a_4^4 X^2 - \left(\frac{\gamma-1}{2}\right)\left(\frac{A_d}{A(t)}\right)^2 u_3^2 a_3^4 \qquad (22)$$

where $X = e^{\frac{\gamma-1}{\gamma R}(s_d - s_c(t))}$.

Equation (22) is then in terms of the unknowns u_3, a_4, a_3. The solution for subsonic flow is then obtained using equations (13), (14) and (22), as there are only three unknowns. The value s_4 has, of course, been eliminated by incorporating equation (15) in equation (22).

Using equation (13), a relation for a_4 may be found. Then, substituting for a_4 in equation (22) and rearranging gives:-

$$u_3 = \left(\frac{2}{\gamma-1}\right)^{\frac{1}{2}} \frac{A(t)}{A_d a_3^2} \left[a_c(t)^2 - \left(\frac{\gamma-1}{2}\right) u_3^2\right] \times \left[a_c(t)^2 X - a_3^2\right]^{\frac{1}{2}} X^{\frac{1}{2}} \qquad (23)$$

where X is as for equation (22).

Equation (14) may now be used to get an expression for a_3 in terms of u_3:-

$$a_3 = a_o(\frac{\gamma-1}{2})\, Q_1 + (\frac{\gamma-1}{2})\, u_3 \qquad (24)$$

Equations (23) and (24) may then be solved using an iteration procedure similar to that described in section 1.3 of this appendix. When u_3 and a_3 are obtained, the remainder of the solution is simple.

2.3 CHOKED OUTFLOW

As mentioned in the previous section, the solution for choked outflow may be obtained from equations (13) to (17). Equation (16) represents the constant mass flow relation. For convenience, this relation may now be rewritten by substituting for $p_d(t)$ from equation (17) and for C(t) from equation (14) of Appendix 2:-

$$(\frac{2}{\gamma+1})^{\frac{\gamma+1}{2(\gamma-1)}} \frac{A(t)}{A_d}\, e^{\frac{(s_4 - s_c(t))}{R}} = \frac{u_3 a_4^{\frac{2}{\gamma-1}}}{a_c(t)^{(\frac{\gamma+1}{\gamma-1})}}$$

Now, using substitutions from equations (13) and (15) in the above equation, a relation in terms of u_3 and a_3 is obtained.

$$u_3 = [a_c(t)^2 - (\frac{\gamma-1}{2})\, u_3^{\,2}]\, e^{\frac{(s_d - s_c(t))}{R}} (\frac{2}{\gamma+1})^{\frac{\gamma+1}{2(\gamma-1)}} \frac{A(t)}{A_d} \frac{a_c(t)^{(\frac{\gamma+1}{\gamma-1})}}{a_3^{(\frac{2\gamma}{\gamma-1})}} \qquad (25)$$

Equation (14) may now be used to obtain an expression for a_3 in terms of u_3:-

$$a_3 = a_o(\frac{\gamma-1}{2})\, Q_1 + (\frac{\gamma-1}{2})\, u_3 \qquad (26)$$

Now the values of u_3 and a_3 may be found from equations (25) and (26) using an iteration procedure similar to that described in section 1.3 of this appendix. The remainder of the solution is then straightforward.

2.4 COMPUTATION METHOD

In the subroutine FLWØUT which performs the calculations for outflow from the cylinder, two other limiting flow cases are considered in addition to the event of barely sonic flow in the exhaust port. These limiting cases concern the occurrence of barely sonic flow in the duct in either regions (3) or (4).

As mentioned in section 2 of this appendix, only subsonic flows are assumed to exist in the main duct. The program, in fact, does not handle sonic or supersonic flow in the duct, although, of course, it could be altered to do so. Therefore, if the value of the Riemann invariant, Q_1, of a C_- characteristic is so low that supersonic flow would occur in the duct, the computation is stopped and an error message printed.

It is obvious that the occurrence of sonic flow in either regions (3) or (4) is quite unlikely, however, the study of these limiting cases helps to set fine limits on the iterations which must be performed in the program. As a result, such iterations have been found to rapidly converge to very accurate solutions.

The subroutine which performs all the calculations for outflow form the cylinder, FLWØUT, is listed in Appendix 6.

APPENDIX 5

INFLOW AT TAILPIPE OUTLET

The derivation of the flow existing after a C_+ characteristic reaches the tailpipe outlet, causing inflow, is given below.

Figure (1) shows an x - t diagram describing the event. The incident C_+ is reflected as a C_- characteristic and, as there is inflow, a P characteristic is introduced. Given that inflow occurs, the final situation is determined using steady flow relations and by assuming that the flow from the atmosphere is isentropic. Only subsonic flows are considered. The information required to obtain the final flow is a description of the incident C_+ characteristic, and the conditions in the atmosphere. These values, in terms of figure (1) are:-

for C_+: s_d

u_2

a_2

$P_1 = (\frac{2}{\gamma-1})\frac{a_2}{a_o} + \frac{u_2}{a_o}$

for atmosphere: s_5

$p_5 = p_o$ reference value

As mentioned in section 2.7.2 the final flow is calculated using the energy equation, the equation for the Riemann invariant, equation (2.7) and the fact that the pressures and velocities either side of the resultant P characteristic are the same.

In figure (1) by equating pressures in regions (3) and (4), the following relation is obtained:-

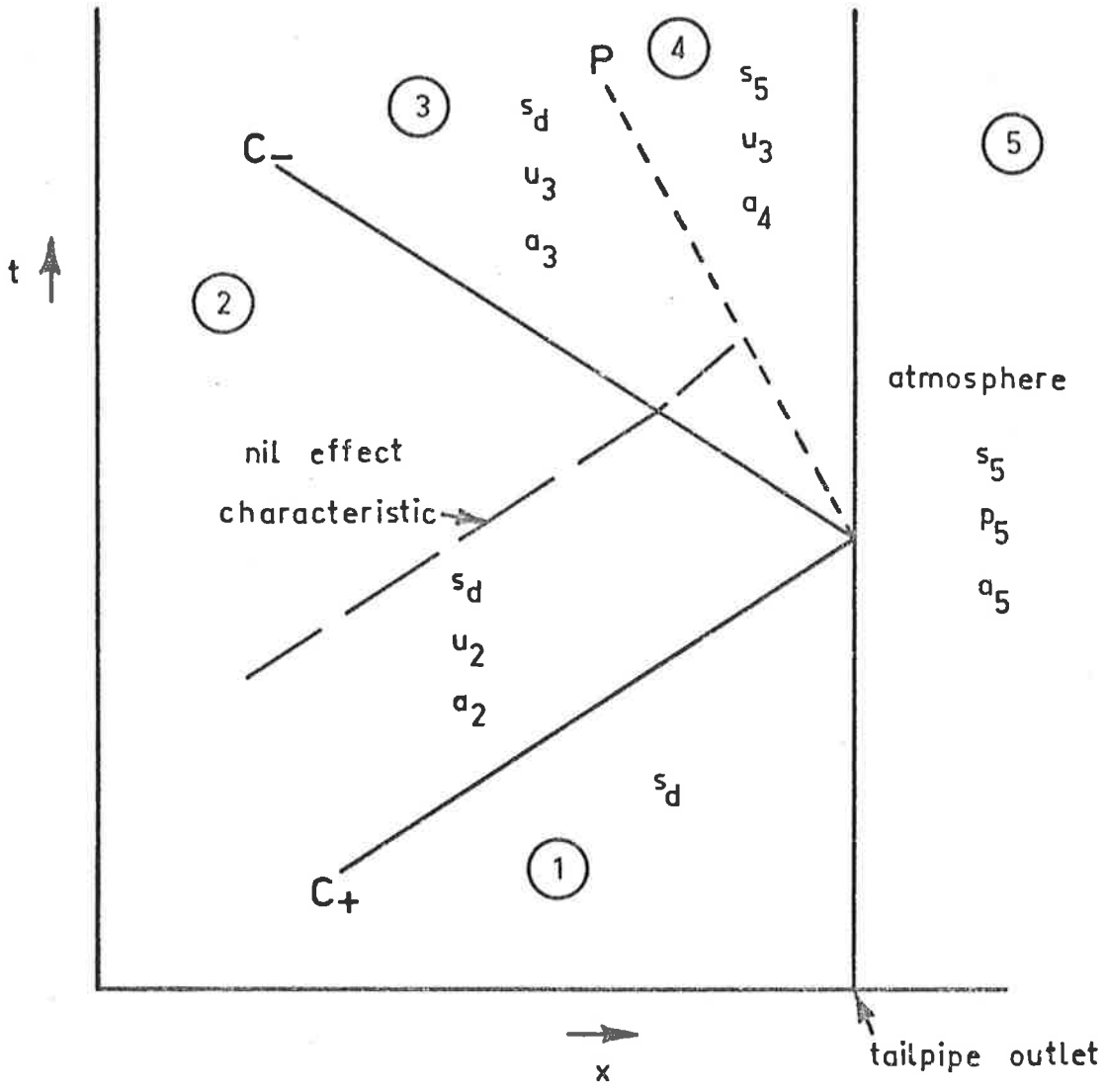

FIG.1 C_+ CHARACTERISTIC CAUSING INFLOW AT TAILPIPE OUTLET

$$\frac{a_4}{a_3} = e^{\frac{\gamma-1}{2\gamma R}(s_5 - s_d)} \qquad (1)$$

(see Appendix 2 equation (20))

The energy equation for the flow from the atmosphere gives:-

$$(\frac{\gamma-1}{2})\, u_3^2 + a_4^2 = a_5^2 \qquad (2)$$

as the velocities in regions (3) and (4) are the same.

If, as in Appendix 3, a nil effect C_+ characteristic, with the same Riemann invariant as the initial one, enters region (3), the following is true:-

$$P_1 = (\frac{2}{\gamma-1})\frac{a_3}{a_o} + \frac{u_3}{a_o} \qquad (3)$$

Finally, as the atmospheric pressure, p_5, is the same as the reference pressure p_o, the atmospheric speed of sound may be expressed in terms of the other reference conditions. Hence:-

$$a_5 = a_o\, e^{\frac{\gamma-1}{2\gamma R}(s_5 - s_o)} \qquad (4)$$

(see Appendix 2 equation (20)).

The solution is now obtained from equations (1) to (4) above as a_4, a_3, u_3, a_5 are the only unknowns. Terms may be eliminated to solve for the most convenient of the unknowns. For example, u_3 may eventually be solved in terms of a quadratic:-

$$\frac{u_3}{a_o} = \frac{-B \pm \sqrt{4AC + B^2}}{2A}$$

where $$A = 1 + \left(\frac{2}{\gamma - 1}\right) e^{\left(\frac{\gamma-1}{\gamma R}\right)(s_d - s_5)}$$

$$B = -2P_1$$

$$C = \left(\frac{2}{\gamma-1}\right)^2 \left(\frac{a_5}{a_o}\right)^2 e^{\left(\frac{\gamma-1}{\gamma R}\right)(s_d - s_5)} - P_1^2$$

The question of whether to take the positive or negative root in the expression for u_3 needs to be considered. If equation (2.12) is re-written in terms of the requirement for inflow to the tailpipe, the following is obtained:-

$$\text{for inflow to occur} \quad \left(\frac{2}{\gamma-1}\right) e^{\left(\frac{\gamma-1}{2\gamma R}\right)(s_d - s_o)} - P_1 > 0 \qquad (5)$$

Using relations (5) and (4), after some manipulation C may be proved to be positive. It is clear that A is always positive, while B is always negative. Therefore if u_3 is to be negative, as it must be if there is inflow, then only the negative root may be taken. Therefore:-

$$\frac{u_3}{a_o} = \frac{-B - \sqrt{4AC + B^2}}{2A} \qquad (6)$$

where A, B, C are as shown above. The remainder of the solution is straightforward.

APPENDIX 6

COMPUTER PROGRAM LISTING

A listing of the main program together with all the sub-routines which are used in performing a calculation for a 2-stroke engine with a tuned expansion chamber exhaust is given in the enclosed microfiche. Some small changes have been made to the program since the completion of the research, however, answers obtained are effectively the same. The author acknowledges that the original program has been further modified by Mr. W.M. Pearce of the University of Adelaide Computing Centre, so as to make it suitable for use on computers other than that installed at the University of Adelaide.

APPENDIX 7

LAWNMOWER SPECIFICATIONS

The lawnmower used is the Simpson-Pope rotary action 2-stroke. The cutting action is provided by a 4 bladed cutting system with an 18 inch (0.46 m) diameter cut and the grass clippings are collected in a rear catcher. The mower is not self propelled.

The engine is an air cooled single cylinder type with piston ports and crankcase induction, developing about 2 h.p. at 3500 r.p.m. Lubrication is by a petrol-oil mixture. The drive shaft of the engine is vertical. A brief list of the engine specifications follows:-

Basic Dimensions of Engine

compression ratio	5:1
bore x stroke	$2\frac{1}{8}$ inches x $2\frac{1}{8}$ inches
swept volume	125 cc

Construction of Engine

crankcase	- light weight aluminium alloy casting
cylinder	- fine grained normalized cast iron
cylinder head	- aluminium, with central sparkplug
crankshaft	- spheroidal graphite iron
connecting rod	- spheroidal graphite iron, with big end roller bearing
piston	- aluminium alloy
carburettor	- float type, side draught
ignition	- flywheel magneto

Port Timing

Inlet	open	72° BTDC
	close	72° ATDC

Exhaust	open	119° ATDC
	close	119° BTDC
Transfer	open	127° ATDC
	close	127° BTDC

BIBLIOGRAPHY

1. BERANEK, L.L. (Ed) (1971) — Noise and Vibration Control (McGraw-Hill)

2. BANNISTER, F.K. & MUCKLOW, G.F. (1948) — Wave action following sudden release of compressed gas from a cylinder. Proc. Instn. Mech. Engrs. 159, 269-300.

3. BENSON, R.S., GARG, R.D. & WOOLLATT, D. (1964) — A numerical solution of unsteady flow problems. Int. J. Mech. Sci. 6, 117-144.

4. BENSON, R.S. (1968) — A computer program for calculating the performance of an internal combustion engine exhaust system. Proc. Instn. Mech. Engrs. 182, (Pt.3L), 91-108.

5. MUTYALA, B.R.C. & SOEDEL, W. (1976) — A mathematical model of Helmholtz resonator type gas oscillation discharges of two-stroke cycle engines. J. Sound Vib., 44 (4), 479-491.

6. DAVIS, D.D., STOKES, G.M., MOORE, D. & STEVENS, G.L. (1954) — Theoretical and Experimental Investigation of mufflers with comments on engine - exhaust muffler design. N.A.C.A. Report 1192.

7. WATTERS, B.G., HOOVER, R.M. & FRANKEN, P.A. (1959) — Designing a muffler for small engines. Noise Control 5 (2), 18-22.

8. DAVIES, P.O.A.L. (1964) — The design of silencers for internal combustion engines. J. Sound Vib. 1 (2), 185-201.

9. ALFREDSON, R.J. (1970) — The design and optimization of exhaust silencers. Ph.D. thesis, Institute of Sound and Vibration Research, University of Southampton.

10. RUDINGER, G. (1955) — Wave diagrams for non-steady flow in ducts (D. Van Nostrand).

11. WHITHAM, G.B. (1974) — Linear and non-linear waves (J. Wiley)

12. LIEPMANN, H.W. & ROSHKO, A. (1957) — Elements of gas dynamics. (J. Wiley)

13. MORSE, P.M. (1948) — Vibration and sound. (McGraw-Hill)

14. SREENATH, A.V. & MUNJAL, M.L. (1970) — Evaluation of noise attenuation due to exhaust mufflers. J. Sound Vib., 12 (1), 1-19.

15. BIES, D.A. (private communication) — Work conducted at Ray W. Herrick Laboratories, Purdue University

16. BIES, D.A. & WILSON, O.B. (1957) — Acoustic impedance of a Helmholtz resonator at very high amplitude. J. Acoust. Soc. Am. 29 (6), 711-714.

BIBLIOGRAPHY

17. RUDD, M.J. & BENDER, E.K. (1974) — Lawnmowers: noise and cost of abatement. E.P.A. report Pb-234 932.

18. SPERRY, W.C. & SANDERS, G.J. (1959) — Quiet blades for 18-inch rotary type power lawnmowers. Noise Control 5 (May) 26-31.

19. Tasmanian Statutory Rules (1974) No. 59

20. CLARK, W.D. & WILLIAMS, K.C. — (private communication)

21. ANDERTON, D. & BAKER, J. (1973) — Influence of operating cycle on noise of diesel engines. S.A.E. paper 730241.

22. GROVER, E.C. & LALOR, N. (1973) — A review of low noise diesel engine design at I.S.V.R. J. Sound Vib. 28 (3), 403-431.

23. ANDERTON, D., LALOR, N., GROVER, E.C. & PRIEDE, T. (1969) — Assessment and control of combustion - induced noise in I.C. engines. Combustion Engine Progress. 48-53.

24. MABIE, H.H. & OCVIRK, F.W. (1963) — Mechanisms and dynamics of machinery. (J. Wiley)

25. CREMER, L., HECKL, M. & UNGAR, E.E. (1973) — Structure-borne sound. (Springer-Verlag)

26. MUGRIDGE, B.D. & MORFEY, C.L. (1972) — Sources of noise in axial flow fans. J. Acoust. Soc. Am. 51, (No. 5, Pt. 1), 1411-1426.

27. MORFEY, C.L. (1973) — Rotating blades and aerodynamic sound. J. Sound Vib. 28, (3), 587-617.

28. BARRY, B. & MOORE, C.J. (1971) — Subsonic fan noise. J. Sound Vib. 17, (2), 207-220.

29. COATES, S.W. & BLAIR, G.P. (1974) — Further studies of noise characteristics of internal combustion engine exhaust systems. S.A.E. paper 740713.

30. KARNOPP, D.C., DWYER, H.A. & MARGOLIS, D.L. (1975) — Computer prediction of power and noise for two-stroke engines with power tuned, silenced exhausts. S.A.E. paper 750708.